Naturally occurring nuclear reactions in rock formations and groundwaters

Smith, Barry

Award date:
1989

Awarding institution:
University of Bath

NATURALLY OCCURRING NUCLEAR REACTIONS IN ROCK FORMATIONS AND GROUNDWATERS.

submitted by Barry Smith
for the degree of PhD
of the University of Bath
1989

ProQuest LLC
789 East Eisenhower Parkway
P.O. Box 1346
Ann Arbor, MI 48106-1346

5043946

ACKNOWLEDGEMENTS.

I Wish to express my sincere thanks to my supervisor, Dr J.N.Andrews for his continued guidance and encouragement throughout this work.

I am indebted to and would like to thank the following :

The staff of the University of Bath who were always ready with help and advice.

The Bath and Portland Group, RTZ and Nottingham City Council for permission to use their mines and caves.

The Natural Environment Research Council for funding this research.

My wife, friends and the staff of the British Geological Survey who have contributed by offering constant encouragement in the course of this thesis.

ABSTRACT

A theoretical methodology has been developed for the calculation of rates of neutron and cosmogenic nuclide production in subsurface rock formations and groundwaters. Estimates made using this methodology are compared with experimentally measured neutron flux and nuclide concentrations and conclusions are drawn as to the validity of the theoretical approach.

The production rate of neutrons below the Earth's surface was estimated by considering production from (α,n) reactions, spontaneous fission, muons, protons and pions. Using correction factors for the attenuation of initial particle fluxes by material of the regolith, and for latitude and altitude effects production rates for specific sites were calculated. Calculations suggest that production from protons and pions dominate at depths < 4 meters below the Earth's surface.

The development of neutron flux within rock matrices was investigated to validate the calculation of thermal neutron flux from neutron production rates. Measurement of the neutron flux at sites for which theoretical fluxes were calculated based on chemical rock analysis of surrounding strata show that the flux may be estimated with reasonable confidence at depths below the influence of cosmic ray protons and pions. At shallower depths calculations overestimate the neutron flux.

Neutron induced reactions are the dominant processes producing ^{3}H, ^{14}C, ^{36}Cl, ^{37}Ar and ^{39}Ar in the deep subsurface. In the majority of cases regolithic production is dominated by spallation reactions. Direct production of all these isotopes by negative muon capture is possible, however, an accurate assessment of their importance requires more data. The movement of produced isotopes into groundwater requires a detailed understanding of fluid flow paths and rock mineralogy.

Investigation of the neutron induced production of radio-isotopes in the Stripa and Carnmenellis granites shows evidence for the in-situ production of ^{3}He, ^{36}Cl, ^{37}Ar and ^{39}Ar. For these isotopes measured concentrations are not inconsistent with predicted values.

CONTENTS

1 INTRODUCTION.

Cosmogenic nuclides produced in the Earth's atmosphere by the interaction of cosmic rays have been used for studying geochemical and hydrogeological processes for more than 40 years. The most common applications have been age-dating of groundwaters and estimation of the extent of mixing between waters of different ages. During this period, the atmospheric production and geochemical fate of nuclides, such as ^{3}H, ^{14}C, ^{36}Cl, ^{37}Ar and ^{39}Ar, have been extensively investigated (CURRIE., 1982, FRITZ and FONTES., 1984 and 1986).

The importance attached to the study of such isotopes is attributable to their short half-lives in the geological context. This makes them particularly useful for investigating the recent geological past (present day to one million years before present, see Fig 1.1). During this period many geochemical cycles which shape todays climate and topography were active. Extrapolation of these cycles into the future, as is required to predict changes in the Earth's climate depend upon accurate dating.

During the 1970's and 1980's advances in analytical instrumentation increased the sensitivity, accuracy and precision of measurment for these isotopes in both the solid and aqueous phase. This has enabled the detailed study of isotopes that were previously impossible to detect at natural levels (for example ^{36}Cl). Such an increase in sensitivity, accuracy and precision of measurement cannot lead to more accurate dating of geological processes unless it is matched by improvements in sampling techniques and in understanding of the factors that effect the interpretation of such measurements.

The most basic assumption in the use of any cosmogenic nuclide for dating geochemical events is that the initial concentration in a sample is fixed by atmospheric levels and that once isolated from the atmosphere only radioactive decay causes the concentration in the sample to change. The validity of such an assumption for ^{3}H and ^{36}Cl was disputed as early as the 1950's by DAVIS and SCHAEFFER, (1955) and MORRISON and PINE, (1955). These authors theoretically predicted the production of these isotopes in the subsurface rocks by neutron induced nuclear reactions (this effect has historically been known as "in-situ production").

However the validation of such hypothesis was, at that time, impossible since measurement techniques were not accurate enough to produce direct evidence. Increasingly detailed investigation of the greenhouse effect, and the integrity of proposed nuclear waste disposal sites has renewed interest in dating groundwaters with these isotopes (DAVIS and BENTLEY., 1982). This has led to the need for an accurate assessment of the possible effects of in-situ production processes on levels of cosmogenic nuclides used to date old groundwaters.

To assess the effects of in-situ production on the concentrations of radionuclides in groundwaters requires that:-

(a) It is possible to accurately calculate the neutron production rate.
(b) The contribution from other rare nuclear reactions is known.
(c) The transfer of the produced isotope into flowing groundwater is favorable.
(d) The effect of geochemical variation on (a), (b) and (c) is predictable.

This thesis re-examines point (a) in view of new data and validates methods for the calculation of neutron production rates and for the experimental measurement of neutron flux. These methods are used to compare in-situ production due to neutron induced reactions with that due to other nuclear reactions and to test the sensitivity of production rate to geochemical variations. Case studies are presented for groundwaters from the Stripa and Carnmenellis granites for which isotope production by in-situ reactions are of particular interest, for both groundwater dating and for determining solute origin.

Sections 1.1 to 1.4 review basic nuclear theory for the calculation of particle induced production rates and radioactive decay. Section 1.5 reviews the geochemical cycle and the hydrological applications of the cosmogenic nuclides that have been selected for detailed study (^{3}H, ^{14}C, ^{36}Cl, ^{37}Ar and ^{39}Ar).

1.1 Nuclear stability and the radioactive decay process.

1.1.1 Energetics and nuclear properties.

1.1.1.1 Energy units. The energies involved in nuclear processes are many orders of magnitude greater than those associated with chemical processes, and it is usual to refer to energy changes atom^{-1} rather than mole^{-1} as in chemical processes. The most common energy unit used in nuclear physics and radio chemistry is the electron volt (usually abbreviated to eV) which is equivalent to 1.6021×10^{-19} J. By convention energy liberated in nuclear transitions is positive, as opposed to the opposite convention in chemical processes.

1.1.1.2 Mass and energy. EINSTEIN (1907) showed that mass and energy are not independent and may be related according to the equation :-

$$E = mc^2 \qquad \text{Eqn 1.1}$$

where E is an amount of energy, m its mass equivalent, and c is the velocity of light consequently, a system which loses energy will lose an equivalent amount of mass.

1.1.1.3 Binding energy and Coulombic forces. The total energy required to completely separate the constituent parts of a nuclus (protons and neutrons) from each other is termed the "total binding energy" of the nucleus. When divided by the total number of nucleons (A) this yields the "average binding energy" per nucleon (E_B). However in a nucleus, protons and neutrons are not all bound to the same extent (analogous to an atom, where the inner electrons are more tightly bound than the outer ones). E_B remains virtually constant for nuclei of mass 16 or greater, however for nuclei of low mass (<16) E_B is reduced because of the large "surface to volume" ratio in such nuclei (nucleons near the surface do not have a complete set of near neighbours).

E_B may be expressed in terms of the liquid-drop binding energy equation given by MEYERS and SWIATECKI (1966) :-

$$E_B = (E_V - E_S - E_C + E_P)/A \qquad \text{Eqn 1.2}$$

where E_B is the binding energy per nucleon, E_V is the volume energy which increases with increasing mass and has a positive sign, E_S is the surface energy which decreases with increasing mass, E_C is the coulomb energy which arises from the electrostatic repulsion between protons and increases with the atomic number (Z) and E_P is the pairing energy which accounts for the preference of nuclides with even numbers of protons and neutrons.

In any nucleus a balance exists between nuclear forces (attractive) and Coulombic forces (repulsive) acting on individual nucleons within that nucleus. The variation in the state of such balance (in terms of potential energy) with distance r from the nucleus is approximately described by a square-well of radius R, where R is the radius in which nuclear attractive forces act (FRIEDLANDER et al., 1981). Square-wells are shown for a charged particle (proton) and neutral particle (neutron) interactions in Fig 1.2a and 1.2b from which it may be seen that a "positive potential energy barrier" would inhibit the transfer of a charged particle into, or out from the nucleus. This potential energy barrier is termed the "Coulombic barrier" and its height strongly influences the stability of nuclei with respect to decay and nuclear reactions. Note that such a barrier does not exist for the passage of a neutral particle and that quantum mechanics has shown that there is a finite probability of charged particles "tunneling" through such a barrier.

1.1.2 Nuclear stability.

The total number of different known nuclides is approximately 1,700, however only about 260 of these are stable suggesting that stability is the exception rather than the rule. These stable nuclides and some naturally occurring unstable nuclides such as U and Th make up the elements in the periodic table. A careful examination of the relative stability of isotopes has led to the concept of "magic numbers" for Z, the atomic number (the number of protons) and n (the number of neutrons). Nuclides having magic proton numbers or magic neutron numbers, or both, are usually stable as indicated by their greater isotopic abundance or slower

decay rate. The magic numbers for Z and n are 2, 8, 10, 20, 28, 50, 82, and 126.

Radionuclides decay by spontaneous nuclear transformation until a stable nuclear configuration is attained. Most of the known radionuclides do not occur naturally because their half-lives are short and they have totally decayed in the time since the solar system was formed. Four groups of radionuclides exist naturally on the earth:-

(a) Radionuclides with very long half lives so that a measurable amount of that found in the pre-solar system nucleosynthesis, still remains. Radionuclides in this group include ^{238}U, ^{235}U, ^{232}Th, ^{87}Rb and ^{40}K.

(b) Radionuclides produced by the decay of the long lived radionuclides in (a). Such radionuclides include ^{226}Ra and ^{222}Rn which occur in the ^{238}U decay series.

(c) Radionuclides produced by the interaction of high energy cosmic rays with the atmosphere and surface of the earth. Such radionuclides include ^{3}H, ^{10}Be, ^{14}C, ^{36}Cl and ^{129}I.

A further group of nuclides are those that are produced by nuclear reactions subsequent to the decay of the natural radionuclides. It is these nuclides which are of particular interest in this thesis.

In addition, some radionuclides have been introduced into the environment by man (anthropogenic sources), for example, those released from nuclear reactors and during the testing of nuclear weapons. Such nuclides include ^{129}I, ^{3}H, ^{14}C, ^{85}Kr.

1.1.3 Nuclear decay rates.

The decay or disintegration rate of any radioactive nuclide is proportional to the number of atoms present in a particular sample. As an unstable element decays, the number of radioactive atoms decreases causing an equivalent decrease in the decay rate according to equation 1.3.

$$-\frac{dn}{dt} = -\lambda\, n(t) \qquad \text{Eqn 1.3}$$

where n is the number of radioactive nuclei in a sample at a given time t and λ is the decay constant with dimensions of $time^{-1}$. Integration of equation 1.3 yields equation 1.4 which shows that the number of radioactive atoms in a given sample decreases exponentially with time.

$$n = n_o\, e^{-\lambda t} \qquad \text{Eqn 1.4}$$

where n_o is the initial number of radioactive atoms and n is the number remaining after time t. The time required for half of the original number of radioactive atoms to decay $t_{1/2}$ (the half-life) may be derived from equation 1.4 to be :-

$$t_{1/2} = \frac{0.693}{\lambda} \qquad \text{Eqn 1.5}$$

Equations 1.3 to 1.5 apply to the formation of a stable nuclide from the decay of an unstable nuclide, however in some cases such as radioactive "series" an unstable nuclide may decay into a stable nuclide via a number of unstable intermediates. The mathematics of decay in radiochemical series have been reviewed in many texts (KAPLAN., 1955, FAURE., 1986). The major conclusions of such treatments is that a condition known as "secular equilibrium" exists when the product of the decay constant and number of unstable atoms for each member of the series are equal. The time required for such a condition to be established depends on the decay constant (or half-life) of the longest lived decay product in the series.

1.2 Nuclear decay processes.

1.2.1 Alpha decay.

Whenever a nucleus decays to a lower energy state by α-particle emission, it loses a total of four nucleons, two protons and two neutrons. The residual nucleus is therefore a new element whose atomic number (Z) is two less than the parent nuclide. The disintegration of a nuclide (A,Z) by a emission is summarised by :-

$$(A,Z) \rightarrow (A-4,Z-2) + \alpha + \text{energy} \qquad \text{Eqn. 1.6}$$

where A and Z are the atomic mass and atomic number respectively, and (A-4,Z-2) represents the product nuclide. This decay mode is favourable for nuclides having atomic numbers of 58 (Cerium) or greater and for a few light nuclides, including ^{5}He, ^{5}Li and ^{8}Be.

A successful theoretical interpretation of α-decay was first made by GAMOW (1928) and GURNEY and CONDON (1928), and used to explain a relationship between half-lives and α energies. Their theoretical approach is based on the quantum mechanical "tunneling" of α-particles through the nuclear potential well (also termed "Coulombic barrier" which is a consequence of the competition between short range nuclear forces and repulsive electrostatic forces) and has been well validated by experimental results (FRIEDLANDER., 1981).

1.2.1.1 The energetics of alpha decay. The energy spectra of α particles, emitted from a radio-nuclide are characterised by definite and discrete groups of energies indicating that when a nucleus undergoes such a transition it does so between specific energy states. For example when ^{228}Th decays to ^{224}Ra the α-particle spectrum consists of 5 well defined lines with energies from 5.138 MeV to 5.423 MeV (FRIEDLANDER et al., 1981). These spectral lines do not occur with the same intensities, for instance in the case of ^{228}Th decay the most intense line contains 72.7% of the total number of α particles emitted. Spontaneous α-decay will only occur in a nucleus if the energy of the parent nuclide (A,Z) is greater than that of the products.

The difference in the energy sates is referred to as the reaction energy , Q.

$$Q = M_{Z,A}c^2 - [M_{Z-2,A-4} + M_\alpha]c^2 \quad \text{(joule)} \qquad \text{Eqn 1.7}$$

where c is the speed of light in a vacuum and $M_{Z,A}$, $M_{Z-2,A-4}$ and M_α are the rest-mass of the initial nucleus, product nucleus and α-particle, respectively. When expressed in MeV, Q gives the maximum disintegration energy for the decay process. This energy is shared between the products of the disintegration process, hence the disintegration energy, Q, is shared between the α-particle and the recoil nucleus, M_{Z-2}.
The maximum α energy (E_α) for such a reaction is related to Q by the equation :-

$$E_\alpha = Q \frac{M_{Z-2,A-4}}{M_{Z-2,A-4} + M\alpha} \qquad \text{Eqn. 1.8}$$

As stated above not all α particles have this maximum energy and to conserve the total rest mass the product nuclide must be left in an excited state. This excited state may then de-excite by the emission of γ radiation (see Fig 1.3).
Conservation of momentum also requires that the product nuclide attains a momentum equal in magnitude and opposite in direction to that of the emitted α-particle. The "recoil energy" ($E_{Z-2,A-4}$ MeV) for such a decay process may then be calculated from :-

$$\frac{M_\alpha E_\alpha}{M_{Z-2,A-4}} = E_{Z-2,A-4} \qquad \text{Eqn. 1.9}$$

where M_α and E_α are the rest mass and energy of the emitted alpha particle and $M_{Z-2,A-4}$ is the rest mass of the product nuclide.

1.2.2 Beta decay.

Beta decay is more common than α decay and every element has several isotopes which decay by this mode. In ß decay, the mass number A of the isotope does not change and such transitions are referred to as isobaric transitions. There are three different kinds of ß decay process :-

(a) Negatron emission. This occurs in isotopes which have an excess of neutrons and can be considered to be the transformation of a neutron into a proton and an electron. The negative electron (called a negatron, $ß^-$) is expelled from the nucleus so that the nuclear charge, Z, increases by one unit.

(b) Positron emission. This is a similar process to negatron emission but occurs in isotopes that have an excess of protons. The nucleus emits a positively charged electron (positron, $ß^+$) and therefore the nuclear charge, Z, decreases by one.

(c) Electron capture. This also occurs in isotopes which have an excess of protons. In this process the nucleus captures one of the atomic electrons, usually from the K shell so that the nuclear charge decreases by one unit. Both positron emission and electron capture may occur in the same isotope.

1.2.2.1 The energetics of beta decay. (a) Negatron decay. The energy released by this decay mode may be found in a similar way to that for α decay. As in the case of α decay, spontaneous ß decay is only energetically possible if the parent atom is heavier than the product atom. However in negatron decay this energy does not appear simply as the kinetic energy of the emitted particle. As may be seen from the ß particle energy spectrum for ^{40}K (Fig 1.4) all emitted ß particles do not have the same energy. This is because in ß decay a further neutral particle (the anti-neutrino $\bar{\upsilon}$) is emitted (FERMI., 1934 and REINES and COWAN., 1957) and the energy available for decay is shared between the ß particle and the neutrino. For example the maximum energy of ß particle released during the decay of ^{14}C (E_{max}) corresponds to Q for the reaction (0.156 MeV (Fig 1.5).

In some cases the product nucleus formed by ß decay is left in an excited state. This excess energy is emitted

either as a γ ray, or it is transferred to an extra nuclear electron which is then ejected from its orbital. These ejected electrons are mono-energetic and are superimposed on the continuous ß particle spectrum. This process is termed internal conversion.

Some nuclei may remain in such excited states, prior to decay by internal conversion or γ emission, for measurable lengths of time (metastable states) and are referred to as isomers being in an isomeric state.

(b) Positron decay. The energetics of positron decay are similar to those for negatron decay in that the energy spectrum forms a continuum where the decay energy is shared between two emitted particles. However in the case of positron decay the energy is shared between the positron (a positive electron or anti-electron) and a neutrino. The positron that is emitted by such processes is slowed by collision with atoms and when nearly at rest interacts with an electron. In this reaction, matter (the electron) meets anti-matter (the positron) and both are annihilated yielding two 0.511 MeV γ-rays. Thus the total decay energy of the reaction is the endpoint energy plus 1.02 MeV arising from the annihilation as is seen in the decay of ^{14}O to ^{14}N (see Fig 1.6).

(c) Electron capture. An alternative method by which a nucleus can decrease Z by 1 whilst keeping A constant is by capturing one of its extra-nuclear electrons. This capture is most probable for K shell electrons as they are close to the nucleus. Electrons from other shells,however, also have a finite capture probability. In the capture process a mono-energetic neutrino is emitted from the nucleus. An example of such decay is the branched decay of ^{40}K to ^{40}Ca and ^{40}Ar (See Fig 1.7). In the decay process the vacancy left by the extra-nuclear electron may be filled by one from an outer shell. This causes the emission of an energetic x-ray which in turn may stimulate the release of an "Auger" electron.

1.2.3 Gamma decay.

The emission of γ-rays are analogous to the emission of photons of optical and x-ray frequencies by an atom. In γ decay a γ-ray photon results when a nucleon undergoes transitions

between nuclear energy levels. These energy levels in nuclei are quantized as is evidenced by the discrete α particle and γ ray energies encountered during α decay. Generally the lifetime of such states are short ($<10^{-14}$ s), depending on the amount of reorganisation that must take place within the nucleus. However some states may exist for periods of longer than a year, such nuclei are known as isomers and their decay is termed isomeric transition.

$$(A,Z)^* \longrightarrow (A,Z) + \text{photon}$$

γ emission does not induce nuclear transmutations, however the mass energy of the nuclide is reduced by an amount equal to the energy of the emitted photon.

Not all possible γ transitions are observed as some are forbidden by selection rules.

1.2.4 Decay by spontaneous fission.

Spontaneous fission is a very rare mode of decay and only occurs among the heaviest elements in the periodic table. During fission the nucleus splits into two smaller nuclei of approximately equal mass, with the release of about 200 MeV which appears mainly as the kinetic energy of the two fragments. Spontaneous fission was discovered by FLEROV and PETRZHAK (1940), after it had been theoretically predicted by the "liquid drop" model of BOHR and WHEELER (1939). Since Flerov and Petrzhaks discovery of spontaneous fission in U this mode of decay has been observed in more than twenty heavy nuclides including ^{235}U for which it is an alternative mode of decay. Recently the emission of small nuclei such as ^{14}C from U and Th series isotopes has been observed (ROSE and JONES., 1984). Such emissions represent the extremes of non-symmetrical fission.

1.2.4.1 The energetics of spontaneous fission. In terms of reaction energetics the fission of any isotope with an atomic mass > 100, are exoergic and, as a consequence are unstable with respect to spontaneous fission (FRIEDLANDER et al., 1981).

However measurable rates of spontaneous fission are only found among the heaviest elements due to the Coulomb barrier which prevents the emission of large highly charged fission fragments.

1.3 Nuclear reactions.

Nuclear reactions occur when a particle such as a neutron, proton or a "heavy ion" interacts with a target nucleus, to produce a number of products. These products include a nuclei which may or may not be itself undergo further radioactive decay, and reaction products which depend upon the exact nature of the reaction. Reactions are described by the use of equations such as :-

$$ {}^{A}_{Z}X\ (a,b)\ {}^{A}_{Z}Y \qquad \text{Eqn 1.10} $$

where ${}_{z}X$ describes the initial nuclei, a and b are the reacting and produced particles/ions and ${}_{z}Y$ describes the produced nuclide. Many reactions occur via an excited intermediate nuclei which may de-excite via a number of processes (reaction channels) which have associated probabilities. Channels involving charged particle emission generally have smaller probability than that for those involving neutral particles due to the particles having to traverse the Coulomb barrier (See Fig 1.2).

1.3.1 Reaction energetics.

Q the reaction energy may be calculated for given reaction channels provided that the rest mass (in terms of energy) of the products and target, and the kinetic energy of the reacting particle are known. For example the reaction $^{14}N(^{4}He,^{1}H)^{17}O$ may be described as :-

$$ {}^{4}He + {}^{14}N \longrightarrow {}^{18}F^{\star} \longrightarrow {}^{17}O + {}^{1}H + Q $$

and Q calculated by balancing the equation in terms of mass or energy.

The energy Q appears as kinetic energy of the final reaction products whose energy portion may be calculated based on classical mechanics given that their kinetic energies are inversely proportional to their mass. For the case above :-

$$\frac{\text{kinetic energy } {}^{1}H}{\text{kinetic energy } {}^{17}O} = \frac{\text{mass } {}^{16}O}{\text{mass } {}^{1}H} \qquad \text{Eqn 1.11}$$

Q may be +, 0 or -, reactions with negative Q values require that the reacting particle have a minimum threshold energy below which the reaction has little probability. This threshold energy (E_{tr}) may be calculated using equation 1.12 (GIBSON., 1971).

$$E_{tr} = -Q \frac{A+1}{A} \qquad \text{Eqn 1.12}$$

where A is the atomic mass of the target nucleus and Q is the reaction energy (MeV).

1.3.2 Reaction cross-sections.

The probability of a reaction occurring is dependent on the energy of the reacting and ejected particles, and is expressed as the energy dependent reaction cross-section ($\sigma_{(E)}$), which has units of barns or cm^2 (1 barn = $1x10^{-24}$ cm^2). The cross-section for a particular reaction is defined as :-

$$\sigma_{(E)} = \frac{\lambda N_r}{N_{tg}\phi} \qquad \text{Eqn 1.13}$$

where λ is decay constant, N_{tg} is the number of target nuclei per unit volume of target material, N_r is the production rate per unit volume and ϕ is the particle flux.

Cross-sections for reactions may be determined in many ways the more common being from measured values of λ, from measured yields of nuclides produced in reactions and from calculations based on nuclear energetics. A particularly

useful method of calculating cross-sections has been described by INTHOFF (1955) which uses nomograms to calculate cross-sections for (n,p) and (n,α) reactions.

For low energy reactions the cross-section and hence reaction probability of :-
neutron induced reactions > proton induced reactions > alpha induced reactions > pion induced reactions > muon induced reactions > gamma induced reactions

A similar generalisation applies to the probability of particle emission in nuclear reactions. Thus, the cross-sections of reactions involving :-
neutron emission > proton emission > alpha emission.
This generalisation breaks down for light nuclei where particular reactions, such as $^{6}Li(n,\alpha)^{3}H$, are energetically very favourable.

Neutron induced reactions are the most likely naturally occurring nuclear reactions to produce significant amounts of nuclides in the subsurface. The validity of this statement applied to the subsurface production of ^{3}H, ^{14}C, ^{36}Cl, ^{37}Ar and ^{39}Ar is tested in Section 4.0.

1.3.3 Reaction rates.

The rate of a nuclear reaction is expressed as the number of desired product nuclei produced per unit time (R). This is calculated using equation 1.14.

$$R = \sigma_{(E)}\ n\ \phi_{(E)} \qquad \text{Eqn 1.14}$$

where R is the number of nuclei produced from the reaction (s^{-1}), $\sigma_{(E)}$ is the reaction cross-section (cm^2) at a given energy E, n is the number target nuclei cm^{-3} and $\phi_{(E)}$ is the particle flux ($cm^{-2}\ s^{-1}$) for particles of energy E. Note the production rate (R) is constant with respect to time provided that the number of target nuclei is not significantly reduced.

However if the produced nuclide is radioactive and the number of atoms of product present after a given time is required, equation 1.14 must be adapted to account for the decay of any produced nuclide during irradiation. The irradiation of a target with a constant flux of particles acts like a radioactive parent with an infinite half life.

Thus the number of atoms of product present after time t ($N_{(t)}$) is equal to :-

$$N_{(t)} = \frac{R}{\lambda}(1-e^{-\lambda\tau}) \qquad \text{Eqn 1.15}$$

where $N_{(t)}$ is the number of atoms of product produced after irradiation time t (s), λ is the decay constant for the produced nuclide (s^{-1}) and t is the length of the irradiation period (s). The number of atoms present increases until the irradiation time approaches infinity

$$\lim\ (1-e^{-\lambda t}) = 1 \qquad \text{Eqn 1.16}$$

and for $\lambda t >> 1$ (t> several half-lives)

$$N = \frac{R}{\lambda} \qquad \text{Eqn 1.17}$$

where ($\tilde{N}$) is the number of atoms of product at saturation. This equilibrium will persist until the number of target nuclei is significantly reduced, provided that the system remains closed with respect to the mass transport of material.

In nature mono-energetic particles are rare and to accurately obtain R, $N_{(t)}$ or $\tilde{N}$, equations 1.14, 1.15 and 1.17 must be integrated over the energy distribution of the reacting particles. In many cases such an integration is impossible since $\phi_{(E)}$ is not generally known with great certainty. The same also applies in many case for $\sigma_{(E)}$ which is often only known for a few discrete energies. Because of this a number of reaction dependent approaches have been adopted to obtain estimates of R, $N_{(t)}$ or $\tilde{N}$ these are discussed with respect to the type of reacting particle below.

1.3.3.1 Neutron reactions. MORRISON and PINE. (1955) and DAVIS and SCHAEFFER. (1955) first predicted that nuclear processes, involving the reaction of neutrons with the component elements of the rock matrix, were likely to be the greatest source of radioisotopes in the subsurface. This is

because no Coulomb barrier prevents the formation of an intermediate excited state for such reactions (See Fig 1.2). Consequently reaction probabilities for low energy neutrons are high compared to those for charged particle reactions.

After a neutron enters a nucleus the resulting excited compound nucleus may emit a charged particle, which is subject to Coulomb barrier effects, a gamma ray or one or more neutrons, whilst in heavy nuclei fission may take place. These reactions are known symbolically as (n,p), (n,α), (n,γ), (n,n), (n,2n) and (n,f) reactions.

(n,n) reactions are scattering reactions which may be either elastic or in-elastic. At relatively low neutron energies (for instance 0.025 eV) elastic scattering predominates, however at energies above 0.1 MeV in-elastic scattering dominates. In in-elastic scattering large amounts of kinetic energy are lost from the scattered neutron. This energy loss is commonly called thermalisation and is further discussed with respect to rock matrices in Section 3 and APPENDIX 3.

The probability of specific reaction channels (ie/ cross-sections for (n,p), (n,α), (n,γ), (n,2n) and (n,f) reactions) are energy dependent. The energy dependence is complex (See Fig 1.8) however three regions may be identified :-

(1) In the thermal region (0.001 to approximately 0.5 eV), many target elements have cross-sections proportional to 1/v, where v is the neutron velocity (see Fig 1.8). In terms of energy the cross-section is proportional to $E^{-1/2}$ since :-

$$v = \sqrt[2]{\frac{E}{0.523 \times 10^{-8}}} \qquad \text{Eqn 1.18}$$

where E is the neutron energy (eV) and v is its velocity (m s^{-1})

(2) In the intermediate energy region (0.5 to approximately 5000 eV) cross-sections show sharp maxima at energies equal to the resonance energy levels of the compound nucleus. These absorptions are particularly complex for heavy nuclei.

(3) In the fast energy region (energies above 5000 eV) cross-sections are generally lower than in the thermal and resonance regions. However cross-sections in this region may show large increases with energy due to neutron induced reactions with energy thresholds.

Because of the complexity of the variation in σ with energy the only correct way to calculate reaction rates is to group cross-sections into energy intervals and sum the reaction rate over the total number of intervals (multi-group neutron theory). Unfortunately at present, this approach is impractical as it requires a detailed knowledge of the neutron energy spectrum. This is particularly hard to determine experimentally in rock matrices due to limitations in the size and detection limit of neutron spectrometers (CENTRONIC., 1986, MARSHALL., 1983, TRS No 107., 1970, ICRU., 1969. and ALLEN., 1960).

Theoretical estimation of the required neutron energy distribution is also difficult since it must be based on a knowledge of the initial neutron energies and moderating properties of the rock matrix. These are often not well known and are also likely to show wide variability between rock types. However, calculations by KREFT., 1973 indicate that in rock matrices the majority of neutrons are likely to reach thermal energies and the importance of neutron reactions in the fast and intermediate energy regions is low. Thus in rock matrices reaction rates calculated using thermal neutron cross-section should be consistent with the true reaction rate. If the degree of thermalisation is low the use of thermal neutron cross-sections yield the maximum possible production rate as thermal cross-sections are generally higher than either intermediate region or fast region cross-sections for neutron reactions with negative Q values.

The use of thermal cross-sections in calculations for specific sites may be validated by "broad brush" measurements of the neutron flux distribution, using Cd thermal neutron filters (ANDREWS et al., 1986, YAMASHITA et al., 1966 and MORRISON and PINE., 1955). These techniques have been used in this thesis to validate the correctness of using thermal neutron cross-sections for the calculation of reaction rates in the Stripa and Carnmenellis granites.

If more accurate production rates are to be calculated it

is imperative that the dependence of σ with neutron energy be investigated for the rarer (n,p) and (n,α) cross-sections and that better energy dependent cross-section data should be obtained.

1.3.3.2 Charged particle reactions. Charged particle reactions are predominantly high energy reactions since charged particles suffer electrostatic repulsion by nuclei (See Fig 1.2). The most common naturally occurring charge particle reactions are those initiated by primary and secondary cosmic rays (protons, pions, muons and heavy nuclei). At depths below the influence of cosmic rays alpha particles produced from the decay of the naturally occurring radionuclides (U and Th series isotopes) also initiate charged particle reactions (MORRISON and PINE., 1955).

When charged particles pass through matter, energy is lost by scattering from atomic electrons and more importantly at low energies by scattering from atomic nuclei. During this process considerable ionisation occurs making the detection of the charged particle relatively easy.

Because of the wide range in the energies of cosmic ray and nuclear decay particles two classes of charged particle reactions may defined:-

(1) Reactions at energies of less than 50 MeV. This includes reactions of "slowed" cosmic ray particles and a particles from U and Th decay series. These reactions may be described by the "compound-nucleus" approach (FRIEDLANDER et al., 1981) in which a compound "meta-stable" intermediate nuclei is formed. This subsequently decays by appropriate reaction channels. Because of coulombic repulsion these reactions generally show a threshold energy dependence despite having positive Q values (See Section 1.3.1). An example of the energy dependence of the reaction cross section for a low energy charged particle reaction is shown in Fig 1.9.

Reaction rates for these reactions may be calculated in a similar way to that used for neutron reaction rates provided that the energy dependence of the cross-section and particle flux are known. Alternatively "Thick" or "Thin" target yields may be used.

Thick target yields automatically integrate the yield of a bombarding particle whilst its energy is degraded by the

absorbing target material and are particularly useful for calculating the number of neutrons produced by (α,n) reactions (Section 2) and the yield of the $^{11}B(\alpha,p)^{14}C$ reaction (Section 4). Thin target yields, on the other hand, are based on target thicknesses that do not significantly degrade the energy of the bombarding particle and may be used to calculate the reaction cross-section at discrete energies ($\sigma_{(E)}$).

(2) Reactions that occur at energies greater than 50 MeV. These reactions are only produced in nature by cosmic rays and their secondaries. At energies above 50 MeV "direct reaction" predominates and spallation products are formed. An example of the energy dependance of the reaction cross section for a high energy charged particle reaction is shown in Fig 1.9.

In spallation reactions (also called "nuclear evaporation reactions") small fragments (neutrons, protons, α particles, etc.) are removed from the nucleus by the interaction of the bombarding particle. At such high energies fission reactions are also possible, these however differ considerably in their mass yield relationship from low energy fission processes.

Production rates from these high energy interactions are calculated from either thick or thin target yields (isotopic yields), or form the average number of particles produced per interaction based on evidence from "nuclear stars" formed in emulsion detectors (particle yields).

1.4 Cosmic rays

Thousands of meters above the earths surface, the outer atmosphere experiences a continuous bombardment from photons and subatomic particles. The photons cover the whole range of the electromagnetic spectrum (from radio waves through visible light to gammay rays) whilst most of the subatomic particles are energetic nuclei (atoms stripped of all their electrons). This high energy rain of particles has become known as cosmic radiation. Cosmic radiation is distinguished from radiation produced by radioactive decay by the fact that cosmic ray particles have much higher energies and are thinly spread. Cosmic rays arriving from space (the primary component) interact with the atoms and molecules of the upper atmosphere and produce "showers" of subatomic particles (See Fig 1.10) the "secondary" component. Most of this secondary radiation is absorbed before reaching the Earth's surface (producing cosmogenic radio nuclides such as ^{14}C in the process) leaving

a residual comonent of weakly interacting particles which pass through the air/ground interface. This residual component interacts with the dense medium of the earth's surface to produce neutrons and radioactive nuclei which may then interact further or decay. Roughly 20 cosmic ray particles cm^2 s^{-1} arrive at the top of the atmosphere. At sea level this is reduced to approximately 1 particle cm^2 s^{-1} (CLOSE et al., 1987) and represents approximately one third of the natural radiation dose to man (KAYE and LABY., 1986). In comparison, one gram of a radioactive substance such as radium emits thousands of millions of particles a second. The constituents and properties of the primary and secondary components of cosmic rays are discussed further below.

1.4.1 The primary component.

The primary component of cosmic rays is mainly composed of galactic rather than solar particles. These include energetic (0.1 GeV to 20 GeV) protons (approximately 94%) and nuclei with $Z < 20$. The remainder being predominantly high energy gamma rays and nuclei with $Z > 20$. A small percentage of the total particle flux have energies in excess 1000 GeV. The distribution of elements within the primary component has been shown to be close to that found in stars (LAL and PETERS., 1967).

The flux of the primary component reaching the solar system is isotropic and virtually unchanging with time (to within 0.1% below 10^{14} eV (KAYE and LABEY., 1986)) however the flux observed at the top of the Earth's atmosphere varies slightly due to the effect of interplanetary magnetic fields (modulated by solar activity on a 11 year cycle) and the Earth's magnetic field that deflects low energy particles towards the polar regions. The effect of the Earth's magnetic field is more pronounced for primary cosmic radiation than for the secondary particles (at sea level); the primary flux at the geomagnetic poles being 20 times that at the geomagnetic equator (ROSSI., 1948).

Occasionally bursts of particles originating in solar flares can have energies of a few GeV, and can be classed as cosmic rays. Such bursts have caused the cosmic ray activity to increase by factors in excess of 50 (23^{rd} February 1956) for periods of less than one day (QUENBY., 1967). Solar events such as the 11 year sun spot cycle show a negative

correlation with primary cosmic ray intensity due to their effect on the interplanetary magnetic field.

1.4.2 The secondary component.

The secondary component of cosmic rays that reach the Earth's surface is composed of subatomic particles including positrons, μ-mesons, pi-mesons, neutrons, protons etc, the properties of the most abundant of these particles are summarised in Table 1. These secondary particles are produced by the interaction of primary cosmic ray particles with molecules and atoms present in the Earths atmosphere (principally, in order of abundance N_2, O_2, Ar, CO_2, Ne). As well as secondary particles these interactions also produce cosmogenic radionuclides in the atmosphere and to a limited amount in the Earth's surface (LAL and PETERS., 1967).

Because of the high energy of the primary component, production of secondary particles and direct production of cosmogenic nuclides occur via spallation reactions. Secondary particles once produced either decay or undergo further interaction with atmospheric nuclei via processes summarised in Fig 1.11. Such interactions attenuate the primary radiation and secondary component during their passage from the high atmosphere to the Earth's surface.

1.4.2.1 The N-Component. The N-component of secondary cosmic rays is that portion which is capable of producing further nuclear interactions, such as spallation, with high efficiency (primarily high energy protons, neutrons and charged pi-mesons). The intensity of these particles decreases in an exponential manner with atmospheric depth (half thickness approximately 76 g cm^{-2} (KAYE and LABEY., 1986) depending upon the exact depth interval (SIMPSON and FAGOT., 1953)). The latitude dependence of the N-component (including the contribution from neutrons (HENDRICK and EDGE., 1966)) is dependent upon atmospheric depth. At large atmospheric depths (> 700 g cm^{-2}, or approximately 10000 m above sea level) the variation in intensity due to latitude, is approximately constant. The flux of particles at the geomagnetic equator is 20 to 30 % of the flux at geomagnetic latitudes greater than 60^{o} N, above which the flux is constant (YOKOYAMA et al., 1977, HENDRICK and EDGE., 1966 and SIMPSON and FAGGOT., 1953). There is a small variation in the flux of N-component

particles with longitude due to the nature of Earth's geomagnetic dipole (YOKOYAMA et al., 1977 and SIMPSON., 1951). These factors are further discussed in Section 2.3.

1.4.2.2 The μ-meson component. The μ-meson component of secondary cosmic rays is produced by the decay of pi-mesons and these retain about 80% of the energy of their parents. Energy lost through ionisation rather than through nuclear interactions such as is the case with the N-component. Positive and negative μ-mesons occur in approximately equal proportions. Most of the μ-mesons reach ground level and subsequently penetrate the regolith to depths in excess of 5 m (HAMPEL and KIRSTEN., 1975, CHARALAMBUS., 1971 and ROSSI., 1948). During this penetration μ-mesons either decay or become captured by nuclei of the regolith. The attenuation of the μ-meson component by different thicknesses of regolithic material follows a complicated relationship (ROSSI., 1948) that is dependent on the μ-meson energy spectrum at the air/ground interface (Section 2).

The latitude and atmospheric depth dependence of the intensity of μ-mesons produced during the decay and interaction of primary and secondary particles varies to a smaller degree than the intensity of the N-component (KAYE and LABY., 1985 and SUBRAMANIAN et al., 1958). The dependence of μ-meson intensity with latitude and atmospheric depth are discussed further in Section 2.4.

1.5 Cosmogenic nuclides.

The term "cosmogenic" may be applied to any nuclide produced by the interaction of cosmic rays. Those of particular interest because of their use as tools in the interpretation of hydrological processes are:-

^{3}H, ^{14}C, ^{36}Cl, ^{37}Ar and ^{39}Ar

These nuclides have been used for both radio-chemically dating groundwaters and the investigation of rock-water interaction (DAVIS and BENTLEY., 1982). Their atmospheric production, detection and use for groundwater studies are reviewed briefly in Sections 1.5.1 to 1.5.5.

1.5.1 Tritium.

1.5.1.1 Atmospheric production. Tritium (^3H) is produced in the atmosphere by interaction of cosmic ray particles with gases present in the stratosphere through the endothermic reaction, $^{14}N(n,^3H)^{12}C$ (LIBBY., 1946 and CRAIG and LAL., 1961) and by spallation of O_2 (threshold energy 10 MeV, REEDY and ARNOLD., 1972). Production in the troposphere is much lower than that in the stratosphere (LAL and PETERS., 1967).

Tritium once produced, is rapidly incorporated into water molecules and removed from the atmosphere by meteoric precipitation. The residence time of tritiated water in the lower stratosphere is between 1 and 10 years but after it reaches the lower troposphere it is rained out in 5 to 20 days (GAT., 1980). Anthropogenic ^3H has mainly been added to the stratosphere by nuclear weapon tests. Nuclear reactors and particle accelerators have also added measurable quantities of ^3H.

1.5.1.2 Determination of ^3H in natural waters. The ^3H content of water is general expressed in "Tritium Units" (T.U.) where 1 T.U. is an abundance of 1 atom ^3H per 10^{18} atoms of hydrogen (equivalent to 7.1 disintegrations of ^3H per minute per liter of water). Tritium may be determined at levels greater than 2 T.U. by direct liquid scintillation counting; at levels lower than this electrolytic preconcentration followed by either liquid scintillation counting or gas-proportional counting of propane (WOLF et al., 1981) is required. This latter method has a detection limit of 0.1 T.U. (97.5% confidence level) for a 1000 minute count.

1.5.1.3 The use of ^3H in hydrological studies. Natural ^3H has been used in hydrological studies to either approximately date young groundwaters or to infer the mixing of old and new groundwaters (DAVIS and BENTLEY., 1982). Its potential use to accurately date young groundwater is impossible because of the wide variation in the ^3H content of rainfall over the past 60 years. However a qualitative estimate of the time of recharge is possible using an I.A.E.A. recommendation (I.A.E.A. 1973) that :-

(1) Water with concentrations of ^3H less than 3 T.U.indicates groundwater ages in excess of 35 years.

(2) Water with concentrations between 3 and 20 T.U. indicates the presence of some bomb pulse ^{3}H and that recharge occurred between 1953 and 1961.
(3) Water with concentrations in excess of 20 T.U. would suggest water originating since 1962.
Note that the short half life of ^{3}H requires modification of the above dates since approximately 1.3 half lives has passed since the above rules were defined.

1.5.1.4 The ^{3}H content of natural waters. The natural ^{3}H content of rainfall in the northern hemisphere prior to weapon testing was generally less than 25 T.U. (GAT., 1980) with a range of 2.0-10 T.U. for middle and low latitude surface waters (VON BUTTLAR and LIBBY, 1955). Rainfall values peaked at more than 4000 T.U. during 1963 following extensive atmospheric weapon tests (WEISS and ROETHER, 1975).

Bomb-produced ^{3}H levels in the southern hemisphere were lower than in those in the northern hemisphere, and the decline after cessation of atmospheric weapon testing has been more gradual due to the predominance of ocean surface which acts as a sink (DAVIS and BENTLEY., 1982 and FAURE., 1986).

Tritium contents of natural subsurface waters are generally expected to be less than meteoric waters due to radioactive decay since recharge (IAEA., 1973). However significant levels of ^{3}H (> 1 TU) have unexpectedly been found in old groundwaters (> 1000 years since recharge) associated with the Stripa and Carnmenellis granites (ANDREWS and KAY., 1982, NORDSTROM et al., 1985). These authors have considered the attribution of this to subsurface insitu production of ^{3}H via the reaction $^{6}Li(n,\alpha)^{3}H$ (this reaction has also been shown to be a major source of ^{3}He in subsurface fluids (MORRISON and PINE., 1955 and MAMYRIN and TOLSTIKHIN., 1984)). However, it was concluded that the levels of ^{3}H must be due either to mixing with recent groundwater or contamination during sampling. Sections 5 and 6 of this thesis re-examine these conclusions using measured neutron fluxes and more detailed geochemical data.

1.5.2 Carbon-14.

1.5.2.1 Atmospheric production. Production of ^{14}C in the atmosphere occurs through the interaction of neutrons produced by cosmic rays with nitrogen and to a lesser degree oxygen via $^{14}N(n,p)^{14}C$ and $^{17}O(n,\alpha)^{14}C$ reactions. Both of these reactions are exotheric and have cross-sections of 1.8 and 0.24 barns respectively for thermal neutrons (KAYE and LABY., 1986). The production rate is dependent on latitude and altitude. Unlike ^{3}H and ^{36}Cl, the production rate of ^{14}C in the troposphere is almost equal to that in the stratosphere (LAL and PETERS., 1967) due to increase of neutron flux with atmospheric depth. Rapid mixing of ^{14}C in the atmosphere evens out latitude effects and makes the specific activity of atmospheric ^{14}C essentially independent of latitude (ANDERSON and LIBBY., (1951). After formation carbon-14 rapidly oxidises to produce $^{14}CO_2$ which either enters the biosphere and/or is exchanged at the ocean surface.

1.5.2.2 Determination of ^{14}C in natural waters. Carbon-14 emits a low energy beta particle (mean energy 50 KeV) and may be measured at environmental levels by a number of techniques. The earliest measurements were made on solid carbon using a Geiger counter (LIBBY., 1955) however this method was inefficient and was superseded by the use of gas counting in low background counters (RALPH., 1971). More recently the development of Accelerator Mass Spectrometery (AMS) has improved the precision and accuracy of ^{14}C measurements especially those made on small samples of carbon.

The ^{14}C content of a sample of C extracted from a groundwater is general expressed as the samples specific activity relative to that of a standard such as NBS oxalic acid (MOOK., 1980).

1.5.2.3 The use of ^{14}C in hydrological studies. Natural ^{14}C has been used in hydrological studies to either date post glacial groundwaters or to infer the mixing of very old and new groundwaters (DAVIS and BENTLEY., 1982). The use of ^{14}C to date groundwaters was first suggested by MUNNICH (1957) and it has since become the most developed dating method. With new detection techniques such as TAMS, ^{14}C dating of

groundwaters in excess of 30,000 years old is theoretically possible ,however, numerous difficulties still exist with its application. The greatest of these is due to isotopic exchange with the large number of C sources present in the subsurface (ie/ carbonate rocks and organic carbon).

Carbon-14 principally enters groundwater during recharge in the soil zone where the partial pressure of soil CO_2 may be up to two orders of magnitude greater than CO_2 present in the atmosphere (NORDSTROM et al., 1985). The absorption of soil CO_2 by the groundwater produces carbonic acid by the reaction:-

$$CO_2(g) + H_2O(l) \rightleftharpoons H_2CO_3(aq) \qquad \text{Eqn 1.18}$$

Dissociation of the carbonic acid then takes place producing H^+ :-

$$H_2CO_3(aq) \rightleftharpoons H^+(aq) + HCO_3^-(aq) \qquad \text{Eqn 1.19}$$

This reaction is followed by a second dissociation to form CO_3^{-2} and more H^+:-

$$HCO_3^-(aq) \rightleftharpoons H^+(aq) + CO_3^{2-}(aq) \qquad \text{Eqn 1.20}$$

However this dissociation occurs to a much smaller degree than that in equation 1.19. The H^+ liberated by these reactions is free to react with soil constituents and minerals present in the matrix with which the groundwater is in contact. Of the common minerals carbonates such as aragonite are most easily attacked under these weakly acidic conditions to form bicarbonate ions (FYFE et al., 1978):-

$$CaCO_3(s) + H^+ \rightleftharpoons Ca^{2+}(aq) + HCO_3^-(aq) \qquad \text{Eqn 1.21}$$

Equations 1.19 to 1.21 may be summarised with respect to carbonate dissolution by soil CO_2 :-

$$CaCO_3(s) + CO_2(g) + H_2O(l) \rightleftharpoons Ca^{2+} + 2HCO_3^-(aq) \qquad \text{Eqn 1.22}$$

In this reaction only half of the carbon present as bicarbonate comes from soil CO_2. Carbon contained in rock matrices is generally assumed to have zero ^{14}C content since rocks are old with respect to the half life of ^{14}C. Thus the

concentration of ^{14}C which enters groundwater during its passage through the soil zone is rapidly diluted by a factor of two due to the dissolution of carbonate minerals. In an evolved groundwater further dilution may occur due to equilibrium exchange processes with C present in the rock matrix (EVANS et al., 1984). Thus the use of ^{14}C for dating groundwaters requires a considered approach which may introduce many correction factors, many of which are reviewed in MOOK (1980). Even using these techniques recharge dates may have errors in excess of +/- 100% (DAVIS and BENTLEY., 1982).

1.5.2.4 The ^{14}C content of natural waters. As is the case for many cosmogenic nuclides, the ^{14}C content of the atmosphere has been increased by nuclear weapon testing and other anthropogenic sources such as releases from nuclear power stations. The atmospheric ^{14}C content increased by 100% during the 1960's due to the above effects and is still 30% in excess of pre 1950 levels (OESCHGER., 1982). In contrast, the specific activity of atmospheric carbon has been reduced by the burning of large amounts of fossil fuel since the industrial revolution (SUESS., 1955). Levels of ^{14}C found in natural surface waters reflect such variations in atmospheric effects and show a large variation due to the chemical dilution effects outlined in Section 1.5.2.3.

Levels of ^{14}C around 1 to 10 pmc in old groundwaters have been interpreted as mixing with much younger waters or sample contamination (NORDSTROM et al., 1985). The possibility of such levels being produced by insitu nuclear reactions initiated by neutrons and alpha particles from the U and Th decay series have previously been investigated (ZITO et al., 1980; ANDREWS et al., 1989). Conclusions from these studies showed that although ^{14}C can be produced in the subsurface, it was, unlikely to label groundwater in excess of 1 pmc even under favourable conditions. Section 4 of this thesis evaluates the importance of other sub-surface nuclear reactions, such exotic decay, that could produce ^{14}C.

1.5.3 Chlorine-36

1.5.3.1 Atmospheric production. Chlorine-36 is produced in the atmosphere by cosmic ray induced reactions on Ar and Cl. The greatest production occurs in the stratosphere mainly due to proton induced spallation of ^{40}Ar. Production in the troposphere is lower, the most significant production processes being the $^{36}Ar(n,p)^{36}Cl$ reaction and the $^{35}Cl(n,\gamma)^{36}Cl$ reaction with aerosol chloride (LAL and PETERS., 1967).

From 1953 to 1964 atmospheric nuclear weapons tests at low altitudes produced a substantial excess of ^{36}Cl by neutron irradiation of marine aerosols (SCHAEFFER et al., 1960, ELMORE et al., 1982 and BENTLEY et al., 1982). This excess was high enough to enable the detection of ^{36}Cl by either low background counting using a screen wall counter (DAVIS and SCHAFFER., 1955 and SCHAEFFER et al., 1960) or liquid scintillation counting using $SiCl_4$ (RONZANI and TAMERS., 1966). The effect of this anthropogenic source has since declined due to the residence time of Cl in the atmosphere being <3 years (ELMORE et al., 1982) (natural fallout levels have thus been regained since early seventies).

Stratospheric production is latitude dependent due to the effect of the earths magnetic field on the flux of primary cosmic ray particles, however stratospheric mixing is rapid and the concentration of ^{36}Cl is produced in this region is considered to be uniform (ANDREWS et al., 1986). Tropospheric production again varies with latitude but to a lesser degree as the latitude dependence of the neutron flux at these altitudes is smaller than the stratospheric latitude variation (SIMPSON and FAGGOT., 1953).

Chlorine-36 atoms become attached to atmospheric aerosols in the sub-micron size range which are subsequently removed by precipitation in the lower troposphere. The entry of ^{36}Cl from the stratosphere into the troposphere varies seasonally and occurs via the tropopause. Thus the ^{36}Cl fallout fate is higher in middle latitudes than at the equator or poles. The latitude dependence of the fallout rate has been calculated by LAL and PETERS. (1967) and is shown in Fig 1.12.

These fallout rates have been used extensively as a basis for the calculation of recharge ^{36}Cl concentrations and

$^{36}Cl/Cl$ ratios for paleo-ground waters (FINKEL., 1980, BENTLEY et al., 1982, PHILLIPS et al., 1984, BENTLEY et al., 1986a, BENTLEY et al., 1986b and ANDREWS et al., 1986).

1.5.3.2 Determination of ^{36}Cl in natural waters. High levels of chlorine-36 may be determined by a number of different methods. During the early 1960`s when atmospheric nuclear weapon testing was taking place it was possible to detect ^{36}Cl by liquid scintillation, and screen wall counting. However as levels in meteoric waters returned to normal it became apparent that these techniques did not have the required sensitivity to determine $^{36}Cl/Cl$ ratios of less than 10^{-12} without considerable difficulty (RONZANI and TAMERS., 1966). The development of accelerator mass spectrometric (A.M.S) techniques for nuclide determination at the University of Rochester by D.Elmore and others provided a means for the precise measurement of $^{36}Cl/Cl$ ratios as low as $5x10^{-15}$ in natural waters (ELMORE et al., 1979 and DAVIS and BENTLEY., 1982). Since then a number of other A.M.S systems have been built utilising slightly different acceleration techniques (FINK et al., 1984 and KUBIC et al., 1984). The general principals of A.M.S are reviewed in PURSER et al (1982).

A major consideration with respect to ^{36}Cl determination is that contamination of the sample (Cl^- precipitated from solution as AgCl) by S should be minimised to reduce any signal from the relatively very abundant isobar ^{36}S. The degree to which S contamination affects the accuracy of the determination differs between AMS techniques. For instance the technique of KUBIC et al (1984), is less sensitive to S contamination than that of ELMORE et al (1979) due to its better isobaric resolution. The typical minimum sample size required by these methods is 100 mg of AgCl. This is easily precipitated from groundwater samples. The extraction of Cl from solid rock, however, is hampered by the generally low Cl concentration and the resistance of the matrix to dissolution.

1.5.3.3 The use of ^{36}Cl in hydrological studies. Chlorine-36 has a half-life of approximately 300,000 years making it theoretically possible to date groundwaters in excess of one million years old. This is considerable older than that achievable with other cosmogenic nuclei such as ^{14}C or ^{3}H. and makes ^{36}Cl particularly useful for dating groundwater and

estimating groundwater flow patterns in low permeability rocks.

The use of ^{36}Cl as a dating tool for ground waters was first suggested during the 1950's (DAVIS and SCHAEFFER., 1955 and SCHAEFFER et al., 1960). The lack of a suitably sensitive detection method prevented the investigation of pre-bomb pulse levels (DAVIS and DEWEIST., 1966 and TAMERS et al., 1969) until the developement of AMS techniques (ELMORE et al., 1979) and to a limited extent ultra high sensitivity scintillation counting (ROMAN and AIREY., 1981). Since the developement of AMS techniques ^{36}Cl concentrations have been measured in ice (FINKEL et al., 1980 , ELMORE et al., 1982, NISHIIZUMI et al., 1983), in saline sediments (PHILLIPS et al., 1983), and in groundwaters (ELMORE et al., 1979, FINKEL et al., 1980, BENTLEY et al., 1982, BENTLEY et al., 1983, PHILLIPS et al., 1984, KUBIC et al., 1984, BENTLEY et al., 1986a+b, ANDREWS et al., 1986, PAUL et al., 1986, ANDREWS et al., 1989).

Studies on groundwater systems that have attempted to use ^{36}Cl as dating tool for old groundwaters (DAVIS and BENTLEY., 1982, BENTLEY et al., 1986a+b and ANDREWS et al., 1986) all show different degrees of success. Major uncertainties such as the constancy of recharge conditions and the effect of in-situ production of ^{36}Cl have been cited as possible factors which complicate the use of ^{36}Cl in these studies. Whilst the results were not exact they have enabled gross estimates of the rate and direction of movement for groundwaters older than 30,000 years to be made.

Chlorine-36 has also been used to investigate rock water interaction and to predict the origin of groundwater salinity (ANDREWS et al., 1986 and ANDREWS et al., 1989). Such studies rely upon accurate estimates of the magnitude of in-situ production of ^{36}Cl and show that ^{36}Cl concentrations in groundwaters are considerably affected by the transfer of in-situ produced ^{36}Cl from the rock matrix.

1.5.3.4 The ^{36}Cl content of natural waters. The ^{36}Cl content of the atmosphere and subsequently groundwaters has been increased by nuclear weapons testing and other anthropogenic sources such as releases from nuclear power stations. The ^{36}Cl content of Greenland ice increased by two orders of magnitude during the 1950's due to the low altitude testing of nuclear weapons (ELMORE et al., 1982). Levels of ^{36}Cl found

in modern surface waters reflected such "bomb pulse" variations and have now reached pre 1950 levels of around $5x10^7$ atoms l^{-1} for middle latitudes (BENTLEY et al., 1982).

The successful use of ^{36}Cl dating methods require that the concentration of ^{36}Cl at recharge be known. This may be estimated from atmospheric fallout provided that rainfall and evapo-transpiration during the period when recharge occurred are known (BENTLEY et al., 1982 and ANDREWS et al., 1986). In the case of waters in excess of 20,000 years old, or of waters in areas of widely varying climatic conditions these cannot be known accurately, hence such estimates should be treated with caution.

Concentrations of ^{36}Cl in groundwaters have been shown to be significantly affected by neutron irradiation of rock borne chloride as well as by irradiation of chloride in solution, especially in high radioelement rocks such as granites (ANDREWS et al., 1986). In other rock matrices such as sandstones the in-situ production of ^{36}Cl is generally less important. As in-situ production is very site specific its effects must always be considered.

The production of large amounts of ^{36}Cl by the interaction of cosmic rays at the earths surface act as a further input of ^{36}Cl into recharging groundwater. The importance of this effect is dependent upon the penetration depth of each cosmic ray component and is discussed further in Section 4.

1.5.4 Argon-37 and Argon-39.

Argon has three stable isotopes ^{36}Ar, ^{38}Ar and ^{40}Ar. The presence of the cosmogenic nuclides ^{37}Ar (decay mode ^{37}Ar (electron capture)^{37}Cl; half-life = 35.1 days) and ^{39}Ar (decay mode $^{39}Ar(\beta^-)^{39}K$; half-life = 269 years) in the atmosphere was theoretically suggested by LAL and PETERS. (1967).

1.5.5.1 Atmospheric production. The atmospheric production of both ^{37}Ar and ^{39}Ar principally occur by neutron induced reactions on stable Ar isotopes. LAL and PETERS. (1967) suggest that ^{37}Ar is produced mainly in the stratosphere due to the reaction $^{40}Ar(n,4n)^{37}Ar$ and that tropospheric production is a factor of 2 lower. However measurements by LOOSLI and OESCHGER (1969) show an excess level of ^{37}Ar in tropospheric air and the authors suggest that this may either

be due to ^{37}Ar produced by the reaction of cosmic ray protons with the earths surface and/or by anthropogenic sources such as nuclear weapon testing. The same authors suggest that ^{39}Ar is produced by the reaction $^{40}Ar(n,2n)^{39}Ar$. Incontrast with ^{37}Ar, production of ^{39}Ar occurs mainly in the troposphere (LAL and PETERS., 1967) and does not appear to have been affected by anthropogenic production (LOOSLI., 1983).

Both isotopes are inert gases and undergo no chemical reactions in the atmosphere; thus both exchange with water at the earths surface or undergo thorough atmospheric mixing. The concentration of ^{39}Ar in the atmosphere is probably constant both in terms of time and geographic location due to its long atmospheric residence time which damps out fluctuations in its production rate (FAURE., 1986).

The same is not true for ^{37}Ar whose atmospheric residence time is short due to its small half-life. The concentration of this isotope would thus be expected to closely follow the variation in the cosmic ray derived neutron flux with time and geographical position, or to reflect the proximity of anthropogenic sources.

1.5.4.2 Measurement of ^{37}Ar and ^{39}Ar concentrations.

LAL and PETERS. (1967) predicted, the presence of atmospheric ^{37}Ar and ^{39}Ar and their atmospheric concentrations were measured using ultra-low background proportional counters (LOOSLI and OESCHGER., 1968 and 1969). To achieve an ultra-low background the counters were housed in an underground laboratory coated with specially selected low radioactivity concrete. The methodology employed for sampling Ar from groundwaters requires the degassing of approximately 15,000 l of groundwater which is carried out using an in-line stripper (LOOSLI et al., 1989).

1.5.4.3 Hydrological uses of ^{37}Ar and ^{39}Ar and their concentrations in groundwaters. LAL and PETERS. (1967) pointed out the usefulness of these isotopes for studying natural circulation systems since their half-lives complement those of other cosmogenically produced nuclides (that of $^{37}Ar < {}^{3}H$ whilst that of $^{39}Ar > {}^{3}H < {}^{14}C$). Their use for dating groundwaters was first suggested by OESGHGER et al. (1974) and the method has since been refined by H.H. Loosli and colleagues at the University of Bern.

Argon-39 dates obtained for a number of groundwaters have been compared with ^{14}C dates of the same samples (LOOSLI and OESCHGER., 1980; LOOSLI., 1983). Agreement was poor and unexpectedly large discrepancies were noted. Postulated reasons for these discrepancies were in-situ production of ^{39}Ar or inaccurate ^{14}C dates due to factors discussed in section 1.5.2. Whilst ^{37}Ar has only recently been detected in groundwater (LOOSLI et al., 1989) its has too short a half life to be used for dating groundwater in low permeability rocks. Measurement in such groundwaters should enable spatial variations of the in-situ neutron flux to be studied, since all atmospheric input will have decayed and only the in-situ produced component will be measured.

Typical atmospheric levels of these two isotopes are 2.03×10^{-3} Bq L^{-1} Ar (OESCHGER., 1982) and 3×10^{-3} Bq L^{-1} Ar (ANDREWS et al., 1989 and LOOSLI et al., 1989). In a recharging groundwater saturated with atmospheric Ar at 10°C these would correspond to concentrations of 4×10^{-3} and 6×10^{-3} atoms L^{-1} respectively. The importance of in-situ production of both these isotopes is demonstrated by the fact that many times this atmospheric input has been found in groundwaters which are old enough to be uncontaminated by bomb pulse production (LOOSLI., 1983, and LOOSLI et al., 1989).

The relative importance of nuclear reactions which may produce these argon isotopes are discussed in Section 4 and their levels in groundwaters at the Stripa site are reviewed in Section 5.

Table 1.1 Properties of particles that constitute the secondary component of cosmic rays.

particle	charge	mass (MeV)	principal decay mode	mean life (s)
π^+	+1	140	$\pi^+ \longrightarrow \mu^+ + \nu$	2.6×10^{-8}
π^-	-1	140	$\pi^- \longrightarrow \mu^- + \bar{\nu}$	2.6×10^{-8}
π^0	0	135	$\pi^0 \longrightarrow \bar{\nu} + \nu$	0.8×10^{-16}
μ^+	+1	105.6	$\mu^+ \longrightarrow e^+ + \bar{\nu} + \nu$	2.2×10^{-6}
μ^-	-1	105.6	$\mu^- \longrightarrow e^- + \bar{\nu} + \nu$	2.2×10^{-6}
e^-	-1	0.511	stable	stable
e^+	+1	0.511	stable	stable
γ	0	0.0	stable	stable
p	+1	938.3	stable	stable
n	0	939.6	stable in nuclei	stable
nuclei	-	-----	stable/radioactive	------

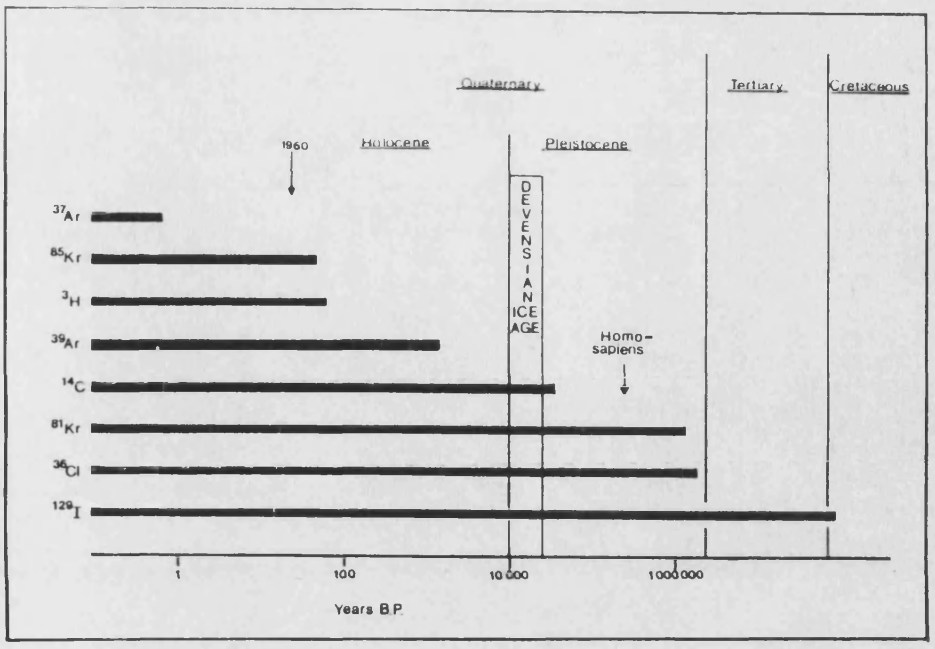

Fig 1.1 Diagram showing the useful "ideal" dating ranges for a selection of cosmogenic isotopes used in hydrogeological studies. The maximum datable age is defined in this diagram as 5 half lives (97% decay) of the particular isotope.

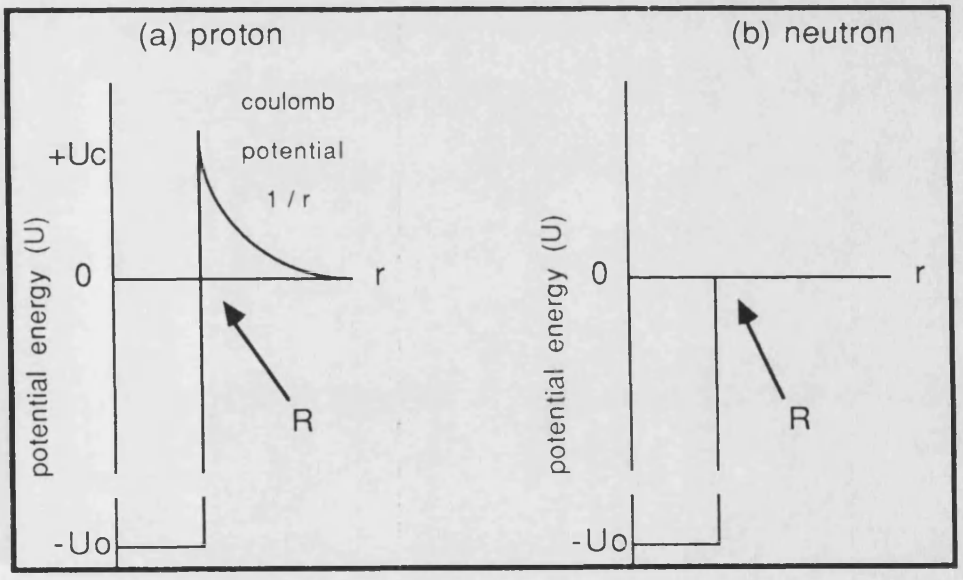

U_0 typically -30 to -40 MeV.
U_C typically 10 MeV for Z = 50 at R
R = nuclear radius approximately 10^{-13} cm.

Fig 1.2 Potential energy diagram for (a) a proton and (b) a neutron at a distance r from the atomic nucleus.

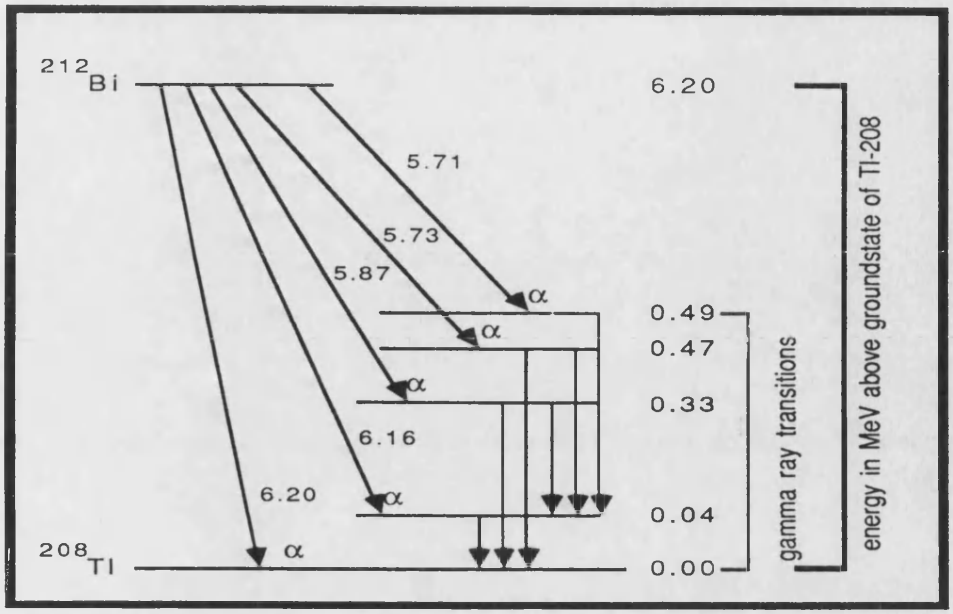

Fig 1.3 Energy level diagram for alpha and gamma ray transitions between ^{212}Bi and ^{208}Tl. Energies in are in MeV.

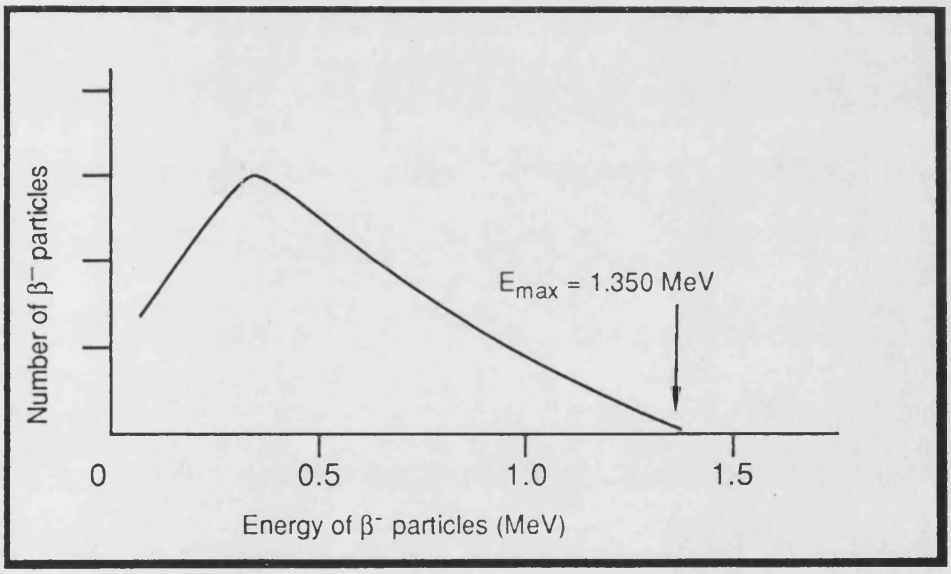

Fig 1.4 Energy spectrum of Beta particle emitted during the decay of ^{40}K.

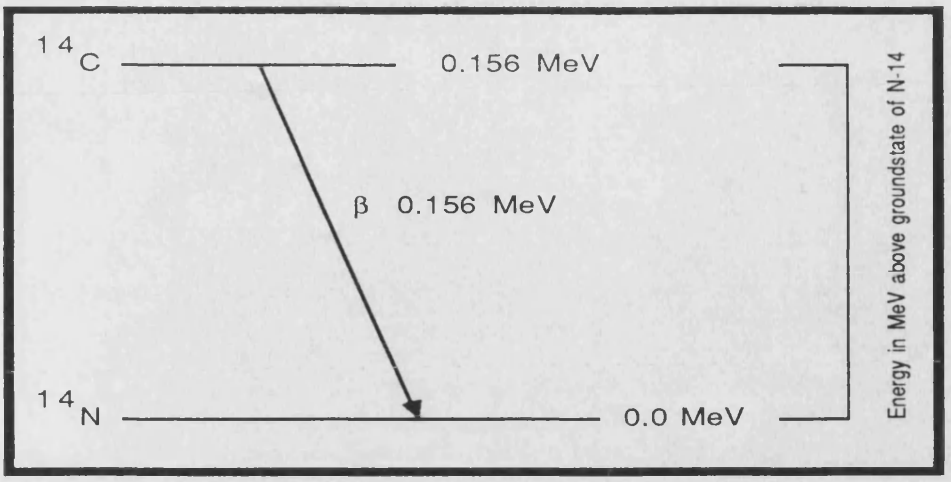

Fig 1.5 Energy level diagram for the beta decay of ^{14}C into ^{14}N.

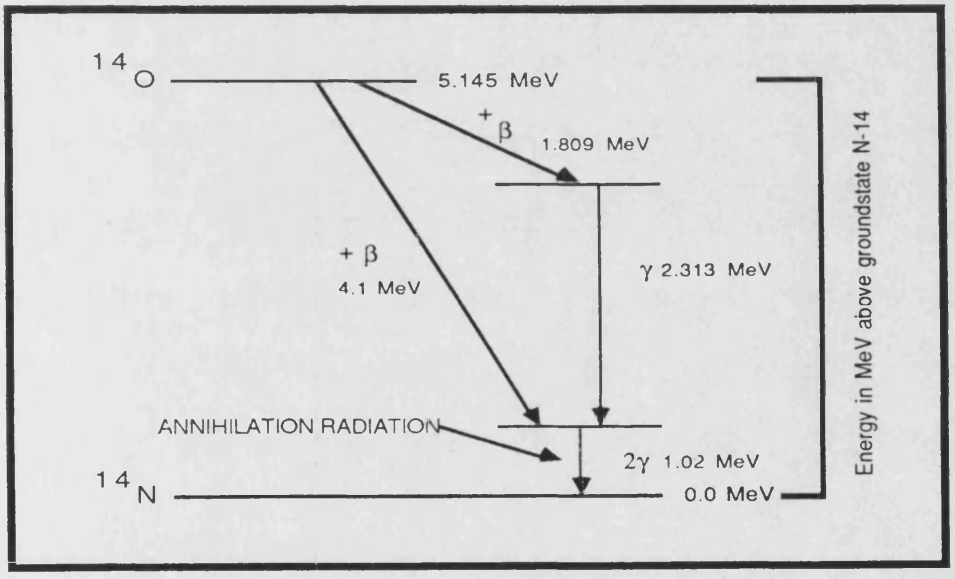

Fig 1.6 Energy level diagram for the decay of ^{14}O into ^{14}N by positron emission.

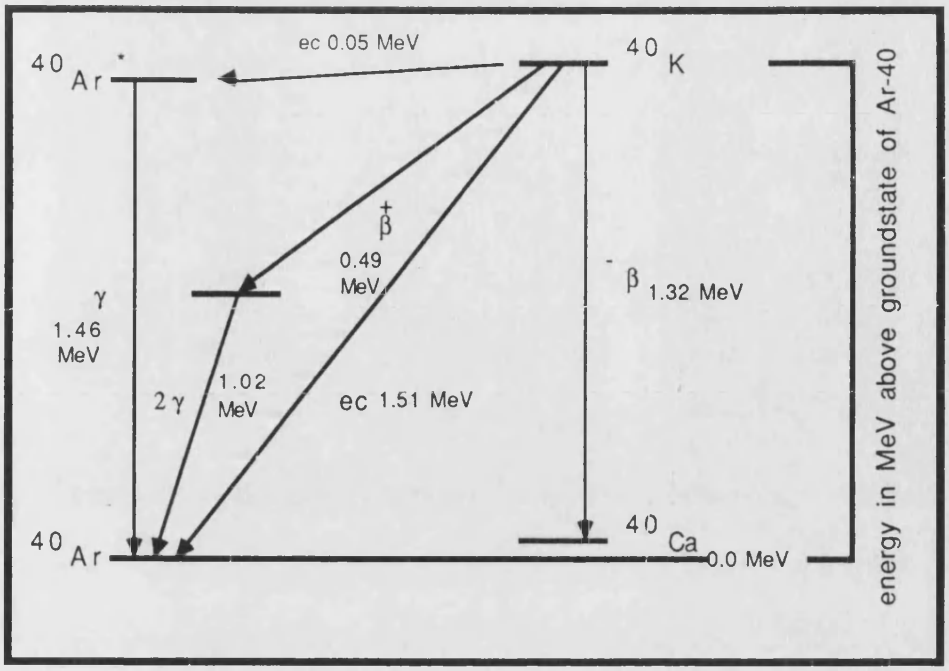

Fig 1.7 Energy level diagram for the decay of ^{40}K into ^{40}Ar by electron capture (ec), beta and gamma emission.

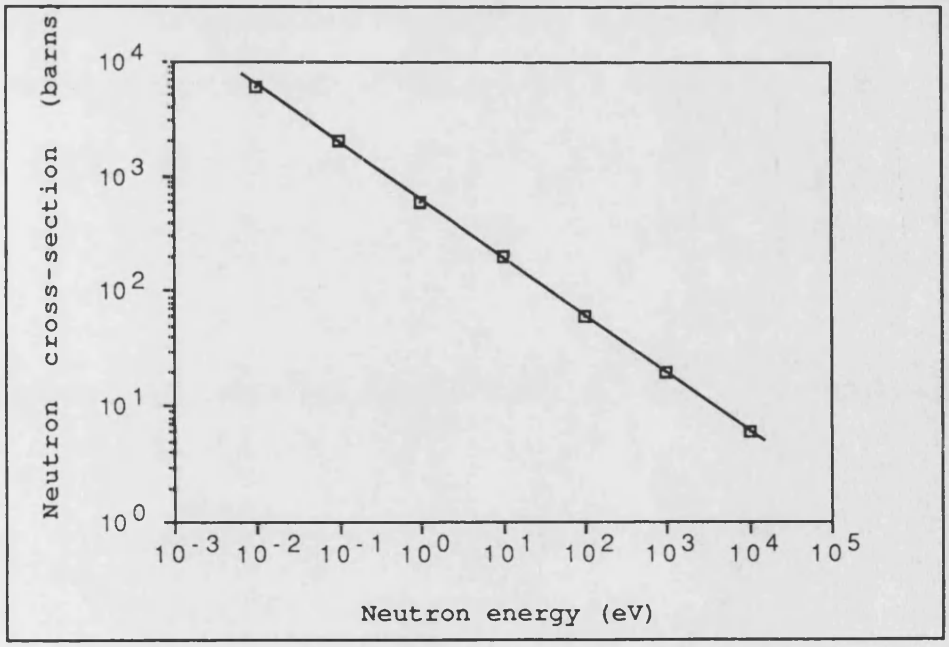

Fig 1.8 The variation in cross-section with neutron energy for the reaction $^{10}B(n,\alpha)^{3}H$ (KAYE and LABY., 1985).

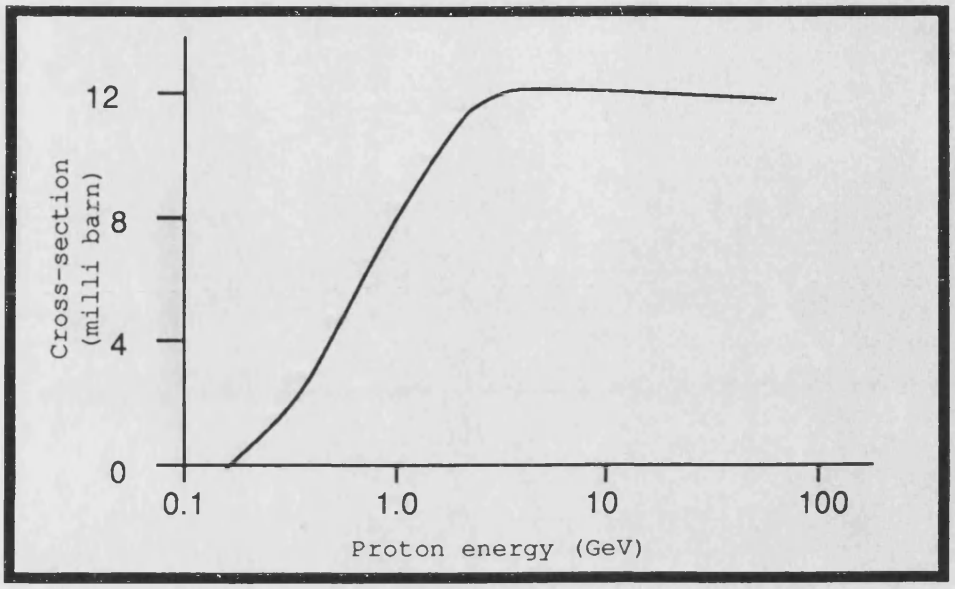

Fig 1.9 The variation in cross-section with proton energy for the spallation of Fe to form ^{36}Cl (REGNIER et al., 1977).

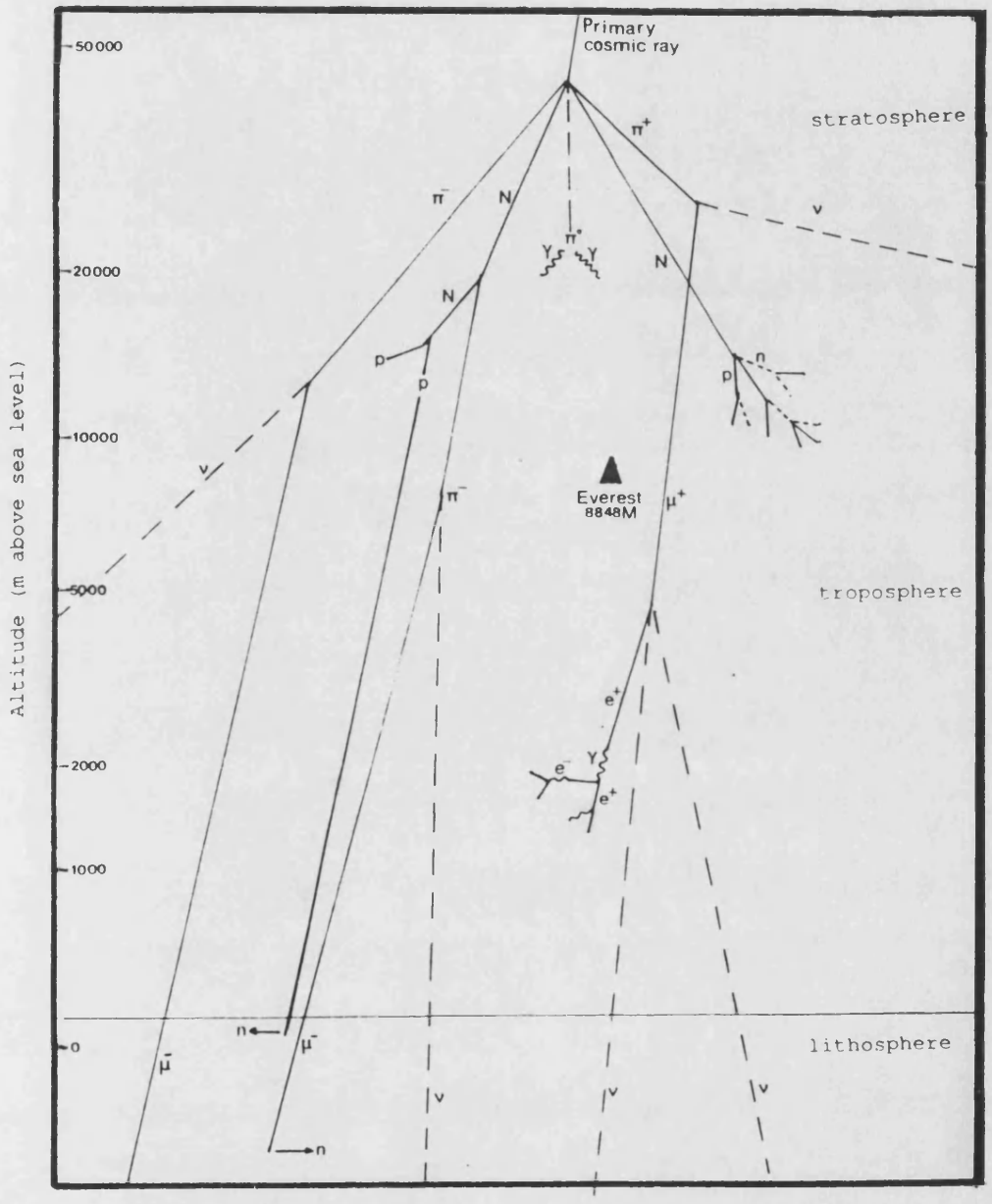

Fig 1.10 Diagramatic representation of the propagation of secondary cosmic ray particles from a single primary particle.

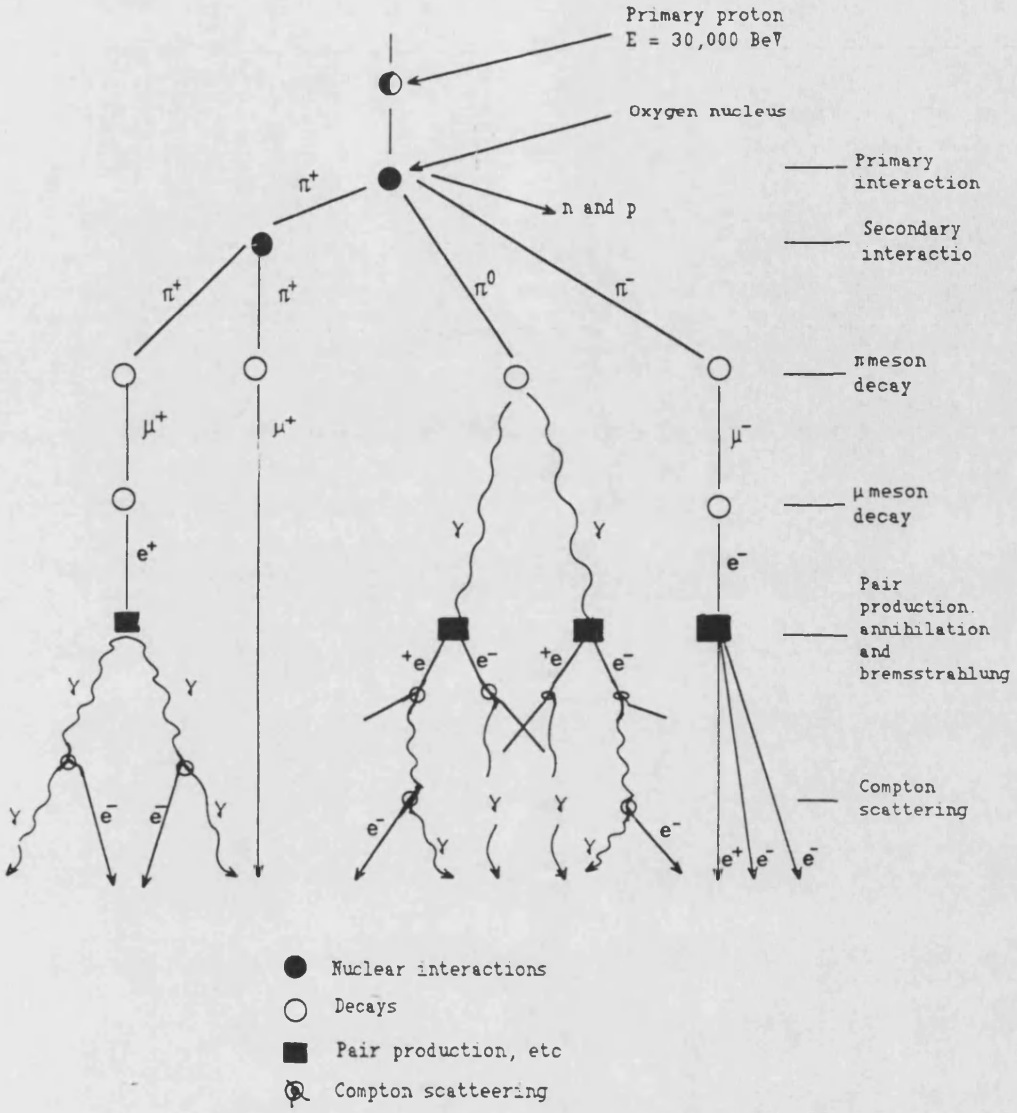

Fig 1.11 Cosmic ray secondary decay reactions.

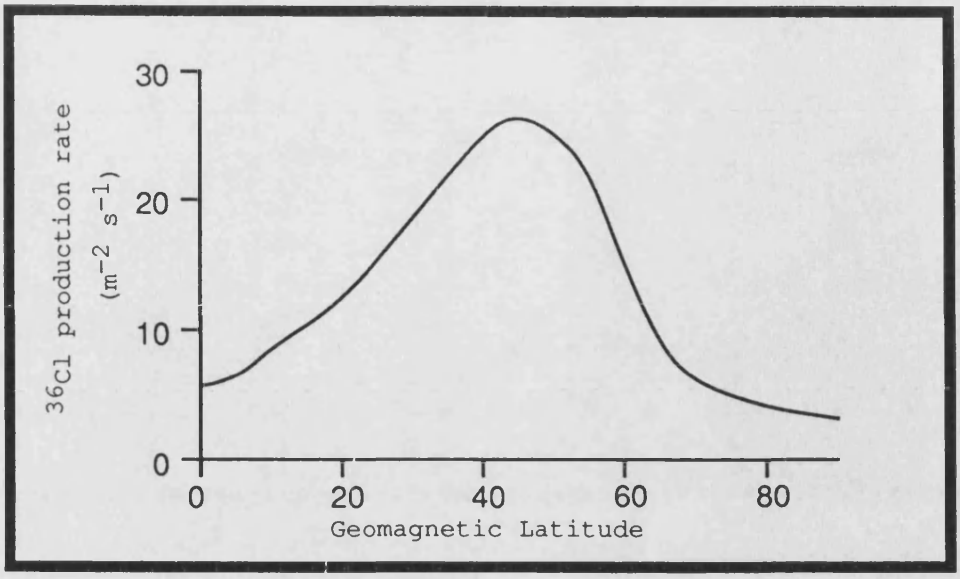

Fig 1.12 The variation of ^{36}Cl fallout rate (atoms m^{-2} s^{-1}) with geomagnetic latitude (LAL and PETERS., 1967).

2.0 THE GENERATION OF NEUTRONS IN THE SUBSURFACE.

This section describes how neutrons may be produced in the subsurface and introduces methods by which neutron production rates may be estimated. Sub-Sections 2.1 to 2.4 examine neutron production by (α,n) reactions, fission of heavy nuclei, reactions of protons and pions from cosmic rays and reactions with negative muons. In each of these sub-sections production has been investigated in six "average" rock types which were selected to represent the bulk of the Earth's crust. The chemical and physical properties of these rocks were taken from PARKER (1967) and are summarised in Appendix 1. Sub-section 2.5 compares the relative importance and magnitude of each of these production reactions. Calculations of the total neutron production rates based on theories developed in Section 2 have been combined into a computer program ("ISOTOPE PRODUCTION") to enable the calculation of neutron production rates in any given rock matrix. A listing of this program is given in Appendix 5.

2.1 Neutron production due to (α,n) reactions.

The number of neutrons produced per α particle by an (α,n) reaction in a given medium depends on the energy dependant (α,n) cross section, and on the rate of energy loss of the α particle. Two important parameters which determine the (α,n) cross section are the reaction energy (Q) and the height of the coulombic barrier (B) (MORRISON and PINE (1955), FEIGE et al (1968)). For an (α,n) reaction :-

$$X(\alpha,n)Y$$

where X, Y, α and n are the reacting isotope, product isotope, α particle and neutron respectively, the value of Q and B may be calculated from equations 2.1 and 2.2

$$Q = (M_X + M_\alpha - M_Y + M_n)\ c^2 \text{ MeV} \qquad \text{Eqn. 2.1}$$

$$B = \frac{2\ e^2\ Z}{R} = \frac{2.88\ Z}{R} \text{ MeV} \qquad \text{Eqn. 2.2}$$

where R is approximately $(1.4A^{0.33} + 1.2)$, A and Z are the atomic weight and atomic number of the reacting isotope and M_X, M_Y, M_α and M_n are the atomic masses of the reacting nuclei and particles. The threshold energy E_{th} (obtained from Q via equation 2.3) is the minimum kinetic energy which the α particle must have for the reaction to be energetically possible.

$$E_{th} = -[(M_x+M_\alpha)\ /\ M_X]\ Q \text{ MeV} \qquad \text{Eqn. 2.3}$$

For exothermic reactions (Q+) $E_{th} =< 0$. The highest energy α particle emitted by naturally occuring radionuclides is 8.78 MeV (from ^{212}Po). Thus (α,n) reactions with $E_{th} > 8.78$ MeV cannot be initiated by naturally occuring radionuclides. Most α particles will be slowed down by interaction with the electrons of the surrounding matrix as well as having to penetrate the potential barrier surrounding the nucleus. This decreases the likelihood of any interaction even with nuclei for which the (α,n) reaction is energetically favourable. Thus the contribution to the total neutron production rate from isotopes for which B>8 MeV (for Z>16) will be small. Table 2.1 lists values of Q, E_{th} and B for (α,n) reactions with light to medium nuclei.

Table 2.1 shows that only Li, Be, B, C, N, O, F, Ne, Na, Mg, Al, Si, and P are capable of producing a significant number neutrons by reaction with natural series α particles. The major isotopes of C, O, Si and elements heavier than Ca do not contribute significantly to neutron production due to the size of their Coulombic barriers (and consequently high threshold energies). Of the light elements only C, O, Na, Mg, Al, and Si are in abundances of greater than one percent in

many rock matrices. These elements account for the majority of produced neutrons. FEIGE et al (1968) and GORSHKOV et al (1962) have measured neutron yields for the relatively heavy elements Ti and Fe. The contribution to the total neutron production rate by these elements is small as these reactions are initiated by high energy α particles (>6 Mev) which are rare in nature. Heavy elements ,however, do contribute to the overall α particle stopping power of the compound.

Reactions of major rock forming elements which contribute to the neutron production are :-

$^{13}C(\alpha,n)^{16}O$	$^{17}O(\alpha,n)^{20}Ne$
$^{18}O(\alpha,n)^{21}Ne$	$^{23}Na(\alpha,n)^{26}AL$
$^{24}Mg(\alpha,N)^{27}Si$	$^{25}Mg(\alpha,n)^{28}Si$
$^{26}Mg(\alpha,n)^{29}Si$	$^{27}Al(\alpha,n)^{30}P$
$^{29}Si(\alpha,n)^{32}Si$	$^{30}Si(\alpha,n)^{33}S$

2.1.1 Experimental measurement of (α,n) yields.

Early measurements of thick target neutron yields were made using a natural series radionuclide as the source of monoenergetic α-particles and simple gas filled moderated proportional counter as a detector. (ROBERTS., 1947 and GORSHKOV., 1962). The major problem with this type of apparatus was that the energy of the α particles although monoenergetic could not be varied, hence the variation of neutron yield with α-particle energy could not be studied. Another problem was that the intensities of these α-sources were low and errors in the detection of the low neutron fluxes produced were high. FEIGE et al (1968) were the first to use a linear accelerator as the source of α-particles. This enabled the energy of the α-particles to be varied and an energy/yield profile to be measured. Their method also had the advantage of exposing the target to much greater intensities of α-particles and this increased the accuracy and reduced the time required for each measurement.

The measurement and in some cases calculation of neutron yields from cross-section data has been continued throughout the seventies. Major improvements have been in the use of

spherical graphite or polyethylene moderators and ^3He detectors which have a well known efficiency (WEST and SHERWOOD., 1982).

For further details reference should may be made to :- ROBERTS (1947), GORSHKOV (1962), FEIGE et al (1968), LISKIEN and PAULSEN (1977), BAIR and GOMEZ del CAMPO (1979), WEST and SHERWOOD (1982) and NAKASIMA (1982).

2.1.2 Mono-energetic (α,n) yields for single elements.

Experimentally derived (α,n) yields quoted by a number of authors for 5.3 Mev α particles are shown in Table 2.2. It may be seen that the results of FEIGE et al (1968), GORSHKOV et al (1962) and ROBERTS (1947) are in reasonable agreement. The results obtained by WEST and SHERWOOD (1982) and BAIR and GOMEZ del CAMPO et al (1979) are in good agreement with each other but are about 30 % lower than those of the earlier authors. This difference is because the yields reported by earlier authors were calculated relative to the yield for Al which was set to 1 at 5.3 Mev. Absolute yields were then calculated based on an absolute yield for Al at 5.3 Mev of 75 neutrons per 10^8 α-particles. WEST and SHERWOOD (1982) and BAIR and GOMEZ del CAMPO(1979) quote their absolute yields for Al at these energies to be 51 +/- 1.0 neutrons per 10^8 α-particles. This value is in agreement with those of LISKIEN and PAULSEN (1977) who reported 52 neutrons per 10^8 α-particles and NAKASIMA (1982) who reported 53 neutrons per 10^8 α-particles. Since the more recent data are based on better experimentation (see Section 2.1.1) I have assumed that that the absolute neutron yield for Al at 5.3 MeV is 51 neutrons per 10^8 α particles, and the data of FEIGE et al (1968), GORSHKOV et al (1962) and ROBERTS (1947) have been corrected accordingly.

2.1.3 Monoenergetic (α,n) yields for multi element matrices.

According to FEIGE et al (1968) and WEST (1979) the (α,n) yield for a mono isotopic element (Yi) may be expressed as :-

$$Y_i = \int_0^R n_i \sigma_i \, dx = \int_0^{E_\alpha} \frac{n_i \, \sigma_i(E)}{-dE/dx} \, dE \qquad \text{Eqn. 2.4}$$

Where -dE/dx is the linear stopping power of the element or isotope i. Converting to mass stopping powers.

$$Y_i = \int_0^{E_\alpha} \frac{n_i \, \sigma_i(E)}{\rho_i \, S_i} \, dE = \int_o^{E_\alpha} \frac{n_i \, \sigma_i(E) \, N_o}{n_i \, A_i \, S_i} \, dE \qquad \text{Eqn. 2.5}$$

or on simplification :-

$$Y_i = \frac{N_0}{A_i} \int_0^{E_\alpha} \frac{\sigma_i(E)}{S_i} \, dE \qquad \text{Eqn. 2.6}$$

Where :-

R = the range for an α-particle in an element or isotope i

n_i = number of atoms per cm^3 of element or isotope i

A_i = atomic weight of element or isotope i

S_i = mass stopping power of element or isotope i, MeV g^{-1} cm^2

$\sigma_i(E)$ = the (α,n) cross section for element or isotope i at an energy E

ρ_i = density of i = $n_i A_i / N_0$

N_0 = Avogadro's number

Thus the neutron production function requires integration over the energy range E_α to E_0 due to the continuous energy loss of the α-particle in the material. Provided that a large proportion of incident α-particles stop in a mono-isotopic

target, Y_i may be evaluated from the measured thick target (α,n) yield for that isotope. The neutron yield Y_{ci} due to an isotope, i, in a chemical compound,c, may be defined, in terms of the linear stopping power of the compound S_{lc} and the linear stopping power of the element i (S_{li}) as :-

$$Y_{ci} = \int_0^{E_\alpha} \frac{n_i \ \sigma_i(E)}{S_{lc}} \ dE = \int_0^{E_\alpha} \frac{S_{li}}{S_{lc}} \ \frac{n_i \ \sigma_i(E)}{S_{li}} \ dE \qquad \text{Eqn.2.7}$$

FEIGE et al (1968) and WEST (1979) have shown that the ratio of the stopping powers S_{li}/S_{lc} is effectivly independent of energy and may be removed from the integral of equation 2.7. (WEST (1979) showed that this ratio does not alter by more than 4% for the elements from Be to Ca and between 4 and 8 MeV)

$$Y_{ci} = \frac{S_{li}}{S_{lc}} \ Y_i \qquad \text{Eqn. 2.8}$$

The (α,n) yield of the compound, Y_c is thus the sum of its elemental or isotopic yields weighted by the ratio of the linear stopping powers.

$$Y_c \qquad \sum_i \frac{S_{li} \ Y_i}{S_{lc}} \qquad \text{Eqn. 2.9}$$

which is equivalent to :-

$$Y_c \ S_{lc} = \sum_i S_{li} \ Y_i \qquad \text{Eqn.2.9b}$$

Converting into mass stopping powers (multiplication of S_{1i} by the density of the element or isotope (n_iA_i/N_0) and S_{1c} by the density of the compound ($\Sigma\rho\ n_iA_i/N_0$)) yields:-

$$Y_c = \frac{\sum_i n_i\ A_i\ S_i\ Y_i}{\sum_i n_i\ A_i\ S_c} \qquad \text{Eqa. 2.10}$$

using the Bragg law of additive stopping powers which states:-

$$S_c = \frac{\sum_i S_i\ n_i \frac{A_i}{\rho_i}}{\sum_i n_i\ A_i} \qquad \text{Eqa. 2.11}$$

equation 2.10 following simplification becomes :-

$$Y_c = \frac{\sum_i S_i\ n_i\ A_i\ y_i}{\sum_i S_c\ n_i\ A_i} \qquad \text{Eqa. 2.12}$$

Where $n_i\ A_i$ is equivalent to the fractional weight abundance (W_i) of an element i or isotope the compound.

$$Y_c = \frac{\sum_i W_i\ S_i\ Y_i}{\sum_i W_i\ S_i} \qquad \text{Eqa. 2.13}$$

Thus the (α,n) yield for a compound is the sum of the (α,n) yields of its components weighted by relative mass stopping powers. Equation 2.13 may be used to calculate elemental yields for elements from experimentally determined values of the total yields for compounds (Y_c). An example of such a calculation is outlined below:-

For a compound C containing two elements A and B, where the neutron yield of the compound (Y_C) and element A (Y_A) are known.

$$S_c = W_A S_A + W_B F_B \qquad \text{Eqn. 2.14}$$

$$Y_B = \frac{Y_C S_C - W_A S_A Y_A}{W_B S_B} \qquad \text{Eqn. 2.15}$$

For Al_2O_3, where element A=Al and element B=O, S_A = 493, S_B = 609, W_A = 0.53, W_B = 0.47, Y_A = 435, Y_C = 221.

$$Y_B = [(221 \times 548) - (261 \times 435)]$$

$$Y_B = 26.5$$

2.1.4 Yields from U and Th series decay.

To calculate the (α,n) yields for the decay of U and Th and their daughter products present in either a compound or rock matrix it must be assumed that all of the elements present are distributed homogeneously. As will be discussed later this is often not the case but this assumption is necessary to enable an estimate of the neutron production rate to be made from experimentally measured neutron yields. It must also be assumed that each of the natural series is in secular equilibrium. This is the case for rock matrices in which U and Th have been trapped for more than 10^6 years.

To calculate the total (α,n) yields due to U and Th series isotopes it is necessary to weight the mono-energetic (α,n) yield according to the abundance and energy of a particular α particle. The (α,n) yield for each α-particle energy in the ^{232}Th, ^{238}U and ^{235}U decay series must be interpolated from the (α,n) yields for discrete energy intervals given by the above authors. This may either be carried out graphically (see Fig 2.1) or by using a computer derived cubic spline interpolation. These yields must then be multiplied by the fractional abundance of each α-particle for nuclides which have a number of α-energies and then summed over each decay series. This gives the total number of

neutrons produced per series for 10^8 α-particles. On division by the of number α-emitting nuclides the weighted average number of neutrons emitted per 10^8 α-particles for each series in equilibrium is obtained. In the case of natural U a further weighting process is required to correct for the different abundances and decay rates of the ^{238}U and ^{235}U series. This weighting may be carried out by assuming that both the ^{238}U and ^{235}U series are in equilibrium and applying equation 2.16.

$$^{NAT}U = (\lambda_{238}\ n_{238}\ \alpha_{238}\ Y_{238}) + (\lambda_{235}\ n_{235}\ \alpha_{235}\ Y_{235}) \qquad \text{Eqn.2.16}$$

Where ^{NAT}U is the neutron yield per 10^8 α particles from natural U, λ_{238} and λ_{235} are the decay constants for ^{238}U and ^{235}U, n_{238} and n_{235} are the number of atoms of ^{238}U and ^{235}U per g of natural U, α_{238} and α_{235} are the number of α particles per decay series and Y_{238} and Y_{235} are the average neutron yields per 10^8 α particles for the ^{238}U and ^{235}U decay series. This simplifies to :-

$$^{NAT}U = (0.961\ Y_{235}) + (0.039\ Y_{235}) \qquad \text{Eqn. 2.17}$$

Values of the (α,n) yield derived from the data of FEIGE et al (1968) are given in Table 2.3a. Yields derived from the data of other authors are given in Tables 2.3b and 2.3c. These Tables are summarised in Table 2.4 which shows a variation in the neutron yield between authors of about 8% (1σ) for Al and Mg. Extrapolation of this variation to other elements where less data are available for comparison would indicate that the (α,n) yields are accurate to better than +/- 10%. The data in Table 2.4 together with that of Table 2.6 may be used with equation 2.13 to calculate the neutron yields for individual elements where measurements have only been made on compounds (namely Na_2CO_3, K_2CO_3, TiO_2 and $CaCO_3$). These results are given in Table 2.5. The absolute neutron yields in Table 2.5 may be converted into a more useful form by calculating the neutron yield that would result from 1 μg of either natural U

or Th present in 1 g of another element. This requires that the data to be multiplied by 10^8 and then divided by the number of α particles emitted per micro gram per annum of natural U or Th. (3.09×10^6 and 1.24×10^5 for natural U and Th respectively). The results of this are given in Table 2.7 and are 5-10 % lower than those quoted in Table 9 of FEIGE et al (1968). This would make neutron production rates calculated according to the yields of FEIGE et al (1968) marginally too high.

2.1.5. Alpha particle induced neutron yields in rock matrices.

The neutron yield for a rock matrix per ppm of Th or U at equilibrium with their daughters may be calculated by use of equation 2.13 where Y_i refers to the yields quoted in Table 2.7 and W_i is the weight fractional abundance of an element i in the matrix. The total yield g^{-1} of rock per annum from (α,n) reactions (P_α) may then be calculated from:-

$$P_\alpha = [U]\ Y_U + [Th]\ Y_{th} \qquad \text{Eqn. 2.18}$$

Where [U] and [Th] are the U and Th concentrations (ppm) in the rock matrix and Y_U and Y_{Th} are the yields per ppm U and Th calculated from equation 2.13. This equation holds only where the U, Th and major (α,n) producing elements such as Na, Al and Mg are distributed evenly throughout the rock matrix. Since the range of α particles in rock matrices is small (from 0.001 to 0.005 cm (FAURE, 1986)) this is more likely for micro-granular matrices such as basalts than, for instance, granites. The degree to which the neutron production rate is affected by micro-distribution within the rock matrix may be estimated by comparing calculated and measured production rates. This is, however, open to error since differences may be due to other factors. A better way to estimate this effect would be by comparing calculated and measured production rates within specific minerals. Unfortunately present analytical techniques have not achieved suitable sensitivity together with spatial resolution to enable this to be carried out.

If the chemical composition of a matrix is known with respect to the (α,n) producing elements, U and Th, and is assumed to be homogeneous, then the expected (α,n) yield and associated error may be calculated using equations 2.18, 2.13 and error propagation. This is carried out in the computer program "ISOTOPE PRODUCTION" a listing and description of which is given in Appendix 5. The error propagation is based on a standard deviation of 8% for the (α,n) yield for a specific element, a standard deviation of 10% for the mass stopping-power of an element and a 1σ error on the abundance of all elements involved in the (α,n) production process. The (α,n) yields for six average rock types (defined by PARKER., 1967) assuming a standard deviation of 10 % on elemental abundances were calculated using the above program to assess the relative (α,n) yields of some general rock types. The results of this given in Table 2.8. Figures 2.2 to 2.7 show the relative importance of each of the light elements to the total neutron production rate. It may be seen in all cases that the majority of neutrons are produced by (α,n) reactions with elements from O to Si. The major (α,n) producers in silicates are Na, Al and Si. The neutron yield from Ca in carbonates is negligible (since Ca has an (α,n) yield of <0.5 per 10^8 α-particles (FEIGE et al., 1968)). However Ca may contribute significantly to the total stopping power (especially in carbonates) and hence must be included when calculating (α,n) yields. For the average rocks used in Table 2.8 the Th decay chain produces more neutrons than the U decay chain due to the to the low U/Th ratio exhibited by these particular rocks.

2.2 Neutron Production by fission of heavy elements.

Spontaneous fission of the heavy element U was first noted by FLEROV and PETRZHAK (1940), after it had been theoretically predicted by the "liquid drop" model of BOHR and WHEELER (1939). Since Flerov and Petrzhaks discovery of spontaneous fission in U this mode of decay has been observed in more than twenty heavy nuclides including ^{235}U for which it is an alternative mode of decay. The basic calculation of the

number of neutrons produced by this decay mode has remained the same except that more accurate fission half-lives have been used for the spontaneous fission of ^{238}U. The decay of isotopes by spontaneous or neutron induced fission have also been of interest to geochemists studying fission track dating methods (Reviewed in FAURE., 1986) and those studying the production of nuclides by spontaneous fission especially in situations of high U concentration.

2.2.1 Neutron production by spontaneous fission.

Of the isotopes which undergo spontaneous fission (^{238}U, ^{235}U, ^{232}Th, etc) the most important in nature because of its relatively low fission half-life is ^{238}U (PRICE and WALKER., 1963). ^{238}U decays by spontaneous fission and α decay, the latest estimate of its spontaneous fission half-life is 8.5×10^{17} years (De CARVALHO et al., 1982). This is much larger than its α-decay half-life of 4.5×10^{9} years (LEDERER and SHIRLEY., 1978). The number of neutrons produced per year from one micro gram of ^{238}U may be estimated from equation 2.19.

$$Y_{sf} = n_{238} \ \lambda_{sf} \ n_{sf} \qquad \text{Eqn. 2.19}$$

Where Y_{sf} is the number of neutrons produced from spontaneous fission per microgram per annum, n_{238} is the number of atoms of ^{238}U in one micro gram of natural U, λ_{238} is the spontaneous fission decay constant for ^{238}U (a^{-1}) and n_{sf} is the neutron multiplicity for spontaneous fission, 2.2 neutrons per fission (U.E.A.E.C., 1963).

2.2.2 Neutron production by induced fission.

Neutron induced fission of other U isotopes such as ^{235}U may also produce neutrons in areas of high U content. ^{235}U is 128 times more abundant than ^{234}U the next most abundant isotope of U which is capable of neutron induced fission. Thus ^{235}U is the most likley isotope to produce significant numbers of neutrons from induced fission.

The number of neutrons produced by neutron induced fission may be calculated using the equation :-

$$Y_{nf} = n_{235} \ \sigma_{235} \ \phi \ n_{nf} \qquad \text{Eqn. 2.20}$$

where Y_{nf} is the number of neutrons produced per micro gram U per annum from neutron induced fission, n_{235} is the number of atoms of ^{235}U per micro gram of U, σ_{235} is the thermal fission cross section of ^{235}U, ϕ is the thermal neutron flux ($cm^{-2}a-1$), and n_{nf} is the average number of neutrons emitted per induced fission ([2.43] KAYE and LABY.,1986).

2.2.3 Neutron production by fission processes.

The estimation of the relative importance of each of the above reactions in the natural environment (where localised areas of high U concentrations maybe found) is difficult since the neutron production rate due to the (α,n) reaction is extremely sensitive to the presence of other light elements such as B and Na which may be associated with U minerals (ATTREP et al., 1979) and also because the distance between such localised concentrations have an effect on the neutron flux experienced by each other. The following discussion illustrates the difficulties of estimating the importance of fission processes in uranium bearing ores.

Spontaneous fission releases 2.2 neutrons per fission. Prompt fission neutrons are are emmitted at energies of approximately 5 MeV (KAYE and LABY., 1986), whilst energies of neutrons from (α,n) reactions are about 4 MeV GORSHKOV (1962). U ore such as uraninite contains ^{238}U with an abundance of 99.28 atom percent and ^{235}U with an abundance of 0.72 atom percent together with a number of other elements; the fission cross sections for these two isotopes of U in the energy ranges of both fission and (α,n) neutrons are not very different. Hence, if neutrons due to spontaneous fission or (α,n) reactions cause further fissions, these will occur chiefly in ^{238}U with a negligibly small amount of fast fission in ^{235}U. For neutrons produced by this initial, high energy, interaction fission is more probable than the capture but less probable than either elastic or inelastic scattering.

Neutrons that undergo capture cause a corresponding decrease in the population of free neutrons.

Elastic scattering by heavy nuclei such as U has little effect on the neutron energy and, after such a collision, the neutron is free to undergo further interaction. Inelastic scattering at neutron energies above 1 MeV, has a relativly high probability and such an interaction is able to reduce the neutron energy to a value below that of the fission threshold for ^{238}U (0.3 MeV). Consequently neutrons from spontaneous fission and (α,n) reactions are only slightly increased in number by fast fission of ^{238}U.

Neutrons which have been degraded in energy below the thresholds for fission and inelastic scattering may either undergo capture or elastic scattering. Those which are captured are undergo no further interaction. Neutrons which are scattered elastically lose energy in small decrements and after many collisions reduce their energy to that of the "resonance" region. The probability of capture in this energy region (the resonance capture probability) for ^{238}U is much greater than the probability of fission in ^{235}U due to the low abundance of that isotope. Thus in an ore with a high concentration of uranium few neutrons will reach thermal energy and udergo fission reactions with ^{235}U. Alternatively if the ore contains large amounts of light elements such as oxygen and hydrogen resonance capture is less likely and a large proportion of neutrons may initiate fission of ^{235}U.

From this discussion it is evident that the number of neutrons produced from induced fission will depend strongly on the moderation properties and spatial distribution of U and trace elements in a particular rock matrix. For instance a U bearing ore with a high porosity which is also saturated with water will produce more neutrons from induced fission than a similar matrix with a low water content. For most matrices however (which have concentrations of U $<<$1000 ppm) production of neutrons due to neutron induced fission is insignificant and the neutron production rate per gram per annum due to fission processes (P_f) may calculated using equation 2.21.

$$P_f = Y_{sf} \times [U] \quad (n\ g^{-1}\ a^{-1}) \quad \text{Eqn. 2.19}$$

Where [U] is the number of micro grams of U in one gram of the rock matrix and Y_{sf} is 0.473 neutrons μg^{-1} of natural U a^{-1}. The number of neutrons produced by spontaneous fission for six average rock matrices (analysis of PARKER., 1967) are given in Table 2.9. The results simply reflect the uranium content of each rock type. The number of neutrons produced by this process are compared with those produced by (α,n) reactions in Section 2.5

2.3 Neutron production by protons and pions.

Protons and pions are strongly interacting particles produced from the reactions of energetic cosmic rays in the high atmosphere. Protons have unit nuclear mass and unit positive charge whilst pions have a mass 0.14 that of the proton, a charge of +1, 0, or -1 and are responsible for short range internuclear forces. Pions are mainly produced by spallation reactions (otherwise known as star reactions) on oxygen and nitrogen nuclei at heights in excess of 15 km. Protons when are stable to decay processes for at least for 10^{32} years (CLOSE et al., 1987) and are attenuated by undergoing further nuclear reactions in the atmosphere until they reach the air/ground interface. Pions produced with a positive, or negative charge may decay into muons and neutrinos before further interaction with either the atmosphere or air/ground interface. These pions have a mean lifetime of less than 10^{-8} s and this together with their strong affinity for nuclear matter means that few survive to reach the air/ground interface. Neutral pions may also be produced, these have a much shorter lifetime decaying into gamma ray photons which then produce electron-positron pairs in less than 10^{-16} s. Kaons may also be produced in this cascade process. However due to their short lifetime (1×10^{-8} s) they decay in the atmosphere before undergoing a nuclear collision. Protons and pions which reach the Earth's surface are attenuated in the

regolith by reactions which release neutrons among other products. Neutron producing reactions occurring in this zone cause the number of neutrons produced in the atmosphere to be "swamped" by neutrons escaping from the air/ground interface (HENDRICK and EDGE., 1966 and YAMASHITA et al., 1966).

Protons may either produce neutrons as "evaporation" products or through low energy nuclear reactions such as (p,xn). Negative pions, on coming to rest, undergo Coulombic capture, but de-excitation for this reaction is more violent than for negative muon induced capture reactions (see Section 2.4) leading to complete disruption of the capturing nucleus. These energetic reactions are generally termed "star producing" reactions due to the characteristic star shape formed in photographic emulsion detectors. Alternatively positive pions when brought to rest by ionisation are repelled by the like-charge of the nucleus and decay to a positive muon and a neutrino.

At the Earth's surface the principal neutron producing reactions involve nuclear evaporation since the high energy component is dominant. However with increasing depth low energy proton and pion induced reactions dominate (O'BRIEN et al., 1978). The intensity of these particles and consequent neutron production rate are dependent upon the geomagnetic latitude (λ) and height above sea level. For the purpose of this thesis a reference point at sea level with $\lambda = 40°N$ has been selected due to the large amount of data available for this location. Factors that govern the neutron production rate due to these interactions are discussed in the following sections.

2.3.1 Neutron production by proton/pion interaction at various depths.

The calculation of neutron production rates for various depths below the air/ground interface at sea level may be based either on experimental measurement of the production profile of neutrons in the regolith, or on the attenuation of neutron producing particles by regolithic material.

Both the attenuation of neutron producing particles and the production of neutrons have been found to decrease exponentialy with depth into the regolith. The neutron production rate (P_p) at a depth d (meters) is thus :-

$$P_p = P_{ps} \; e^{-a_p (d \rho \times 100)} \qquad \text{Eqn. 2.22}$$

Where P_{ps} is the neutron production rate at the surface ($g^{-1}a^{-1}$), d is the depth below the air ground interface (m), ρ is the matrix density (g cm^{-3}) and a_p is the attenuation factor for the decrease either in the neutron production rate or in the neutron producing component ($cm^2 g^{-1}$) for a particular regolithic material.

COCCONI and COCCONI TONGIORGI (1951) measured an attenuation coefficient of 0.00625 cm^2 g^{-1} for proton and pion induced neutron production in water at a geomagnetic latitude of 54°N whilst YAMASHITA et al (1966) measured an attenuation coefficient for the neutrons produced from cosmic radiation to a depth of 100 g cm^{-2} of 0.0059 cm^2 g^{-1} through concrete at 44°N.

O'BRIEN et al (1978) calculated the depth dependence of the neutron production rate based on a nucleonic cascade model at 40°N. Their results yield an attenuation coefficient of 0.0045 cm^2 g^{-1}. NISHIIZUMI et al (1984) measured attenuation coefficients for proton/pion induced isotopes of 0.0056 to 0.0058 cm^2 g^{-1} in the lunar regolith. These values agree well with the above terrestrial estimates which is surprising considering the different energy and particle distributions of cosmic rays on the moon. The value obtained for water (COCCONI and COCCONI TONGIORGI., 1951) also agrees well with attenuation factors calculated for rock matrices, this is in agreement with theory in that the chemical nature of the regolith has little effect provided the average atomic number is fairly constant. The calculated attenuation factor of O'BRIEN et al (1978) has been taken to represent the lower limit of the attenuation factor in rock matrices, and the measured value of YAMASHITA et al (1966) to represent the

highest. Thus the depth attenuation factor (a_p) for neutron production by protons/pions ranges from 0.0045 to 0.0059 cm^2 g^{-1}. The neutron production rate at the surface (P_{ps}) has again either been calculated or measured by the above authors. As stated previously the production rate at the air/ground interface will depend on geomagnetic latitude, altitude and to a lesser extent on chemical composition.

The results of cascade calculations by O'BRIEN et al (1978) agree with the measured fluxes of YAMASHITA et al (1966) and P_{ps} has been taken to be 1190 neutrons g^{-1} a^{-1} (this represents 1.6 times the neutron production rate of 740 neutrons $g^{-1}a^{-1}$ for $\lambda = 40^{\circ}N$ at sea level over a silicate rock (O'BRIEN et al., 1978)). Calculated neutron production rates for depths below the air ground interface based on these values are given in Table 2.10.

2.3.2 The effect of altitude on neutron production by proton and pion interaction.

Neutron production due to the proton/pion flux varies to a much greater extent with altitude than that from negative muons. By comparing the data of O'BRIEN et al (1978) and ROSSI (1948), the proton/pion intensity increases by 500% for 0-2000 m above sea level whilst the muon intensity increases by only 200% for a similar change in altitude.

The value of P_{ps} at a given altitude may be obtained by multiplying P_{ps} at sea level (740 neutrons g^{-1} a^{-1}) by an altitude correction factor (R_{pa}).

The altitude variation of P_{ps} has been well studied and averaged values of R_{pa} are shown in Table 2.11. These have been based on the results of YOKOYAMA et al (1977), YAMISHITA et al (1966), LAL and PETERS (1967) and SCHOPPER et al (1967) all of which show a exponential decrease in neutron production with atmospheric depth from 5000 m to sea level. The given R_{pa} values are based on an average attenuation factor of 0.0061 +/- 0.0006 cm^2 g^{-1}. This attenuation factor varies by a maximum of 10% with geomagnetic latitude and solar activity (SCHOPPER et al., 1967) which is within the above quoted error and thus may be neglected. The R_{pa} values given in Table 2.11

have been fitted to a third degree polynomial equation :-

$$R_{pa} = 9.456\times10^{-11} A_1^3 + 9.880\times10^{-8} A_1^2 + 8.529\times10^{-4} A_1 + 0.984 \quad \text{Eqn. 2.23}$$

where A_1 is altidude in m above sea level. This has been used to interpolate R_{pl} values (for the altitude interval 0 to 5000 m above sea level) and allow correction factors to be calculated by the computer program "ISOTOPE PRODUCTION" (see Appendix 5).

2.3.3 Effect of latitude on neutron production by proton/pion interactions.

The latitude dependence of the neutron production rate due to proton/pion interaction is due to the Earth's magnetic field preventing the transport of charge particles below a certain threshold energy (the "geomagnetic rigidity"). This effect is less pronounced at low altitude since it primarily affects the low energy component of the primary cosmic radiation, little of which reaches lower altitudes. The geomagnetic latitude effect may again be corrected for by multiplication of P_{ps} by a factor (R_{pl}) based on the variation of neutron production. Quoted R_{pl} values have been based on the data of YOKOYAMA et al (1977) and have been corrected to give $R_{pl} = 1$ at a geomagnetic latitude of $> 60^{\circ}N$. R_{pl} also varies slightly with altitude and with the solar cycle (SCHOPPER et al., 1967 and SIMPSON and FAGGOT., 1953). For instance R_{pl} values for $\lambda=90^{\circ}N$ vary by a factor of 1.5 between a solar minimum and maximum, the variation at 5000 meters is a factor of 1.3 times that at sea level (SCHOPPER et al., 1967). Overall the accuracy to which R_{pl} may be calculated is small due to a combination of the above effects.

Small variations in the geomagnetic cutoff with longitude also affect R_{pl} (BLAND and CIONI., 1968). These are small compared with the overall uncertanties associated with the calculation of R_{pl} may genarally be ignored. If required errors may be minimised by calculating the R_{pl} value for ranges of longitude based on continental areas. Variation in R_{pl} for different continents based on the calculations of YOKOYAMA et

al (1977) are given in Table 2.12 and are shown in Fig 2.8.

The variation of R_{pl} with geomagnetic latitude (λ) is approximately linear from 25 to 55 degrees and may be interpolated over the range 0 to 60° using equations 2.23a and 2.23b for $32.5>\lambda<60$ and $0>\lambda<32.5$ respectivly.

$$-2.52\times10^{-5}\lambda^3 + 3.22\times10^{-3}\lambda^2 - 0.122\lambda + 1.583 \qquad \text{Eqn. 2.23a}$$

$$2.08\times10^{-5}\lambda^3 - 9.23\times10^{-4}\lambda^2 + 0.019\lambda + 0.120 \qquad \text{Eqn. 2.23b}$$

where λ is the geomagnetic latitude. These equations have been included in the computer program "ISOTOPE PRODUCTION" (see Appendix 5). R_{pl} remains approximately constant in the region $\lambda > 60°$ at 1.

2.3.4 The effect of the chemical nature of the regolith on the neutron production by proton/pion interactions.

The dependence of the proton/pion induced neutron production rate on the chemical nature of the regolith may be estimated from the data of O'BRIEN et al (1978). This data gives average neutron multiplicities for stars ($\bar{n}_m$) produced by proton and pion interactions in a number of single and multi-element matrices at depths of 100 g cm^{-2} below the air/ground interface for a geomagnetic latitude of 40°N and a solar minimum. These results show a correlation between weighted mean atomic number ($\bar{Z}$) (weighted according to atomic concentration for a multi-element matrix) and $\bar{n}_m$ see Table 2.13 and Fig 2.9. $\bar{Z}$ varies between 9 and 12 for most common rock matrices ($\bar{Z}$ limestone=10.51, $\bar{Z}$ sandstone=9.89, $\bar{Z}$ granite=10.24 (calculated using the chemical analysis of PARKER (1967))) thus the variation of $\bar{n}_m$ and the the neutron production rate may be estimated. $\bar{n}_m$ varies between 7.3 and 10 neutrons per star for the above defined range in $\bar{Z}$ and, within errors, the variation in production rate due to the chemical nature of the regolith may be said to be negligible provided that the proportion of heavy or light elements is small.

2.3.5 Calculations of neutron production by proton/pion interactions for some rock matrices.

As discussed above (Section 2.3.4) the neutron production rate due to proton and pion interaction with the Earth's regolith (P_p) does not vary to any appreciable extent with the chemical composition of the regolith. It does however vary with depth (d), altitude above sea level (A_l) and geomagnetic latitude (λ). These factors may be corrected for and P_p calculated for any specific material and depth in the regolith provided that the depth below the air ground interface, the altitude and geographical positions of the air ground interface and the density of the regolithic material are known. Corrections for these effects are combined in equation 2.24.

$$P_p = R_{pa}\, R_{pl}\, 1190\, e^{a_p(d\ \rho\ 100)} \qquad \text{Eqn. 2.24}$$

The evaluation of the factors a_p, R_{pa} and R_{pl} have been discussed above in sections 2.3.2, 2.3.3 and 2.3.4 respectively. The computer program "ISOTOPE PRODUCTION" (see Appendix 5) calculates the total neutron production depth profile, taking into account all possible variables. Figs 2.10 and 2.11 show that for common rock types the contribution to neutron production from cosmic proton/pion events becomes negligible below 5 meters. At shallower depths the attenuation of the neutron production by these processes show a half thickness of ca. 0.75 meters. It is also evident (Fig 2.11) that the altitude of the air ground interface can have a significant effect on the neutron production rate at a given depth. A source of uncertainty in these results is the correction factor for latitude since this is strongly dependent on solar conditions. An average correction factor may be used for exposure over a number of solar cycles if there has been no long term change in solar activity. A further source of error is uncertainty over the depth attenuation coefficient (a_p), especially at depths in excess of

1 meter.

The relative importance of this neutron production process compared to (α,n), fission and negative muon capture production is discussed in Section 2.5.

2.4 Neutron production by negative muon capture.

Muons are weakly interacting particles produced from the decay of free pions and K mesons, which are themselves produced from the interaction of high energy cosmic protons with nuclei in the high atmosphere. Muons may be produced with positive or negative charge and these may either decay with a typical lifetime of $< 10^{-6}$ seconds in free space, or interact with the Earth's surface. On passing through the air/ground interface muons lose energy predominantly by pair production and bremsstrahlung however some energy is also lost by nuclear interactions through virtual photons. These processes are discussed in detail by GEORGE (1957) and PAL and BHATTACHARYYA (1985). If the muon has not decayed during this slowing down process further reactions may occur depending on the muonic charge. Positive muons may form "muonium atoms" by capturing electrons from the dense media of the regolith. These positive muons then decay into a positron and two neutrinos with the release of the captured electron. On the other hand negative muons become captured by the coulombic field of atoms present in the regolith. This interaction of negative muons may either to decay or lead to the production of a new isotope and the emission of one or more neutrons.

Negative muons produced from cosmic ray interaction after slowing down may be "stopped" by nuclei deep within the Earth's surface to produce μ-mesic atoms. On "stopping", such muons are captured by the coulombic field of a nucleus and cascade rapidly (in about 10^{-11} s) to the metastable 1S level of the μ-mesic atom. For negative muons this muonic orbital is closer to the nucleus than the innermost electrons and hence there is a large probability of the muon interacting with a proton according to the nuclear capture reaction :-

$$\mu^- + p \rightarrow n + \upsilon$$

The probability of this reaction is dependent upon the separation of muonic energy levels from the nuclear surface and has been shown to be greater for elements of high Z (MARSHAK et al., 1969). In competition with this reaction is the muons decay :-

$$\mu^- \rightarrow e^- + \tilde{\upsilon} + \upsilon$$

For most nuclei the weak interaction process (nuclear capture) predominates and in these cases the fraction of muons captured from the μ-mesic atom almost equals one. If in the capture process the proton is at rest then the neutron recoils with about 5 MeV. However since the proton may be moving at the time of capture, the recoil energy of the neutron will be different from the above value. The emission of neutrons generally predominates due to the coulombic barrier which prevents the escape of charged particles at the above energies. However WYTTENBACH et al (1978) have measured the probability of proton and a particle emmission following negative muon capture. They report probabilities ranging from $1x10^{-2}$ to $1x10^{-4}$ which are small compared with neutron emission probabilities typically in excess of $8x10^{-1}$. These charged particle reactions are discussed further in section 4 of this thesis with respect to production of specific radionuclides. The interaction of a negative muon with matter as described above is summarised in Fig 2.12 This process may produce isotopes by :-

(1) direct muon interaction

$$\mu^- + (Z,A) \rightarrow (Z-1,A)^* \rightarrow (Z-1,A-x) + x\ n$$

(2) secondary neutron interaction

$$(Z,A) + n \rightarrow (Z,A+n)$$

Theoretical calculations of isotope production rates due to muon interactions via process (1) have been described by LAL (1963) and CHARALAMBUS (1971). To estimate the neutron production rate due to negative muon capture it is necessary to sum process (1) over all the constituents of the matrix under study. This neutron production rate may then be used to

estimate the contribution to the total neutron production rate from negative muon capture.

The neutron production rate (P_μ) at a depth d meters below the air ground interface for a given altitude and geomagnetic latitude is given by equation 2.25

$$P_\mu = N_d F f \qquad \text{Eqn. 2.25}$$

Where N_d is the negative muon stopping rate (g^{-1} a^{-1}) at a depth d, F is the fraction of "stopping" muons which reach the 1S muonic level and undergo nuclear capture causing neutron emission and f is the average number of neutrons emitted per muon capture in the rock matrix.

2.4.1 The negative muon stopping rate (N_d).

The negative muon stopping rate is the derivative of the experimental muon intensity/depth curve at a depth d. CHARALAMBUS (1971) and TAKAGI and TANAKA (1968) have derived negative muon stopping rates as a function of depth in this manner for 40°N geomagnetic and sea level. Their results are about ten times greater than earlier estimates by LAL (1962).

These revised stopping rates are confirmed by the experimental data of HAMPEL and KIRSTEN (1975) and stopping rate data is presented in Table 2.14 and plotted against depth in Fig 2.13 The intensity and subsequent stopping rate of muons at a given point must follow the time variation of the galactic component of cosmic radiation. This has been shown to have been constant within 10% for the last 10^7 years (QUENBY., 1967). Small periodic variations exist in muon intensity at the Earth's surface which may effect the production of neutrons and short lived isotopes. These may be due to atmospheric conditions, magnetic storms or solar related events. The overall accuracy to which N_d may be obtained will hence be related to the effect of these phenomenon. CHARALAMBUS (1971) has estimated that the probable error in N_d should not exceed 20% over a long period where the effects of transient events have evened out. Further to these variations the capture rate must also depend

upon the variation of the muon flux with altitude and geomagnetic latitude. Correction factors for these variations are discussed below.

2.4.1.1 Effect of altitude and latitude on the negative muon stopping rate (N_d).

The variation of the negative muon stopping rate with altitude is smaller than that of protons and pions due to their much lower attenuation in air and because they are produced mainly in the upper atmosphere (see Section 2.3.3). Since the range in energy of cosmic ray derived muons is large (from less than 0.01 Gev to greater than 100 Gev with about 30 % having energies greater than 0.3 Gev) and methods of energy discrimination poor, two energy regions have historically been measured. These are < 0.3 Gev (slow muons) and > 0.3 Gev (fast muons) which relate to the muons ability to pass through 167 gcm^{-2} of Pb (ROSSI., 1948). If it is assumed that variation in altitude (over the range 0 to 5000 meters) and geomagnetic latitude produce little change in the negative muon energy spectrum (an artifact of the muon's low reactivity) the negative muon stopping rate at a depth (d meters) will consequently follow any such variations.

To a first approximation this holds true and correction may be made for both latitude and altitude effects using data for slow muons (ROSSI., 1948) and by assuming no variation due to geomagnetic latitude. However a more careful approach shows that both latitude and altitude effect the muons energy distribution in a complex way. SUBRAMANIAN et al (1958) and CONVERSI et al (1950) have shown that the slow muon intensity increases towards the pole and varies by a factor of 3 between 50°N and 40°N and a factor of 1.5 between 40°N and 29°N. The variation in fast muon intensity is much smaller and is quoted by KAYE and LABY (1986) as being less than 1.15 between 90°N and 0°N. Furthermore, the energy ranges of these muons are such that the slow muons (range < one meter in rock matrices) effect neutron production in the uppermost layers of the Earth's crust. However in these surface layers neutron production is mainly due to the stopping of protons and pions

(see Section 2.3), and any difference caused by the different intensities of slow muons due to latitude and altitude effects will be small compared to neutron production from protons and pions. The latitude and altitude variation of fast muons whose range in rocks enable them to penetrate past the zone of surface neutron production, is however much more important in assessing the neutron production profile since fast muons are the predominant source of neutrons in this intermediate region (4-60 meters depending on rock type). In view of the above and general inaccuracies in the measurement of other parameters required to estimate the production rate of neutrons from negative muon capture (N_d, F, and f) only the variation in muon intensity with altitude has been considered. This has been based on the data of ROSSI (1948) (for geomagnetic latitudes greater than 40°N).

The negative muon intensity at a given altitude was obtained by integration of the vertical muon intensity over 2π radians and multiplying the result by the muonic charge ratio. The variation of muon intensity with zenith angle (θ) has been studied by a number of authors and has been found to be of the form:-

$$I_\mu = I_{\mu v} \cos^n \theta \qquad \text{Eqn. 2.26}$$

Where $I_{\mu v}$ is the vertical intensity $g^{-1}a^{-1}str^{-1}$, n is a power factor, θ is the zenith angle in radians and I_μ is the total negative muon intensity, $g^{-1}a^{-1}$. Both n and the muonic charge ratio vary slightly with altitude and have values of 2.16 and 0.44 at sea level (TAKAGI and TANAKA., 1968). From these results (Table 2.15) an altitude correction factor ($R_{\mu a}$) for negative muons was calculated and then fitted to an polynomial equation to allow interpolation between altitude values. The resulting equation is valid for altitudes up to 5000 meters.

$$R_{\mu a} = 6.01\times10^{-12}A_1^3+1.40\times10^{-7}A_1^2+2.8\times10^{-4}A_1+0.977 \qquad \text{Eqn.2.27}$$

Where $R_{\mu a}$ is the altitude correction factor for an air/ground interface at an altitude (A_1) meters. The data of Table 2.14 may be corrected for altitude by multiplication with the appropriate $R_{\mu a}$ value.

2.4.2 The fraction (F) of stopped muons captured by the nucleus.

Stopped muons are captured in a rock matrix to an extent which depends upon the elemental composition of the rock and the probabilities of muon capture by individual nuclei. The fraction of stopped negative muons (F) that are captured by nuclei in the rock matrix and subsequently emit neutrons rather than decaying may be calculated from the equation :-

$$F = \frac{\sum_z M_z \, p_z \, r_z}{\sum_z M_z \, p_z} \qquad \text{Eqn. 2.28}$$

Where M_z is the fractional molar abundance of element z in the rock matrix, p_z is the probability that a stopped negative muon reaches the 1S muonic level of element z relative to that for oxygen and r_z is the probability of nuclear capture from the 1S muonic level of element z. The latter probability does not vary greatly with atomic number over the range Z=8 to Z=20, that is, for the major rock forming elements. The probability data of Table 2.16 have been used together with average rock composition data (PARKER 1967) to calculate the fraction of muons which undergo nuclear capture reactions relative to those that decay or undergo reactions not involving neutron emission. The results for average granite, basalt, sandstone, ultramafics, clays & shales and carbonate rocks are shown in Table 2.17. From this it may be seen that F varies little between rock types especially considering the accuracy with which p_z values are known. It is reasonable to assume for most common rocks matrices that the value of F = 0.41.

2.4.3 The number (f) of neutrons emitted per muon capture.

Neutrons may be emitted directly from the nucleus or from a compound nucleus. Neutrons emitted from either of these processes may be very energetic. KOZCOWSKI et al (1985) have measured neutron energies as high as 50 Mev but such energetic neutrons form only a small fraction of the total neutron yield for a specific element. Direct neutron emission is less common than compound emission (SINGER., 1974) which may produce up to six neutrons per capture. The multiplicity of neutron emission has been studied theoretically using a modified Fermi gas approach, and experimentally using radiochemical methods for the detection of reaction products (McDONALD et al., 1965). There is no direct correlation between this model and experiment (MUKHOPADHYAY., 1977). The results of experiments up to 1973 are reviewed by SINGER. (1974). The average number of neutrons emitted per capture varies slightly with Z and may found by weighting each neutron multiplicity by its probability. To obtain the muon-induced neutron emission, f, for a rock matrix this result should then be further weighted according to the element's atomic abundance in the rock matrix. However difficulties arrive in this approach due to the lack of experimental data for some key elements such as O, Na and K, and breakdown of any empirical relationship for light elements (For instance the relationship of BOBODYANOV (1970) which suggests that :-

$$f = 0.3\ A^{0.33} \qquad \text{Eqn. 2.29}$$

where f is the average neutron multiplicity and A is the atomic weight of an isotope, yields values of f which are 20 to 30 % lower than experimental results for Al and Ca). In view of this the average value of f suggested by CHARALAMBUS (1971) of 1.23 neutrons per capture (which neglects any variation of f with Z) has been used for a rock matrix of "average composition".

2.4.4 Calculation for some rock matrices.

As discussed in section 2.5.1 the neutron production rate (P_μ) at a depth below the Earth's surface may be calculated from the nature of the regolith, the geomagnetic latitude and the altitude of a particular site. Equation 2.25 when corrected to allow for variation in the geomagnetic latitude and altitude of a particular site becomes:-

$$P_\mu = N_d R_{\mu a} R_{\mu l} F f \qquad \text{Eqn. 2.30}$$

Where N_d is the negative muon stopping rate (g^{-1} a^{-1}) at a depth d, $R_{\mu a}$ is the altitude correction factor, $R_{\mu l}$ is the geomagnetic latitude correction factor, F is the fraction of "stopping" muons which reach the 1S muonic level and undergo nuclear capture causing neutron emission and f is the average number of neutrons emitted per muon capture in the rock matrix. Sections 2.4.1 to 2.4.4 show that this equation may be simplified by assuming that $R_{\mu l}$ does not vary significantly with latitude, that F is approximately 0.41 for average rock matrices, and that f=1.23. Equation 2.30 thus becomes:-

$$P_\mu = (N_d R_{\mu a}) \ 0.50 \qquad \text{Eqn. 2.31}$$

Neutron production rates calculated for a sandstone matrix at sea-level are given in Table 2.18 and plotted against depth in Fig 2.13. This depth dependence was fitted to a complex equation to enable the computer program "ISOTOPE PRODUCTION" (see Appendix 5) to interpolate between depth intervals. A best fit was found by taking the natural logarithm of P_μ for a depth (in terms of g cm^{-2}) and fitting the resulting values to a 5 degree polynomial. The resulting program calculates P_μ at any depth interval between 20 and 20000 g cm^{-2} (see Appendix 5). The depth dependence and relative importance of neutron production due to negative muon capture compared to other neutron production processes are discussed in Section 2.5.

2.5 Comparison of neutron production reactions.

The mechanisms by which (α,n) reactions, spontaneous fission, proton/pion reactions and negative muon induced reactions produce neutrons in the Earth's surface are discussed in Sections 2.1, 2.2, 2.3, 2.4 and 2.5. This Section compares and summarises the relative contribution of each of these reactions to the total neutron production rate. The total neutron production rate (P_{tot}) for a given site may be calculated from a combination of equations 2.18, 2.21, 2.24 and 2.30 which yields:-

$$P_{tot} = P_{\alpha}+P_f + P_p + P_{\mu} \qquad \text{Eqn. 2.32}$$

Where P_{α}, P_f, P_p and P_{μ} are the neutron production rates ($g^{-1}a^{-1}$) for (α,n), spontaneous fission, proton/pion and negative muon reactions respectively. P_{α} and P_f vary with chemical composition and not depth below the Earth's surface.

The number of neutrons produced by each of these two processes for the six average rocks types defined earlier in this chapter are given in Table 2.19. From this it may be seen that the number of neutrons produced by spontaneous fission is small compared to the total number of neutrons produce by (α,n) reactions due to the high Th/U ratios of these average rocks. For a matrix with a ratio nearer to unity (such as average limestone) the spontaneous fission yield may account for as much as 40% of the total neutron yield from these processes. Typical errors in the determination of the neutron production rate due to these processes are less than 6% (based on a 8% error in (α,n) neutron yields, a 10% error in spontaneous fission yield and 10% errors in the chemical composition of the matrix.

P_p and P_{μ} vary with both latitude and depth below the Earth's surface but not appreciably with composition. The variation of P_{tot} with depth below the Earth's surface for six average rock types (at sea level, 40°N geomagnetic latitude and chemical analysis of PARKER (1967)) calculated using equation 2.32 is shown in Fig 2.14. The individual contributions to P_{tot} from P_p and P_{μ} are also plotted on this

figure which shows that :

a/ Within the uppermost layers of the Earth's surface the contributions from (α,n) and spontaneous fission reactions are negligible.

b/ Between 0 and approximately 1.7 meters depth neutrons from the reaction of protons and pions with nuclei in the rock matrix contribute >50 % of neutron production.

c/ Below 1.7 meters depth neutron production is due to neutrons from (α,n) reactions, spontaneous fission and negative muon capture.

d/ The depth to which negative muon capture contributes significantly to the total neutron production rate depends upon the neutron production rate from (α,n) and spontaneous fission reactions which in turn are dependent on the U and Th content of the rock matrix.

e/ At large depths (>10m) differences between rock-type densityes have have an increasingly large effect on the neutron production rate.

Table 2.1. Reaction thresholds (E_{th}) and Coulombic barriers (B) for alpha particle reactions with light nuclei.

Reaction	Isotopic abundance %	Q KeV	E_{th} MeV	B MeV	
$^{1}H(\alpha,n)$----	99.99	-------	------	-----	
$^{4}H(\alpha,n)^{5}Li$	0.01	-4.192	12.576	0.972	*
$^{3}He(\alpha,n)$---	-----	-------	------	-----	
$^{4}He(\alpha,n)^{7}Be$	99.99	-18990	37.98	1.683	*
$^{6}Li(\alpha,n)^{9}B$	7.5	-3977	6.628	2.308	
$^{7}Li(\alpha,n)^{10}Be$	92.5	-2790	4.384	2.228	
$^{9}Be(\alpha,n)^{12}C$	100.	5704	-----	2.802	
$^{10}B(\alpha,n)^{13}N$	20.	1060	-----	3.416	
$^{11}B(\alpha,n)^{14}N$	80.	157	-----	3.338	
$^{12}C(\alpha,n)^{15}O$	98.89	-8507	11.34	3.923	*
$^{13}C(\alpha,n)^{16}O$	1.11	2215	-----	3.847	
$^{14}N(\alpha,n)^{17}F$	99.64	-4737	6.09	4.408	
$^{15}N(\alpha,n)^{18}F$	0.36	-6430	8.145	4.333	
$^{16}O(\alpha,n)^{19}Ne$	99.76	-12145	15.181	4.874	*
$^{17}O(\alpha,n)^{20}Ne$	0.04	588	-----	4.801	
$^{18}O(\alpha,n)^{21}Ne$	0.20	-699	0.854	4.733	
$^{19}F(\alpha,n)^{22}Na$	100.	-1949	2.359	5.252	
$^{20}Ne(\alpha,n)^{23}Mg$	90.5	-7221	8.665	5.760	*
$^{21}Ne(\alpha,n)^{24}Mg$	0.27	2555	-----	5.689	
$^{22}Ne(\alpha,n)^{25}Mg$	9.2	-482	0.570	5.622	
$^{23}Na(\alpha,n)^{26}Al$	100.	-2971	3.488	6.115	
$^{24}Mg(\alpha,n)^{27}Si$	78.99	3139	-----	6.598	
$^{25}Mg(\alpha,n)^{28}Si$	10.	1820	-----	6.529	
$^{26}Mg(\alpha,n)^{29}Si$	11.0	36	-----	6.463	
$^{27}Al(\alpha,n)^{30}P$	100.	-2652	3.045	6.934	
$^{28}Si(\alpha,n)^{31}S$	92.2	-8135	9.297	7.397	*
$^{29}Si(\alpha,n)^{32}S$	4.7	-1532	1.743	7.329	
$^{30}Si(\alpha,n)^{33}S$	3.1	-3504	3.971	7.265	
$^{31}P(\alpha,n)^{34}Cl$	100.	-5572	6.291	7.718	
$^{32}S(\alpha,n)^{35}Ar$	95.	-8628	9.707	8.164	*

Reaction	Isotopic abundance %	Q KeV	E_{th} MeV	B MeV	
$^{33}S(\alpha,n)^{36}Ar$	0.75	-2002	2.245	8.098	
$^{34}S(\alpha,n)^{37}Ar$	4.2	-4629	5.174	8.034	
$^{35}Cl(\alpha,n)^{38}K$	75.8	-5866	6.536	8.472	
$^{37}Cl(\alpha,n)^{40}K$	24.2	-3888	4.308	8.348	
$^{36}Ar(\alpha,n)^{39}Ca$	0.34	-8685	9.650	8.904	*
$^{38}Ar(\alpha,n)^{41}Ca$	0.07	-5231	5.782	8.777	
$^{40}Ar(\alpha,n)^{43}Ca$	99.6	-2289	2.518	8.658	
$^{39}K(\alpha,n)^{42}Sc$	93.3	-6800	7.497	9.201	
$^{41}K(\alpha,n)^{44}Sc$	6.7	-3384	3.714	9.079	
$^{40}Ca(\alpha,n)^{43}Ti$	96.94	-11160	11.26	9.620	*
$^{42}Ca(\alpha,n)^{45}Ti$	0.65	-5182	5.28	9.496	
$^{43}Ca(\alpha,n)^{46}Ti$	0.14	79	-----	9.436	
$^{44}Ca(\alpha,n)^{47}Ti$	2.08	-2170	2.26	9.378	
$^{46}Ca(\alpha,n)^{49}Ti$	0.003	-223	0.242	9.267	
$^{48}Ca(\alpha,n)^{51}Ti$	0.19	-156	0.169	9.161	

* Energy threshold too high for natural series (α,n) reactions.

Table 2.2. Neutron yields per 10^8 α for 5.3 MeV α particles

Target	neutron yield per 10^8 α				
	1	2	3	4	5
Li	-	-	-	-	168.
Be	-	8440.	-	6980.	6286.
B	-	1960.	-	-	1860.
C	8.6*	11.2	11.2	9.1	-
O	-	-	7.1	-	6.
F	-	-	-	-	1860.
Na	-	-	152.	-	-
Na_2CO_3	104.	-	-	-	-
Mg	133.	133.	142.	102.	100.
Al	75.	76.	75.	51.	53.
Al_2O_3	39.	-	-	-	-
Si	10.6*	16.8	16.2	8.9	8.9
SiO_2	8.78	10.7	-	-	-
K_2CO_3	5.2	-	-	-	-
CaF_2	540.	645.	584.	-	-
$CaCO_3$	5.6	-	-	-	-
Fe	-	-	-	0.03	-
Ti	1.05	-	-	-	-
TiO_2	4.8	-	-	-	-
UO_2	-	-	-	<0.01	2.1

1/ FEIGE et al (1968)
2/ GORSHKOV et al (1962)
3/ ROBERTS (1947)
4/ WEST and SHERWOOD (1982)
5/ BAIR and GOMEZ del CAMPO (1979)
* Calculated using method of FEIGE et al (1968)

Table 2.3a. Neutron yields per 10^8 α particles for ^{232}Th, ^{238}U, ^{235}U and ^{NAT}U decay.

Target	neutron yield per 10^8 α			
	^{232}Th	^{238}U	^{235}U	^{NAT}U
SiO_2	20.9	10.2	15.9	10.4
Na_2O_3	298.	154.	221.	157.
K_2CO_3	24.7	11.2	16.4	11.4
Al	298.	144.	213.	146.
Mg	278.	155.	225.	157.
Fe	22.9	4.86	3.30	4.80
CaF_2	940.	564.	818.	578.
$Al2O_3$	151.	76.3	109.	77.7
$CaCO_3$	9.67	5.57	7.56	5.66
TiO_2	63.4	19.9	22.2	20.0
Ti	108.	29.4	30.9	29.5

Calculated from data of FEIGE et al (1968).

Table 2.3b. Neutron yields per 10^8 α particles for ^{232}Th, ^{238}U, 235U and NATU decay.

Target	neutron yield per 10^8 α			
	^{232}Th	^{238}U	^{235}U	^{NAT}U
Be	11800.	8050.	10900.	8160.
BeO	4390.	3070.	4010.	3110.
C	22.9	14.3	19.4	14.5
Al	330.	158.	239.	161.
Mg	328.	184.	269.	187.
Si	43.2	21.5	32.0	21.9
Fe	26.2	5.57	4.40	5.52
UO_2	3.46	2.41	3.26	2.44

Calculated from the data of WEST and SHERWOOD (1982).

Table 2.3c. Neutron yields per 10^8 α particles for ^{232}Th, ^{238}U, ^{235}U and ^{NAT}U decay.

Target	neutron yield per 10^8 α			
	^{232}Th	^{238}U	^{235}U	^{NAT}U
Li	1200.	655.	964.	667.
Be	10700.	7570.	9930.	7660.
B	2430.	1980.	2420.	2000.
O	10.2	7.28	9.29	7.36
F	1620.	967.	1380.	983.
Mg	300.	170.	247.	173.
Al	305.	147.	220.	150.
Si	40.0	20.0	29.7	20.4
UO2	3.42	2.44	3.30	2.47

Calculated from the data of BAIR and GOMEZ del CAMPO (1979).

Table 2.4. Summary of neutron yield data (per 10^8 α particles) for ^{232}Th and ^{NAT}U decay.

Target	Absolute neutron yield per 10^8 α ^{232}Th			^{NAT}U		
	1	2	3	1	2	3
Li	-	1200.	-	-	667.	-
Be	-	10700.	11800.	-	7660.	8160.
B	-	2430.	-	-	2000.	-
C	-	-	22.9	-	-	14.5
O	-	10.2	-	-	7.36	-
F	-	1620.	-	-	983.	-
Na_2CO_3	298.	-	-	157.	-	-
Mg	278.	300.	328.	157.	173.	187.
Al	298.	305.	330.	146.	150.	161.
Si	-	40.0	43.2	-	20.4	21.9
SiO_2	20.9	-	-	10.4	-	-
K_2CO_3	24.7	-	-	11.4	-	-
$CaCO_3$	9.67	-	-	5.66	-	-
CaF_2	940.	-	-	578.	-	-
Ti	108.	-	-	29.5	-	-
TiO	63.4	-	-	20.0	-	-
Fe	22.9	-	26.2	4.80	-	5.52
UO_2	-	3.42	3.46	-	2.47	2.44

1/ FEIGE et al (1968).
2/ BAIR and GOMEZ del CAMPO (1979).
3/ WEST and SHERWOOD (1982).

Table 2.5. Summary of neutron yields per 10^8 α particles for ^{232}Th and ^{NAT}U decay series.

Target	Absolute neutron yield per 10^8 α	
	^{232}Th	^{NAT}U
Li	1200.	667.
Be	11250.	7910.
B	2430.	2000.
C	22.9	14.5
O	10.2	7.36
F	1620.	983.
Na	747.	389.
Mg	302.	172.
Al	311.	152.
Si	41.6	21.2
K	11.3	11.7
Ca	<0.5	<0.5
Ti	108.	29.5
Fe	24.6	5.16
U	0.34	0.34

Table 2.6.Mass stopping powers for α particles at 6.8 MeV

Target	Mass stopping Power MeV $g^{-1}cm^{-2}$	Target	Mass stopping Power MeV $g^{-1}cm^{-2}$
H	1779	Ag	290**
He	745*	Cd	---
Li	652*	In	---
Be	623*	Sn	---
B	619*	Sb	280**
C	635	Te	---
N	614*	I	275**
O	609	Xe	---
F	531	Cs	---
Ne	551*	Ba	260**
Na	503	La	---
Mg	520**	Ce	---
Al	493	Pr	260**
Si	501	Nd	---
P	---	Pm	---
S	480*	Sm	---
Cl	452*	Eu	250**
K	455	Gd	---
Ca	453	Tb	---
Sc	---	Dy	240**
Ti	406	Ho	---
V	---	Er	---
Cr	400**	Tm	---
Mn	---	Yb	230**
Fe	395**	Lu	---
Co	---	Hf	---
Ni	385**	Ta	220**
Cu	360**	W	220**
Zn	360**	Re	---
Ga	---	Os	---
Ge	340**	Ir	---
As	---	Pt	205**
Se	325**	Au	210**
Br	320**	Hg	---
Kr	---	Tl	---
Rb	---	Pb	200**
Sr	325**	Bi	200**
Y	---	Po	---
Zr	320**	At	---

Table 2.6. continued

Target	Mass stopping Power MeV $g^{-1}cm^{-2}$	Target	Mass stopping Power MeV $g^{-1}cm^{-2}$
Nb	---	Rn	---
Mo	310**	Fr	---
Tc	---	Ra	---
Ru	---	Ac	---
Rh	295**	Th	---
Pd	---	U	190**

Data from FEIGE et al (1968) unless otherwise stated.
* From WILLIAMSON et al (1966).
** From ZIEGLER (1980).

Table 2.7. Summarised absolute neutron yields per ppm Th and U at equilibrium.

Target	Absolute neutron yield per ppm :- Th	U
Li	9.24	21.4
Be	86.60	254.
B	18.70	64.2
C	0.176	0.465
O	0.0785	0.236
F	12.50	31.6
Na	5.75	12.5
Mg	2.33	5.52
Al	2.39	4.88
Si	0.320	0.681
K	0.087	0.366
Ca	<0.004	<0.016
Ti	0.832	0.947
Fe	0.189	0.166
U	0.0026	0.0109

Estimated errors at < 10% based on comparison of yields for Mg and Al between authors.

Table 2.8. Neutron yields from (α,n) reactions with average rock matrices when irradiated with U and Th series alpha particles.

Rock Type	[Th] ppm	[U] ppm	(α,n) neutron yield $g^{-1}a^{-1}$ Th	+/-	U	+/-
Granite	18	3.5	8.82	0.67	3.74	0.28
Sandstone	1.7	0.45	0.41	0.03	0.25	0.02
Basalt	4	1.0	2.04	0.15	1.12	0.08
Limestone	1.7	2.2	0.34	0.03	1.08	0.09
Clays+Shales	11	3.2	4.73	0.38	3.00	0.24
Ultramafic	0.004	0.001	0.0026	0.0002	0.0015	0.0001

Based on chemical analysis of average rock matrices by PARKER (1967) (see Appendix 1) and an average error in individual (α,n) yield of 8% (see text).

Table 2.9. Neutron yields from spontaneous fission in selected average rock matrices.

Rock Type	[U] ppm	spontaneous fission yield g^{-1} a^{-1}
Granite	3.5	1.66
Sandstone	0.45	0.21
Basalt	1.0	0.47
Limestone	2.2	1.04
Clay + Shales	3.2	1.51
Ultramafic	0.001	0.00047

Based on chemical analysis of average rock matrices by PARKER (1967) (see Appendix 1).

Table 2.10. Neutron production rate due to proton and pion interactions (P_p) at varying depths below the air ground interface for a site at λ = 40 °N.

Depth m(1)	g cm^{-2}	Production rate (P_p) neutrons g^{-1} a^{-1} (2)	(3)
0	0	740	740
0.1	22	650	670
0.25	56	530	580
0.5	112	380	450
0.75	168	275	350
1	224	200	270
2	448	53	99
3	672	14	36
4	896	3.7	13
5	1120	1.0	4.8
10	2240	<1.0	<1.0
20	4480	<1.0	<1.0

(1) Based on a rock matrix density of 2.24 g cm^{-3}.
(2) Attenuation coefficient (a_p) = 0.0059 cm^{2}g^{-1}.
(3) Attenuation coefficient (a_p) = 0.0045 cm^{2}g^{-1}.

Table 2.11. Variation in the production rate of neutrons due to proton and pion interactions (P_p) with altitude.

Altitude* m	Relative production (sea level = 1) R_{pa}
0	1.0
1000	2.0
2000	3.9
3000	6.9
4000	12.0
5000	19.0

* standard atmospheric pressure

Table 2.12. Variation in the production rate of neutrons due to proton and pion interactions (P_p) with geomagnetic latitude.

latitude degrees,N	Relative production $R_{pl}(1)$	$R_{pl}(2)$	$R_{pl}(3)$	R_{pl}
0	0.260	0.260	0.260	0.260
20	0.260	0.304	0.260	0.274
30	0.304	0.418	0.443	0.388
40	0.500	0.633	0.728	0.620
50	0.943	0.956	0.956	0.952
60	1.000	1.000	1.000	1.000
80	1.000	1.000	1.000	1.000

$R_{pl} = 1$ for $\lambda > 60°N$

Calculated from the data of YOKOYAMA et al., 1977

(1) Europe and North Africa
(2) North America
(3) Asia

Table 2.13. Variation of the average number of neutrons produced per interaction ($\bar{n}_m$) with the average atomic number of target material.

Element/matrix	$\bar{Z}$	$\bar{n}_m$(1)
H_2O	3.4	4.60
Soil(1)	8.4	7.85
Al	13.0	10.5
Fe	26.0	24.0

(1) Based on the data of O'BRIEN et al (1978) for depths of 100 gcm^{-2} below the air ground interface at sea level.

Table 2.14. Negative muon stopping rates for different depths below the air ground interface at a geomagnetic latitude of 40°N and sea level.

Depth m*	Depth gcm^{-2}	stopping rate g^{-1} a^{-1}
0.1	22.4	165.
0.25	56.	184.
0.5	112.	199.
0.75	168.	244.
1.	224.	231.
2.	448.	163.
3.	672.	119.
4.	896.	85.
5.	1120.	67.
10.	2240.	26.
20.	4480.	8.1
40.	8960.	2.1
80.	17920.	0.45
100.	22400.	0.14
500.	112000.	<0.14

* Based on a rock matrix density of 2.24 gcm^{-3}

Table 2.15. Variation in muon intensity (I_μ) and correction factor ($R_{\mu a}$) with altitude.

Altitude m	$I\mu v$ $g^{-1}a^{-1}str^{-1}$	$I\mu$ $g^{-1}a^{-1}$	$R_{\mu a}$
0	147	98	1
1000	196	130	1.48
2000	331	220	2.18
3000	473	314	3.22
4000	694	461	4.76
5000	978	650	7.04

Table 2.16. The probability of negative muon capture (P_z) and of subsequent neutron emission (r_z).

Element	Z	P_z*	r_z**
O	8	1.0	0.28
Na	11	1.0	0.42
Mg	12	0.93	0.46
Al	13	0.76	0.51
Si	14	0.84	0.56
K	19	1.54	0.79
Ca	20	1.90	0.84
Fe	26	3.28	0.90

* VON EGIDY and HARTMANN., 1982, ** CHARALAMBUS., 1971

Table 2.17. Total probability for negative muon capture by average rocks.

Rock type	Capture probability
Basalt	0.45
Clays and Shales	0.39
Granite	0.40
Limestone	0.44
Sandstone	0.38
Ultramafic	0.43

Table 2.18. Negative muon induced production of neutrons (P_μ) in a sandstone for a geomagnetic latitude of 40°N at sea level calculated from equation 2.31 using N_d values given in Table 2.14.

Depth m*	neutron production rate gcm^{-2}	$g^{-1}\ a^{-1}$
0.1	22.4	77.
0.25	56.	86.
0.5	112.	93.
0.75	168.	114.
1.	224.	108.
2.	448.	76.
3.	672.	56.
4.	896.	40.
5.	1120.	31.
10.	2240.	12.
20.	4480.	3.8
40.	8960.	0.96
80.	17920.	0.21
100.	22400.	0.07
500.	112000.	<0.07

* Based on a rock density of 2.24 g cm^{-3}

Table 2.19. Comparison of neutron production rates from spontaneous fission and (α,n) reactions.

Rock Type	Neutron production rate ($g^{-1}a^{-1}$)			
	spontaneous fission	(α,n)	total(1)	+/-
Granite	1.7	13.0	14.1	0.7
Sandstone	0.21	0.66	0.88	0.04
Clays and shales	1.5	7.7	9.26	0.46
Limestone	1.0	1.4	2.45	0.15
Basalt	0.47	3.2	3.62	0.17
Ultramafic	0.00047	0.0041	0.0046	0.0003

(1) Calculated using computer program not from addition of values in this table.

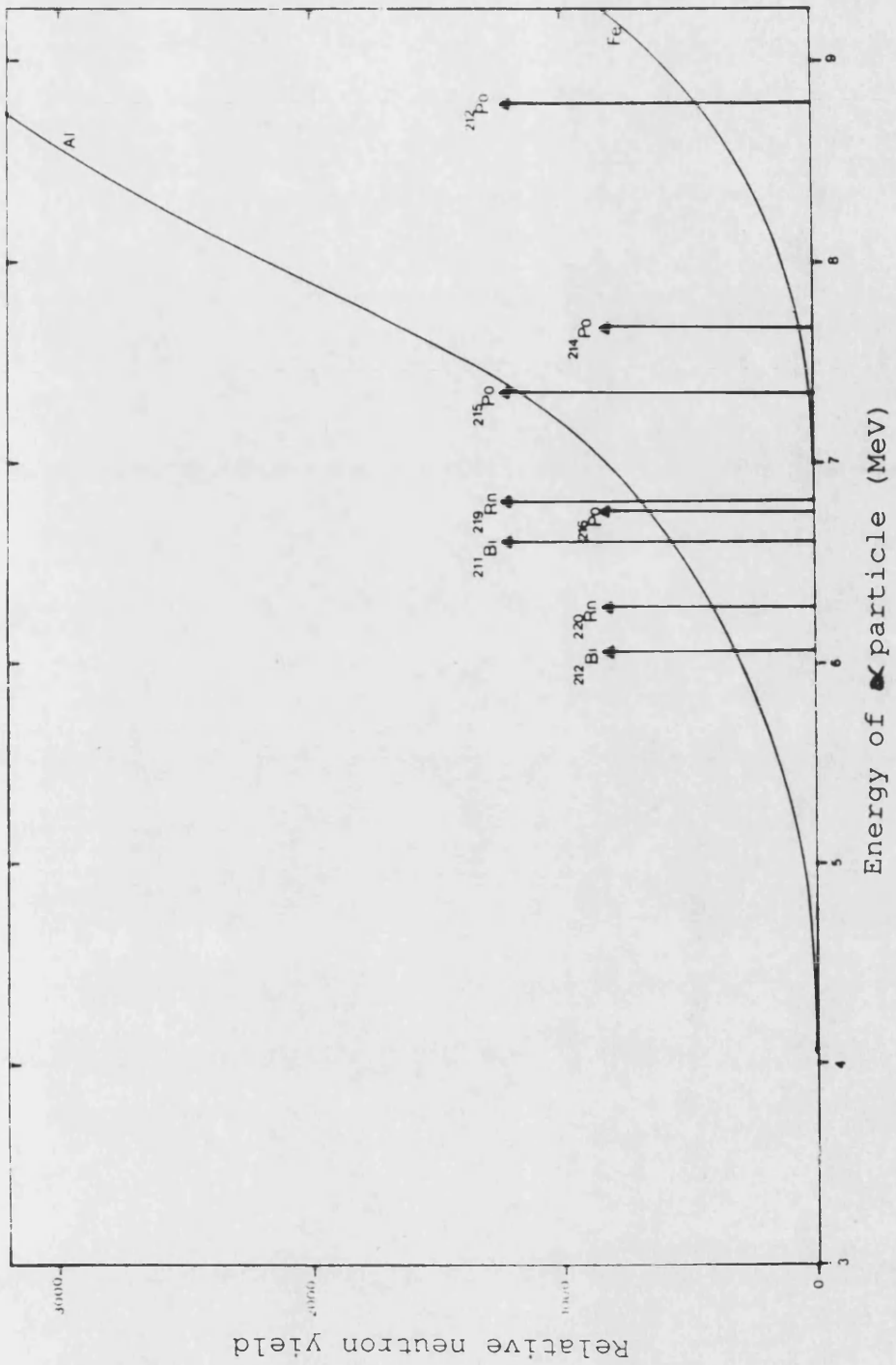

Fig. 2.1. Typical neutron yield vs alpha particle energy curves for (α,n) reactions. The data presented is for Al and Fe and is taken from FEIGE et al (1968). Energies of major alpha particles from the U and Th decay chains are marked.

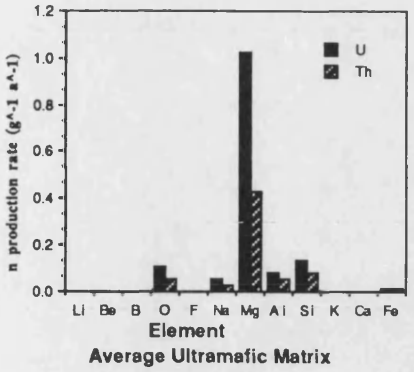

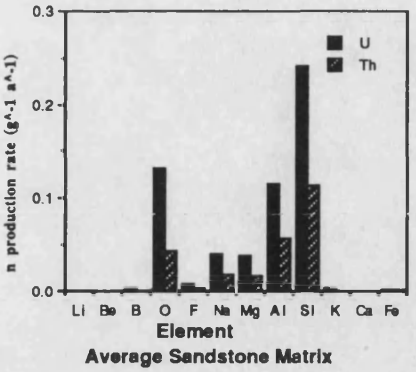

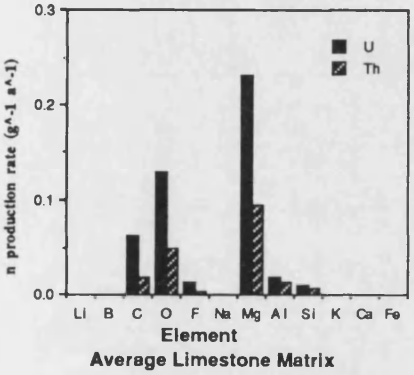

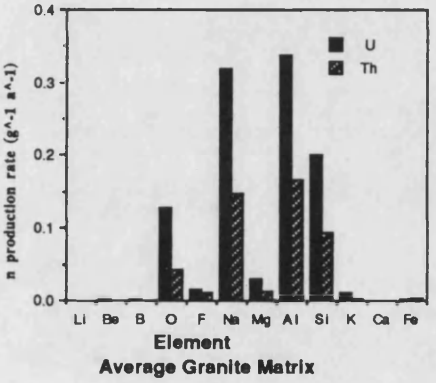

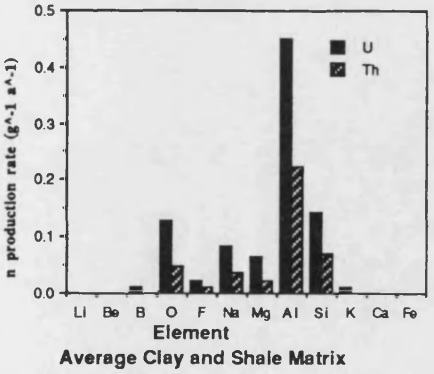

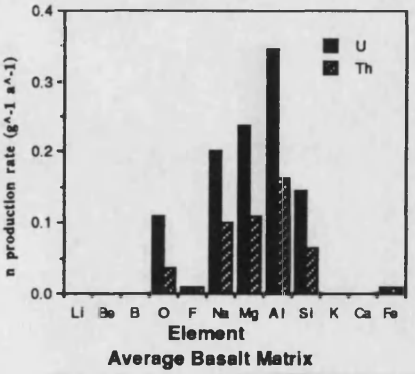

Fig. 2.2. to 2.7. Neutron yields from light elements in rock matrices due to bombardment with U and Th series alpha particles. The yields are based on the chemical analysis of PARKER (1967) and are in units of $g^{-1}\ a^{-1}\ \mu g^{-1}$ of U and Th in equilibrium with their daughters.

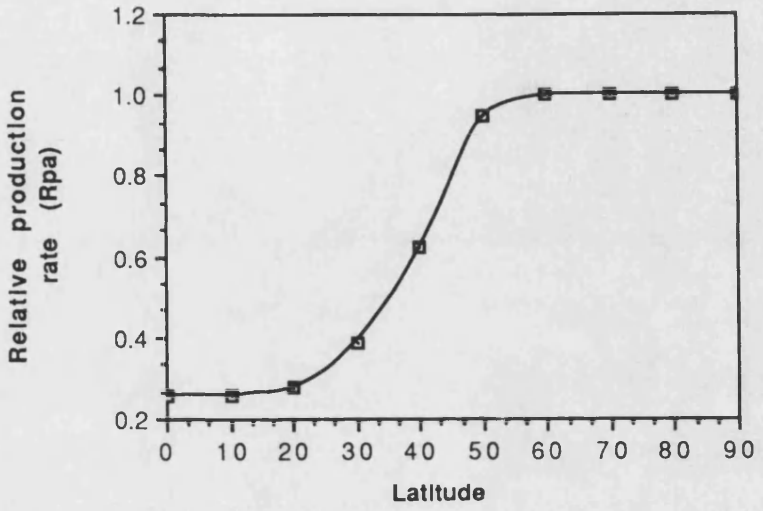

Fig. 2.8. Variation in neutron production rate and R_{pl} with geomagnetic latitude for the longitudinal divisions:- Asia, North America and Europe. Data from YOKOYAMA et al (1977).

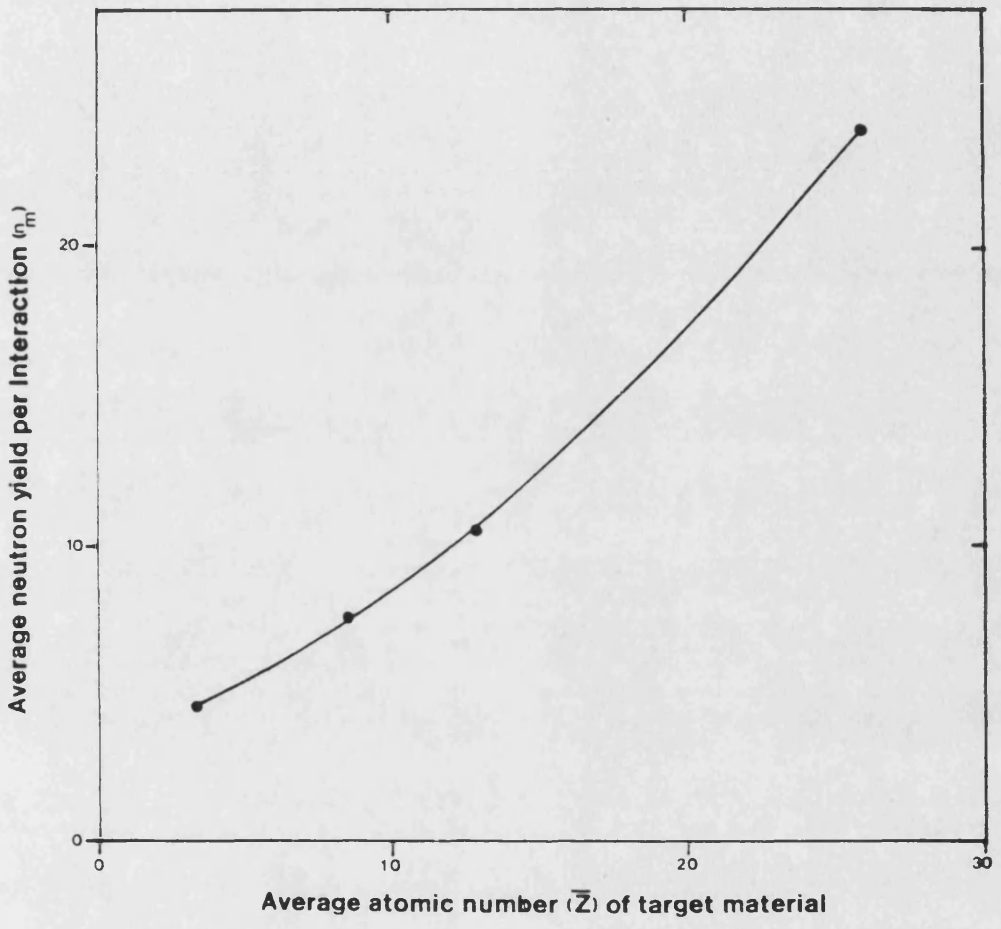

Fig. 2.9. Variation in the average neutron yield due to spallation interactions (n_m) with the average atomic number of target material ($\overline{Z}$). The data is valid for target material placed at 100 gcm^{-2} below the air/ground interface at sea level.

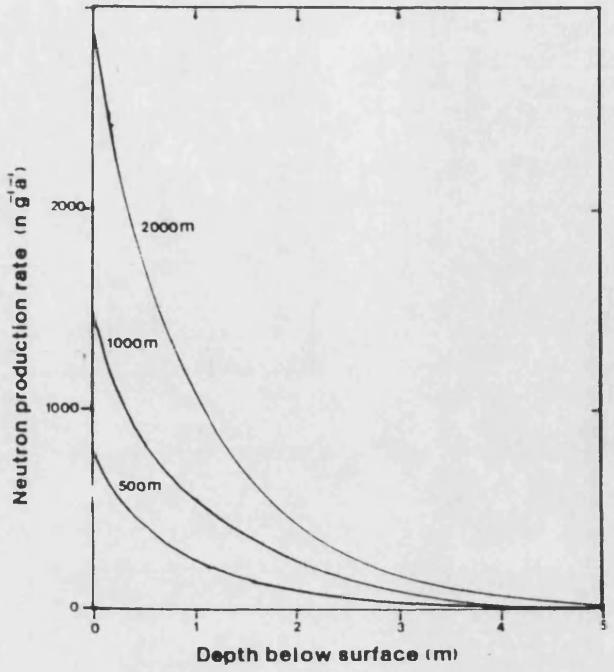

Fig. 2.11. Variation of the neutron production rate due to proton and pion interaction (P_p) with depth below the air/ground interface at different altitudes. The data valid for a rock matrix with a density of 2.24 gcm $^{-3}$, sited at 40°N geomagnetic latitude.

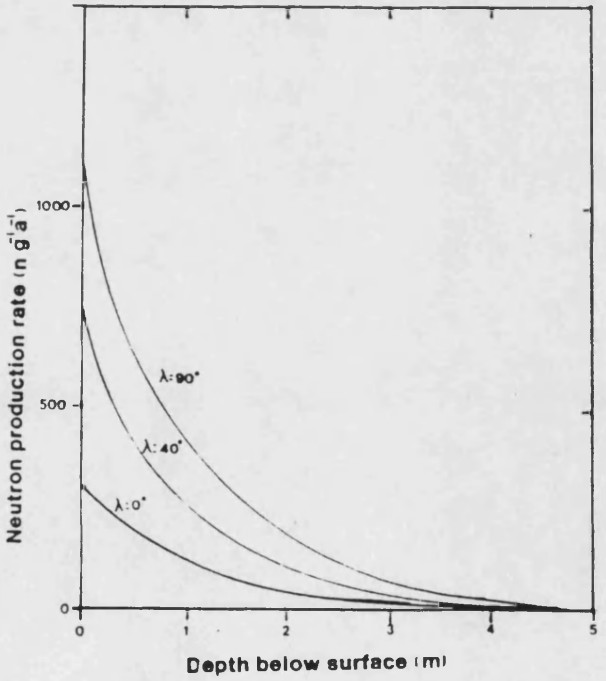

Fig. 2.10. Variation of the neutron production rate due to proton and pion interaction (P_p) with depth below the air/ground interface at different geomagnetic latitudes. The data valid for a rock matrix with a density of 2.24 gcm $^{-3}$, sited at 40°N geomagnetic latitude.

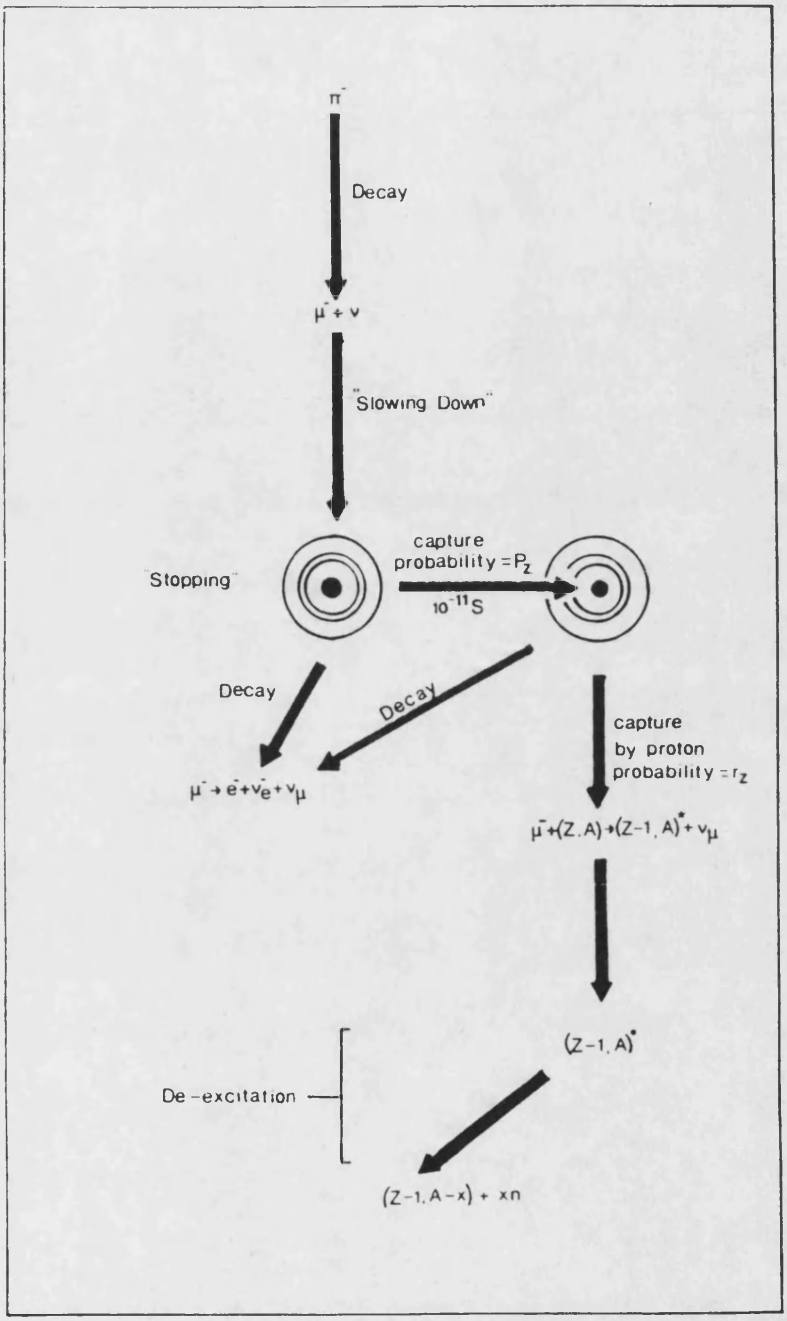

Fig. 2.12. Diagram showing the process by which negative muons may become captured and subsequently cause emmission of neutrons from nuclei present in a rock matrix.

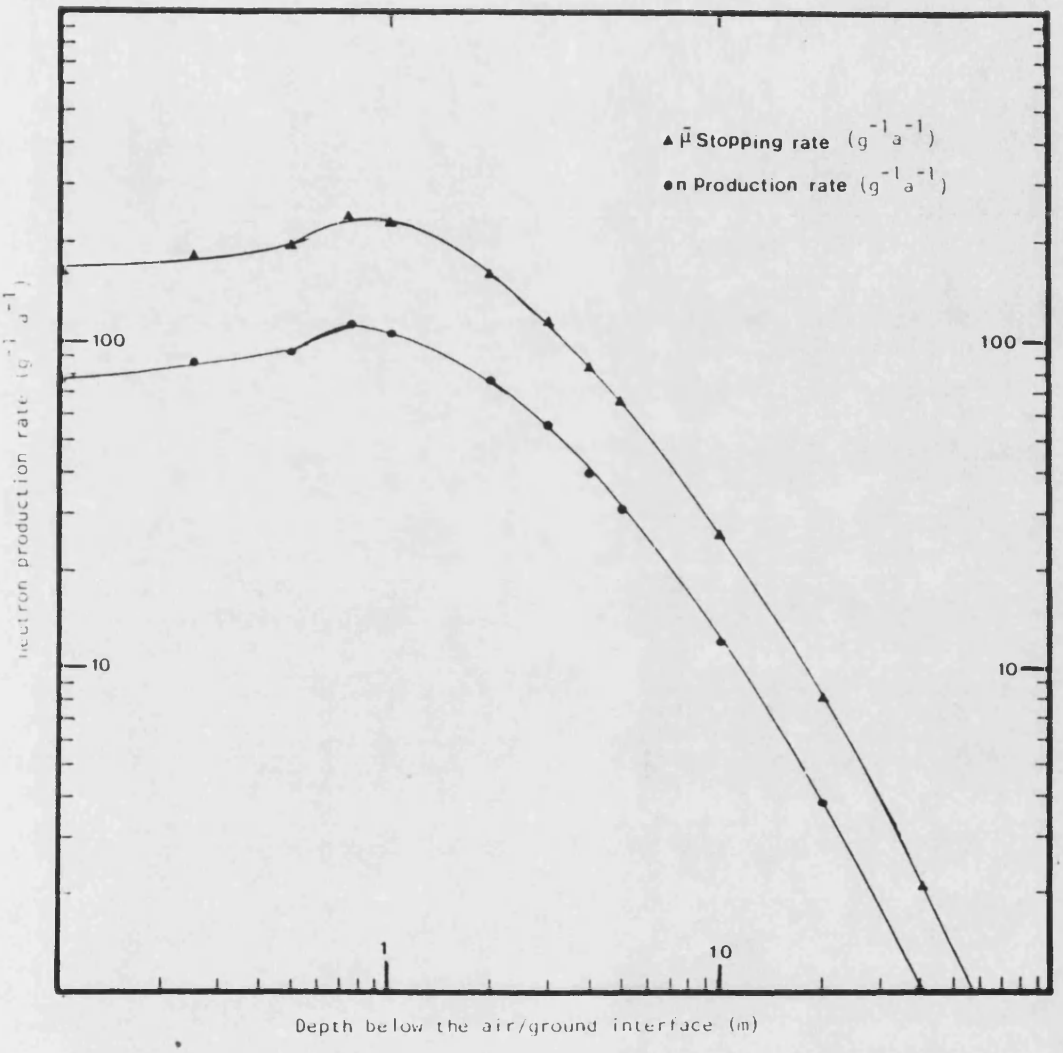

Fig. 2.13. Variation in negative muon stopping rate (N_d) and subsequent neutron production rate with depth below the air ground interface. The data is valid for a rock matrix with a density of 2.24 gcm^{-3} located at sea level and 40°N geomagnetic latitude.

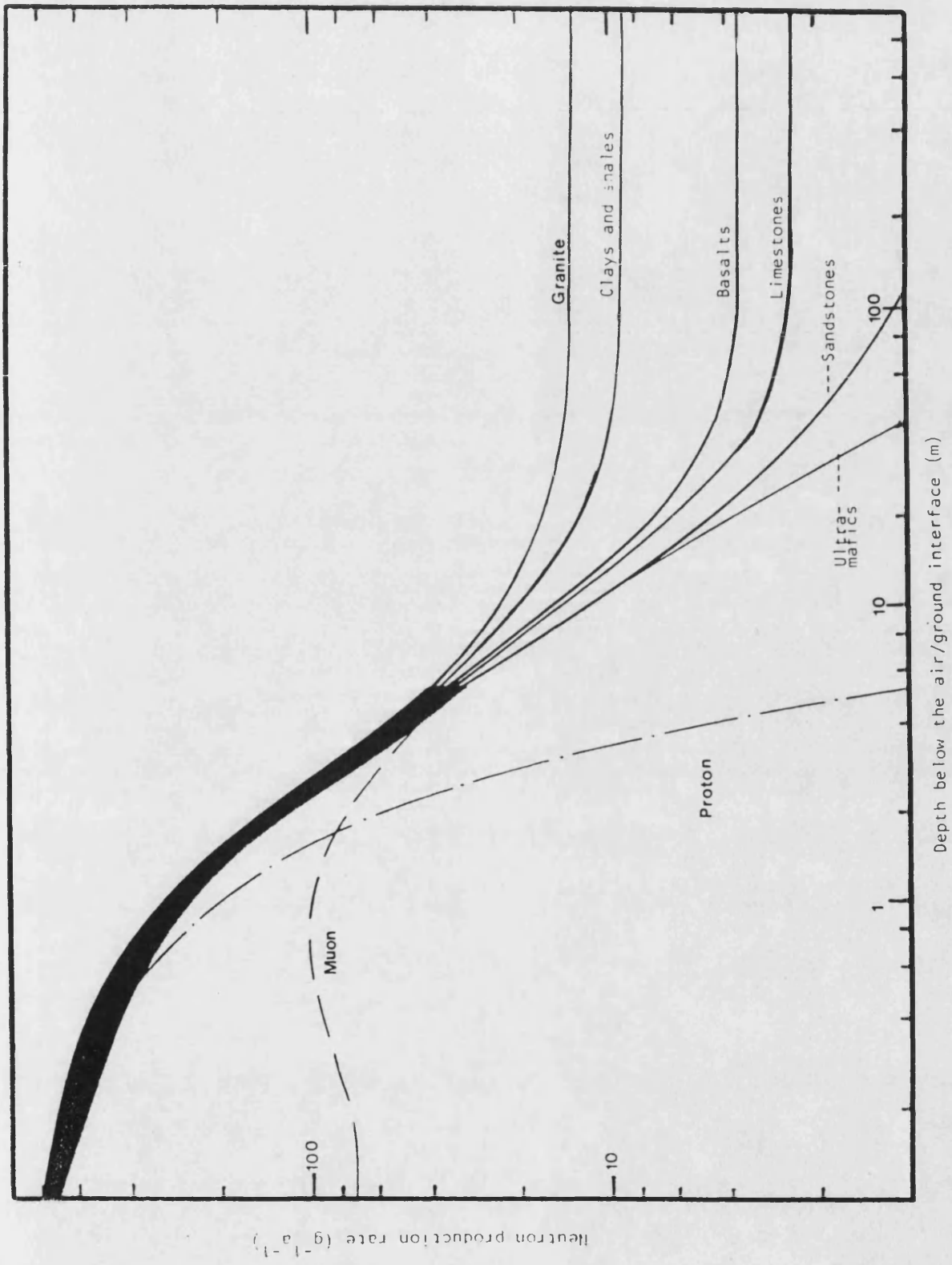

Fig. 2.14. Variation in total neutron production rate (P_{tot}) with depth below the air/ground interface for average granite, basalt, limestone, sandstone, clays and shales and ultramafic rocks. The figure illustrates the depth to which cosmic ray interactions influence the total neutron production rate. The data is valid for rock located at sea level at 40°N.

3.0. THE MAGNITUDE AND ENERGY DISTRIBUTION OF THE IN-SITU NEUTRON FLUX.

Both the magnitude and energy distribution of the neutron flux within a particular rock matrix (due to the production of neutrons by processes described in section 2) are dependent on the neutron absorption properties of the matrix. These properties are predominantly dependent on the chemical composition of the matrix, a knowledge of which enables the neutron flux developed within a given matrix to be estimated (MORRISON and PINE., 1955, KUHN et al., 1984 and ANDREWS et al., 1986).

The objective of this Section is to show how these absorptive properties may vary with the neutron energy distribution; may be calculated or measured for rocks, and to how these results may be used to calculate neutron fluxes for both average rock types and for specific sites at which the neutron flux has been measured. These calculated fluxes are compared with the measured fluxes to gauge the accuracy of such calculations.

3.1 Thermalisation of neutrons within rock matrices.

Neutrons produced by processes described in section 2 are slowed down and elastically scattered by material of the rock matrix until they ideally reach a Maxwellian energy distribution (SATCHLER., 1980) that is characteristic of thermal motions in the matrix (Fig. 3.1), or are absorbed.

In rocks near the Earth's surface such a Maxwellian energy distribution would have a most probable energy of approximately 0.0259 +/- 0.0017 eV (ie/ temperatures of 30 +/- 20^{o}C). Similar energy distributions are also found in the core of a well moderated fission reactor (Fig. 3.2). The neutron energy distribution in the intermediate and fast energy regions of a rock matrix may be expected to show a similar structure to that of a well moderated fission reactor (Fig 3.2) if neutron absorption in the resonance region is low and the initial neutron energies reflect that of a fission neutron source. These factors are discussed further below.

3.1.1 The energy distribution of source neutrons.

Neutrons in the source region represent the energy distribution of specific neutron sources discussed in section 2. GORSHKOV et al. (1962) measured the mean energy distribution of neutrons produced by the interaction of ^{210}Po α particles (5.305 MeV) on major rock forming elements. The mean neutron energies for Be, B, C, CaF_2, Mg, Al, Si, SiO_2 and granite targets ranged from approximately 5.0 MeV for Be to 2.0 MeV for Al. The mean neutron energy for a granite matrix was found to be approximately 2.5 MeV. This data and the mean α particle energy for the ^{238}U and ^{232}Th decay chains (between 5 and 6 MeV) is consistent with the initial neutron energy distribution in geological materials being slightly higher than that of fission neutrons (initial energies in the range 1 to 2 MeV (IAEA.,1970)). However it should be noted that neutrons from cosmic ray interactions (such as negative muon capture) produce some neutrons with initial energies in excess of 10 MeV (KOZOWSKI et al., 1985) which are considerably higher than fission neutron energies.

3.1.2 Neutron absorption.

Neutron absorption occurs due to neutron induced reactions in which the neutron is not re-emitted. In a medium that absorbes a large number of neutrons the number of free neutrons is reduced (causing a reduction in the neutron flux). Also if this absorption occurs in the thermal energy region the neutron energy distribution will no longer be in thermal equilibrium with the surroundings.

Absorption reactions are inelastic and comprise (n,γ), (n,p) , $(n,2n)$ and (n,α) reactions. The total reaction probability for these reactions, the absorption cross-section (σ_a), is the sum of the individual reaction cross-sections (ie/ σ_γ, σ_p, σ_α). Absorption may take place during the thermalisation process or after thermalisation has taken place. These two processes are discussed separately below.

3.1.2.1 Absorption of epi-thermal neutrons. Neutrons are slowed down from the fast region to thermal energies by elastic scattering in the rock matrix. The principal elements responsible for this process in an average rock matrix are O and Si due to their high abundance.

During this slowing down process a number of neutrons will be lost principally due to resonance capture. The fraction of neutrons reaching thermal energies (F_{th}) may be calculated by a simple empirical approach (MORRISON and PINE., 1955) or by multi-group neutron transport theory (KREFT., 1973). The approach adopted by MORRISON and PINE (1955) estimates F_{th} to be between 0.6 and 0.9 for typical silicate matrices and assumes that slowing down is mainly due to collisions with oxygen.

KREFT (1973) calculated the probability of non-capture during the slowing down process (which is equivalent to F_{th}) for Pu-Be and ^{252}Cf source neutrons (Pu-Be mean neutron energy 5 MeV (KREFT (1973), ^{252}Cf mean neutron energy 1.42 MeV (ICRU., 1969)) for sandstone, limestone and dolomite. His results show that values of F_{th} vary little with the concentration of major elements in the rock matrix. However they also show that F_{th} is dependent upon the moisture content of the medium. For the rocks studied F_{th} varied between 0.8 and 0.99 for moisture contents of 1% to 100%. This variation is however small compared to the error in calculation of the neutron production rate for a rock matrix. Bearing this in mind the following conclusions may be drawn:-

1/ In permeable rocks, such as sandstones, pore volumes are saturated with water and F_{th} may be taken to be 1.

2/ For rocks of low permeability such as granites the value of F_{th} may be as low as 0.8.

3/ Since the value of F_{th} represents absorption of neutrons in the intermediate energy region any element present in the rock matrix which has a large absorption cross-section in this region will reduce the value of F_{th}. Such elements include B and Li which are strong neutron absorbers in this region (Li and B have resonance integral cross-sections of 40 and 325 barns respectively for the energy interval 0.55 eV to 2 MeV (KAYE and LABY., 1986)).

3.1.2.2 Absorption of thermal neutrons. When in thermal equilibrium with rock matrices neutrons have a most probable energy of approximately 0.025 eV. In free space such neutrons may travel very large distances (>10^5 m) before decaying to protons by β emission. In rock matrices thermal neutrons undergo scattering and absorption reactions within much shorter distances, so that their ultimate fate is absorption. The thermal absorption cross-section for a multicomponent matrix may be calculated, by weighting the individual thermal absorption cross-section for each element by its abundance in the said matrix (this Section), or by direct measurement (see Appendix 3).

The thermal mass absorption cross-section (Σ_m (cm^2g^{-1})) may be calculated from individual elemental abundances (ppm) in the rock and associated thermal neutron absorption cross-sections (barns) using equation 3.1.

$$\Sigma_m = \sum_i \frac{Wt_i \ \sigma_{ai} \ 10^{-6}}{At_i} \times \frac{6.023 \times 10^{23}}{1 \times 10^{24}} \qquad \text{Eqn 3.1}$$

where Wt_i is the elemental abundance of element i, σ_{ai} is the thermal neutron absorption cross-section for element i (ie/ at 0.025 eV) and At_i is the atomic weight of element i in grams. Exact evaluation of this summation requires a complete chemical analysis of the particular rock. However a good estimate may be made from the data for just 17 elements (Li, B, Na, Mg, Al, Si, Cl, K, Ca, Ti, Cr, Mn, Fe, Co, Ni, Sm, and Gd) (ANDREWS and KAY., 1982) although these include some trace elements which are not often determined. To aid the calculation of such cross-sections a computer program has been written which also propagates uncertainties in absorption cross-section and elemental abundance (see Appendix 5).

Σ_m has been calculated using this program for the six average rock types described earlier in Section 2, and for samples of rock collected from sites at which measurements of neutron flux were made (See Appendix 2). Results of calculations on average rock types are presented in Table 3.1. This table shows that for most rock matrices Σ_m lies between

0.001 and 0.0001 cm^2g^{-1} and that the average error in such calculations of Σ_m is approximately 5%. The absorbance due to each of the 17 elements in each of these 6 rock types are shown in Figs 3.3 to 3.8 and show no general trend in the way Σ_m is "distributed" within different matrices. However Figs 3.3 to 3.8 emphasise the large contribution to Σ_m from the trace elements B and Gd. Iron and Si also show large contribution in silicate matrices, whilst Ca shows a substantial contribution in limestones.

The diversity of analytical techniques required to analyse the 17 elements required for an accurate calculation of Σ_m means that such analysis are time consuming and expensive. It is for this reason that a method was developed to experimentally measure Σ_m. The development and validation of this method of determining Σ_m is described in Appendix 3.

3.1.3 The effect of neutron absorption on the neutron energy distribution.

From the data of Table 3.1 it can be seen that the thermal absorption cross-sections of rock matrices are at least an order of magnitude greater than that of a well moderated reactor (Σ_m approximately $1x10^{-4}$ cm^2 g^{-1}). In such cases the energy distribution has a Maxwellian form, however the most probable neutron energy is shifted to energies higher than that of the thermal energy for its surroundings (IAEA., 1970). The magnitude of this shift to higher energies is difficult to calculate for rock matrices due to the large number of uncertainties associated with elemental distributions and abundances. As a consequence previous authors have assumed for the purpose of calculations of neutron flux (YAMASHITA et al., 1966, ANDREWS and KAY., 1982 and KUHN et al., 1984) and neutron induced in-situ production of isotopes (MORRISON and PINE., 1955 and MAMYRIN and TOLSTIKHIN., 1984) that the effect of such energy shifts are either small or negligible.

This assumption facilitates the use of standard neutron absorption (and reaction) cross-sections which are quoted for a neutron energy of 0.0253 eV (KAYE and LABY., 1985). This energy corresponds to the most probable neutron energy for a Maxwellian energy distribution at 293.6°K.

YAMASHITA et al. (1966) have attempted to assess the effect of thermal neutron absorption on the neutron energy distribution within soils. Using equation 3.2 they calculated that the absorption of thermal neutrons in soils would shift the most probable neutron energy from 0.0253 eV to 0.042 eV. (such a shift would result in a 20% decrease in σ_a for 1/v absorber).

$$T_n = T_0 \ (1+0.9 \sum_i F_i M_i \frac{\sigma_{ai}}{\sigma_{si}}) \qquad \text{Eqn 3.2}$$

where T_n is the shifted neutron temperature (K), T_o is the moderator temperature (K), F_i is the fraction of atoms of element i in the rock matrix, m_i is the atomic mass of element i, σ_a is the absorption cross-section of element i and σ_s is the scattering cross-section of element i. The accuracy of this calculation as made by YAMISHITA et al. (1966) is questionable because the shifted neutron temperature (T_n) was estimated ignoring contributions from neutron absorbers such as B and Gd which although present at low concentrations have high values for σ_a/σ_s. If these are included T_n becomes 3 to 4 times T_o for the average rock types given in Appendix 1 (this would result in a 40 to 50% decrease in σ_a for 1/v absorber). More importantly equation 3.2 is only valid for situations where $0 < T_n/T_o < 0.5$ (IAEA., 1970) making the basis of such calculations questionable. To more accurately predict the effect of absorption within rock matrices requires a more complex mathematical treatment using computer based Monte Carlo type calculations. Even using these methodologies assumptions as to the distribution of absorbers within the matrix and the initial energy distribution would still have to be made.

The best theoretical estimate of these effects that can be made at present is that the neutron energy distribution within rock matrices is likely to have a higher average energy than that of its surroundings. This effect will be greater for rocks with a higher absorption cross-section. The effect of this assumption on the calculation of neutron flux and

production rate will be to over estimate the calculated thermal flux and thence also the in-situ production rate from neutron induced processes.

From the above discussion of initial neutron energies and neutron absorption it may be concluded that :-

(1) Energies of neutrons produced from (α,n) reactions are slightly higher than those produced during nuclear fission.

(2) A large proportion of produced neutrons reach thermal energies before absorption ($F_{th} > 80\%$) even though initial neutrons energies are slightly higher than fission energies. The neutron energy distribution during this slowing down process is difficult to predict without detailed neutron transport calculations.

(3) The proportion of neutrons reaching thermal energy is likely to be effected by the presence of strong 1/v absorbers such as B and Li.

(4) At thermal energies in rock matrices neutron absorption is not dominated by any major element. However even low concentrations of B and Gd strongly effect such absorption.

(5) Absorption of thermal neutrons by rock matrices increases the relative flux of fast thermal neutrons. The magnitude of this increase is difficult to calculate and present estimates are unreliable.

(6) Whilst the influence of neutron absorption on the thermal neutron flux should not be ignored, the assumption that a thermal energy distribution centered near 0.025 eV exists greatly aids the calculation of neutron flux and isotope production rates. The validity of this assumption may only be tested using neutron flux measurements.

(7) The use of multi-group neutron transport theory provides invaluable information as to the neutron energy distribution in rock matrices. This information is impossible to obtain by any other means and it should be used in future to investigate variations in neutron energy distributions between rock types.

3.2 Calculation of thermal neutron flux.

The thermal neutron flux for an absorber at 20°C (ϕ_{th}) may be defined as :-

$$\phi_{th} = n\ v_{th} \qquad \text{Eqn. 3.3}$$

where n is the neutron density and v_{th} is the velocity of the thermal neutrons 2200 m s^{-1} (ICRU., 1969). This velocity corresponds to the most probable velocity of a Maxwellian density distribution at 20°C (0.025 eV).

From discussion of the thermalisation and absorption of neutrons it can be seen that the absorptive properties of a rock matrix influence both the density and velocity (energy) distribution of neutrons in a complicated manner which is at present undefined. However the calculation of neutron flux may be simplified by assuming that neutrons that reach thermal energies are in true thermal equilibrium with their surroundings at temperatures near 20 C. If this is assumed the thermal neutron flux may be calculated from the absorption mean free path, λ_a, for thermal neutrons which is given by :-

$$\lambda_a = \frac{1}{o\,\Sigma_m} \qquad \text{Eqn 3.4}$$

where o is the matrix density in g cm^{-3}. The value of λ_a in rock matrices typically lies between 25 and 150 cm. The corresponding mean life time, t_m, and time constant, k, for the absorption of thermal neutrons (Energy = 0.025 eV equivalent to a velocity of 220000 cm s^{-1}) are given by :-

$$t_m = \frac{\lambda_a}{220000} \qquad \text{Eqn 3.5}$$

$$k = \frac{1}{t_m} \qquad \text{Eqn 3.6}$$

k controls the removal of neutrons from the rock matrix by absorption reactions and the equilibrium between neutron production and absorption is established according to equations 3.7 and 3.8.

$$n_t = \frac{P_{tot}}{k}\ (1-e^{-kt}) \qquad \text{Eqn 3.7}$$

or

$$n_t = \frac{P_{tot}}{k} \quad \text{when } t > 0.001 \text{ s} \qquad \text{Eqn 3.8}$$

Where n_t is the neutron density after time t (cm^{-3} of rock) and P_{tot} ($g^{-1}s^{-1}$) is the total neutron production rate from sources discussed in Section 2. Equilibrium is established almost immediately since k is about 2200 s^{-1}.

From equation 3.3 the thermal neutron flux, ϕ_{th}, is then equal to $n_t v_{th}$ $cm^{-2}s^{-1}$. Where v_{th} is the thermal neutron velocity in cm s^{-1} (ANDREWS et al., 1986). Equations 3.3 to 3.8 may be simplified and corrected to account for the fraction of produced neutrons which do not reach thermal energies :-

$$\phi_{th} = \frac{P_{tot}\ F_{th}}{\Sigma_m} \quad (cm^{-2}s^{-1}) \qquad \text{Eqn 3.9}$$

Where P_{tot} is the total neutron production rate ($g^{-1}s^{-1}$), F_{th} is the fraction of produced neutrons which reach thermal energies and Σ_m is the macroscopic absorption cross-section for thermal neutrons (cm^2g^{-1}).

The neutron flux has been calculated using the above procedure for six average rock types (Table 3.2), for the purpose of these calculations it has been assumed that all produced neutrons reach thermal energies as is suggested in Section 3.1.

The variation in neutron flux with depth below the air/ground interface would be expected to follow the variation in neutron production rate (Fig. 2.14). However the flux within the first few centimeters of the Earth's surface does not follow the neutron production rate because of neutrons escaping into the atmosphere (O'BRIEN et al., 1978 and YAMASHITA et al., 1966). At depths below the influence of cosmic radiation (for most rocks > 100 m see Section 2) the neutron production rate and thence flux is controlled jointly by the radio-element content and the abundance of neutron absorbing elements such as B. It is thus not surprising to find the highest flux produced for average rock types (Table 3.2) is within a granite.

3.3 Comparison of calculated and measured neutron flux.

Very few studies have been published that compare measurements of neutron flux in the deep subsurface and with calculated values. In the studies that have been published it is mainly neutron production rates that have been compared. MORRISON and PINE. (1955) attempted to measure the neutron production rate within a block of granite, shielded from cosmic rays in a salt mine. The results of this experiment were poor due to the relative insensitivity of their counting equipment. However a further successful experiment was carried out by the same authors using a simulated granite with a much higher U and Th content. In this experiment the predicted neutron emission rate was greater by a factor of two than the measured rate.

The next well documented experiment to compare calculated and measured neutron production rates was made by KUHN et al (1984). In this experiment a high sensitivity ^{3}He proportional counter was used with and without Cd shielding to measure the thermal neutron production rate in rock formations at depths of up to 1300 m below the Earth's surface. Chemical analysis of the respective formations were then used to calculate, neutron yields (based on the data of FEIGE et al., (1968)) and absorption cross-sections.

These were used to derive the neutron production rate from the counting rate of the detector.

Results of this experiment show an order of magnitude agreement between measured and predicted neutron production rates. The agreement is worse for measurements made in boreholes at shallow depths (12 to 30 m below surface). At these depths discrepancies were interpreted as being due to the production of neutrons from the interaction of muons as well as from (α,n) and spontaneous fission reactions.

ANDREWS et al. (1986) carried out a series of neutron flux measurements in the Stripa granite and Leptite using a high sensitivity calibrated BF_3 proportional counter and compared the calculated flux with that estimated form a chemical analysis of the rock matrix and (α,n) and spontaneous fission neutron yields (FEIGE et al., 1968). The calculated and measured fluxes showed good agreement (within 20%). In these experiments the thermal/epi-Cd flux ratio was also measured and showed that the majority of neutrons in the granite were thermalised. The general principals of the methodology used in ANDREWS et al. (1986) were modified and developed in the course of this thesis and applied to the measurement and calculation of neutron flux.

3.3.1 Methodology, results and comparison.

The accuracy by which the neutron flux could be calculated was tested by collecting, and carrying out chemical analysis of rock from a number of sites at which the neutron flux was also measured (using methods described in Appendix 4). The sites at which measurements were carried out were selected to enable results to be compared with calculated flux for a wide range of geological formations and depths below surface. Details of the selected sites and of the results of chemical analysis of rocks collected from these sites are given in Appendix 2.

Calculations of neutron flux for these sites (neutron production from (α,n), spontaneous fission and cosmic ray induced sources) have been based on the assumption that all produced neutrons reach thermal energy ie/ $F_{th} = 1$. The bases used for these calculations are presented in Sections 2 and 3 of this thesis and were performed using the computer program "ISOTOPE PRODUCTION" a listing of which is given in Appendix 5

Results of measurement of the thermal and total neutron flux at each site are given in Tables 3.3 (the raw data for these measurements is presented in Appendix 4) along with the results of flux calculations for the particular site in question.

3.3.1.1 Comparison of measured and calculated neutron flux

Results from Table 3.3 have been plotted in Figs. 3.9 and 3.10 as measured thermal neutron fluxes against calculated thermal neutron fluxes, and in Figs. 3.11 and 3.12 as measured total neutron fluxes against calculated total neutron fluxes (note that calculated thermal neutron flux is equal to the total calculated flux since it has been assumed in the calculations that all neutrons reach thermal energies)

In Fig. 3.9 a logarithmic scale has been applied to each axis so as to give a complete picture of all measured and calculated data. Fig. 3.9 shows that for the measured sites calculated thermal flux is generally greater than the measured thermal flux. A similar trend is evident when data for sites > 5 m below the surface (FM2, FM3, FM9, FM10, FM13, FM14, FM15, FM17, FM20, FM21, FM22, FM23, FM24 and FM25) is presented using linear axis (Fig. 3.10). This trend is the opposite effect to that experienced by KHUN et al., (1984) where measured fluxes were higher than calculated fluxes. Fig. 3.10 shows that the measured thermal flux is in the majority of cases half the calculated flux. The exception to this are measurements made in Rosemanowes Quarry B/H C which show a good agreement between calculated and measured thermal flux. Unfortunately there are insufficient measurements of near surface thermal flux to compare with calculated values.

Fig. 3.11 shows that two groups of sites may be identified :-

(a) Those that yield values that lie close to the line at which measured values equal calculated values (the line of equality). The sites within this group (FM2, FM3, FM4, FM9, FM10, FM13, FM14, FM15, FM16, FM17, FM20, FM21, FM22, FM23, FM24 and FM25) have been plotted with linear scales in Fig. 3.12 to illustrate the agreement between measured and calculated values for this group of measurement sites (error bars represent an assumed error of 10% in the calculated flux and actual counting errors (1σ) in the measured flux).

Note that there is only good agreement for sites at which measurements were made below the influence of cosmic ray protons and pions.

(b) Those that lie above the line of equality (FM6, FM7, FM8, FM5 and FM1). This group consists of measurements made at sites at or near the Earth's surface and Fig. 3.11 shows that the calculated flux for these sites is in excess of the measured flux.

From the comparisons of calculated and measured fluxes made above it must be concluded that in majority of sites calculated neutron flux at depths deeper than approximately 5 m reflect the total flux rather than the thermal flux. Note that the one exception, Rosemanowes Quarry B/H C has a high permeability and is often oversaturated with meteoric water. This aids thermalisation and is consistent with the calculated and measured thermal fluxes being in close agreement.

It is possible that disparity between calculated and measured thermal neutron fluxes may be caused by the high neutron absorption cross-sections found in rock matrices. As discussed in Section 3.1 absorption of thermal neutrons shifts the "free" neutron energy distribution to higher energies.

This hypothesis was tested by plotting the ratio of the measured thermal flux to the measured epi-cadmium flux (R_{Cd}) :-

$$R_{Cd} = \frac{\text{measured epi-cadmium neutron flux}}{\text{measured thermal neutron flux}}$$

against the absorption cross-section (Σ_m) (Fig 3.13). A weak negative correlation was observed, even if non-borehole measurements were not considered. This suggests that the degree of thermalisation increases with absorption cross-section which is not consistent with the above hypothesis. The effect may also have been caused by neutron absorption during thermalisation, however in this case a positive correlation between R_{Cd} and Σ_m would also be observed, since strong 1/v absorbers that would be expected to cause such effects (ie/ B and Li) contribute greatly to Σ_m.

Changes in the energy distribution of free neutrons due to absorption by the BF_3 detector could also reduce the agreement between predicted and measured thermal flux. Such an effect should be constant and is unlikely to be an important factor since it could not be used to explain observations where good agreement is found (Rosemanowes Quarry B/H C and in the Stripa Granite (ANDREWS et al., 1986).

It is therefore concluded that whist prediction of the total in-situ produced neutron flux is possible from a theoretical basis prediction of thermal flux by using present theory is less accurate. Where it is important to know neutron energy distributions to a greater accuracy measurement of R_{Cd} is the only reliable technique.

The agreement between measured and calculated flux (thermal or total) at the Earth's surface or at depths < 3 m is poor. Since production is this zone is almost exclusively from the reaction of protons and pions this strongly suggests that production rates used in the calculations are overestimates. Alternatively neutrons produced by such processes may be of to high an energy too be detected by the equipment described in Appendix 4. This hypothesis is supported by measurements by YAMASHITA et al., 1968 who used moderated neutron counters to measure flux in the near surface regions. These counters measured the flux of epi-cadmium neutrons at the Earth's surface to be 8 times the thermal flux. The un-moderated BF_3 counter used in this work gave a very low epi-cadmium count rate under similar conditions. This effect does not fully explain the overestimates for depths of approximately 1m since it should decrease rapidly below 0.5 due to thermalisation by the matrix (O'BRIEN et al., 1978).

At larger depths the agreement between measured and calculated flux is better. This agreement is demonstrated in Fig. 3.14 which shows the variation of calculated and measured neutron flux with depth. The values agree well in the depth range 5 to 60 m which is consistent with the described treatment of negative muon interactions (Section 2.4).

Fig 3.11 also shows that in measurements carried out in this work the effect of measurement position (ie/ in center of passage, borehole, against wall of chamber) is small compared to the accuracy of flux calculations and variations caused by geochemical effects.

This is consistent with theory as air is a weak absorber of neutrons and the detector geometry is such that end effects are negligible (see Appendix 4).

Table 3.1. Comparison of neutron absorption cross sections calculated for average granite, sandstone, clays and shales, limestone, basalt and ultramafic rocks.

Rock Type	Neutron absorption cross-section (Σ_m) cm^2g^{-1}
Granite	0.0068 +/- 0.0003
Sandstone	0.0060 +/- 0.0003
Clays and shales	0.0097 +/- 0.0005
Limestone	0.0045 +/- 0.0002
Basalt	0.0073 +/- 0.0003
Ultramafic	0.0047 +/- 0.0003

Errors based on a 10% error in the elemental abundances of PARKER (1967). Absorption cross-sections and associated errors from HUGHES and SCHWARZ (1958).

Table 3.2. Comparison of neutron fluxes calculated for average granite, sandstone, clays and shales, limestone, basalt and ultramafic rocks at 2m and 200m below the earths surface.

Rock Type	Neutron flux (ϕ) $x10^{-4}$ $cm^{-2}s^{-1}$			
	2m		200m	
		+/-		+/-
Granite	5.6	0.7	0.66	0.04
Sandstone	7.0	0.7	0.046	0.003
Clays and shales	4.6	0.5	0.30	0.02
Limestone	9.6	0.9	0.17	0.013
Basalt	5.9	0.6	0.16	0.010
Ultramafic	8.9	0.9	3.0 +/- 0.3 * 10^{-4}	

Errors based on a 10% error in the elemental abundances of PARKER (1967). Fluxes at 2m based on corrections for a rock density of 2.24 g cm^{-3}, a site at 40°N geomagnetic latitude over North America and at sea level.

Table 3.3. Calculated and measured total and thermal neutron flux for each of the sites described in Appendix 2.

Measurement and site	site depth (1) m	sample analysis	measured total neutron flux $x10^{-4}$ cm^{-2} s^{-1}	+/-	measured thermal neutron flux $x10^{-4}$ cm^{-2} s^{-1}	+/-	calculated total neutron flux (2) $x10^{-4}$ cm^{-2} s^{-1}	+/-
measurements made in boreholes								
FM13 Rosemanowes B/H C	6	SA4	1.67	0.22	1.17	0.04	0.80	0.05
FM14 average of 4 measure-							1.47	(3)
FM15 ments between 3.8 and								
FM17 5.98 m into the face.								
FM16 Rosemanowes B/H B	6	SA4	1.47	0.04	----	----	0.80	0.05
3.80 m into face.							1.47	(3)
FM20 South Crofty B/H A	560	SA1	0.61	0.01	0.37	0.02	0.78	0.05
FM21 South Crofty B/H B	560	SA1	0.63	0.02	0.38	0.02	0.78	0.05
FM24 Pendarves B/H A	100	SA2	0.53	0.02	0.32	0.03	0.48	0.04
FM9 Bath Stone mine slot	30	SA15	0.23	0.01	0.13	0.01	0.055	0.004
							0.18	(3)
FM6 Bath University	0	---	16.5	0.25	----	----	137.0	(3)
FM7 sand pit.	0.5	---	19.2	0.08	----	----	93.0	(3)
FM8	1.2	---	13.4	0.12	----	----	61.0	(3)

Table 3.3 cont. Calculated and measured total and thermal neutron flux for each of the sites described in Appendix 2.

Measurement and site	site depth (1) m	sample analysis	measured total neutron flux $x10^{-4}$ cm^{-2} s^{-1}	+/-	measured thermal neutron flux $x10^{-4}$ cm^{-2} s^{-1}	+/-	calculated total neutron flux (2) $x10^{-4}$ cm^{-2} s^{-1}	+/-
non borehole measurements								
FM5 Bath University surface	-0.5	---	21.8	0.08	19.8	0.08	80.0	(3)
FM22 South Crofty centre	560	SA1	0.51	0.02	0.34	0.02	0.48	0.04
FM23 South Crofty wall	560	SA1	0.49	0.02	0.35	0.03	0.48	0.04
FM25 Pendarves against wall	100	SA2	0.30	0.03	0.22	0.02	0.48	0.04
FM1 Nottingham at surface	-1.0	---	18.0	0.3	----	----	79.0	(3)
FM2 Nottingham against wall	17	SA16	0.60	0.02	0.32	0.02	0.16	0.01
							0.55	(3)
FM3 Nottingham near wall	17	SA16	0.57	0.03	0.23	0.03	0.16	0.01
							0.55	(3)
FM4 Nottingham centre	17	SA16	0.57	0.01	----	----	0.16	0.01
							0.55	(3)
FM10 Bath stone mine centre	30	SA15	0.21	0.01	0.13	0.01	0.055	0.004
							0.18	(3)

Key :-

(1) Depth below air/ground interface in metres.

(2) Calculated flux based neutron yields for (a,n) and spontaneous fission processes and calculated values of Σ_m unless stated otherwise (see Appendix 2 for values). In these calculations it has been assumed that $F_{th} = 1$.

(3) Calculated flux corrected for neutron production by cosmic ray interaction.

(4) B/H = Borehole.

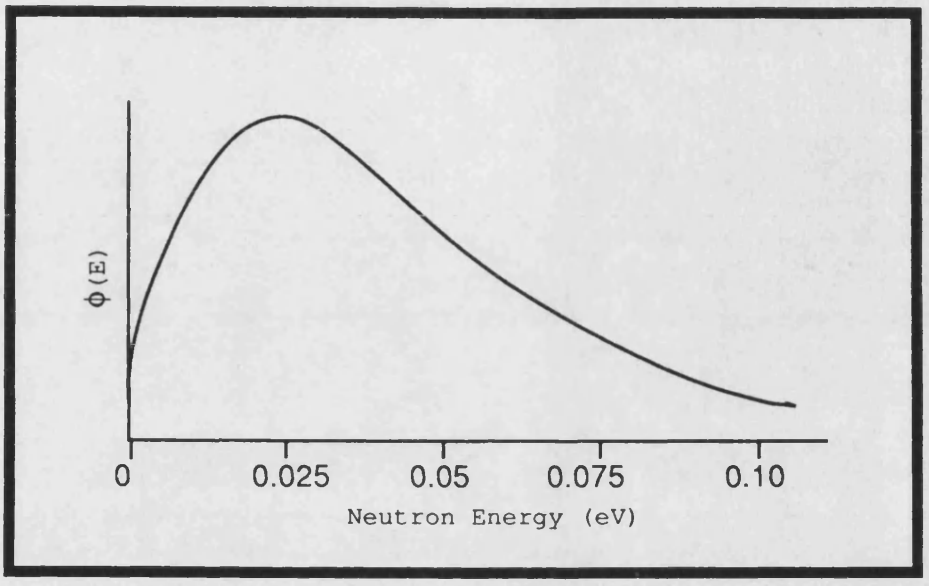

Fig. 3.1 Maxwellian neutron flux distribution for medium at 20.4°C.

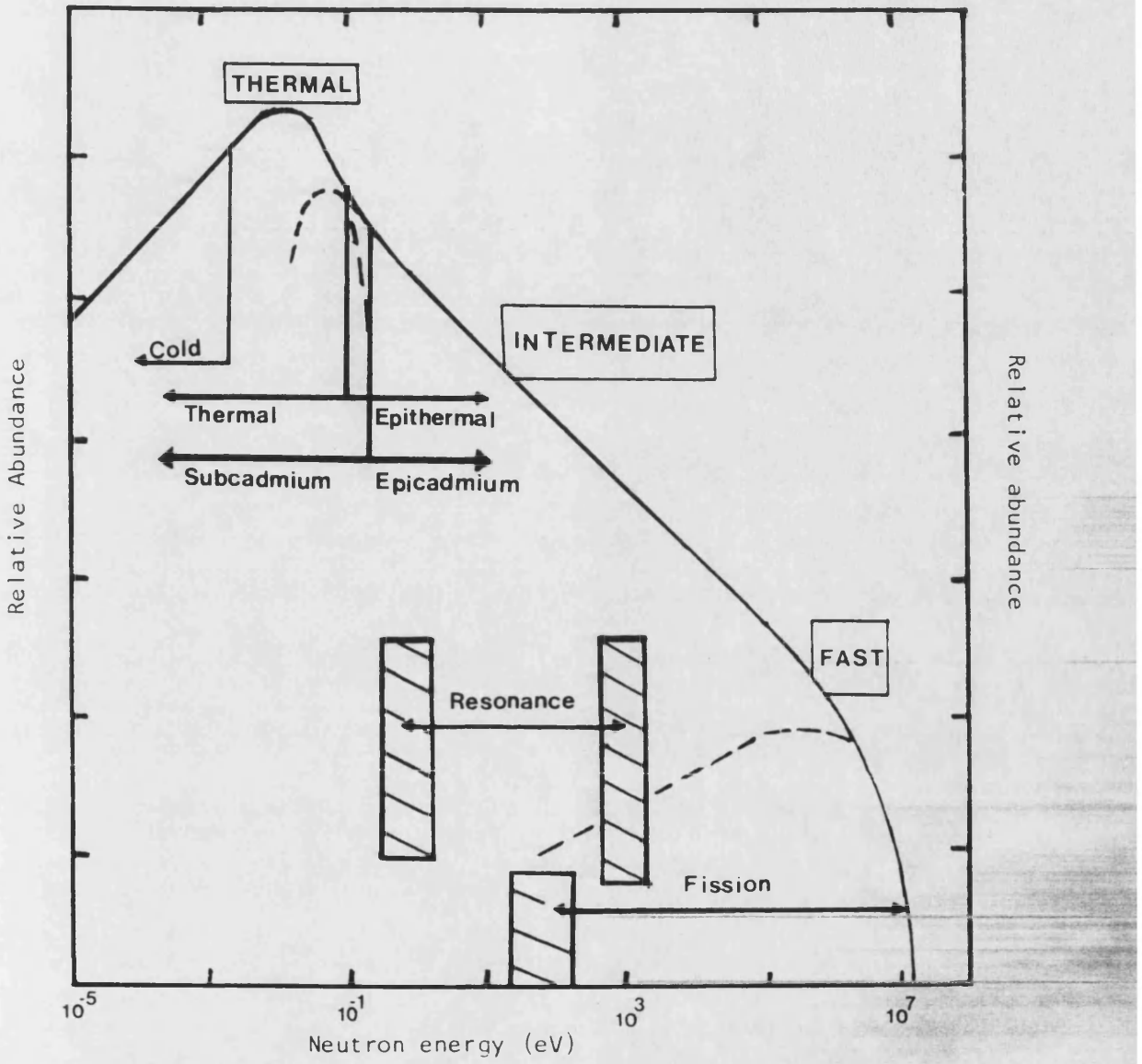

Fig. 3.2 Schematic diagram of the differential neutron flux spectra in a moderated reactor. The Fig. illustrates major energy divisions and terms referred to in the text.

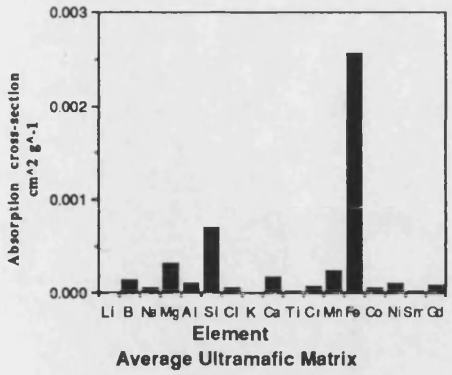

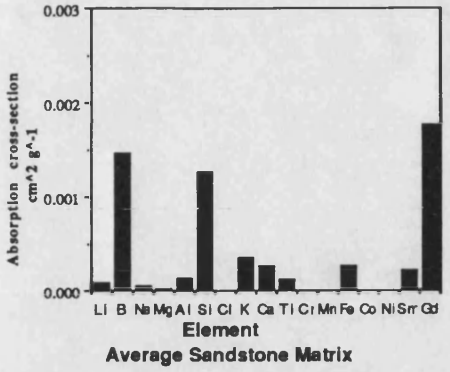

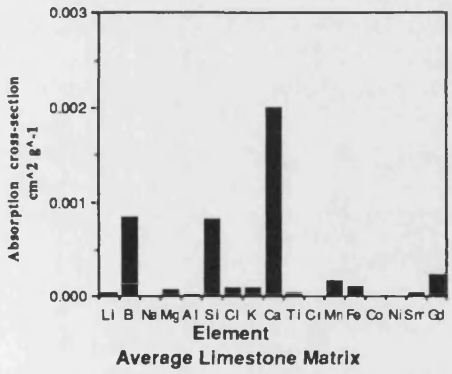

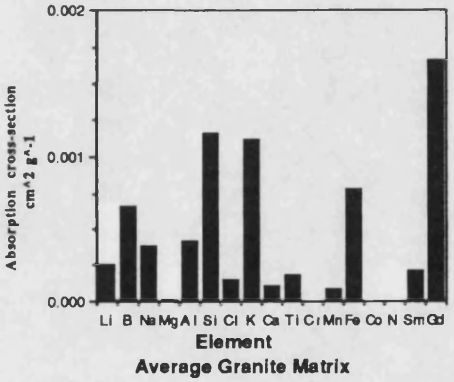

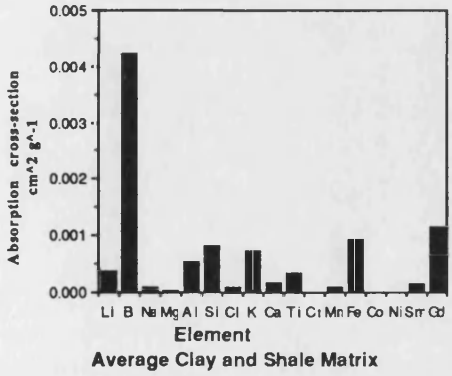

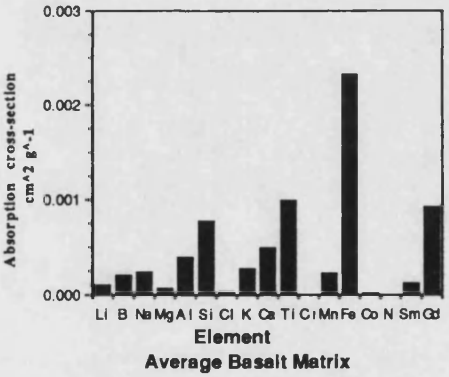

Figs. 3.3 to 3.8. Neutron absorption plotted against element for six average rock types. Units of neutron absorbance are cm^2g^{-1}. These Fig.s show little similarity in the influence or distribution of elements that contribute to Σ_m between rock types.

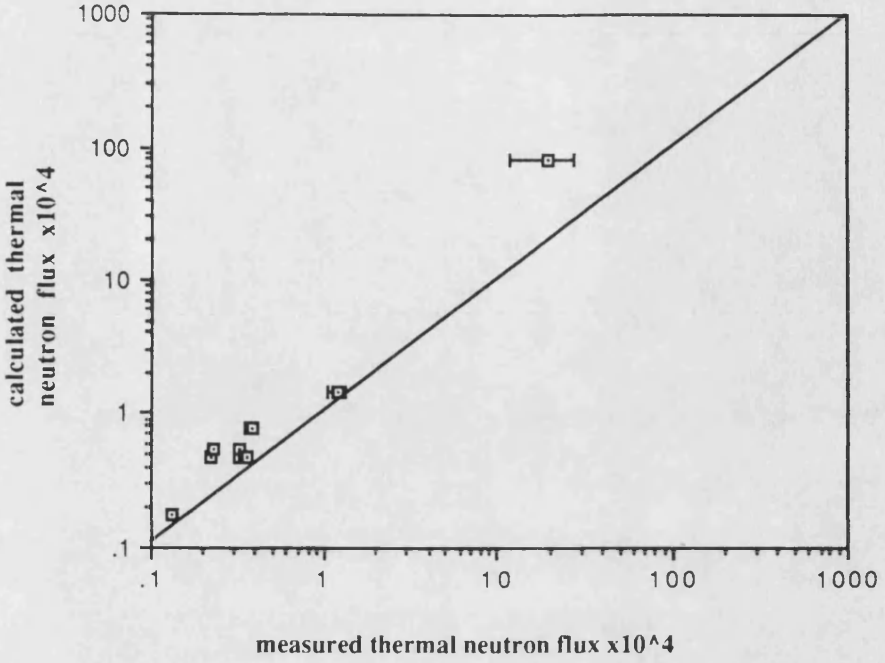

Fig. 3.9. Measured thermal neutron flux plotted against calculated thermal neutron flux (log scales).

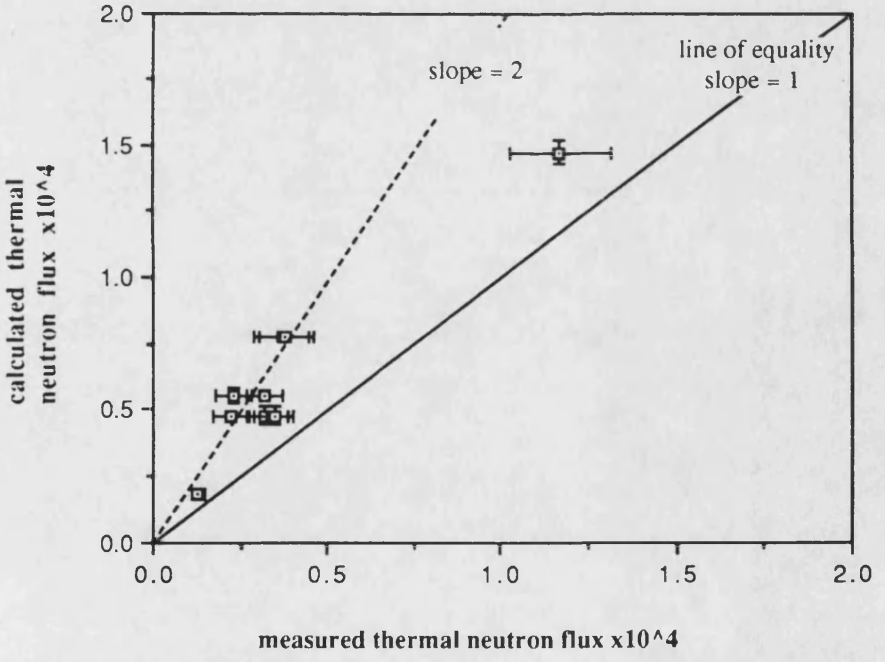

Fig. 3.10. Measured thermal neutron flux plotted against calculated thermal neutron flux (linear scales).

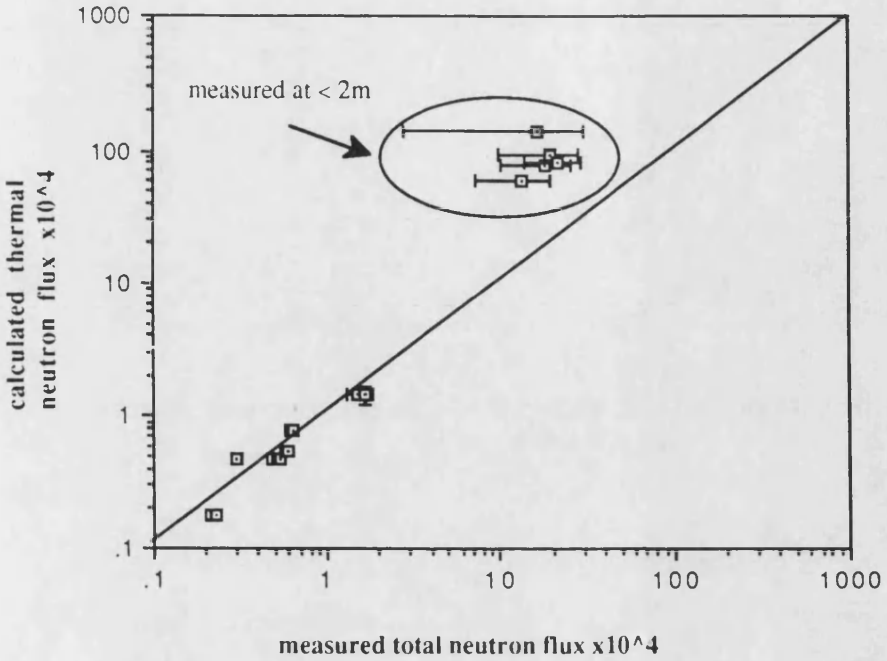

Fig. 3.11. Measured total neutron flux plotted against calculated thermal neutron flux (log scales).

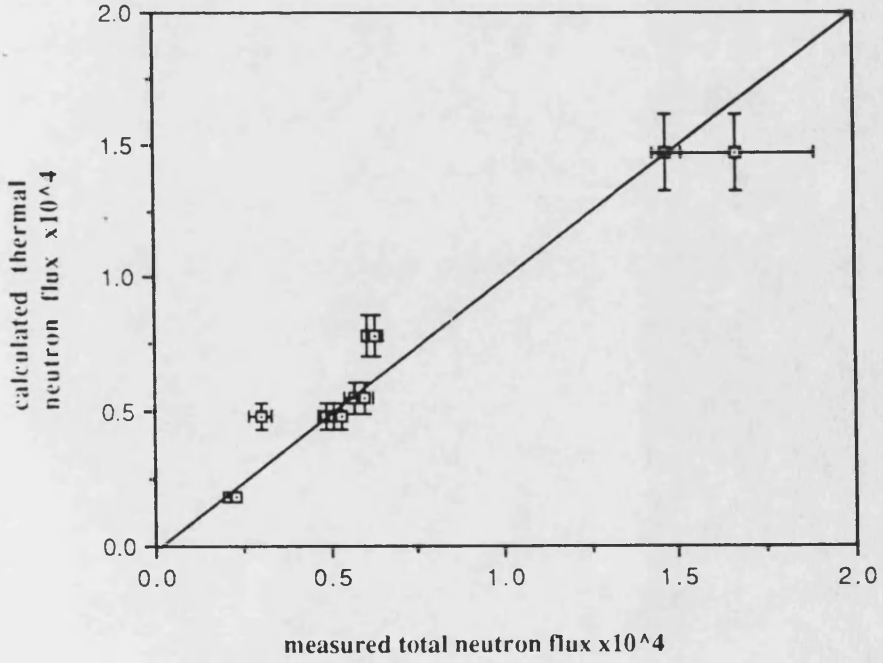

Fig. 3.12. Measured total neutron flux plotted against calculated thermal neutron flux (linear scales).

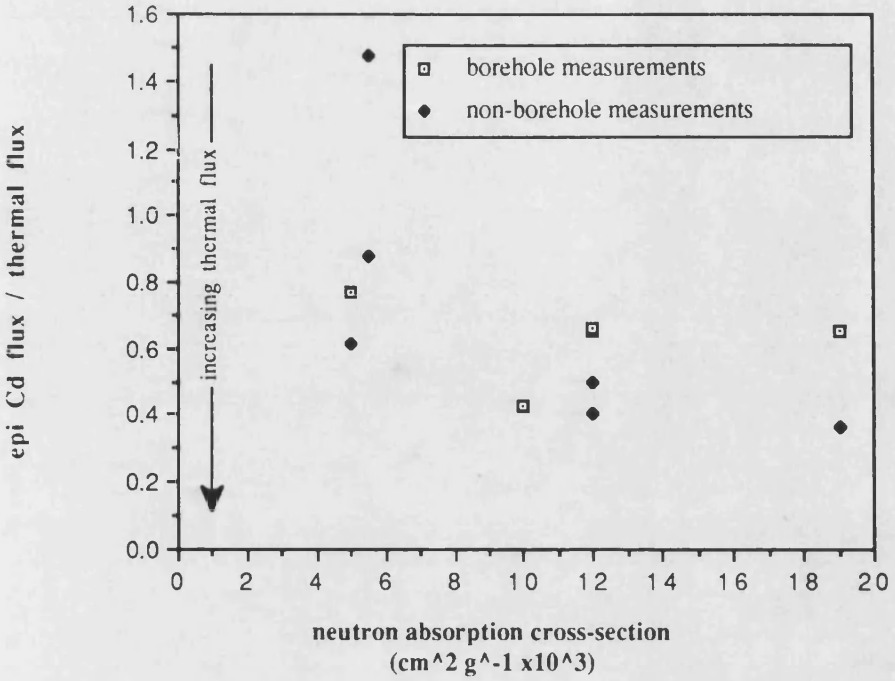

Fig. 3.13. Neutron absorption cross-section (Σ_m) plotted against measured epi-Cd flux ratio (R_{Cd}), for borehole and non-borehole measurements.

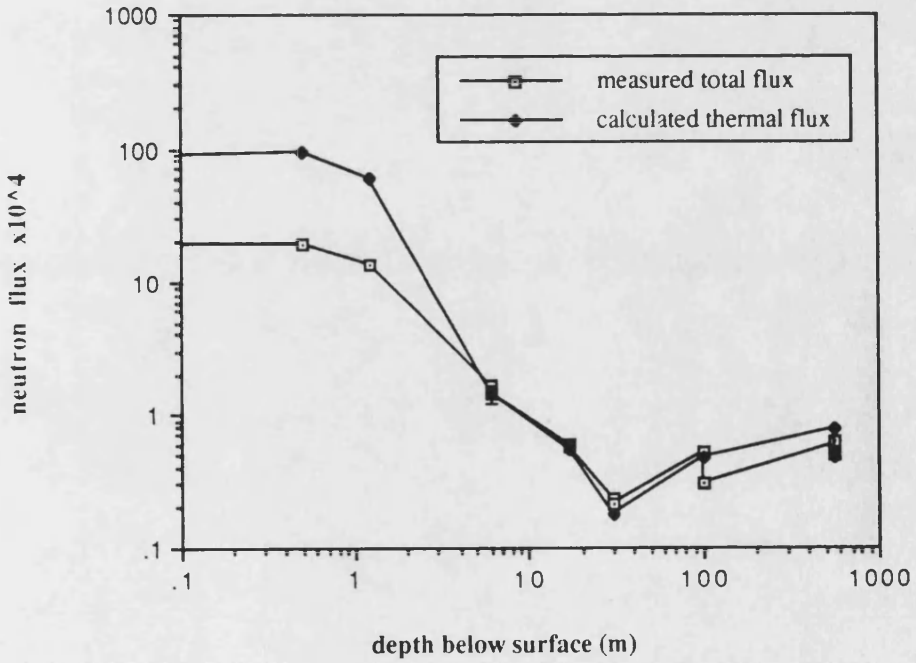

Fig. 3.14. Depth below surface plotted against measured measured total neutron flux.

4.0 NUCLIDE PRODUCTION IN THE SUBSURFACE.

4.1 Introduction.

The production of neutrons and attenuation of cosmic ray primary and secondary particles have been discussed in Section 2. This Section uses the proposed thermal neutron fluxes and cosmic ray intensities derived in Sections 2 and 3 to discuss the relative importance of various in-situ production reactions for :- ^{3}H, ^{14}C, ^{36}Cl, ^{37}Ar and ^{39}Ar.

The discovery, atmospheric production, detection and application of each of these isotopes in geochemical studies are briefly discussed in Section 1. Each may be produced by a multitude of naturally occurring nuclear reactions which include the direct interaction of cosmic ray primary or secondary particles, the decay of other radionuclides and the interaction of neutrons produced from spontaneous fission, (α,n) or cosmic ray induced processes. The estimation of production rates due to these reactions is introduced generally in Section 4.1.1 and discussed in more detail in Sections 4.2 to 4.6. As well as discussing the production of each isotope each Section also attempts to assess the likelihood of the produced nuclide migrating into a flowing groundwater based on criteria given in Section 4.1.2.

4.1.1 Production reactions

The reactions considered for the production of each isotope fall into four groups:-

(a) Reactions involving the interaction of cosmic ray primary or secondary particles.

(b) The decay of other radionuclides.

(c) The interaction of neutrons produced from spontaneous fission, (α,n) or cosmic ray induced processes.

(d) Other low energy reactions.

Reactions in group (a) are due to the interaction of high energy protons, muons and pions which are present in the regolith to a depth of 60m (see Section 2). High energy protons and secondary pions mainly interact with nuclei at the Earths surface by spallation. Production rates due to these particles have been calculated from a mixture of theoretical & measured reaction rates, and attenuation coefficients. Appropriate corrections have been made for matrix composition and altitude/latitude effects. Reactions with muons are less

energetic and the compound nucleus generally de-excites by the emission of one or more neutrons. The emission of small numbers of charged particles is also possible following muon capture and the most recent data have been used to extrapolate results to the nuclides detailed above. Production rates from muon induced reactions have been calculated from experimentally derived muon stopping rates and capture and emission probabilities (see Section 2).

Of the isotopes detailed above only ^{14}C is the product of nuclear decay by naturally occurring isotopes. The production rate of ^{14}C due to the bi-modal decay of U and Th series isotopes has been calculated based on the most recent data.

Reaction (c) would be expected to yield the highest production rate below the influence of the cosmic ray particles described above (60m). The production rate due to these reactions has been calculated based on the best available cross-section data. The rates due to neutrons produced from the interaction of cosmic ray primaries and secondaries have also been calculated. As stated in Section 3 the theoretically predicted thermal neutron flux produced in the upper meter of the Earths surface is not consistent with measurements made during the course of this thesis. Since reasons for this are at present unclear it was decided to calculate production rates based on the theoretical estimates which agree with those made elsewhere.

Other reactions such as (α,X) and (p,X) reactions where X may be any particle have been considered for the production of the isotopes detailed above. Calculation of production rates are given where appropriate.

4.1.2 Nuclide transport.

As the concentration of isotopes of interest to this study are more often measured in groundwaters (due to their present in rock matrices at very low concentrations, and given that they may be more easily concentrated and separated from groundwaters) the mechanisms of transfer of in-situ produced nuclides from their site of production and into flowing groundwater must be considered. Two major modes of transport may be envisaged :-

(a) The isotope once produced moves away from the site of production and into flowing groundwater. This movement may be as a result of diffusion or the "recoil" of reacting nuclei. This process will be referred to as "direct injection".

(b) The isotope once produced accumulates at the site of production until, at some later stage the isotope is released into the flowing groundwater due to weathering. This process will be referred to as "delayed injection".
The criteria for estimating the importance of these processes are discussed in Section 4.1.2.1.

4.1.2.1 Transfer process (a) "direct injection". The transfer of nuclides into groundwater by this process will be dependent upon their kinetic energy of formation, their half life, their diffusive properties, the ease with which they may be accommodated in their immediate crystalline surroundings and upon the distance between their site of production and the flow porosity of the matrix. It is not generally possible to assess all of these parameters and two approaches have been adopted to estimate the extent of transport from the rock matrix into a groundwater.
(1) A maximum concentration in the groundwater may be estimated on the assumption that all of the radionuclides produced within the rock matrix are transferred to fluids present in pore spaces. In the case of an interstitial flow system (such as may be found in a sandstone aquifer) the rock porosity is host to the groundwater. However for crystalline rocks water may be present bound to the crystalline lattice, as non-conductive fluid inclusions, and as fracture fluids. Thus in crystalline rocks areas of flowing groundwater may be far removed from production sites. Using this method the resulting concentration of a nuclide in fracture fluids (${}^{w}\tilde{N}$) (cm^{-3}) may be calculated given its equilibrium concentration in the rock matrix ($\tilde{N}$) (cm^{-3}) and the matrix porosity (p) (%) using :-

$$ {}^{w}\tilde{N} = \tilde{N} \frac{1}{p * 0.01} \qquad \text{Eqn. 4.1} $$

This estimate is independent of the micro-distribution of radionuclide production in relation to the aqueous phase.

(2) Such a total transfer model as discussed above is not well suited to the problem of estimating transfer of isotopes into the fracture fluids of crystalline rocks such as granites. A more appropriate method of estimation should assess the migration of isotopes from their in-situ production sites into the fracture fluids. Such migration can only take place over relatively short distances which are determined by the recoil energy, half life, and diffusive properties of the produced isotope. The resulting concentration in the fracture fluids is consequently strongly influenced by any enhanced in-situ production in secondary fracture mineralisation.

For this fracture based model (see Fig 4.1), isotope concentrations in the fluids depend upon the fracture width (fracture widths may be estimated from the ^{222}Rn contents of groundwaters (ANDREWS et al., 1986)); upon the composition of the fracture walls (newly fractured or mineralised surfaces) and upon the migration distance from the fracture wall. If the above are known the resulting maximum concentration in a fracture fluid may be calculated by assuming complete transport of the nuclide from a distance l_t (defined by its diffusive properties, half-life and recoil energy) either side of the fracture into the fluid filled fracture volume. ANDREWS et al (1986) consider that fractures in crystalline rocks are essentially planar. Using this approximation the concentration of in-situ produced nuclide in fracture fluids ($^{w}\tilde{N}$) (cm^{-3}) may be calculated using:-

$$ {}^{w}\tilde{N} = \frac{4\ l_t}{f_w}\ \tilde{N} \qquad (cm^{-3}) \qquad \text{Eqn.4.2} $$

where l_t is the transport length for the nuclide of interest in fracture wall material (μm), f_w is the average fracture width (μm) and $\tilde{N}$ is the concentration of nuclide in fracture wall material (cm^{-3}). An accurate evaluation of l_t for each of the nuclides of interest is not possible since l_t would be expected to be site specific (it would depend upon the partition of diffusion between lattice diffusion and "inter-pore diffusion"). For this reason an "average" value of 150 μm has been assumed in crystalline rocks (ANDREWS et al.,

1989). From a qualitative viewpoint l_t would be larger for inert gases with long half-lives (^{39}Ar) or large recoil energies (^{85}Kr). l_t would be expected to be small for nuclides such as ^{3}H and ^{14}C which may be fixed" by chemical reactions within the rock matrix. The relative importance of each of the discussed parameters for specific isotopes are evaluated in Sections 6.2 to 6.6.

4.1.2.2 Transfer process (b) "delayed injection". In this process the isotope once produced accumulates at the site of production until, at a later stage the isotope is transported into the flowing groundwater due to "weathering" processes. These weathering processes may either be dissolution of minerals forming the production site or mechanical processes such as fracturing.

Groundwaters exhibit a range of chemical compositions which may be related to the mineralogical and chemical constitution of the enclosing rock. Under flow conditions groundwaters constantly adjust their composition to that of the new environment by dissolution and precipitation of minerals. The amount of isotope released during the dissolution process, will depend on the degree of undersaturation of the fluid with respect to the mineral it is in contact with, and the fluid contact time (ie/ is both thermodynamically and kinetically controlled). The rate of release of isotopes into the flowing groundwater by this method may be estimated from a knowledge of the prevailing thermodynamic conditions (estimated from chemical analysis and equilibrium models such as WATEQ), fluid flow rates and fracture widths (calculated from either isotopic or chemical tracers). The total amount of isotope that may be released into the groundwater depends upon the time since the mineral/rock matrix became closed. In the case of radio isotopes produced within the mineral phases of the rock matrix secular equilibrium will most probably have been achieved and maximum concentrations may be found by assuming that all of the isotope is removed into the volume of fluid required to dissolve an equal quantity of mineral/rock matrix. Similar calculations may be made for the case of stable isotopes produced by the decay of in-situ radioisotopes. In this case however the exact time since the mineral/rock matrix became closed must be estimated as the concentration of the isotope is integrated with respect to time.

Isotopes may also be removed from groundwater by precipitation of minerals, for instance Evans et al (1984) have shown that ^{14}C is removed from modern water by exchange with ^{14}C dead carbon in calcite. The relative importance of this removal process depends upon the solubility and equilibrium dynamics of each species. For instance the equilibrium constant for the reaction:-

$$Cl^-(S) \text{ ----- } Cl^-(aq)$$

lies far to the right hand side and remains relatively unaffected by pH. However the equilibrium constant for the reaction :-

$$CaCO_3(S) \text{ ------- } Ca^{2+}(aq) + CO_3^-(aq)$$

lies much nearer the left hand side and is very sensitive to pH conditions. Inert gases such as Ar may also be incorporated into vacant sites within precipitating minerals although this effect should be small as this would raise the disorder of the crystal and hence decrease its stability.

The relative importance of these processes compared to that of the direct injection process is discussed for each nuclide in Sections 4.2 to 4.6.

4.2 Production of Tritium

The production of ^3H in the terrestrial environment is discussed briefly in Section 1. As well as being useful as an indicator of groundwater age decay of ^3H is also a major source of ^3He in crustal rocks (MORRISON and PINE., 1958 and LAL., 1987). The following Sections first examine how ^3H could be produced in the subsurface and then assess processes by which ^3H may escape from its production site and into the water phase. Processes leading to the production of ^3H in the subsurface are summarised in Fig 4.2.

4.2.1 Low energy neutron induced reactions.

MORRISON and PINE, (1955) first suggested that ^3H (and thence ^3He) could be produced via the $^6Li(n,\alpha)^3H$ reaction. The production of neutrons which initiate this reaction are discussed in Section 2. The production of ^3H from these neutron induced reactions follows the variation in neutron production rate and consequently neutron flux with composition and depth below the air ground interface. Thus at depths greater than 60 meters the major source of neutrons is spontaneous fission and (α,n) reactions. Up to these depths

neutron production is mainly due to cosmic ray secondaries. ^{3}H may also be produced to a smaller extent by the neutron induced reactions :-

(a) $^{2}H(n,\gamma)^{3}H$

(b) $^{3}He(n,p)^{3}H$

(c) $^{10}B(n,2\alpha)^{3}H$

All of these reactions have much smaller cross-sections than the $^{6}Li(n,\alpha)$ reaction, and consequently have correspondingly low production reaction rates except in situations where the abundance of the respective target isotope is high in comparison to that of Li. The abundance of ^{2}H and ^{3}He in rock matrices is very low, making the contribution to the total ^{3}H production rate from reactions (a) and (b) extremely small. The cross-section for reaction (c) is about 1 barn (LAL and CRAIG pers comm, 1986) hence the contribution from this reaction would be insignificant for many rock matrices. However if the B to Li concentration ratio exceeds 55 then the contribution from reaction (c) exceeds 10% of the total production rate and hence may no longer be considered insignificant. Assuming that the relative contributions from these reactions are small the production rate for a given neutron flux and rock composition may be calculated from equation 4.3.

$$N_{H3} = \phi \ (\ n_{Li} \ \sigma_{Li} \ ) \qquad \text{Eqn. 4.3}$$

where N_{H3} is the ^{3}H production rate ($g^{-1}\ a^{-1}$) for a given altitude, geomagnetic latitude and depth below the air/ground interface, n_{Li} is the number of atoms of $^{6}Li\ g^{-1}$, σ_{Li} is the (n,α) reaction cross-section for ^{6}Li in cm^{2} and ϕ is the neutron flux ($cm^{-2}\ a^{-1}$). Results of such calculations made for a number of average rock types are given in Table 4.1. The variation of neutron flux with depth discussed in Section 3 means that the production rate of ^{3}H also varies with depth in a similar manner. The depth profile for ^{3}H production due to neutron induced processes at a given geomagnetic latitude and altitude is shown in Fig 4.3.

4.2.2 Low energy (p,x) reactions.

Simple (p,x) reactions such as (p,α), (p,γ) and (p,n) which have a relatively low energy threshold do not contribute ^{3}H to the epigene zone because of the lack of suitable target

nuclides. Reactions involving the emission of even a number of particles (p,2n), (p,2p) etc having much higher energy thresholds (> 10 MeV) which are well below the typical energies of cosmic protons (10-500 MeV) will again not contribute ^{3}H due to the lack of suitable target nuclides. However reactions such as $^{A}X(p,^{3}H)^{A-4}X$ would be expected to produce significant levels of ^{3}H in surface rocks even though their reaction threshold energies are greater than 10 MeV (REEDY and ARNOLD., 1972). YOKOYAMA et al (1977) calculated a "surface" ^{3}H production rate for spallation and low energy proton reactions of 117 atoms $g^{-1}a^{-1}$ when corrected to sea level and a geomagnetic latitude of >60° N. Their calculated rate did not vary by more than 5% between granite, limestone and basalt. This is consistent with the major production reactions being due to O and other light elements, whose concentration does not change greatly between these rock types. (see Section 4.2.4)

4.2.3 Negative muon capture reactions.

High energy protons react with nuclei (N_2, O_2 and Ar) in the stratosphere causing evaporation of pions during braking, these in turn decay into muons. Muons either decay to neutrinos before interacting, or react with nuclei at or below the Earths surface.
Both negative muons and negative pions may be captured according to reaction schemes discussed in Section 2.4.1. Once capture has taken place the excited nucleus may de-excite by the emission of a particle or group of particles. Tritium may be produced in this process as either the product of a reaction (ie/ $^{6}Li(\mu,p2n)^{3}H$) or as the emitted particle (ie/ $^{A}_{Z}X(\mu,^{3}H)^{A-3}_{Z-2}X$).

The probabilities for these reactions are smaller than those for neutron emission following capture since they require the emission of charged particles through the Coulombic barrier. However the height of the Coulombic barrier increases with atomic number, so the probability of these reactions should increase with decreasing atomic number. WYTTENBACH et al (1978) have measured the probabilities for these types of reactions. Their method however, only measures the probability of the loss of one proton and two neutrons and does not measure the emission of one discrete ^{3}H nuclei. They do, report that the ratio of the probability of the emission

of a deuteron to that of the emission of one proton and one neutron is 6, this may be used to estimate the lower limit for the production of ^{3}H by this process since the nuclear binding energy for ^{3}H is three times that of deuterium (hence making the emission of a discrete particle more probable). Interpolation of their results give fractional reaction probability R_p values for the reactions :-

(a) $^{6}Li + ^{-}\mu \text{ --- } ^{6}He^{*} \text{ --- } ^{3}H + p2n$

(b) $^{16}O + ^{-}\mu \text{ --- } ^{16}N^{*} \text{ --- } p2n + ^{13}C$

(c) $^{28}Si + ^{-}\mu \text{ --- } ^{28}Al^{*} \text{ --- } p2n + ^{25}Mg$

Of 0.09 to 0.015, 0.05 to 0.008 and 0.026 to 0.004 respectively. The production rate of ^{3}H due to these reactions (N_{H3} g^{-1} a^{-1}) may be calculated following the method of CHARALAMBUS (1969).

$$N_{H3} = \frac{N_d \, M_z \, P_z \, r_z \, R_p}{{}_i\Sigma \, M_i \, P_i} \qquad \text{Eqn. 4.4}$$

where N_d is the negative muon stopping rate (g^{-1} a^{-1}) at depth d (see Section 2.4.2), M_z and M_i are the fractional molar abundance of elements z or i, P_z and P_i are the probability that the stopped muon is captured by the muonic 1S level of element z or i relative to that for Oxygen, r_z is the probability that the captured muon reaches the nucleus of element z before decaying and R_p is the fractional reaction probability for the emission of one discrete particle. (The range of elements over which summation of M_iP_i should be carried out is discussed in Section 2.4). Values of N_d, P_z and r_z are given in Table 2.16. The results of calculations of N_{H3} for an average sandstone (Analysis of PARKER., 1967) are given in Table 4.2.

From these it can be seen that the largest contribution to the ^{3}H production rate is from reaction (b) due to the large abundance of O. This is likely to be so for all of the average rock types described in Appendix 1 since the abundance of O is approximately constant at 50 +/- 10 %. The yield from reaction (a) is negligible due to low abundance of Li and that

of reaction (c) is low because of the lower abundance of ^{28}Si and smaller reaction probability. The relative importance of these reactions compared to other production reactions are discussed in Section 4.2.6.

4.2.4 Spallation reactions.

High energy protons react by colliding with nuclei to produce spallation products which consist of light nuclei and residual "heavy" nuclei. Spallation reactions between protons, and O and Al nuclei have been shown to be a source of ^{3}H in the epigene zone of the moon and hence similar reactions would be expected to produce ^{3}H in the terrestrial epigene zone (REEDY and ARNOLD., 1972, YOKOYAMA et al., 1977, KURTZ et al., 1986). Since the majority rock matrices contain mainly low Z elements the ^{3}H production rate is independent of rock composition (see Table 4.3). YOKOYAMA et al (1977) has calculated ^{3}H production rates for both types of proton induced reactions (see Section 4.2.2). The production rate due to these reactions will follow the variation of the cosmic proton flux with height and geomagnetic latitude (see Section 2.3). Using this variation and the attenuation coefficient for the absorption of protons from cosmic rays (Section 2.3) the production rate of ^{3}H due to these spallation reactions may be calculated at different depths below the air/ground interface for a rock of average composition. This depth variation has been calculated for an average granite, sandstone and limestone (Table 4.4). The depth variation for an average granite is shown in Fig 4.3. The relative importance of this reaction compared to other production reactions are discussed in Section 4.2.6.

4.2.5 Spontaneous and neutron induced fission reactions.

The amount of ^{3}H produced during neutron induced fission of ^{235}U and spontaneous fission of ^{238}U is theoretically small since this would require ternary fission which is energetically unfavorable. MAMYRIN and TOLSTIKHIN (1984) estimated ^{3}H production based on interpolation of measured fission yields for the elements U to Cf. Their results indicate that ^{3}H produced from these reactions is insignificant compared to other production reactions.

4.2.6 Summary of ^{3}H production reactions.

The contribution to the total ^{3}H production rate from

each of these reactions is summarised for the average rock types granite, sandstone and limestone in Table 4.4. From this table it can be seen that:-

(a) Spallation reactions produce the majority of ^{3}H near the Earths surface. The magnitude of this production does not vary greatly between rock types and is negligible below 5 meters.

(b) Low energy neutron reactions ($^{6}Li(n,\alpha)$) produce significant quantities of ^{3}H near the surface. The exact magnitude of these production rates depend upon the thermal neutron flux at the surface and the Li concentration of the matrix. Values in Table 4.4 reflect the maximum rates based on all produced neutrons reaching thermal energy. At depths below the influence of cosmic rays this reaction is responsible for production of ^{3}H.

(c) The rate of production due to negative muon capture reactions depend on the reaction probability. If upper limits for the reaction probability are used, then these reactions yield production rates of ^{3}H as high as that produced by neutron induced reactions in rocks with a low Li content. The majority of ^{3}H is produced by negative muon capture on oxygen and thus these production rates are virtually independent of rock composition.

Fig 4.3 shows the depth variation of the production rate in an average granitic rock. From this it may be seen that the production rate of ^{3}H below 2m is predominantly due to low energy neutron induced reactions with ^{6}Li. A similar profile would be expected for the production of ^{3}He from beta decay of ^{3}H.

4.2.7 Transport of in-situ produced ^{3}H.

As discussed in the above Section the major source of ^{3}H in rock matrices is Li. Any discussion of how ^{3}H enters a flowing groundwater should thus first consider the distribution of this element.

In crystalline rocks Li generally occurs in the minerals muscovite and biotite and less commonly in lepidotite, zinnwaldite, spodumene, tourmaline, hectorite and amblygonite. In sedimentary rocks Li may be present either where the minerals mentioned above are present as detrital material or as residual salts precipitated from fluids. In both of these cases Li may be inhomogenously distributed on both the micro

(sub mm) and macro scales throughout the matrix. Inhomogeneity on the macro scale being created by secondary and tertiary mineralisation associated with hydrothermal activity. Each of these minerals provided they are not large compared to the associated neutron pathlength in the mineral will experience the average neutron flux and produce ^{3}H.

The degree of inhomogeneity will be site specific and it is thus difficult to generalise, however the general treatment below should be applicable to all of the above minerals.

In a typical system the following processes may lead to transport of in-situ produced ^{3}H (ANDREWS et al., 1989).

(a) Ejection into pore water.

(b) Exchange with hydrogen in bound/free water molecules.

(c) Exchange with hydroxyl sites in the crystal lattice.

Following the $^{6}Li(n,\alpha)$ reaction ^{3}H nuclei are emitted as free radicals with a maximum energy of 2.73 MeV. This gives it a range in typical crystal lattices of 0.0035 cm (WILLIAMSON et al., 1966). Thus ejection of tritium into pore fluids followed by exchange with H in free water molecules would be more important in highly porous media such as sandstones than in crystalline rocks such as granite.

If the in-situ produced ^{3}H does not enter the fracture fluids directly then it may either exchange with bound water or hydroxyl sites within the crystalline lattice. To enter the flowing groundwater this bound ^{3}H must then be released by alteration processes. This may well be the case in the Cornish granites (Section 6) where EDMUNDS et al (1986) have shown that release of Li by hydrolysis of biotite readily occurs. Such release of Li must also be accompanied by release of stored in-situ ^{3}H.

4.3 Production of Carbon-14

A number of authors have previously considered subsurface production of ^{14}C, and their conclusions are reviewed in ZITO et al., 1980. However their considerations were limited to either the production of ^{14}C by the alpha induced reaction $^{11}B(\alpha,p)^{14}C$ or via the neutron induced reactions $^{13}C(n,\gamma)^{14}C$, $^{14}N(n,P)^{14}C$ and $^{17}O(n,\alpha)^{14}C$ (See Fig 4.4). This work reviews the importance of the recently discovered rare decay of U and Th series nuclides, the production of ^{14}C via negative muon capture processes and the probability of the produced ^{14}C entering groundwater.

4.3.1 Low energy neutron induced reactions.

The production of ^{14}C from low energy neutron induced reactions follows the variation in neutron production rate and consequently neutron flux with matrix composition and depth below the air ground interface. Thus at depths greater than 60 meters the major source of neutrons is spontaneous fission and (α,n) reactions (see Section 2). Up to these depths neutron production is mainly due to cosmic ray secondaries. ^{14}C can be produced by the neutron induced reactions :-

(a) $^{14}N(n,p)^{14}C$

(b) $^{17}O(n,\alpha)^{14}C$

(c) $^{13}C(n,\gamma)^{14}C$

All of these reactions are exothermic and have well known thermal neutron cross-sections (1.83, 0.235 and 0.0014 barns respectively (MUGHABGHAB et al., 1981).

The production rate of ^{14}C due to these reactions may be calculated from :-

$$N_{C14} = \phi \ (\ n_N \ \sigma_N \ ) \ (n_O \ \sigma_O) \ (n_C \ \sigma_C) \qquad \text{Eqn. 4.5}$$

where N_{C14} is the ^{14}C production rate (g^{-1} a^{-1}) for a given altitude, geomagnetic latitude and depth below the air/ground interface, n_N, n_O and n_C are the number of atoms of ^{14}N, ^{17}O and ^{13}C g^{-1} respectively. σ_N, σ_O and σ_C are the (n,p), (n,α) and (n,γ) reaction cross-sections for reactions (a), (b) and (c) in cm^2 and ϕ is the neutron flux (cm^{-2} a^{-1}).

The production rates of ^{14}C due to reactions (a), (b) and (c) have been calculated for an average sandstone, granite and limestone (analysis of PARKER et al., 1967) (Table 4.5). These results are consistent with the conclusions of ZITO et al (1980) and ANDREWS et al (1988) which state that the low cross-section and abundance ^{13}C make the production of ^{14}C by reaction (c) insignificant with respect to ^{14}C produced by reactions (a) and (b). The low cross-section for reaction (b) is in many cases compensated for by the high abundance of O compared to N. ANDREWS et al (1989) showed that the reactions (a) and (b) produce almost equal amounts of ^{14}C in both silicate rocks and groundwaters, the exact proportion depending on the N content of the matrix and/or fluid.

The variation of neutron production rate with depth discussed in Section 2 means that the production rate of ^{14}C

also varies with depth in a similar manner. The production rates of these reactions have been calculated at varying depths below the surface for an average granite, limestone and sandstone (Appendix 1) see Table 4.9. The importance of these reactions with respect to others production processes are reviewed in Section 4.3.7.

4.3.2 Low energy alpha induced reactions

ZITO et al (1980) suggested that the reaction $^{11}B(\alpha,p)^{14}C$ may produce significant levels of ^{14}C in rock matrices with high levels of U and Th. This reaction is similar to (α,n) reactions discussed in Section 2 in that the α particles arise from the decay of U and Th series isotopes. The reaction is endoergic with Q (the reaction energy) equal to 1.25 MeV and thus has no energy threshold. However the nuclear coulombic field inhibits the transmission of alpha particles with energies less than 3.4 MeV due to electrostatic repulsion (see Section 2). This repulsion effect would be expected to produce a similar "pseudo-threshold" energy dependence to that shown by the analogous $^{10}B(\alpha,n)^{13}C$ reaction (BAIR and GOMEZ del CAMPO., 1979).

The cross-section for this reaction should theoretically be smaller than that for many (α,n) reactions due to the transmission of a charged particle through the coulombic barrier in two directions, and have a "pseudo-threshold energy" of about 3.4 MeV. ZITO et al (1980) considered the cross-section for this reaction to be 20 mb for natural series α particles, however a reappraisal of their method by JULL et al (1988) has estimated a cross-section of 120 mb for natural series α particles. Both of these authors used the concept of "average natural series α particle energy" for their calculations, it would however be better to have used a similar approach to that used for estimating thick target (α,n) yields (see Section 2). This would also correct for the energy loss of the α particle during its travel through the matrix. Unfortunately time has not allowed this to be carried out but the results should be interesting as they could be applied to other isotopes produced by (α,p) reactions (in particular $^{7}Li(\alpha,p)^{10}Be$). The amount of ^{14}C produced by this reaction is thus difficult to estimate, however using the above range of cross-sections and the methods of ZITO et al (1980) and BARKER et al (1985) it is possible to calculate the equilibrium number of ^{14}C atoms produced by this reaction for

a matrix of known B, Th and U concentration. The method used by these authors states that production rate ^{14}C atoms (N_{C14}) (g^{-1} s^{-1}) is :-

$$N_{c14} = \phi_\alpha \, N_{B11} \, \sigma_\alpha \qquad \text{Eqn. 4.6}$$

where ϕ_α is the α particle flux (cm^{-2} s^{-1}), N_{B11} is the number of ^{11}B atoms g^{-1}, and σ_α is the reaction cross-section (cm^2). The αparticle flux is defined as :-

$$\phi_\alpha = R_\alpha \, o \, (\alpha_{Th} + \alpha_U) \qquad \text{Eqn. 4.7}$$

where R_α is the range of α particles (cm) in a silicate matrix, o is the matrix density (g cm^{-3}), and α_{Th} and α_U are the α production rates from U and Th series isotopes. In the calculation of ϕ_α I have assumed an median range for U and Th series α particles of 0.0025 cm (FAURE.,1986), and α particle production rates of 0.0039 and 0.098 s^{-1} for 1 μg^{-1} of Th and U respectively in equilibrium with their daughters (see Section 2).

It should be noted that the range of an α particle depends on its energy and the composition of the matrix, and that the value used here (0.0025 cm) reflects an approximate estimate to reduce the number of variables required in the calculation of N_{C14}. The production of ^{14}C by these reactions would be expected to be of most importance in matrices which have high U and Th together with an appreciable quantity of B. For this reason N_{C14} was calculated for two matrices, a high U, Th granite with low B (represented by the Stripa granite) and a granite enriched in B (represented by the Carnmenellis granite) the results of these calculations are given in Table 4.6. This reaction should also be an important source of ^{14}C in U and Th ores however this is not within the scope of the present work and the reader is guided to BARKER et al (1985) and JULL et al (1988).

The relative importance of these reactions is discussed later in this section, however a cautionary note should be made that since these reactions are initiated by α particles which have a short range in rock matrices the spatial distribution of α source and target nuclides is of great importance, especially since the abundance of B is generally

low.

4.3.3 Low energy (p,x) Reactions.

Simple (p,x) reactions such as (p,α), (p,γ) and (p,n) which have relatively low energy thresholds do not contribute ^{14}C to the epigene zone due to the lack of suitable target nuclides.

4.3.4 Negative muon capture reactions.

The production of negative muons from primary cosmic rays is discussed in Section 2. Negative muons may be captured according to the reaction schemes discussed in Section 2.4.1. Once capture has taken place the excited nucleus may de-excite producing ^{14}C. Where these reactions involve the emission of a charged particle their reaction probabilities will be low compared to those for neutron emission due to the Coulombic barrier. However the height of the Coulombic barrier increases with atomic number, and the probability of charged particle emission will be greater for elements of low atomic number. The only reactions involving negative muon capture which could produce significant quantities of ^{14}C in the subsurface are :-

(a) $^{16}O + {}^{-}\mu \text{ --- } {}^{16}N^{*} \text{ --- } {}^{14}C + pn$

(b) $^{17}O + {}^{-}\mu \text{ --- } {}^{17}N^{*} \text{ --- } {}^{14}C + p2n$

(c) $^{15}N + {}^{-}\mu \text{ --- } {}^{15}C^{*} \text{ --- } {}^{14}C + n$

The fractional probabilities of these reactions are 0.08, 0.05, and 0.2 respectively (interpolated from WYTTENBACH et al (1978) and CHARALAMBUS (1971)). N_{C14} the production rate of ^{14}C atoms due to these reactions ($g^{-1}a^{-1}$) may be calculated in a similar way to the calculation of ^{3}H by these reactions (see Equation 4.2.2).

Results of these calculations made for an average sandstone, granite and limestone (Analysis of PARKER., 1967) are given in Table 4.7.

From these results it can be seen that the ^{14}C production rate from these reactions are virtually constant for different rock types. This is due to the small variation in the abundance of O and total capture probability between rock types. It may also be seen that reaction (a) produces by far the greatest amount of ^{14}C due to negative muon reactions. The relative importance of these reactions compared to other production reactions are discussed in Section 4.3.7.

4.3.5 Spallation reactions.

High energy protons react by colliding with nuclei to produce spallation products which consist of light nuclei and residual "heavy" nuclei. Spallation reactions between protons and O nuclei (reaction threshold of 20 MeV) have been shown to be a source of ^{14}C in the epigene zone of the moon and hence the same reactions would be expected to produce ^{14}C albeit to a lesser extent in the terrestrial epigene zone (REEDY and ARNOLD., 1972, YOKOYAMA et al., 1977). Since most rock matrices contain mainly low Z elements the production rate of ^{14}C due to these reactions are effectively independent of rock composition. YOKOYAMA et al (1977) have calculated ^{14}C production rates for both low and high energy proton induced reactions of 12250 atoms Kg^{-1} a^{-1} at sea level and a geomagnetic latitude of 40°N. The production rates due to these reactions follow the variation of the cosmic proton flux with height and geomagnetic latitude (see Section 2.3). Using this variation and the attenuation coefficient for the absorption of cosmic ray protons the production rate of ^{14}C due to these spallation reactions may be calculated at different depths below the air/ground interface for a rock of average composition (see Table 4.9). The relative importance of this reaction compared to other production reactions are discussed in Section 4.3.7.

4.3.6 Spontaneous emission

The recent discovery (ROSE and JONES., 1984) that ^{223}Ra has a rare decay mode in which energetic ^{14}C nuclei are emitted has important implications for the in-situ production of ^{14}C in Uraniferous rocks. The probability of such decay is expressed as a branching ratio, for such bi-modal decay this is defined as :-

$$R = \frac{\lambda_c}{\lambda_c + \lambda_a} = \frac{\lambda_c}{\lambda_a} \qquad \text{Eqn. 4.8}$$

where λ_c and λ_a are the partial decay constants for ^{14}C and ^{4}He emission respectively. Theoretical estimates of the decay probability show that ^{14}C emission is most likely for Ac and Ra isotopes and that such decay by Th and U series isotopes is relatively unlikely (less than 10^{-4} times the probability for Ac and Ra) even though the reaction is energetically favourable for many of these isotopes. Recent experimental measurements yielded branching ratios of $5.9 \pm 0.6 \times 10^{-10}$ for ^{223}Ra (^{235}U series), $4.3 \pm 1.2 \times 10^{-11}$ for ^{224}Ra (^{232}Th series) and $2.9 \pm 1.0 \times 10^{-11}$ for ^{226}Ra (^{238}U series) (BARWICK et al., 1986; PRICE et al., 1985). BARKER et al (1985) have measured ^{14}C in uranium minerals and estimated an effective branching ratio for all ^{14}C-emitting isotopes present of 1.7×10^{-9} which they attributed mainly to exotic decay in the ^{238}U series. However, JULL et al (1988) have shown that most of the ^{14}C present in these minerals is produced by the reaction $^{11}B(\alpha,p)^{14}C$. The extent of production by such exotic decays in a number of rock matrices has been calculated (Table 4.8) on the basis of the measured branching ratios for ^{223}Ra, ^{226}Ra and ^{224}Ra. From this table it may be seen that although the yield from Th series isotopes is less than that from U series isotopes the production rate due to Th series isotopes may be as important in rocks with average Th:U ratios.

The relative importance of such reactions are further discussed in Section 4.3.7.

4.3.7 Summary of production reactions.

The contribution to the total production rate from low energy neutron induced reactions, spallation reactions and negative muon reactions are summarised for the average rock types sandstone, granite and limestone in Table 4.9. This table also illustrates the depth dependence of such reactions which are also displayed in Fig 4.5. By comparing the results in Table 4.9 with production rates calculated for low energy α particle and spontaneous emission reactions (Tables 4.6 and

4.8 respectively) it may be seen that :-

(a) Spallation reactions and $^{-}\mu$ capture reactions produce the majority of ^{14}C near the Earths surface. Whilst the magnitude of this production does not vary greatly with chemical composition differences in rock density mean that the rate at specific depths vary.

(b) Below the influence of cosmic ray protons ^{14}C is produced by $^{-}\mu$ capture reactions.

(c) Below the influence of negative muons significant amounts of ^{14}C may be produced by low energy α particle reactions and spontaneous emission. In rocks with a high U, Th and B content the production due to (α,p) reactions may greatly exceed that of low energy neutron induced reactions.

4.3.8 Transport of in-situ produced ^{14}C.

The above Section shows that ^{14}C may be produced by a number of reactions within a rock matrix each of which may occur in a major or minor mineral phase, in fluid inclusions, in fracture coatings or in fracture fluids. It may be produced in O sites which are distributed evenly throughout the matrix, in N sites where N may exist as NH_3 which has been found to replace K in micas, and U + Th and B sites.

The transport from each of these sites will differ when produced by low energy reactions recoil release will be low due to the small recoil energies produced by such reactions (<< 1 MeV), however spontaneous emission is highly energetic and significant release could occur via this process. Either during stopping or once stopped the carbon atom could become mobilised due to oxidation by reactions with silicate O to form CO_2 and may become incorporated into the complex carbonate equilibria.

4.4 Production of Chlorine-36.

Possible reactions for the production of ^{36}Cl in the subsurface discussed below and are summarised in Fig 4.6.

4.4.1 Low energy neutron induced reactions.

DAVIS and SCHAEFFER, (1955) suggested that ^{36}Cl may be produced in the surface layers of the Earth by the $^{35}Cl(n,\gamma)^{36}Cl$ reaction. At larger depths they suggested that this reaction could also produce ^{36}Cl due to neutrons from (α,n) reactions on light nuclei. Production processes for

neutrons are discussed in greater detail in Section 2. The production of ^{36}Cl from these reactions follow the variation in neutron production rate and consequently neutron flux with composition and depth below the air ground interface. Thus at depths greater than about 60 meters the major sources of neutrons are spontaneous fission and (α,n) reactions. Up to these depths neutron production is mainly due to cosmic ray secondaries. The production rate for a given neutron flux and rock composition due to these reactions may be calculated from equation 4.9.

$$N_{Cl36} = \phi \, ((n_{Cl} \, \sigma_{Cl}) + (n_K \, \sigma_K)) \qquad \text{Eqn. 4.9}$$

where N_{Cl36} is the ^{36}Cl production rate (g^{-1} a^{-1}) for a given altitude, geomagnetic latitude and depth below the air ground interface, n_{Cl} and n_K are the number of atoms of ^{35}Cl and ^{39}K g^{-1}, σ_{Cl} and σ_K are the (n,γ) and (n,α) reaction cross-sections for ^{35}Cl and ^{39}K in cm^2 and ϕ is the thermal neutron flux (cm^{-2} a^{-1}) at the given altitude, latitude and depth below the air ground interface. For most rocks production from the $^{39}K(n,\alpha)$ reaction is insignificant compared to the $^{35}Cl(n,\gamma)$ reaction due the latter comparatively large cross-section (44 compared to 0.0043 barns (MUGHABGHAB et al., 1981)). However for rocks which have a K/Cl concentration ratio of greater than 900 the contribution from the K reaction is no longer insignificant and exceeds 10% of the production from Cl. For the average rocks defined by PARKER. (1967) this condition is only fulfilled by a sandstone and thus in most cases the K reaction may be ignored.

The variation of neutron flux with depth discussed in Section 3 means that the production rate of ^{36}Cl also varies with depth in a similar manner. The depth profile for ^{36}Cl production due to neutron induced processes at a given geomagnetic latitude and altitude is shown in Fig 4.7.

4.4.2 Low energy (p,x) reactions.

Simple (p,x) reactions such as (p,α), (p,γ) and (p,n) which have a relatively low energy threshold are unlikely to contribute ^{36}Cl to the epigene zone due to the low abundance of suitable target nuclides which would produce ^{36}Cl (ie/ S and Ar). Reactions involving the emission of even a number of particles (p,2n), (p,2p) etc having much higher energy

thresholds (> 10 MeV) which are well below the typical energies of cosmic protons (10-500 MeV) will contribute little in the way of ^{36}Cl since again suitable target isotopes are only present in trace quantities.

4.4.3 Negative muon capture reactions.

High energy protons react with nuclei in the high atmosphere (O, Ar, etc) causing evaporation of muons and pions during braking. Pions then either interact with matter or decay into muons. Negative muons may be captured according to reaction scheme discussed in Section 2.4.1. Once captured the excited nucleus may de-excite by the emission of a charged particle or group of charged particles to produce ^{36}Cl. The probability that these reactions contribute significant amounts of ^{36}Cl is theoretically low since they involve the emission of charged particles through the Coulombic barrier. Production by the emission of neutrons following capture to produce ^{36}Cl is insignificant since the reactions would require Ar as the target material. WYTTENBACH et al (1978) measured the probabilities for reactions such as (μ,pxn) and (μ,α) on elements from Na to Bi. Their results show a good correlation between the height of the Coulombic barrier of the product nucleus and the fractional reaction probability (R_p). Interpolation of their results give R_p values for the reactions :-

$$^{39}K + ^{-}\mu \text{ --- } ^{39}Ar^{*} \text{ --- } 2n + p + ^{36}C$$
$$^{40}Ca + ^{-}\mu \text{ --- } ^{40}K^{*} \text{ --- } \alpha + ^{36}Cl$$

Of 0.02 and 0.0026 respectively. However KUBIC et al (1984) have suggested an R_p value of 0.14 for the reaction $^{40}Ca(^{-}\mu,\alpha)^{36}Cl$ which is approximately two orders of magnitude larger than those interpolated from the data of WYTTENBACH et al (1978). This difference cannot be explained by error in the interpolation and suggests that the calculated value of KUBIC et al (1984) should be treated only as a maximum upper limit. I have assumed that the value of R_p for the reaction $^{40}Ca(^{-}\mu,\alpha)^{36}Cl$ is more likely to be 0.0026 as this is based on interpolation of measured values. The production rate of ^{36}Cl due to these reactions N_{Cl36} may be calculated in a similar way to that used to calculate ^{3}H production from negative muon capture (see Section 4.2.3).

The results of calculations of N_{Cl36} for an average sandstone and limestone (Analysis of PARKER., 1967) are given

in Table 4.10. From these it can be seen that for rocks with a very high Ca concentration (such as limestones) the reaction $^{40}Ca(-\mu,\alpha)$ produces more ^{36}Cl than the reaction $^{39}K(-\mu,pxn)$. However in rocks with a relatively high concentration of K (such as sandstones) the reaction $^{39}K(-\mu,pxn)$ produces more ^{36}Cl. The R_p value for the $^{40}Ca(-\mu,\alpha)$ reaction suggested by KUBIC et al (1984) makes this reaction predominant over the $^{39}K(-\mu,pxn)$ reaction for all rock types. The depth dependence of ^{36}Cl production via these reactions follow that of the negative muon stopping rate (see Section 2.4.3) and is shown for an average granitic matrix, at sea level and a latitude of 40°N geomagnetic in Fig 4.7. The relative importance of these reactions compared to other production reactions are discussed in Section 4.4.5.

4.4.4 Spallation reactions.

In this process high energy protons collide with nuclei to produce spallation products which consist of light nuclei and a residual "heavy" nucleus. Spallation reactions between protons and K, Ca, Fe and Ti nuclei have been shown to be a source of ^{36}Cl in the epigene zone (REEDY and ARNOLD., 1972, REGNIER et al., 1977, YOKOYAMA et al., 1977 and PHILLIPS et al., 1986). Since most rock matrices contain mainly low Z elements the amount of ^{36}Cl produced by this process will be dependent only on the concentration of each of the above mentioned elements. YOKOYAMA et al (1977) calculated ^{36}Cl production rates for the reactions :-

$$K + p \text{ ---- } ^{36}Cl$$

$$Ca + p \text{ ---- } ^{36}Cl$$

at sea level and 40 degrees north (geomagnetic) to be 3.22×10^{-4} atoms g^{-1} a^{-1} per ppm K and 9.93×10^{-5} atoms g^{-1} a^{-1} per ppm Ca. Spallation production from Ti and Fe has been estimated to be insignificant at the Earths surface due to attenuation of high energy cosmic protons by the atmosphere (PHILLIPS et al., 1986). The production rate of these reactions will follow the variation of the cosmic proton flux with height and geomagnetic latitude (see Section 2.4). Using this variation and the attenuation coefficient for the absorption of protons from cosmic rays (Section 2.4) the production rate of ^{36}Cl due to these spallation reactions may be calculated at different depths below the air/ground interface for a rock of specific composition by using equation 4.10.

$$N_{Cl36}=([K]0.000322+[Ca]0.0000993)R_{pl}R_{Pa}R_{Pd} \quad \text{Eqn. 4.10}$$

where N_{Cl36} is the ^{36}Cl production rate due to proton spallation reactions for a specific chemical composition, altitude, latitude, and depth below the air ground interface, [K] and [Ca] are the concentrations of K and Ca in ppm and R_{Pl}, R_{Pa} and R_{Pd} are the correction factors for latitude, altitude and depth respectively (See Sections 2.3 and 2.4). The variation of N_{Cl36} with depth has been calculated for an average granite and the results are shown in Fig 4.7. The relative importance of this reaction compared to other production reactions are discussed in Section 4.4.5.

4.4.5 The relative importance and depth dependence of ^{36}Cl production reactions.

As discussed in Sections 4.4.1 to 4.4.4 the three types of reaction which may produce significant amounts of ^{36}Cl in the subsurface are low energy neutron induced reactions, $^{-}\mu$ capture reactions and spallation reactions. The relative importance of each of these reactions depend upon the depth interval and rock type.

Table 4.11 contains calculated production rates for depths of 1, 5, and 20 m below the air/ground interface for three average rocks types which were selected because they commonly form aquifers. The depths were selected since they define three regions in which differing production reactions dominate.

(a) Form the surface down to a depth of 5 m spallation and low energy neutron induced reactions are both important. The dominant reaction depending on the Cl concentration of the matrix. It should be noted that the production rate of ^{36}Cl from low energy neutrons has been calculated on the assumption that all produced neutrons are thermalised. As discussed in Section 3 this would appear not to be the case for at least the upper meter of the Earths surface. The production rate due to low energy neutrons in this region may thus be up to a factor of ten lower than suggested in Table 4.11.

(b) From 5 to 20 meters the dominant reaction is the production of ^{36}Cl by low energy neutrons. Neutrons in this region are predominantly due to negative muon capture. The production rate of ^{36}Cl in this region by negative muon

capture depends greatly on the value of R_p. However even using the higher probability estimated by KUBIC et al (1984) the production by this reaction is only significant in matrices which have both a very low Cl concentration and neutron flux (such as the sandstone matrix defined by PARKER (1966)).
(c) At depths below 20 m the dominant reaction is again production of ^{36}Cl by low energy neutrons. The source of neutrons in this case being (α,n) and spontaneous fission reactions which are due to natural radioelements dispersed in the matrix.
Calculated ^{36}Cl production rates for these reactions at different depths below the surface of a granitic matrix (PARKER., 1966) are shown in Fig 4.7.

The production rates of ^{36}Cl by these reactions also vary with both geomagnetic latitude and altitude. Corrections may be made for these effects by applying similar correction factors as applied to the neutron production rate.
Calculation of the total ^{36}Cl production rate $(g^{-1}\ a^{-1})$ for given conditions has been simplified by use of the computer program "ISOTOPE PRODUCTION" which calculates all relevant correction factors and production rates.

Results of these calculations may be compared with measured ^{36}Cl production rates of PHILLIPS et al (1986) and FABRYKA-MARTIN perrs comm. PHILLIPS et al (1986) measured the $^{36}Cl/Cl$ ratios of near surface volcanic rocks which had been dated using K/Ar techniques. They then calculated the $^{36}Cl/Cl$ ratio using a method similar to that described above and compared this with the measured values. Table 4.4.3 compares the measured and calculated data of PHILLIPS et al (1986) with that produced using the program "ISOTOPE PRODUCTION". Agreement between the calculated values and those of PHILLIPS et al (1986) are good considering the accuracy of correction factors for altitude, latitude and depth. The calculated values in Table 4.12 are consistent with 4 out of the 7 measured values (a similar proportion to calculated values by PHILLIPS et al (1986)) 2 of the inconsistent samples have a higher $^{36}Cl/Cl$ ratios than expected which may be due to "bomb pulse" contamination. MC84-3 has a much lower $^{36}Cl/Cl$ ratio than expected the reason for this is unclear.

FABRYKA-MARTIN (perrs comm) has reported that measured $^{36}Cl/Cl$ ratios of rock leaches from the Stripa granite and Leptite are consistent in 5 out of 8 cases with ratios

predicted by the above calculations. The inconsistency may be due to experimental methods and are at present being analysed (see Section 5 for a further discussion of the in-situ production of ^{36}Cl at the Stripa site).

4.4.6 Transport of in-situ produced ^{36}Cl.

Once produced if ^{36}Cl is to influence the $^{36}Cl/Cl$ ratio of the groundwater it must escape from its site of production and into fracture fluids. As discussed above ^{36}Cl is predominantly produced by irradiation of chloride in the rock matrix. The energy released when ^{36}Cl is produced from ^{35}Cl is 8.57 MeV, most of which is carried away by the γ photon, and little recoil energy will be imparted to the residual ^{36}Cl nuclei. Thus movement of produced ^{36}Cl from its site of production by recoil is unlikely. ^{36}Cl decays by low energy beta decay (0.71 MeV) and significant radiation damage to its surrounding matrix leading to escape of ^{36}Cl is again unlikely.

It is thus highly likely that any produced ^{36}Cl will become fully mixed with other chloride atoms at its production site and its movement into fracture fluids may be described by the movement of stable chloride into flowing fracture fluids.

The distribution and abundance of chloride in rock matrices varies greatly for instance in rocks it may be present in interlaced evaporites, in formation waters or in detritus. Concentrations in sandstones are typically less than 50 ppm whilst concentrations in limestones and shales may be as high as 200 ppm (FETH., 1981). In crystalline rocks chloride is commonly present in fluid inclusions and along grain boundaries where it may be present as halogen minerals and in micas and amphiboles (primarily biotite and hornblende) where it substitutes for OH^- (FETH., 1981, FUGE., 1979 and NORDSTROM and OLSSON., 1987). Concentrations in granitic, basaltic and ultramafic rocks are generally enriched compared to sedimentary rocks ranging from 100 to 1000 ppm (FETH., 1981). All of these sources are likely to be old compared to the time required for secular equilibrium to be reached (1.5 Ma), thus chloride present in the sites described above will have a $^{36}Cl/Cl$ ratio characteristic of the neutron flux developed within that formation.

The movement of significant amounts of chloride from the matrix is demonstrated in many aquifers which show increase in

salinity with groundwater age. The mechanism of this movement is predominantly dissolution of chloride minerals. In crystalline rocks this dissolution may be concurrent with the opening of fluid inclusions either by hydrolysis or microfracturing following strain relief (NORDSTROM and OLSSON., 1987). A further process which may lead to transport of Cl^- into fracture fluids is the exchange of Cl^- present in biotites with OH^- (FETH., 1981, NORDSTROM and OLSSON., 1987 and EDMUNDS et al., 1987).

Once in solution, Cl^- saturation is rarely reached and Cl^- is said to be "conservative", however some removal of aqueous Cl^- has been observed during kaolinisation. The process of this removal of Cl^- being ion exchange (FUGE., 1979).

Due to the wide distribution of Cl^- in rock matrices ^{36}Cl concentrations in groundwaters above atmospheric input (see Section 1) reflect the availability of matrix Cl^- to the fracture fluids. A corollary of this is that there should be a linear correlation between ^{36}Cl and Cl^- concentrations (and a stable $^{36}Cl/Cl$ ratio) for a particular formation if it is homogeneous with respect to its radioelement composition and its Cl^- distribution. In practice groundwaters may obtain their chlorinity from a number of formations. This leads to discontinuity in the above linear relationship. Andrews et al (1986) have used such discontinuities to investigate the evolution of groundwater chlorinity at the Stripa site (see Section 5) and an attempt is at present being made to use a similar method on natural saline fluids associated with the Carnmenellis granite (see Section 6).

The rate at which any cosmogenic ^{36}Cl input into an aquifer is masked by in-situ produced ^{36}Cl will depend upon the state of secular equilibrium reached by near surface chloride and the ease of solution of such surface chloride and deeper chloride. Under normal temperate conditions a high Cl^- solubility and/or rainfall will mean a short near surface residence time and in such situations the degree to which secular equilibrium will be reached will be small. In such cases the input of ^{36}Cl from deep sources will control the masking of cosmogenic ^{36}Cl (provided that the rate of ^{36}Cl increase, due to solution of matrix Cl^- exceeds that due to neutron irradiation of waterborne Cl^-). However, under arid conditions the degree to which secular equilibrium is reached

will be greater. In this case a high Cl^- solubility will cause meteoric input of ^{36}Cl to be swamped near the surface during infrequent recharge. The $^{36}Cl/Cl$ ratio of Cl^- derived under such circumstances may then be diluted by Cl^- input from deeper sources and radioactive decay until the waterborne Cl^- reaches secular equilibrium with the subsurface neutron flux. In summary :-

(a) The movement of ^{36}Cl produced in rock matrices into groundwater is controlled by the solubility of matrix chloride sources rather than recoil or diffusion.

(b) The movement of ^{36}Cl produced within the matrix may be used to characterise sources of Cl^-.

(c) The irradiation of near surface rocks and chloride deposits by cosmic rays may in certain cases mask meteoric input of ^{36}Cl.

(d) The complex relationship between rainfall, evapo-transpiration, irradiation of surface rocks and solution of matrix chloride strongly suggest a wide variation in recharge levels of ^{36}Cl over climatic cycles.

4.5 Production of Argon-37 and Argon-39.

The subsurface production of ^{39}Ar been considered by a number of authors to explain the poor correlation of ^{39}Ar and ^{14}C dates (LOOSLI and OESCHGER., 1978, LOOSLI., (1983) and ANDREWS et al., 1989). The subsurface production of ^{37}Ar has received less attention due to its half-life which is too short for many hydrological studies. However this short half-life makes it useful as an "in-situ" neutron flux monitor, and attempts are now being made to use it as such (LOOSLI et al., 1989).

Both isotopes may be produced either via neutron induced reactions or by cosmic ray interaction with the Earths surface (See Figs 4.8 and 4.10). The following Section discusses each of these reactions in greater detail.

4.5.1 Low energy neutron induced reactions.

The production rates of ^{37}Ar and ^{39}Ar from low energy neutron induced reactions follow the variation in neutron production rate and consequently neutron flux with matrix composition and depth below the air ground interface. As discussed in Section 2 at depths greater than 60 meters the major sources of neutrons are spontaneous fission and (α,n) reactions. Up to these depths neutron production is mainly due to cosmic ray secondaries.

The following reactions produce either ^{37}Ar or ^{39}Ar:-

(a) $^{36}Ar(n,\gamma)^{37}Ar$ Q= 8.78 MeV

(b) $^{40}Ca(n,\alpha)^{37}Ar$ Q= 1.75 MeV

(c) $^{38}Ar(n,\gamma)^{39}Ar$ Q= 6.59 MeV

(d) $^{39}K(n,p)^{39}Ar$ Q= 0.22 MeV

(e) $^{42}Ca(n,\alpha)^{39}Ar$ Q= 0.34 MeV

All of these reactions are exoergic and their cross-sections would thus be expected to be >0 for thermal neutrons. However even for exoergic reactions the potential barrier against charged particle emission causes cross-sections for the such reactions to exhibit a threshold dependency. Thus the cross-sections for reactions (b), (d) and (e) would be expected to be small for thermal neutrons. Cross-sections for reactions (a) and (c) would be expected to be largest of these reactions since they do not involve the emission of a charged particle. However the concentration of target isotopes for these reactions in rock matrices and associated groundwater would be very small. Hence these reactions cannot produce significant amounts of either ^{37}Ar or ^{39}Ar in rock matrices (LOOSLI and OESCHGER., 1968 and ANDREWS et al., 1988).

The $^{40}Ca(n,\alpha)^{37}Ar$ reaction (reaction (b)) has a cross-section of 2.4 +/- 1.1 mb (MUENNICH., 1958) for thermal neutrons. Cross-sections for reactions (d) and (e) at thermal energies are not well known. The cross-section of the $^{39}K(n,p)^{39}Ar$ reaction has been estimated to be 16 mb (LOOSLI., 1983) which was based on extrapolation. This value is consistent with that obtained for a fission neutron spectrum derived from the nomogram of INTHOFF. (1955) and from interpolation of the results of BASS et al. (1964). The possible error in this cross-section estimate has been quoted to be at least 25% (ANDREWS et al., 1989). There are similarly no cross-section measurements for the $^{42}Ca(n,\alpha)^{39}Ar$ reaction. The cross-section for this reaction is certainly

smaller than the $^{42}Ca(n,\gamma)^{43}Ca$ reaction (0.65 barns). A value for fission spectrum neutrons of 10 mb may be interpolated from the nomogram of INTHOFF. (1955), and it may be assumed that the cross-section for this reaction is of similar order to that for reaction (d). A knowledge of the exact cross-section is not required for silicate rocks since the high isotopic abundance of ^{39}K compared with ^{42}Ca means that, the amount of ^{39}Ar produced from ^{42}Ca is a factor of 10^3 times lower than that from ^{39}K given that the cross-sections and K and Ca concentrations are equal. In estimating production rates of ^{39}Ar in carbonate rocks with a high Ca content the contribution from reaction (e) is almost equal to that from reaction (d) assuming equal reaction cross-sections. The production rate of ^{37}Ar and ^{39}Ar due to these reactions may be calculated from :-

$$N_{Ar37} = \phi \; ((\; n_{Ar36} \; \sigma_{Ar36} \;) + (n_{Ca40} \; \sigma_{Ca40})) \qquad \text{Eqn. 4.11}$$

and

$$N_{Ar39} = \phi \; ((n_{Ar38}\sigma_{Ar38}) + (n_{K39}\sigma_{K39}) + (n_{Ca42}\sigma_{Ca42})) \qquad \text{Eqn. 4.12}$$

where N_{Ar37} and N_{Ar39} are the ^{37}Ar and ^{39}Ar production rates (g^{-1} a^{-1}) for a given altitude, geomagnetic latitude and depth below the air/ground interface, n_{Ar36}, n_{Ca40}, n_{Ar38}, n_{K39} and n_{Ca42} are the number of atoms of target isotope g^{-1}. σ_{Ar36}, σ_{Ca40}, σ_{Ar38}, σ_{K39} and σ_{Ca42} are the (n,γ), (n,α), (n,γ), (n,p) and (n,α) reaction cross-sections for reactions (a), (b), (c), (d) and (e) in cm^2 and ϕ is the thermal neutron flux (cm^{-2} a^{-1}).

The production rates due to reactions (a), (b), (c), (d) and (e) have been calculated for an average sandstone, granite and limestone (Tables 4.13 and 4.14). These results are consistent with the conclusions ANDREWS et al (1989) which state that the low cross-section and abundance ^{36}Ar and ^{38}Ar make production by reactions (a) and (c) insignificant with respect to production by reactions (b) and (d) and (e). The low cross-section for reaction (e) may be compensated for by the high abundance of Ca in carbonate matrices.

The variation of neutron production rate with depth discussed in Section 2 means that the production rate of these radiogenic Ar isotopes also vary with depth in a similar manner (see Fig 4.9 and Fig 4.11). The production rates of

these reactions have been calculated at varying depths below the surface for an average granite, limestone and sandstone (analysis of PARKER et al., 1967) see Tables 4.20 and 4.21. The importance of these reactions with respect to others production processes are reviewed in Section 4.5.5. It should be acknowledged that the measurement of cross-sections for reactions (d) and (e) should be an important priority in the further study of in-situ produced ^{37}Ar and ^{39}Ar.

4.5.2 Low energy (p,x) reactions.

Simple (p,x) reactions such as (p,a), (p,γ) and (p,n) which have relatively low energy thresholds do not contribute ^{37}Ar and ^{39}Ar to the epigene zone due to the lack of suitable target nuclides.

4.5.3 Negative muon capture reactions.

The production of negative muons from primary cosmic rays is discussed in Section 2. Negative muons may be captured according to the reaction schemes discussed in Section 2.4.1. Once capture has taken place the excited nucleus may de-excite producing either ^{37}Ar or ^{39}Ar. Where these reactions involve the emission of a charged particle their reaction probabilities will be low compared to those for neutron emission due to the Coulombic barrier. Reactions involving negative muon capture that could produce significant quantities of ^{37}Ar and ^{39}Ar in the subsurface are :-

(a) $^{39}K + ^{-}\mu \text{ --- } ^{39}Ar^{*} \text{ --- } ^{37}Ar + 2n$
(b) $^{40}K + ^{-}\mu \text{ --- } ^{40}Ar^{*} \text{ --- } ^{37}Ar + 3n$
(c) $^{40}Ca + ^{-}\mu \text{ --- } ^{40}K^{*} \text{ --- } ^{37}Ar + p2n$

(d) $^{39}K + ^{-}\mu \text{ --- } ^{39}Ar^{*} \text{ --- } ^{39}Ar + \upsilon$
(e) $^{40}K + ^{-}\mu \text{ --- } ^{40}Ar^{*} \text{ --- } ^{39}Ar + n$
(f) $^{40}Ca + ^{-}\mu \text{ --- } ^{40}K^{*} \text{ --- } ^{39}Ar + p$
(g) $^{42}Ca + ^{-}\mu \text{ --- } ^{42}K^{*} \text{ --- } ^{39}Ar + p2n$

The fractional probabilities of reactions (a) to (c) are 0.09, <0.001 and 0.018 respectively (interpolated from WYTTENBACH et al (1978) and CHARALAMBUS (1971)). N_{Ar37} the production rate of ^{37}Ar atoms due to these reactions ($g^{-1}a^{-1}$) may be calculated in a similar way to the calculation of ^{3}H by these reactions (see Section 4.2.3).

Results of these calculations made for an average sandstone, granite and limestone (Analysis of PARKER., 1967) are given in Tables 4.15 and 4.16. From these tables it may be seen that both Ca and K produce significant amounts of ^{37}Ar by negative muon capture. The relative contributions depending upon the concentrations of Ca and K in the respective matrix. Reactions (a) and (c) produce the majority of ^{37}Ar due to the high isotopic abundance of each of these target isotopes. The fractional probabilities of reactions (d) to (g) which produce ^{39}Ar are 0.62, 0.50, 0.004 and 0.018 respectively (interpolated from WYTTENBACH et al (1978) and CHARALAMBUS (1971)). N_{Ar39} the production rate of ^{39}Ar atoms due to these reactions ($g^{-1}a^{-1}$) may be calculated in a similar way to the calculation of ^{37}Ar by these reactions.

From Table 4.16 it may be seen that both Ca and K produce significant amounts of ^{39}Ar following negative muon capture. The relative contributions depending upon the concentrations of Ca and K in the respective matrix. As expected reactions (d) and (f) produce the majority of ^{39}Ar due to the high isotopic abundance of each of these target isotopes.

The production rates of these reactions compared to those of other reactions are discussed in Section 4.5.5.

4.5.4 Spallation reactions.

High energy protons react by colliding with nuclei to produce spallation products which consist of light nuclei and residual "heavy" nuclei. Spallation reactions between protons and K, Ca and Fe nuclei have been shown to be a source of ^{37}Ar and ^{39}Ar in the epigene zone of the moon and hence the same reactions would be expected to produce radiogenic Ar albeit to a lesser extent in the terrestrial epigene zone (REEDY and ARNOLD., 1972, YOKOYAMA et al., 1977). Since these reactions occur with elements of atomic number around 20 whose abundance varies widely between rock matrices the production rate due to these reactions is dependent of rock composition. YOKOYAMA et al (1977) have calculated ^{37}Ar and ^{39}Ar production rates for both low and high energy proton induced reactions on K, Ca and Fe (see Table 4.17). The relative contribution to the total spallogenic production rate due to each one of these reactions at the Earths surface may be calculated for a matrix of known K, Ca and Fe content (see Tables 4.18 and 4.19). From these tables it may be seen that :-

(a) Spallogenic ^{37}Ar production in the average rock matrices granite, sandstone and limestone is predominantly (>70%) due to reaction with Ca nuclei.
(b) Spallogenic ^{39}Ar production in the above average rock matrices is due to spallation of Ca and K nuclei. The relative importance of each reaction depending on the Ca/K ratio of each matrix.
The spallogenic production rate will follow the variation of the cosmic proton flux with height and geomagnetic latitude (see Section 2.3). Using this variation and the attenuation coefficient for the absorption of cosmic ray protons (see also Section 2.4) the production rate of radiogenic Ar due to these reactions may be calculated for a rocks of average composition at different depths below the Earths surface (see Tables 4.20 and 4.21).The relative importance of these spallation reactions compared to other production reactions are discussed in Section 4.5.5.

4.5.5 The relative importance and depth dependence of ^{37}Ar and ^{39}Ar production reactions.

As discussed in Sections 4.5.1 to 4.5.4 the three types of reaction which may produce significant amounts of either ^{37}Ar or ^{39}Ar in the subsurface are low energy neutron induced reactions, $^{-}\mu$ capture reactions and spallation reactions. The relative importance of each of these reactions depend upon the depth interval and rock type.

Tables 4.20 and 4.21 contain calculated production rates for depths of 1, 5, and 20 m below the air/ground interface for three average rocks types selected as they commonly form aquifers. It may be seen from these tables that :-
(a) From the surface down to a depth between 3 and 5m spallation reactions produce the majority of both ^{37}Ar and ^{39}Ar.
(b) Below 5 meters both and ^{37}Ar and ^{39}Ar production is dominated by production from negative muon capture even in rocks with a high neutron flux such as granites, or of a high Ca content such as limestones.
(c) Below the influence of negative muons (typically depths greater than approximately 60m (see Section 2)) low energy neutron reactions are responsible for ^{37}Ar and ^{39}Ar production.
Calculated ^{37}Ar and ^{39}Ar production rates for these reactions

at different depths below the surface of a average granitic matrix (PARKER., 1966) are shown in Figs 4.9 and 4.11.

4.5.6 Transport of in-situ produced radiogenic Argon isotopes.

Once produced if either ^{37}Ar or ^{39}Ar are to influence the radiogenic Ar content of the groundwater they must escape from their site of production and into fracture fluids. As discussed above both Ar isotopes are produced by reaction of subatomic particles with K and Ca present in the rock matrix.

In silicate rocks ^{39}Ar is produced almost exclusively by reactions with K. The escape of ^{39}Ar from production sites within silicates would thus depend upon the distribution of K within the matrix. ^{37}Ar production in silicate matrices may occur by reactions involving either K or Ca depending upon the depth below the Earths surface. At sites removed from "groundwater recharge" (which are generally at depths below the influence of negative muons) ^{37}Ar production will take place at Ca sites via the $^{40}Ca(n,\alpha)$ reaction. Because of the short half-life of ^{37}Ar (35 days) any ^{37}Ar input into fracture fluids during recharge will have decayed away, the concentration in the fluids representing local production and transport. The magnitude of transport of produced ^{37}Ar into fracture fluids will depend upon the distribution of Ca within the matrix.

In carbonate rocks significant amounts of both ^{37}Ar and ^{39}Ar are produced following reaction with Ca. A significant amount of ^{39}Ar may also be produced by the small amount of K present in carbonate matrices. In carbonate matrices transport of these radiogenic argon isotopes into fracture fluids is thus controlled by the distribution of both Ca and K.

The energy released when ^{37}Ar and ^{39}Ar are produced from Ca and K by low energy neutron reactions are 1.75 and 0.22 MeV respectively. In the case of the $^{40}Ca(n,\alpha)$ reaction the ^{37}Ar nuclei recoils with an energy of 0.24 MeV. This gives the ^{37}Ar nuclei a range of > 0.1 μm in pure SiO_2 (CARTER and COLLIGON., 1969). The recoil energy imparted to the ^{39}Ar nuclei by the $^{39}K(n,p)$ reaction is much smaller (0.22 MeV) since the mass of a proton is less than that of an α particle. Whilst it is hard to quantitatively calculate the recoil release of these isotopes it may be predicted that release of

^{37}Ar is more likely than that of ^{39}Ar as radiation damage to the surrounding matrix leading to both recoil and diffusive escape of Ar is more probable.

In crystalline rocks potassium is usually distributed throughout the matrix in feldspars and in micas. Whilst Ca is typically associated with secondary mineralisation. The short half-life of ^{37}Ar means that the distance it may diffuse before decaying is small whilst that of ^{39}Ar is considerable longer. This suggests that the probability of the escape of in-situ produced ^{39}Ar into fracture fluids is greater than that for ^{37}Ar. This would be the case if the production sites of ^{37}Ar were the same as those of ^{39}Ar however ^{37}Ar is produced at Ca sites which if associated with secondary mineralisation may be in close proximity to fracture fluids. This factor giving ^{37}Ca a greater escape probability. Measurements carried out by LOOSLI et al (1989) support such a scenario at the Stripa site which is discussed further in Section 5.

In carbonate rocks the ^{37}Ar and ^{39}Ar contents of fracture fluids should reflect a situation in which the fraction of ^{39}Ar released is greater due to some ^{39}Ar production from Ca. Unfortunately at present ^{37}Ar concentrations have not yet been measured fluids from carbonate matrices.

The masking of cosmogenic ^{37}Ar or ^{39}Ar input by in-situ produced radiogenic Ar will depend upon concentration of ^{37}Ar and ^{39}Ar in the matrix and the rate of release of this Ar into the groundwater. The concentration of these isotopes reached in the matrix at secular equilibrium may be found by dividing the production rate by the appropriate decay constant (7.21 a^{-1} and 0.00258 a^{-1} for ^{37}Ar and ^{39}Ar respectively). Given a conservative estimate that 10% of produced Ar is transported from the rock matrix into fracture fluids in the case of the above defined average rocks :-

In the case of ^{37}Ar, levels of atmospheric input (typical concentrations of ^{37}Ar and ^{39}Ar in recharge waters are $4x10^{-3}$ and $6x10^{-3}$ atoms l^{-1} respectively (See Section 1)) are exceeded below the influence of cosmic rays in carbonate rocks. In all rocks atmospheric input levels are exceeded if ^{37}Ar produced in the region influenced by cosmic ray production is transported into the ground water.

The atmospheric input of ^{39}Ar is exceeded in all cases

whether the ^{39}Ar is transported from rocks below or in the influence of cosmic rays.

The parameters used in the generalisation above are site specific and are discussed in detail with respect to the Stripa granite in Section 5.

In summary :-

(a) The movement of ^{37}Ar and ^{39}Ar produced in rock matrices into groundwater is controlled by the recoil energy and diffusion length of the respective nuclide.

(b) The production and transport of ^{37}Ar into fracture fluids is more likely in rocks in which fluid flow occurs in fractures possessing a high Ca content fracture coating.

(c) Levels of ^{37}Ar and ^{39}Ar produced by the irradiation of surface rocks by cosmic rays mask meteoric input of these isotopes if transport of produced isotopes into fracture fluids is rapid.

4.6 Conclusions

From the preceeding discussions of section 4 it is clear that significant quantities of the isotopes ^{3}H, ^{14}C, ^{36}Cl, ^{37}Ar and ^{39}Ar may theoretically be produced in the three selected average rocks (granite, sandstone and limestone, see Appendix 1) by low energy neutron induced reactions. The relative importance of this reaction mode compared to production from reactions involving spallation, negative muon capture, low energy alpha particle capture and spontaneous decay is dependent upon the isotope of interest and the concentration of suitable target nuclides in the particular matrix. The conclusions drawn in this Section for the average rock types described in Appendix 1 show that in the general situation :-

(1) Tritium. Spallation reactions on O and Si produce the majority on ^{3}H near the Earths surface. At depths in excess of approximately 2 m production by low energy neutron irradiation of Li exceeds that of spallation reactions in high Li content rocks such as granites and shales (Appendix 1). In rocks with a low Li content such as sandstones, carbonates and basalts production from negative muon capture reactions on O and Si could produce the majority of ^{3}H in the depth interval 2m to approximately 60m. At depths below the influence of cosmic rays ^{3}H is produced by the low energy

neutron irradiation of Li. The magnitude and general form of these results agree with the predictions of LAL.(1987) who calculated production rates of ^{3}He from near surface cosmic ray interactions via ^{3}H.

(2) Carbon-14. Similarly to ^{3}H, spallation reactions on O and Si produce the majority on ^{14}C near the Earths surface. At depths in excess of approximately 2 m production by negative muon capture reactions with Oxygen exceeds that of spallation reactions. The amount produced by low energy neutron induced reactions is not significant until the influence of these cosmic ray induced reactions are reduced by absorption (> 60 m for an average granite). At these depths the production from neutron induced reactions may be exceeded by low energy (α,p) reactions on B. The spontaneous emission of ^{14}C generally produces less ^{14}C than low energy neutron induced reactions.

(3) Chlorine-36. The relative importance of low energy neutron production reactions on the production of ^{36}Cl is dependent upon the concentration of Cl within the matrix. If this is high then this reaction produces the majority of ^{36}Cl even in rocks of a high Ca and K content. However if the Cl content is low, as may be the case with sedimentary rocks, spallation reaction produce more ^{36}Cl near the earths surface. The importance of negative muon capture reactions is low. At depths below the influence of cosmic rays ^{36}Cl is predominantly produced by the low energy neutron irradiation of Cl.

(4) Argon-37. The relative importance of low energy neutron production reactions on the production of ^{37}Ar near the Earths surface is low. However at depths below the influence of cosmic rays it is the only production reaction. Production near the earths surface is principally due to the irradiation of Ca with cosmic ray protons and pions whilst at slightly deeper depths the irradiation of both Ca and K with negative muons produce ^{37}Ar.

(5) Argon-39. The relative importance of low energy neutron production reactions on the production of ^{39}Ar near the Earths surface is low. However as per ^{37}Ar at depths below the influence of cosmic rays it is the only production reaction.

Production near the earths surface is principally due to the irradiation of K with cosmic ray protons and pions whilst at slightly deeper depths the irradiation of Ca with negative muons produce ^{39}Ar.

(6) The reaction responsible for the production of the majority of these isotopes below the influence of cosmic rays (60 to 100 m below the earths surface, for a site at sea level) is low energy neutron irradiation.

(7) Isotope transport. The probability of ^{3}H, ^{14}C and ^{36}Cl entering flowing fluids depends greatly on the spatial relationship between the fluid and production site due to their low recoil range and chemical reactivity. In fractured rocks where the major production site may be identified as fracture surfaces, the degree of alteration and nature of these surfaces are important. The low chemical reactivity of the inert gas isotopes, ^{37}Ar and ^{39}Ar, make diffusion away from the site of production a much higher probability. However their relatively short half lives mean that diffusion lengths are small and the probability of these isotopes entering flowing fluids depends greatly on the spatial relationship between the fluid and production site.

The accuracy of production rates calculated in this Section are dependent upon the accuracy with which, the flux of reacting particles, the concentration and distribution of the target isotopes throughout the rock matrix and the reaction probabilities are known.

The accuracy of particle flux estimates has been discussed with respect to neutron production in Sections 2 and 3. The accuracy to which the concentration and distribution of target isotopes throughout the rock matrix are known is likely to be low and site dependent, however its reliability may be improved by the analysis of a greater number of samples. The greatest source of inaccuracy in the calculations of this Section are due to the un-availability and hence accuracy of specific reaction probability data for the rarer reactions (such as negative muon capture production and (α,p) reactions). This data could be readily obtained by appropriate laboratory experimentation and would yield a great improvement in the accuracy of with which production rates of isotopes may be calculated.

Table 4.1 Production rates of ^{3}H due to neutron induced reactions at depths in excess of 60m.

Matrix	^{3}H Production Rate (g^{-1} a^{-1})	
	$^{6}Li(n,\alpha)$	$^{10}B(n,2\alpha)$
Sandstone	0.015	0.000057
Granite	0.49	0.00034
Limestone	0.016	0.00014
Stripa granite(*)	1.0	0.00066
Carnmenellis granite(**)	2.9	0.0095

* Neutron flux = 4.71×10^{-4} $cm^{-2}s^{-1}$
[Li] = 11 ppm
[B] = 4 ppm
ANDREWS et al (1989).

** Neutron flux = 6.0×10^{-5} $cm^{-2}s^{-1}$
[Li] = 250 ppm
[B] = 450 ppm.

Table 4.2 ^{3}H production rates for reactions with negative muons in an average rock matrices.

Matrix	Production Rate g^{-1} a^{-1}		
	$^{6}Li(\mu,^{3}H)^{3}H$	$^{16}O(\mu,^{3}H)^{13}C$	$^{28}Si(\mu,^{3}H)^{25}Mg$
Granite	$< 5 \times 10^{-6}$	< 0.58	< 0.18
Sandstone	$< 2 \times 10^{-6}$	< 0.74	< 0.26
Limestone	$< 5 \times 10^{-7}$	< 0.63	< 0.15

Calculated for a site 5m below the surface at 40 N geomagnetic latitude and sea level using maximum reaction probabilities. The production rate for a matrix containing 1 ppm Li and with a neutron flux of 0.5x10-4 $cm^{-2}s^{-1}$ is 0.0097 $g^{-1}a^{-1}$.

Table 4.3 Production rates of ^{3}H due to spallation reactions with light nuclei at the surface of Basalt, Granite and Limestone matrices.

Matrix	^{3}H Production Rate (g-1 a-1)
Basalt	116
Granite	121
Limestone	116

From YOKOYAMA et al. (1977) corrected to sea level at geomagnetic latitudes > 60 N.

Table 4.4 Production rates of ^{3}H due to neutron, spallation and muon induced reactions at depths upto 100m below surface.

	^{3}H Production Rate (g^{-1} a^{-1})		
	neutron induced	spallation induced	muon induced
(Depth = 1m)			
Sandstone	5.0	20.0	< 3.4
Granite	10.6	16.0	< 3.1
Limestone	2.3	18.2	< 2.6
(Depth = 5m)			
Sandstone	0.60	0.10	< 1.0
Granite	1.57	0.03	< 0.75
Limestone	0.28	0.10	< 0.78
(Depth = 20m)			
Sandstone	0.08	< 0.001	< 0.12
Granite	0.61	< 0.001	< 0.08
Limestone	0.047	< 0.001	< 0.09
(Depth = > 100m)			
Sandstone	0.015	< 0.001	< 0.002
Granite	0.49	< 0.001	< 0.001
Limestone	0.017	< 0.001	< 0.001

Calculated for a site at 40 N geomagnetic latitude and sea level.

Table 4.5 Production rates of ^{14}C due to neutron induced reactions at depths in excess of 60m.

Matrix	^{14}C Production Rate ($Kg^{-1}\ a^{-1}$)		
	$^{14}N(n,p)$	$^{17}O(n,\alpha)$	$^{13}C(n,\gamma)$
Sandstone	0.11	0.27	$1x10^{-6}$
Granite	3.3	3.5	0.0005
Limestone	0.40	1.14	0.06
Stripa granite	23.3	24.6	0.0035
Carnmenellis granite	2.97	3.18	0.0004

Table 4.6 Production rates of ^{14}C due to low energy α particle interaction with ^{10}B.

Matrix	[B] $\mu g\ g^{-1}$	^{14}C Production Rate $Kg^{-1}\ a^{-1}$		
		min		max
Sandstone	35.	0.3	---	1.7
Granite	15.	1.1	---	6.7
Limestone	20.	0.7	---	4.1
Stripa granite	4.	3.2	---	19.
Carnmenellis granite	420.	140.	---	844

min based on σ_α = 20 mb : max based on σ_α = 120 mb.

Table 4.7 ^{14}C production rates due to negative muon capture reactions at 5m below the earths surface.

Matrix	^{14}C Production Rate ($Kg^{-1}a^{-1}$)		
	$^{16}O(\mu,pn)$	$^{17}O(\mu,p2n)$	$^{15}N(\mu,n)$
Sandstone	1190	< 1	< 1
Granite	920	< 1	< 1
Limestone	1010	< 1	< 1

Calculated for a site at 40°N geomagnetic latitude and sea level.

Table 4.8 Production rates of ^{14}C due to spontaneous emission of ^{14}C by U and Th series nuclei.

Matrix	[U] $\mu g\ g^{-1}$	[Th] $\mu g\ g^{-1}$	^{14}C Production Rate ($Kg^{-1}\ a^{-1}$) U-series	Th-series
Sandstone (*)	0.45	1.7	0.010	0.009
Granite (*)	3.5	18.	0.077	0.10
Limestone (*)	2.2	1.7	0.048	0.009
Stripa granite	44.1	33.0	0.96	0.18
Carnmenellis granite	18.	16.	0.39	0.088

(*) Analysis of PARKER. (1967).

Table 4.9 Production rates of ^{14}C due to neutron, spallation and muon induced reactions at depths upto 100m below surface.

	^{14}C Production Rate (Kg^{-1} a^{-1})		
	neutron induced	spallation induced	muon induced
(Depth = 1m)			
Sandstone	110.	3560.	4030
Granite	140.	2840.	3770
Limestone	150.	3560.	3380
(Depth = 5m)			
Sandstone	13.	18.	1190
Granite	21.	6.	920
Limestone	19.	18.	1010
(Depth = 20m)			
Sandstone	2.0	<0.001	140
Granite	8.0	<0.001	104
Limestone	3.0	<0.001	120
(Depth > 100m)			
Sandstone	0.38	<0.001	< 2.0
Granite	6.8	<0.001	< 1.0
Limestone	1.5	<0.001	< 2.0

Calculated for a site at 40°N geomagnetic latitude and sea level

Table 4.10 ^{36}Cl production rates for reactions with negative muons.

Depth m	Production Rate g^{-1} a^{-1}			
	Limestone matrix		Sandstone matrix	
	K	Ca	K	Ca
1	.0077	.15	.038	.024
5	.0023	.046	.011	.0073
20	.00030	.005	.0014	.0010

Calculated for a site at 40 N geomagnetic latitude and sea level. (production rate for a matrix containing 1 ppm Cl and with a neutron flux of 0.5×10^{-4} cm^{-2} s^{-1} is 0.000885 g^{-1} a^{-1}.)

Table 4.11 Production rates of ^{36}Cl due to neutron, spallation and muon induced reactions at depths down to 20m.

	^{36}Cl Production Rate (g^{-1} a^{-1})		
	neutron induced	spallation induced	muon induced
(Depth = 1m)			
Sandstone	0.35	1.54	0.06
Granite	6.0	2.11	0.12
Limestone	6.3	6.40	0.16
(Depth = 5m)			
Sandstone	0.041	0.008	0.018
Granite	0.89	0.004	0.029
Limestone	0.78	0.033	0.049
(Depth = 20m)			
Sandstone	0.006	<0.001	0.002
Granite	0.35	<0.001	0.003
Limestone	0.13	<0.001	0.006

Numbers in refer to rates based on R_p values of KUBIC et al (1984).

Table 4.12 Measured and calculated $^{36}Cl/Cl$ ratios for samples discribed in PHILLIPS et al (1986).

Sample	Depth m	$^{36}Cl/Cl$ Ratio $x10^{-15}$ Measured*	Calculated*	Calculated**
SLR-3	0	650+/-50	87	180+/-47
MC84-3	0	50+/-5.8	120	230+/-36
SLR-2	0	650+/-60	135	300+/-100
SLR-7	0	3900+/-200	2550	3960+/-100
C84-41	2	150+/-55	210	140+/-40
SG-1A	0	6770+/-60	6260	7330+/-2480
C84-40	2	390+/-30	380	320+/-20

* Values calculated by "Cl36-Prod".
** Values from PHILLIPS et al (1986).

Table 4.13 Production rates of ^{37}Ar due to neutron induced reactions at depths in excess of 60m.

Matrix	^{37}Ar Production Rate (kg^{-1} a^{-1})	
	$^{40}Ca(n,\alpha)$	$^{36}Ar(n,\gamma)$
Sandstone	0.22	negligible
Granite	1.12	negligible
Limestone	6.0	negligible

Table 4.14 Production rates of ^{39}Ar due to neutron induced reactions at depths in excess of 60m.

Matrix	^{39}Ar Production Rate (kg^{-1} a^{-1})		
	$^{39}K(n,p)$	$^{42}Ca(n,\alpha)$	$^{38}Ar(n,\gamma)$
Sandstone	0.40	0.010	negligible
Granite	16.	0.050	negligible
Limestone	0.35	0.27	negligible

Table 4.15 ^{37}Ar production rates for reactions with negative muons.

Depth m	Production Rate $kg^{-1}\ a^{-1}$					
	Sandstone		Granite		Limestone	
	K	Ca	K	Ca	K	Ca
1	170	165	490	61	36	1070
5	50	49	120	15	11	320
20	5.9	5.7	13	1.7	1.3	38

Calculated for different depths below the surface at a site 40°N geomagnetic latitude and sea level.

Table 4.16 ^{39}Ar production rates for reactions with negative muons.

Depth m	Production Rate $kg^{-1}\ a^{-1}$					
	Sandstone		Granite		Limestone	
	K	Ca	K	Ca	K	Ca
1	1170	38	3350	14	250	245
5	340	11	820	3.4	74	73
20	40	1.3	92	0.38	8.7	8.4

Calculated for different depths below the surface at a site 40°N geomagnetic latitude and sea level.

Table 4.17 Spallogenic production rates of ^{37}Ar and ^{39}Ar from K,Ca and Fe.

Target	Production rate * atoms g^{-1} a^{-1}	
	^{37}Ar	^{39}Ar
K	20.8	910
Ca	595	116
Fe	72	8.0

* Production rates for 1g of target material at sea level and a geomagnetic latitude greater than 60°N.

Table 4.18 Production rates of ^{37}Ar due to spallation reactions with K,Ca and Fe.

Matrix	^{37}Ar Production Rate (kg^{-1} a^{-1})			
	K	Ca	Fe	Total
Sandstone*	---	-----	---	-----
Granite*	95	1290	265	1650
Limestone*	9.6	30800	47	30850

* Chemical analysis of PARKER. (1967)
Calculated for a depth of 1 m below the surface at a site 40 N geomagnetic latitude and sea level.

Table 4.19 Production rates of ^{39}Ar due to spallation reactions with K,Ca and Fe.

Matrix	^{39}Ar Production Rate (kg^{-1} a^{-1})			
	K	Ca	Fe	Total
Sandstone*				
Granite*	4200	250	30	4480
Limestone*	420	6000	5.2	6425

* Chemical analysis of PARKER. (1967)
45 Calculated for a depth of 1m below the surface at a site 40 N geomagnetic latitude and sea level.

Table 4.20 Production rates of ^{37}Ar due to neutron, spallation and muon induced reactions at depths down to 20m.

	^{37}Ar Production Rate (kg^{-1} a^{-1})		
	neutron induced	spallation induced	muon induced
(Depth = 1m)			
Sandstone	76	4140	335
Granite	24	1650	550
Limestone	790	31400	1104
(Depth = 5m)			
Sandstone	9.0	21	98
Granite	3.6	3.5	135
Limestone	98	170	330
(Depth = 20)			
Sandstone	1.2	< 0.01	12
Granite	1.4	< 0.01	15
Limestone	16	< 0.01	39

Calculated for a site at 40 N geomagnetic latitude and sea level.

Table 4.21 Production rates of ^{39}Ar due to neutron, spallation and muon induced reactions at depths down to 20m.

	^{39}Ar Production Rate (kg^{-1} a^{-1})		
	neutron induced	spallation induced	muon induced
(Depth = 1m)			
Sandstone	140	2450	1200
Granite	340	4440	3370
Limestone	81	6430	490
(Depth = 5m)			
Sandstone	17	13	350
Granite	50	9.3	830
Limestone	10	33	150
(Depth = 20m)			
Sandstone	2.2	< 0.01	42
Granite	19	< 0.01	93
Limestone	1.7	< 0.01	17

Calculated for a site at 40 N geomagnetic latitude and sea level.

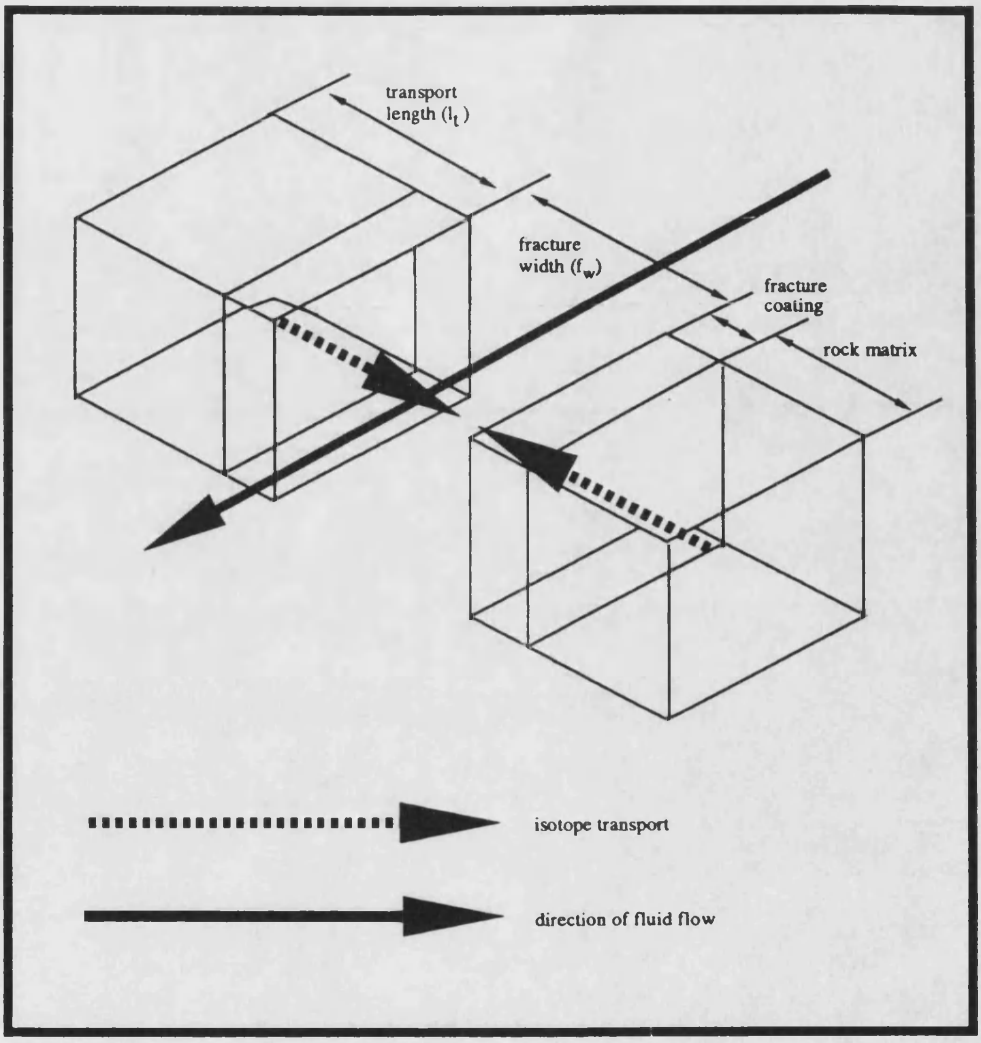

Fig 4.1 Schematic diagram illustrating the release of nuclides into water filled fractures from the surrounding rock matrix.

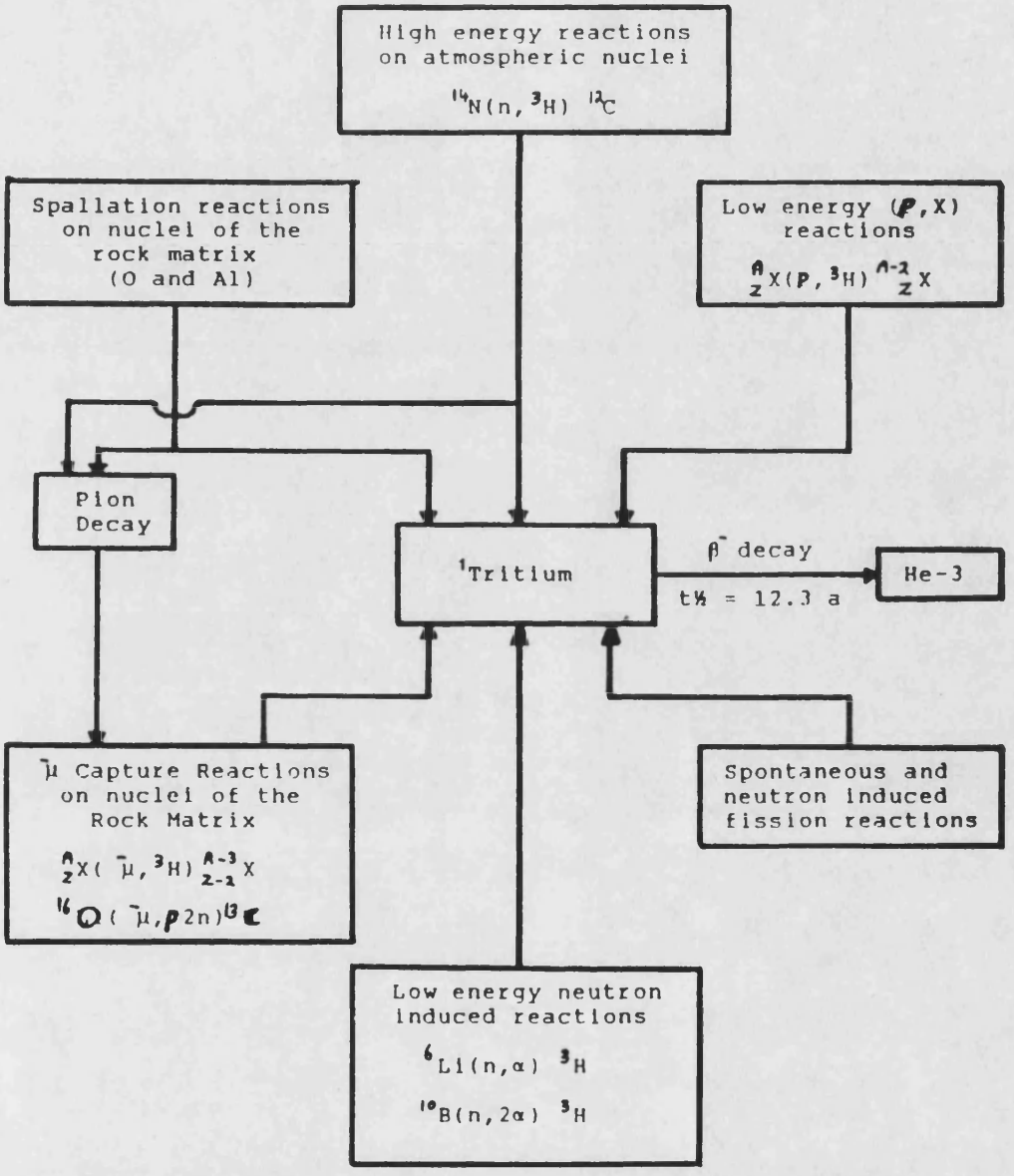

Fig 4.2 Diagram showing nuclear processes by which ^{3}H may be produced in the geosphere.

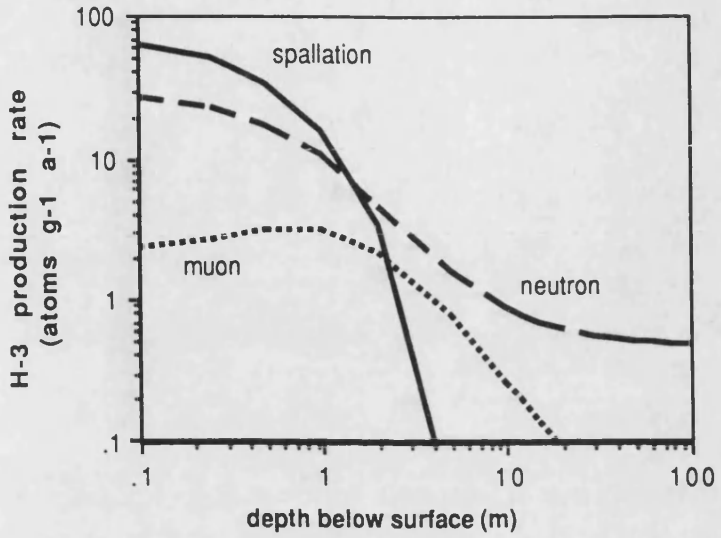

Fig 4.3 Variation in the production rate of ^{3}H with depth below the surface of an average granitic rock (see Appendix 1) for neutron, muon and spallation induced reactions. Rates have been calculated for a sea level site at 40 N geomagnetic latitude.

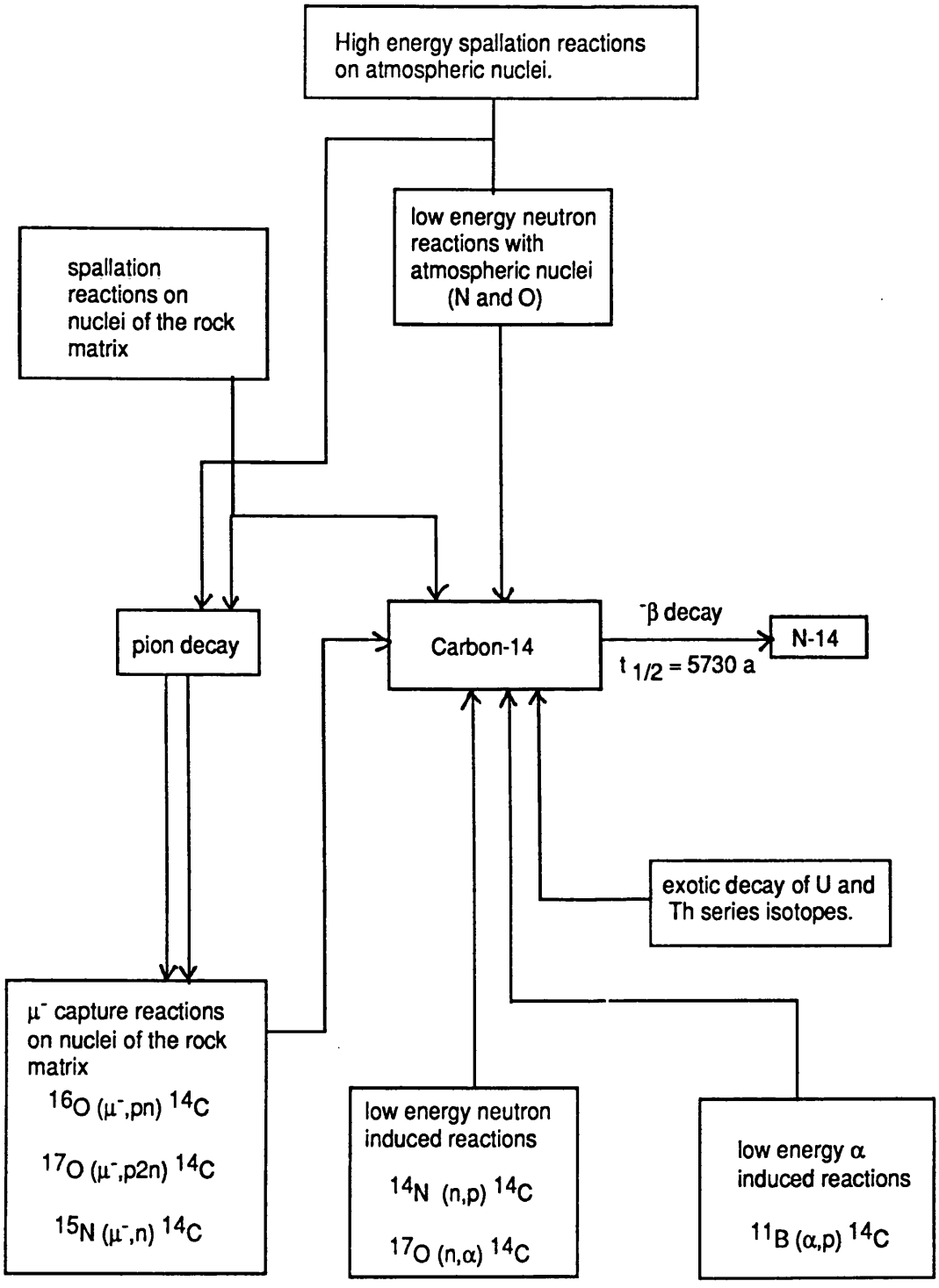

Fig 4.4 Diagram showing nuclear processes by which ^{14}C may be produced in the geosphere.

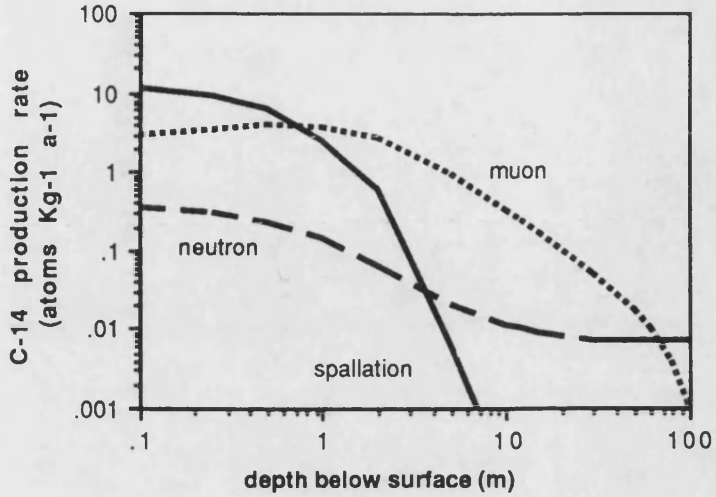

Fig 4.5 Variation in the production rate of ^{14}C with depth below the surface of an average granitic rock (see Appendix 1) for neutron, muon and spallation induced reactions. Rates have been calculated for a sea level site at 40 N geomagnetic latitude.

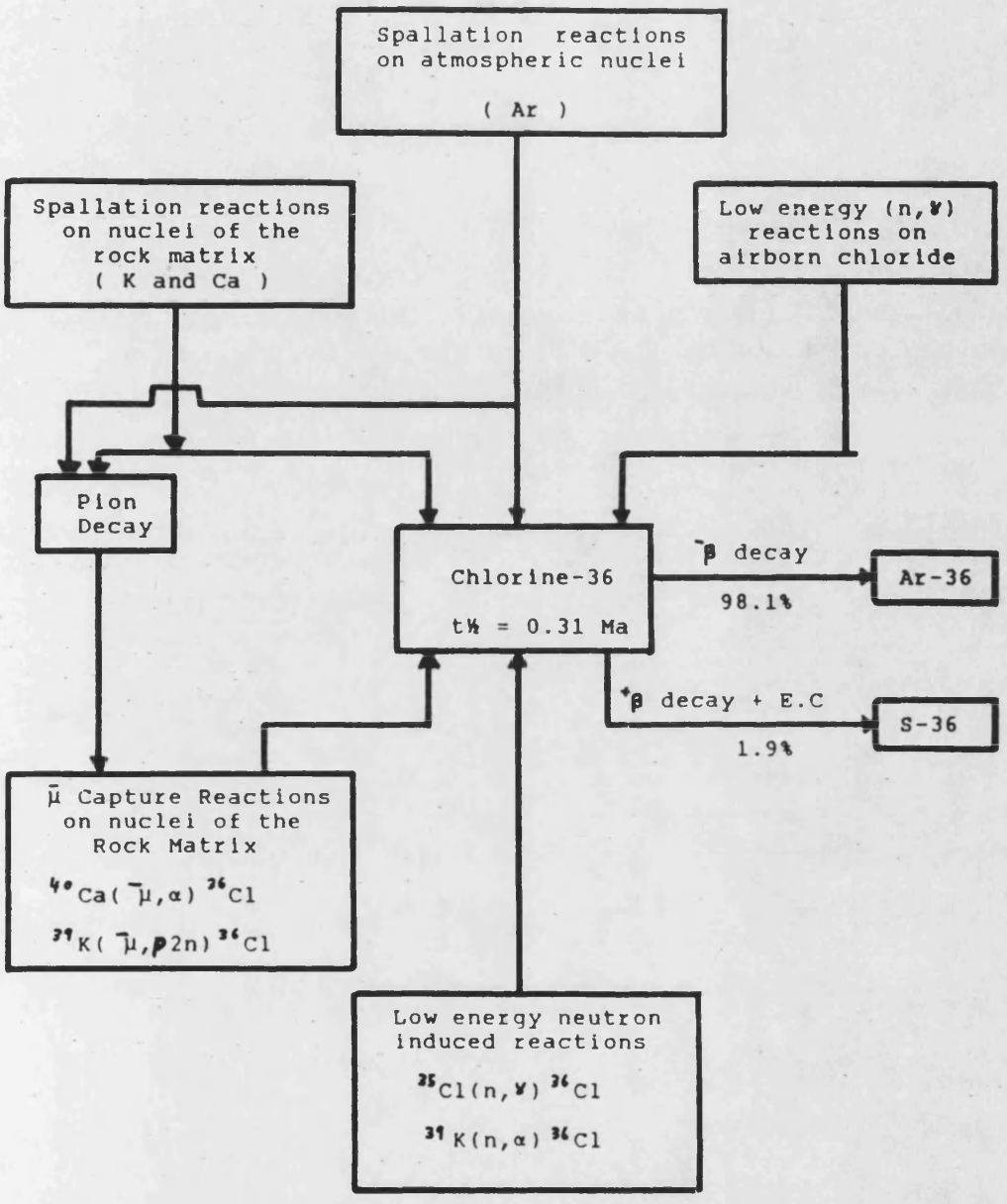

Fig 4.6 Diagram showing nuclear processes by which ^{36}Cl may be produced in the geosphere.

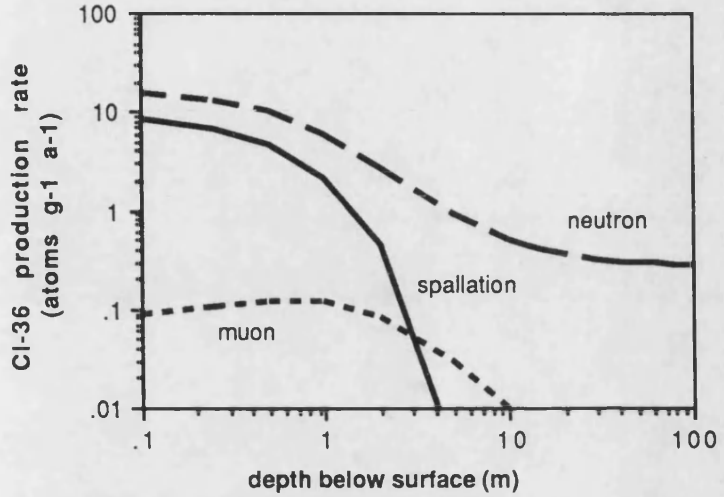

Fig 4.7 Variation in the production rate of ^{36}Cl with depth below the surface of an average granitic rock (see Appendix 1) for neutron, muon and spallation induced reactions. Rates have been calculated for a sea level site at 40 N geomagnetic latitude.

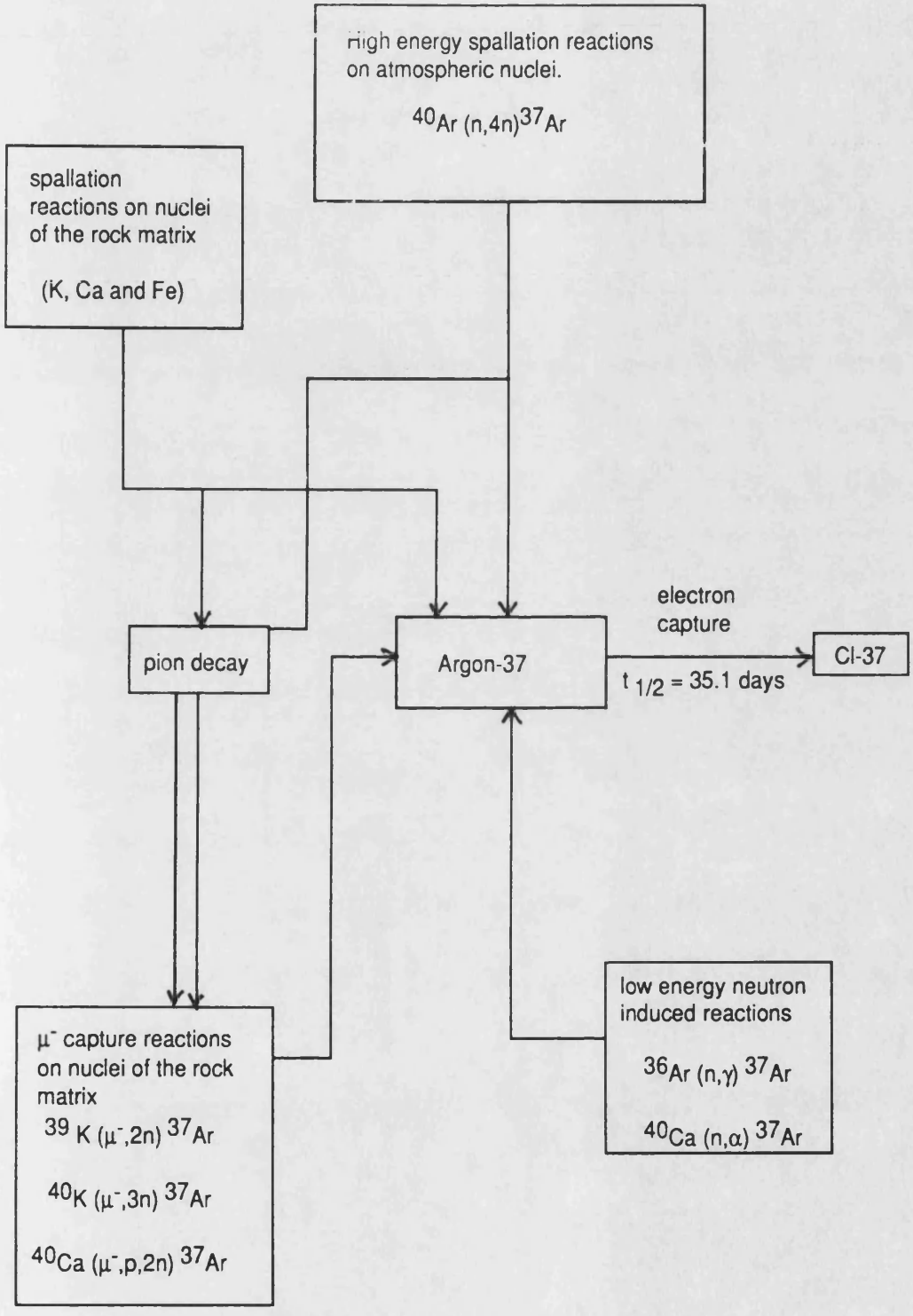

Fig 4.8 Diagram showing nuclear processes by which ^{37}Ar may be produced in the geosphere.

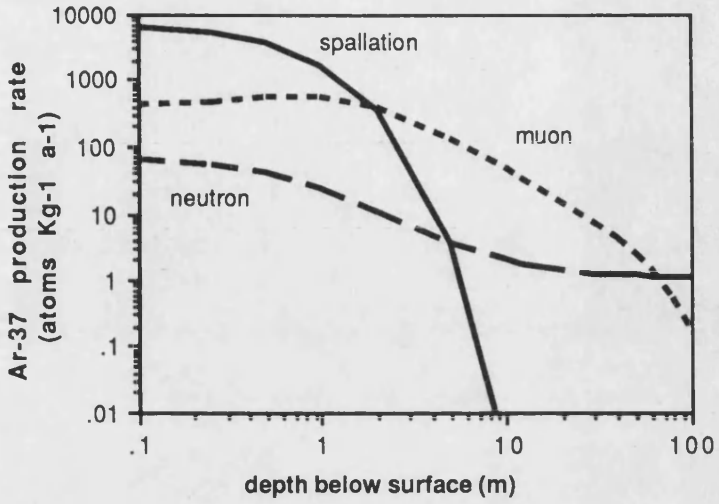

Fig 4.9 Variation in the production rate of ^{37}Ar with depth below the surface of an average granitic rock (see Appendix 1) for neutron, muon and spallation induced reactions. Rates have been calculated for a sea level site at 40 N geomagnetic latitude.

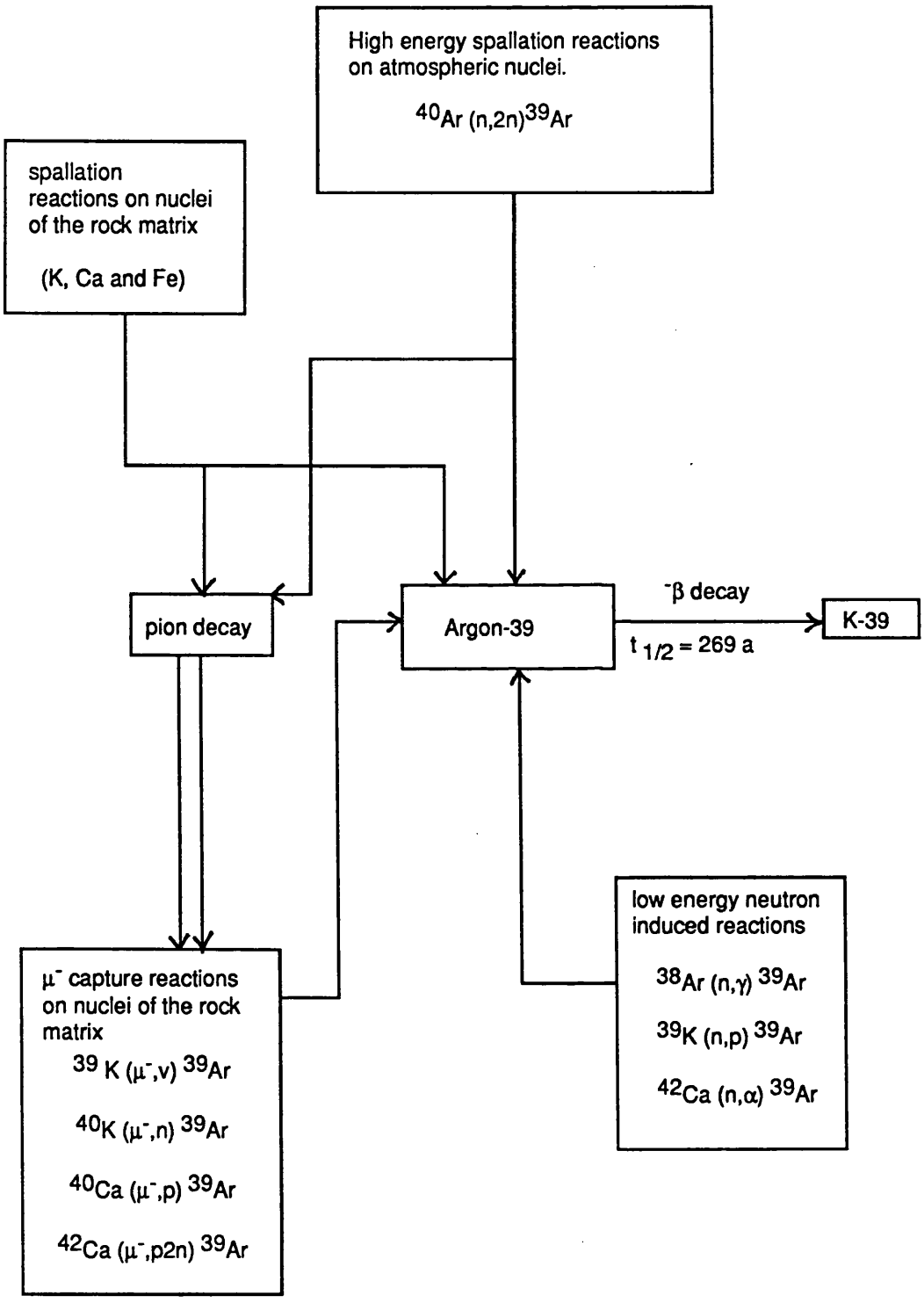

Fig 4.10 Diagram showing nuclear processes by which ^{39}Ar may be produced in the geosphere.

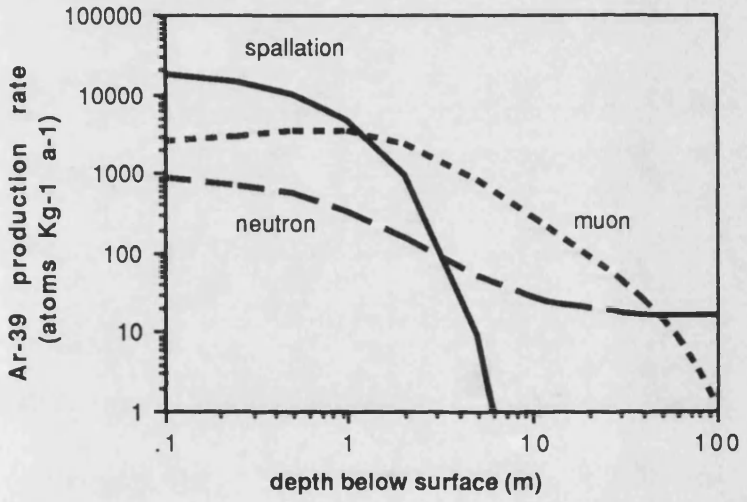

Fig 4.11 Variation in the production rate of ^{39}Ar with depth below the surface of an average granitic rock (see Appendix 1) for neutron, muon and spallation induced reactions. Rates have been calculated for a sea level site at 40 N geomagnetic latitude.

5. IN-SITU PRODUCTION AT THE STRIPA SITE.

5.1 Introduction.

The Stripa Project based at the abandoned Stripa iron-ore mine in south east Sweden (see Fig 5.1), was commissioned in 1977 to investigate the suitability of granite as a nuclear waste depository.

The mine is located in a small intrusion of medium grained granite of precambrian age which is enriched in U and Th compared to average granites. Stripa granite is in contact with local metasedimentary rocks (Leptite) within which are extensive haematite ore bodies. The Stripa site is shown diagrammatically in Fig 5.2 along with associated geology. The site consists of a 360m shaft from which a number of galleries and inclines have been mined, these galleries form experimental stations, the major station being at 360m below surface. To investigate deep groundwater flow patterns a number of boreholes have been drilled from these galleries (GALE and WITHERSPOON., 1979 and NORDSTROM et al., 1985), the two major boreholes being V1 and V2 which are from 360 to 860 and 410 to 1240 meters below the surface respectively. There is a net inflow of water into these boreholes (from the surrounding strata) which has been extensively sampled over different depth intervals by the use of "borehole packers".

The Stripa site is ideal for studying the in-situ production of neutrons and subsequently produced isotopes, discussed in previous Sections, because of its high natural radioelement content, ease of access and the availability of detailed geochemical and geophysical information. This Section uses the methods discussed in Sections 2 and 3 to estimate the in-situ produced neutron flux in both the granitic body and surrounding leptite. This calculated flux is then compared with the measured flux and the results of earlier calculations (NORDSTROM et al., 1985). The measured neutron flux is used to calculate the concentrations of ^{3}H, ^{14}C, ^{36}Cl, ^{37}Ar, ^{39}Ar and ^{85}Kr which enter the groundwater due to in-situ production by reactions described in Sections 1 and 6. These calculated concentrations are compared to the measured concentration of the respective nuclide in the groundwater and evidence is presented for subsurface production and migration of ^{36}Cl, ^{37}Ar, ^{39}Ar and ^{85}Kr in the Stripa granite.

5.2 The subsurface neutron flux at the Stripa site.

The high radioelement content together with relatively low concentrations of the neutron absorbing elements, Li, B and Gd should make the neutron flux generated within the Stripa granite amongst the highest known for crustal rocks. This flux is calculated below.

5.2.1 Neutron production in the Stripa granite and leptite.

At the depth at which the neutron flux measurements of NORDSTROM et al (1985) were made (>300m) neutron production due to cosmic rays is negligible (see Section 2). The in-situ neutron flux is thus due to neutrons produced by (α,n) reactions and spontaneous fission of ^{238}U. The neutron production rate was estimated using an average elemental analysis (based on the determination of light and heavy elements in drill cores from V1 and V2 boreholes (NORDSTROM et al., 1985)) and (α,n) neutron yields derived in Section 2. The average concentrations used in the calculation of neutron fluxes in the Stripa granite and leptite analysis are given in Table 5.1.

The number of neutrons produced per annum by (α,n) reactions was calculated using the computer program "ISOTOPE PRODUCTION" which was developed during the course of this thesis (See Appendix 5). Figs 5.3a and 5.3b show the number of neutrons produced by each of the major light elements present in the lepite and granite respectively. These distributions are typical of silicate rocks and show that elements outside the range O to Si have little influence on the neutron production rate. In both cases the major producers of neutrons are O, Na, Al and Si which would be expected to be distributed evenly throughout the matrix.

The neutron production rates due to (α,n) and spontaneous fission of ^{238}U per gram of Stripa granite and Leptite are given in Table 5.2.

5.2.2 Neutron absorption in the Stripa granite and leptite.

The macroscopic neutron absorption cross section for Stripa granite and leptite was calculated using the computer program "ISOTOPE PRODUCTION" (described in APPENDIX 5) and the average rock analysis given in Table 5.1.

The results of these calculations for the granite were consistent with the absorption cross sections measured on samples of Stripa granite using the method described in Appendix 3 and are given in Table 5.3. Figs 5.4a and 5.4b show the relative contribution of each element to Σ_m of the granite and leptite respectively. It may be seen that in both cases Σ_m is dominated by Gd and the abundant elements Si and K rather than B and Li as found in the case of the Cornish granites. The geochemistry of Gd, Si and K within the Stripa granite suggest that their distribution, and thence the derived value of Σ_m should be more constant in this case than where it is controlled by Li and B.

5.2.3 The in-situ neutron flux.

It has been assumed for the purpose of neutron flux calculations that the fraction of neutrons reaching thermal energies in the Stripa granite and leptite is close to one and that absorption has negligible effect on the neutron energy distribution. This assumption is likely to be valid since the concentration of 1/v neutron absorbers such as Li and B is low in both matrices. The neutron fluxes calculated from average rock analysis of Table 5.1 using the method described in Section 3 are 4.04×10^{-4} $cm^{-2}s^{-1}$ and 0.80×10^{-4} $cm^{-2}s^{-1}$ for the granite and leptite respectively. These values agree to within 15% or better with the experimental measurements of ANDREWS et al. (1986a) which are given in Table 5.1, and are almost an order of magnitude greater than those calculated for average crustal rocks (see Section 3).

It is interesting to note that in the case of the Stripa granite the ratio of thermal to epithermal neutron flux is about 5 (ANDREWS et al., 1986a), indicating that the neutrons are well thermalised. This is consistent with a matrix low in 1/v absorbers (Such as Li and B) and contrasts with the results of measurements made in other locations (see Section 3) where this is not the case.

5.3 Limits for in-situ production of radioisotopes.

The equilibrium number of atoms produced by each of the major neutron induced reactions described in Section 4 have been calculated (Tables 5.4 and 5.5) for the measured neutron

fluxes and measured elemental compositions of the Stripa granite, leptite, fracture fluids and fracture infill. Measured neutron fluxes and chemical compositions of the granite, fracture fluids, typical fracture mineralisation and of the surrounding leptite are summarised in Table 5.1.

Nuclide concentrations in fluids within the granite have been estimated from the results of the above calculations and transfer criteria discussed in Section 4. The fluid composition used for these calculations is that of the most saline groundwater present in borehole V1 at Stripa (NORDSTROM et al., 1985).

The following sections firstly examine the likely processes which control nuclide transfer within the Stripa granite, and then calculates and compares measured concentrations of ^{3}H, ^{14}C, ^{36}Cl, ^{37}Ar, ^{39}Ar and ^{85}Kr in Stripa groundwaters.

5.3.1 Solution and transport of radionuclides.

As discussed briefly in Section 4 the estimation of radionuclide concentrations in flowing groundwaters requires an understanding of the mechanisms of transfer of in-situ produced radionuclides from the rock matrix to the groundwater. In all cases a maximum concentration in the groundwater may be estimated based on the assumption that all of the radioisotopes produced within the rock matrix is transferred to the fluids in the rock pore spaces. (In the case of an interstitial flow system, the rock porosity is host to the groundwater. However, for crystalline rocks, water may be present bound to the crystalline lattice, as non-conductive fluid inclusions and as fracture fluids). The minimum observed porosity for such crystalline rocks is about 1% (ALEXANDER et al., 1981).

This porosity has been assumed for calculation of the maximum radionuclide concentration in the aqueous phase at the Stripa site (see Table 5.6). This estimate is independent of the micro-distribution of radionuclide production in relation to the aqueous phase.

A more appropriate method of estimation in the crystalline rocks found at the Stripa site should assess the migration of radionuclides from their in-situ production sites into the fracture fluids. Such migration can only take place over relatively short distances which are determined by the

recoil energy and diffusive properties of the radionuclide. The resulting concentration in the fracture fluid may consequently be strongly influenced by any enhanced in-situ production in secondary fracture mineralisation as fracture minerals may have compositions which are very different from the mean rock analysis.

For the fracture based model discussed in Section 4, radionuclide concentration in the fluid depends upon the fracture width; upon the composition of the fracture walls (newly fractured granite or fractures with secondary mineralisation) and upon the migration distance for the radionuclide from within the fracture wall. Fracture widths within the Stripa granite have been estimated from the ^{222}Rn contents of the groundwaters (ANDREWS et al, 1986b) and a modal value of 150 μm has been adopted for the purpose of modelling. The migration length of a radionuclide within the rock matrix is dependent upon both the recoil range of the nucleus as it is formed and upon its subsequent diffusion length. The latter is determined by the diffusive properties of the nuclide and by its half-life. The diffusion length of ^{222}Rn within the Stripa granite is 700 μm (ANDREWS et al., 1986b). Lighter noble gas nuclei (e.g.^{39}Ar) would have higher diffusion coefficients than ^{222}Rn and, if their half-lives are longer, much longer diffusion lengths. However, ^{222}Rn is formed in locations within the rock matrix which are readily accessible to the fracture fluids where as for ^{39}Ar, the formation sites are mainly within feldspar crystals so that the diffusion medium for ^{222}Rn is probably water whilst for ^{39}Ar it is a silicate lattice. Sufficient data is not available to assess probable migration distances for all nuclei, and a nominal distance of 300 μm has been assumed for the purpose of assessing the influence of the immediate fracture environment in radionuclide release into fluids.

The possible concentrations of nuclides in groundwaters at the Stripa site calculated using the above method are compared to those based on the total transfer in Table 5.6.

5.3.2 In-situ production of radioelements.

5.3.2.1 Tritium. Tritium in the Stripa waters has been determined by direct liquid scintillation counting (University of Waterloo); by liquid scintillation counting with electrolytic preconcentration (I.A.E.A., Vienna and G.S.F.,

Neuherberg) and by electrolytic preconcentration followed by gas-proportional counting of propane (WOLF et al, 1981) at G.S.F., Neuherberg. The detection limit for this last method is 0.1 T.U. (97.5% confidence level) for a 1000 minute count (0.1 T.U. = 6690 atoms ^3H cm^{-3} H_2O). Groundwater having a natural ^3H input of 5.5 T.U. would need to be isolated from further input for about 70 a to allow decay to this detection limit.

The calculated number of in-situ produced ^3H atoms at equilibrium in the Stripa granite is 46 atoms cm^{-3} of rock matrix (Table 5.4). The production of ^3H due to neutron irradiation of Li in the fracture fluids is comparatively small at about 0.3 atoms ml^{-1} of fluid at equilibrium. On the assumption that all of the atoms formed exchange with the fracture fluids, this corresponds to a ^3H content in the fluid of 0.07 T.U. for 1% fracture porosity or 0.7 T.U. for 0.1% fracture porosity. Intergranular porosities for granites are likely to be about 1% (ALEXANDER et al., 1981; NELSON et al., 1979) and there may be a low percentage of of bound water with which ^3H exchange may take place.

It is unlikely that all of the ^3H atoms formed can migrate to the fracture fluids before being trapped within such intergranular or bound water, so that these ^3H-contents must be regarded as maxima. Table 5.6 compares the estimated ^3H contents of groundwater for total transfer to the fluid phase and for transfer from a limited thickness of rock matrix on either side of a fracture. For the latter model, the ^3H contents of the fracture fluids would be very small.

The ^3H contents of surface and groundwaters at Stripa are reported in NORDSTROM et al (1985) and MOSER et al (1987). All of the surface, shallow groundwaters and mine seepages contain ^3H in excess of 30 T.U. and this must be attributed to the presence of thermonuclear tritium. This proves that the mine seepages must either have fairly rapid flow continuity via fractures to the surface or have exchanged with air-borne ^3H in the mine galleries (ANDREWS et al., 1989). Samples from borehole N1 (a horizontal borehole 360 meters below the surface) have ^3H contents <0.25 T.U. in comparison with contents >60 T.U. for natural seepages into the mine galleries. This indicates that the N1 waters are derived from a region of the granite where fracture flows have not been as

active as now occurs in the mine galleries at similar depths. The concentration of ^{3}H in boreholes other than V2 are significantly above the largest possible value for in-situ production (0.7 T.U.), so that a proportion of post 1952 water must be present in all of these locations. The lower intervals in V2 have ^{3}H contents <0.25 T.U. which, allowing for the precision of measurement, fall in a range which could be attributed to in-situ production. Alternatively, they could be groundwater with natural cosmic ^{3}H inputs with ages up to 70a or much older groundwaters admixed with a very small proportion of groundwater containing thermonuclear ^{3}H.

5.3.2.2 Carbon-14. The extent of in-situ ^{14}C production from neutron interactions in the Stripa granite is shown in Table 5.4 together with contributions of other possible reactions in the rock matrix and the fracture fluids. Significant numbers of ^{14}C atoms are produced in the rock matrix, fracture calcite and in the fracture fluids themselves. However, because of dilution with the stable carbon content of these materials, the ^{14}C specific activity (expressed as a % of that of modern carbon) is significant only for production in the fracture fluids. This is due to the relatively large amounts of carbon present in the rock matrix and especially in calcite. The ^{14}C production in the fracture fluids arises from neutron irradiation of dissolved nitrogen and of the oxygen of the water molecules. Production due to the $^{11}B(\alpha,p)^{14}C$ reaction at the Stripa site is either negligible, or as great as production from either the $^{14}N(n,p)$ or $^{17}O(n,\alpha)$ reactions depending on the cross section used (see Section 4).

Significant production from this reaction due to localised high U concentrations in secondary mineralisation should be small since it is unlikely that boron would be intimately associated with uranium.

The extent of in-situ ^{14}C production by exotic decay has been calculated on the basis of the measured branching ratios for ^{223}Ra and ^{226}Ra. Similar exotic decay of ^{224}Ra (^{232}Th-series) has been neglected since its production rate is only 20% of that for Ra isotopes of the U-series. Also the ^{14}C atoms produced by ^{224}Ra decay are less likely to be accessible to fracture fluids since Th is incorporated in accessory minerals.

The concentration of ^{14}C in fracture fluids as a result of this production mode depends upon the escape probability of ^{14}C from its production site (U concentrations) to the fluid phase, as well as upon the fracture porosity and U-content of the rock matrix.

As discussed in Section 4 the extent and effectiveness of the exotic decay mode of ^{14}C production is at present uncertain. However at the Stripa site, it could be as important as neutron induced reactions in highly mineralised fractures (Table 5.4). The efficiency with which ^{14}C atoms produced at U or Ra sites could migrate into solution is probably less than that for other radionuclides which are produced at similar locations. The noble gases, ^{222}Rn (a ^{226}Ra decay product) and ^{85}Kr (a product of ^{238}U spontaneous fission) would, for example, be expected to diffuse readily from their sites of formation into solution. Similarly, the chemical mobility of the halide, $^{129}I^-$ is likely to be greater than that of ^{14}C atoms The latter could become mobile if oxidised by for instance interaction with uraninite or silicate oxygen but any exchange with the carbonate of fracture calcites would tend to inhibit ^{14}C migration (ANDREWS et al., 1989). Based on the more conservative estimate of ^{14}C production by exotic decay, and if there were little ^{14}C exchange with fracture calcites, it is estimated that in-situ production is likely to label bicarbonate in the Stripa groundwaters to the extent of 1 to 5 % modern carbon (see Table 5.6).

The measurement of ^{14}C contents around 1% modern by radiochemical methods can only be achieved with limited precision for statistical reasons. Even with a well shielded low background counter such as that described by HOUTERMANS AND OESCHGER (1958), determination of 1% modern carbon requires a 24 hour count for a 95% probable error of +/- 0.25% modern. The precision currently achievable with TAMS is similar. The highest possible precision of measurement will thus be necessary to positively demonstrate the occurrence of in-situ ^{14}C-production.

The measured ^{14}C contents of the deep groundwaters at Stripa are generally a few percent modern (NORDSTROM et al., 1985). The low HCO_3^- contents and high pH of these waters make it necessary to take rigorous precautions against contamination by atmospheric carbon dioxide

(NORDSTROM et al., 1985). Careful sampling using a closed circuit CO^2-stripper has been made and the lowest ^{14}C contents measured were 2.0 +/- 1.0 % modern. The presence of ^{3}H in some samples suggests that they contain a proportion of modern possibly anthropogenic ^{14}C. If the possibility of such atmospheric contamination is excluded, most of the groundwaters have a significant residual ^{14}C content. Calcite saturation is approached even for the shallow groundwaters and there is little change in the $^{13}C/^{12}C$ ratio of dissolved bicarbonate within the groundwater system (NORDSTROM et al., 1985). The total carbonate contents decrease with depth and this probably involves calcite precipitation which would not change the ^{14}C specific activity if present as carbonate.

The minimum ^{14}C content resulting from in-situ production in the Stripa fracture fluids (1% modern) corresponds to a decay time of 32 ka for an input of 50% modern carbon due to congruent solution of ^{14}C-dead calcite [$H_2CO_3 + CaCO_3 = Ca(HCO_3)_2$] followed by insignificant ^{14}C exchange with the rock matrix. This is therefore the age limit for application of the ^{14}C method to dating the Stripa groundwaters. As this age is sufficient to approach equilibrium for in-situ ^{14}C-production, the remnant of atmospheric ^{14}C input after subtracting contribution from in-situ production (1%) must be about 1% which corresponds to an age of 32 ka for the oldest groundwater in the system. Alternatively, such a ^{14}C content could be explained by admixture of 2% modern water with very old ^{14}C-free water. For such low ^{14}C-contents, however, the precision of ^{14}C determinations is a limitation to interpretation. The error of measurement is, for example, generally greater than the estimated labelling of dissolved bicarbonate due to in-situ production of ^{14}C. The measured ^{14}C contents in the groundwaters could also be totally attributed to in-situ production.

5.3.2.3 Chlorine-36. The possible presence of in-situ produced ^{36}Cl at Stripa was first suggested by MICHELOT et al (1984) and FONTES et al (1984). The presence was confirmed by NORDSTROM et al (1985) and the phenomenon studied in detail by ANDREWS et al (1986).

As with average granites the only in-situ reaction which produces significant ^{36}Cl in a rock matrix at depths in excess of 100m is the $^{35}Cl(n,\gamma)^{36}Cl$ reaction.

In the Stripa granite the $^{39}K(n,p)^{36}Cl$ reaction produces only 2% of the amount formed by neutron capture on ^{35}Cl. The experimentally measured neutron flux for the Stripa granite produces an equilibrium $^{36}Cl/Cl$ atomic ratio of 215×10^{-15} after 1.5 ma. The neutron flux in the surrounding metasediments (leptite) is lower than in the granite and corresponds to a $^{36}Cl/Cl$ atomic ratio of 41×10^{-15} for chlorine in the leptite. These ratios are the same as those predicted in ANDREWS et al (1986a) since those authors also used the experimental neutron flux in calculations. Use of the calculated neutron flux as a basis for calculation yields values of 185×10^{-15} and 36×10^{-15} for the granite and leptite respectively. These are slightly lower than those calculated from the experimentally determined flux and reflect the slightly lower calculated flux (see Section 3).

Due to the low porosity of the matrix, fracture fluids experience the same neutron flux as in the unfractured granite. (The presence of small amounts of fracture fluids having little influence on the total absorption cross section of the rock and hence on the in-situ neutron flux.) However as stated by ANDREWS et al (1986a) the residence time of fracture fluids could be much less than 1.5 Ma so that in-situ production of ^{36}Cl in the fluids would not attain equilibrium whereas the matrix Cl^- would be at equilibrium for all rocks older than about 1.5 Ma. Groundwaters which increase in salinity during their migration in the fracture system would at least partially derive their chloride from the rock matrix and their $^{36}Cl/Cl$ ratio would gradually attain the ratio of the host rock (in this case granite or leptite).

Measurements of ^{36}Cl at the Stripa site :-

(a) Measurements on matrix chloride.

The analysis of ^{36}Cl present in rock matrices has only recently been achieved due to the difficulty of separating small amounts of uncontaminated chloride from the matrix. Workers in the USA have extracted Cl from a number of rock samples taken from the Stripa site and have determined the $^{36}Cl/Cl$ ratio by tandem accelerator mass spectrometry (J. FABRYKA-MARTIN perrs comm). The preliminary results of these analysis are given in Table 5.5. These results are generally consistent with the equilibrium ratios calculated above. Three of the results (samples N1F, V1F and LEPC), however, are higher than the calculated ratios.

It is at present uncertain if this inconsistency is due to experimental error, local fluctuations in the neutron flux, locally enhanced K:Cl ratios or a combination of these effects. Importantly as of present such high ratios have not been observed in minewaters at the Stripa site, the $^{36}Cl/Cl$ ratios of which are shown in Fig 5.5.. This suggests that such high ratios are localised and that such areas do not contribute substantially to the overall groundwater chlorinity.

(b) Measurements in minewaters.

Samples of minewaters from Stripa were collected in the period 1981-1984 and their ^{36}Cl contents are reported in NORDSTROM et al (1985) and ANDREWS et al (1986a). Further samples were collected and analysed during 1985/86 (DAVIS et al., 1986) and the $^{36}Cl/Cl$ ratio for these and the earlier results are plotted against groundwater chlorinity (after ANDREWS et al., 1986) in Fig. 5.5. On Fig. 5.5, the horizontal lines represent the $^{36}Cl/Cl$ ratios expected for total derivation of groundwater chloride from the granite and the surrounding leptite.

The Cl^- content of local precipitation according to the data of ERIKSSON (1960) is 0.6 mg l^{-1} for an annual precipitation of 760 mm and evapotranspiration of 60%. The corresponding cosmogenic ^{36}Cl content of recharging groundwater is about 1150 atoms ml^{-1} with a $^{36}Cl/Cl$ ratio of 45×10^{-15} using the fallout data quoted above and the method of estimation of the cosmogenic input described in ANDREWS et al., 1986a. The changes in this ratio as such meteoric water derives chlorinity by interaction with the granite or leptite are shown by dotted lines in Fig. 5.5. Dilution lines (broken lines) are shown for a meteoric input which contains bomb-produced ^{36}Cl and derives further Cl^- by interaction with both the granite and the leptite.

Meteoric water containing bomb-pulse ^{36}Cl was found in nearby surface water which has a chloride content of 36 mg l^{-1} with a $^{36}Cl/Cl$ ratio of 1040×10^{-15}. The absence of significant thermonuclear ^{3}H and ^{14}C in the deep minewaters shows that they do not result from solution of matrix chloride by recent meteoric water. All of the minewater samples lie in a region of Fig. 5.5 which falls between the $^{36}Cl/Cl$ ratios characteristic of the leptite and of the granite and most groundwaters in the system must have derived at least part of

their ^{36}Cl, and hence chloride, from the leptite. This supports the earlier conclusion of ANDREWS et al (1986) that ^{36}Cl in Stripa minewaters is mainly due to in-situ irradiation of natural Cl^- and subsequent leaching of ^{36}Cl from the rock matrices along groundwater flow paths.

The time scale for ^{36}Cl increase from equilibrium with the leptite by radiogenic ingrowth within the granitic neutron flux is indicated on Fig. 5.5. Saline water from the leptite would require subsequent residence times up to 300 ka within the granite to derive the observed ^{36}Cl in some of the deep groundwaters from V2 by radiogenic ingrowth if no further chloride were derived from the granite. Alternatively and more probably, these waters may have derived their Cl in part from both the leptite and the granite. Table 5.6 shows that a ^{36}Cl concentration of 1.5×10^8 atoms ml^{-1} would result from total transfer of Cl^- from the granite to pore fluids for a porosity of 1%. Such total transfer would result in a fluid chlorinity of 43 g l^{-1}. The maximum chlorinity present in Stripa groundwaters, however, is only 700 mg l^{-1} which corresponds to about 1.6% of the matrix Cl^- transferred to the pore fluids. It may be concluded that the ^{36}Cl contents observed in the Stripa groundwaters are predominantly caused by in-situ production, either in the leptite or in the granite rather than by inputs of cosmogenic or bomb-pulse ^{36}Cl. Such solution of rock matrix ^{36}Cl is much greater than possible cosmogenic inputs and makes groundwater dating by decay of cosmogenic ^{36}Cl impossible. It is, however, possible to conclude that not all the Cl^- at Stripa has been derived from the granite and that the groundwaters have not resided long enough within the granite to attain the equilibrium $^{36}Cl/Cl$ ratio for the granitic neutron flux.

5.3.2.4 Argon-37. As discussed in Section 4 in-situ production of ^{37}Ar (half-life 35.1 days) is mainly due to the $^{40}Ca\ (n,\alpha)^{37}Ar$ reaction. Compared with the yield of this reaction, the contribution from the reaction $^{36}Ar(n,\gamma)^{37}Ar$ on the argon dissolved in water is several orders of magnitude smaller (Table 5.6). Using an average Ca-content in the Stripa granite of 0.51% (Table 5.1) and the measured neutron flux the equilibrium concentration of ^{37}Ar in the granite is 1.0×10^{-3} atoms cm^{-3}. The equilibrium number produced by the same neutron flux in the fracture fill minerals is 4.0×10^{-2}

atoms cm^{-3}. Using the total transfer model discussed in Section 4 where 100 % of the produce isotope is transferred into the pore fluids, gives an ^{37}Ar content of 0.1 atoms ml^{-1} H_2O for the Stripa granite (Column 2, Table 5.6) . However, for release into fracture fluids from fracture walls concentrations range from 0.004 to 0.16 atoms ml^{-1} and are dependent upon the composition of the fracture wall (Table 5.6). The error in these values may be at least 50% due to the uncertainties associated with the (n,α) reaction cross section. As pointed out in ANDREWS et al (1988) ^{37}Ar could also be introduced into groundwater by admixture of recent water containing anthropogenic ^{37}Ar.

During sampling at Stripa in November 1984, the atmospheric ^{37}Ar content was measured to be $6x10^{-3}$ atoms ml^{-1} H_2O given that the water was saturated at 10°C with argon of recent origin. The estimated concentrations due to in-situ production are of similar or much greater magnitude (Table 5.5). LOOSLI et al (1988) have measured ^{37}Ar concentrations in the Stripa minewaters of 0.10, 0.30 and 0.63 atoms ml^{-1} H_2O. These ^{37}Ar concentrations are equal to or greater than values calculated for the release of in-situ produced ^{37}Ar (Table 5.6). It is unlikely that the measured ^{37}Ar contents of the groundwaters are due to in-situ production involving the average Ca-content of the granite matrix. The measured concentrations are more readily explained if the production site is principally in the high Ca-content fracture infills, which allow easy transport of the produced ^{37}Ar into fracture fluids.

5.3.2.5 Argon-39. The rare radioisotope, ^{39}Ar with a half-life of 269 years, is potentially useful as a dating method in the age range up to 1000 years. The principles of its use for groundwater dating have been discussed by LOOSLI (1983) and other workers (see Section 1). In-situ production of ^{39}Ar can result from the $^{38}Ar(n,\gamma)^{39}Ar$, $^{39}K(n,p)^{39}Ar$ and $^{42}Ca(n,\alpha)^{39}Ar$ reactions whose neutron cross sections are discussed in Section 4.

The relative importance of ^{39}Ar in-situ production reactions in the Stripa granite, its fracture infills and fracture fluids are shown in Table 5.5. All of the reactions within the fracture fluids produce negligible amounts of ^{39}Ar and the major in-situ production results from neutron

interaction with ^{39}K in the feldspars and micas of the rock matrix. ^{39}Ar produced at such sites must escape into the fracture fluids if it is to influence their ^{39}Ar content. For a fracture porosity of 1%, if all the matrix ^{39}Ar were to escape into the fracture fluids (the total transfer model), the ^{39}Ar content of the latter would be 1.3×10^4 atoms ml^{-1} of water (Table 5.6). This is many times the ^{39}Ar content of water which has been equilibrated with the atmosphere (5.8 atoms ml^{-1}, if recent atmospheric Ar is equilibrated with water, LOOSLI (1983)).

Although fracture calcite is likely to be in close contact with fracture fluids, its proportion of the rock matrix is small and its contribution to the total in-situ production of ^{39}Ar will be small relative to the contribution from ^{39}K. Nevertheless, ANDREWS et al. (1988) pointed out that ^{39}Ar atoms (Van der Waals radius 0.19 nm) cannot easily be accommodated at the sites of Ca^{2+} ions (ionic radius 0.10 nm) and it may be released from calcite into fracture fluids with greater efficiency than ^{39}Ar can be released from feldspar or mica lattices. (K^+ ionic radius 0.13 nm). Release of ^{39}Ar into fluids from fracture walls would result in concentrations up to 500 atoms ml^{-1} (Table 5.6). For the Stripa minewaters the measured ^{39}Ar content of the groundwaters range from 50 to 250 atoms ml^{-1} (LOOSLI et al., 1988). These values are much greater than possible inputs of atmospheric ^{39}Ar (5.8 atoms ml^{-1}, above) and must be attributed to in-situ production. They correspond to the loss of 0.5 to 2% of the in-situ production of ^{39}Ar within the granite matrix into fluid filled fractures for a 1% porosity and approximates to total loss of ^{39}Ar from fracture walls. The contribution to the ^{39}Ar content of the groundwater of ^{39}Ar which has been produced in adjacent fracture calcites must also be considered. On a mass balance basis, however, such a contribution is probably less than a few percent of the measured ^{39}Ar content.

5.3.2.6 Krypton-85. ^{85}Kr (half-life 10.8a) is mainly produced underground by spontaneous fission of ^{238}U. In-situ production of ^{85}Kr occurs at U-atom sites and since the U-distribution is inhomogeneous, the concentration of ^{85}Kr in the rock matrix will be variable.

Calculated equilibrium ^{85}Kr contents of the Stripa granite (U-content 44 ppm) and its fracture infills (U-content 1000 ppm) are 0.3 and 6.7 atoms cm^{-3} respectively. The corresponding concentration of ^{85}Kr in fracture fluids within unaltered granite is 30 atoms ml^{-1} for a porosity of 1% and complete release of ^{85}Kr from the rock matrix (the total transfer model). A similar concentration is likely in a fluid which derived all its ^{85}Kr from in-situ production in fracture infills (Table 5.6). The concentration of anthropogenic ^{85}Kr in air-saturated water was negligible prior to 1957 and has gradually increased to the present value of 33-49 atoms ml^{-1} (LOOSLI and OESCHGER, 1979; ROZANSKI and FLORKOWSKI, 1979). In-situ production of ^{85}Kr has not been identified in groundwaters to date because the expected levels are low and are difficult to distinguish from small amounts of atmospheric Kr contamination of the samples. However, at Stripa such anthropogenic input is only likely to exceed the contribution from in-situ production if the efficiency of ^{85}Kr release from the rock matrix is low. The observed concentrations of ^{85}Kr in Stripa groundwaters are 4 - 16 atoms ml^{-1} (LOOSLI et al., 1988). These concentrations range from a fifth to a half that calculated for either total transfer or transfer from fracture minerals and are smaller than that predicted for modern air equilibrated water. If these measured values are due to contamination then this must be in the region of 10% which, in a carefully conducted experiment, should be unlikely. It would thus seem reasonable that the measured values result from in-situ production and that the probability of ^{85}Kr release is high. From a theoretical view point it would seem more likely that ^{85}Kr is produced in and released from fracture infill.

5.4 Conclusions.

(1) The agreement between calculated and measured neutron fluxes in the Stripa granite is good (< +/- 15%), especially when the uncertainties which are associated with the microdistribution of radioelements are considered. The effectiveness of U-series alpha particles for (α,n) reactions at the Stripa site may be reduced by alpha absorption within high concentrations of uraninite in micro-fractures.

(2) The estimated groundwater contents of in-situ produced ^{3}H and ^{14}C are close to the present detection limits for these nuclides. For ^{3}H, the production site is within the minerals of the rock matrix and the efficiency of its transfer to the fluids is probably low. The most significant n-induced ^{14}C production probably occurs within the fracture fluids of a granite matrix. The emission of ^{14}C by exotic decay of Ra and other natural radioelements may also be an important source of in-situ produced ^{14}C.

(3) In groundwaters in the Stripa granite, in-situ production of ^{36}Cl dominates over atmospheric inputs due to both cosmogenic production and nuclear weapon testing. $^{36}Cl^{-}$ may be used for determining the origin of groundwater salinity from comparisons of $^{36}Cl/Cl$ ratios with those calculated for in-situ produced isotopes in the rock.

(4) The in-situ production of ^{39}Ar occurs mainly within the feldspars and micas of a granitic matrix, that is, at the natural K sites. ^{37}Ar production occurs mainly within the fracture minerals within the Stripa granite, that is, at the high concentration of Ca target within the calcite of the fracture infill. ^{85}Kr production occurs at U sites and is controlled by the micro-distribution of U. Fracture infill minerals and microfractures within the matrix minerals are potentially important production sites.

(5) Comparisons of the amounts of in-situ produced isotopes in groundwaters can lead to an understanding of the mechanisms for their release from the rock matrix.

(6) There is a requirement for more precise determinations of nuclear reaction cross sections (especially for some of the noble gas products), and of the probability of ^{14}C exotic decay, to aid the calculation of in-situ production rates.

Table 5.1. Element compositions (μg/g) of the Stripa granite, its fracture infills, fracture fluids and leptite, used to calculate in-situ reaction rates. (1)

Element	Granite	Fracture Infill(5)	Fracture Fluid(1)	Leptite(6)
H	423.(3)	423.(3)	110,000.	423.(3)
Li	11.	0.5	0.18	14.
B	4.0	-	0.24	5.9
C	300.(2)	20.(2)	31.(4)	20.(2)
N	20.(2)	20.(2)	2.56	-
O	480,000.	455,000.	890,000.	485,000.
F	440.	-	4.4	800.(2)
Na	30,200.	-	304.	10,200.
Mg	1,570.	29,450.	0.32	9,200.
Al	74,100.	53,950.	<0.005	60,500.
Si	359,000.	63,800.	6.4	350,500.
Cl	160.	-	700.	105.
Ar	-	-	1.42(4)	-
K	38,400.	1,615.	2.5	33,750.
Ca	5,150.	201,000.	170.	13,500.
Ti	480.	325.	-	1,260.
Cr	1.7	-	-	-
Mn	460.	3,100.	<0.1	155.
Fe	9,300.	129,600.	0.008	19,850.
Co	0.71	-	<0.005	-
Ni	8.0	-	-	-
Kr	-	-	0.0006(4)	-
Rb	200.	-	-	-
Sr	300.(2)	-	1.8	-
Sm	11.4	-	-	7.9
Gd	12.9	-	-	7.5
U	44.1	1,000.	<0.001	5.4(7)
Th	33.0	-	-	17.9(7)
neutron flux	4.71(8)	-	-	0.90(8)

(1) All analytical data from NORDSTROM et al. (1985) unless otherwise stated.
(2) Average granitic values from PARKER. (1967).
(3) For 1% bound or intergranular fluids.
(4) Dissolved gases and ionic species.
(5) For a 50/50 calcite/chlorite fracture filling. (Based on fracture mineral analyses by S.K. FRAPE (personal communication).
(6) Analytical data from S.N. DAVIS (personal communication).
(7) WOLLENBERG et al. (1980).
(8) In units of 10^{-4} cm^{-2} s^{-1} from ANDREWS et al. (1986).

Table 5.2. Neutron production rates from (α,n) and spontaneous fission reactions within the Stripa granite and Leptite.

	Neutron yield (g^{-1} a^{-1})	
	granite	leptite
(α,n) Th series	15.8	6.62
(α,n) U series	46.7	4.47
spontaneous fission ^{238}U	20.5	2.50
Total	83.0	13.6

Table 5.3. Macroscopic total neutron absorption cross sections (Σ_m) for Stripa granite and Leptite.

	Σ_m (cm^2g^{-1})	
	granite	leptite
Calculated from Table 5.1	.0065	0.0054
Measured composite sample from V2 core	.0046	----

Table 5.4. Radioelement production in the Stripa granite, in its fracture infills, fracture fluids and Leptite.

Reaction	Equilibrium number of atoms in 1 cm^{-3} of :- Rock Matrix	Fracture Infill	Fracture Fluid	Leptite
$^{6}Li(n,\alpha)^{3}H$	46	2	0.29	11.3
$^{14}N(n,p)^{14}C$	500	500	300	96
$^{17}O(n,\alpha)^{14}C$	530	500	380	100
$^{223}Ra+^{226}Ra$ decay(1)	21	470	<0.0002	2.5
$^{35}Cl(n,\gamma)^{36}Cl$	$1.5x10^{6}$	negligible	$2.5x10^{6}$	$1.9x10^{5}$
$^{39}K(n,\alpha)^{36}Cl$	$4.0x10^{4}$	$1.7x10^{3}$	1.0	$6.7x10^{3}$

(1) ^{14}C emission for measured branching ratios.

Table 5.5. In-situ production of radioactive noble gases in the Stripa granite, in its fracture infills, fracture fluids and Leptite.

Reaction	Equilibrium number of atoms in 1 cm^{-3} of :- Rock Matrix	Fracture Infill	Fracture Fluid	Leptite
$^{36}Ar(n,\gamma)^{37}Ar$	$<7.5x10^{-7}$	$<7.5x10^{-7}$	$7.5x10^{-7}$	$<7.5x10^{-7}$
$^{40}Ca(n,\alpha)^{37}Ar$	$1x10^{-3}$	$4x10^{-2}$	$1.2x10^{-5}$	$5x10^{-4}$
$^{39}K(n,p)^{39}Ar$	132	5.6	0.003	22
$^{42}Ca(n,\alpha)^{39}Ar$	0.12	4.7	0.002	0.06
$^{238}U(s.f)^{85}Kr$	0.3	6.7	$<3x10^{-6}$	0.036
$^{235}U(n,f)^{85}Kr$	$8.3x10^{-4}$	0.02	$<2x10^{-8}$	$2x10^{-5}$

Table 5.6. Estimated concentrations of in-situ produced radio-nuclides in groundwaters.

Nuclide		Atoms ml^{-1} in water phase: Matrix(1) with 1% porosity	150 µm fracture from (2) adjacent 300 µm of granite matrix	150 µm fracture from (2) adjacent 300 µm of fracture minerals
^{3}H		4600 (0.69 TU)	180 (0.027 TU)	8 (0.001 TU)
^{14}C:	n-induced in fluid	680	680	680
	n-induced in matrix	103000	4100	4000
	Ra isotope decay	2100	84	1880
	Total	106000 (58 pmc (3))	4860 (3.3 pmc (3))	6560 (3.6 pmc (3)
^{36}Cl	n-induced in fluid	0.25×10^{7}	0.25×10^{7}	0.25×10^{7}
	n-induced in matrix	15.0×10^{7}	0.60×10^{7}	negligible
	Total	15.2×10^{7}	0.85×10^{7}	0.25x10
^{37}Ar		0.1	0.004	0.016
^{39}Ar		13200	530	40
^{85}Kr		30	1	27

(1) For total transfer into 1% rock porosity (Fluid content + 100 x rock content.

(2) For total transfer from 300 µm within each wall into the associate fracture fluid . (Fluid content + 4 x matrix/mineral content)

(3) Calculated assuming that the carbon content of the fluid is 2.6 mg l^{-1} and lableing of dissolved carbon is 100%.

Table 5.7. Measured $^{36}Cl/Cl$ ratios for Stripa rocks.

Borehole	depth (m) below surface	$^{36}Cl/Cl$ ratio x 10^{15}
Granite		
N1	376	219
N1F	377	458
V1	751	182
V1F	861	1620
V2	1106	142
V2F	1220	189
Leptite		
LEPF	360	52
LEPC	360	172

Values from J. Fabryka-Martin (perrs comm).

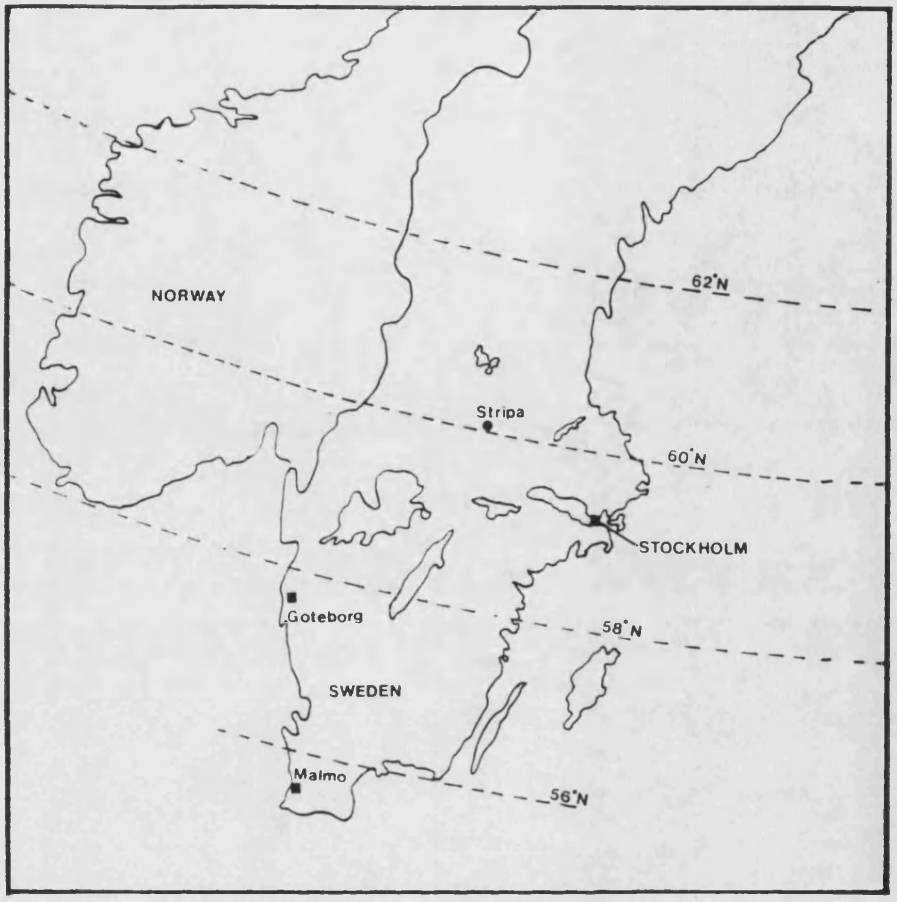

Fig. 5.1 A map of Sweden and Norway showing the location of the Stripa site.

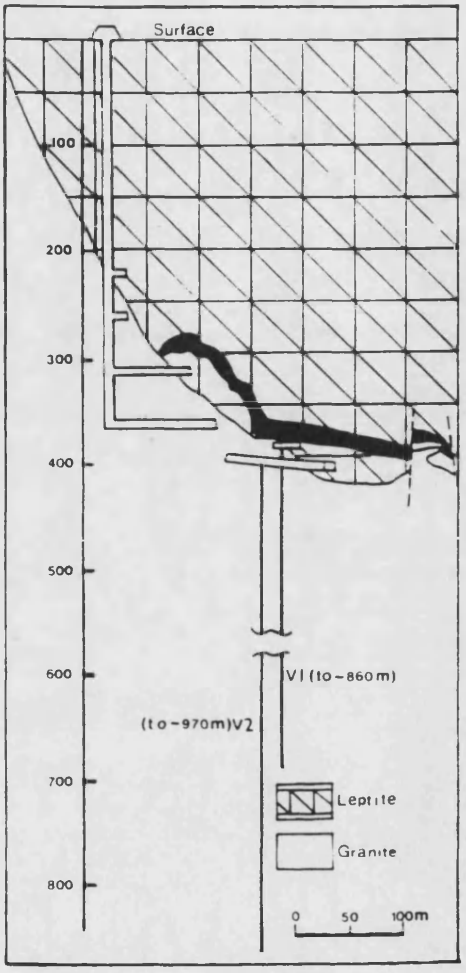

Fig. 5.2 A schematic diagram of the Stripa site showing the location of boreholes V1 and V2, and major geological formations.

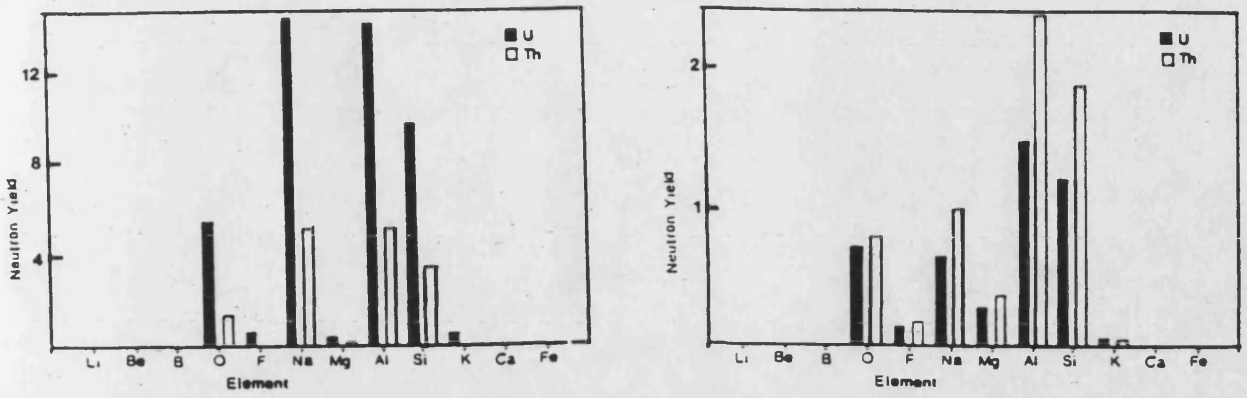

Figs. 5.3a and 5.3b Neutron yields from (α,n) reactions of light elements in Stripa granite (5.3a) and Leptite (5.3b). Neutron yields are in units of $g^{-1}a^{-1}$ for the U and Th contents of the granite and leptite (see Table 5.1). The corresponding neutron yields due to spontaneous fission of ^{238}U are 21 and 2.5 $g^{-1}a^{-1}$ respectively.

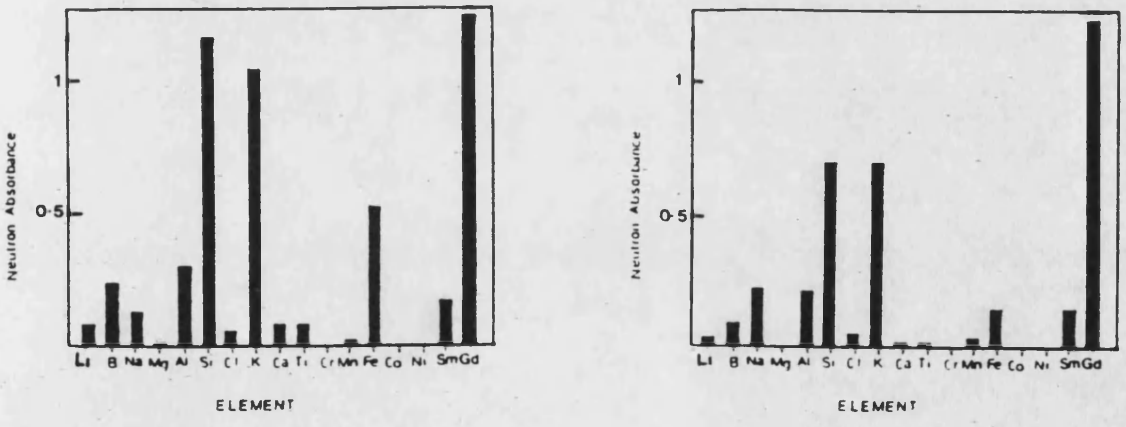

Figs. 5.4a and 5.4b Neutron absorption plotted against element for Stripa granite (5.4a) and leptite (5.4b). Units of neutron absorbance are cm $^2g^{-1}$.

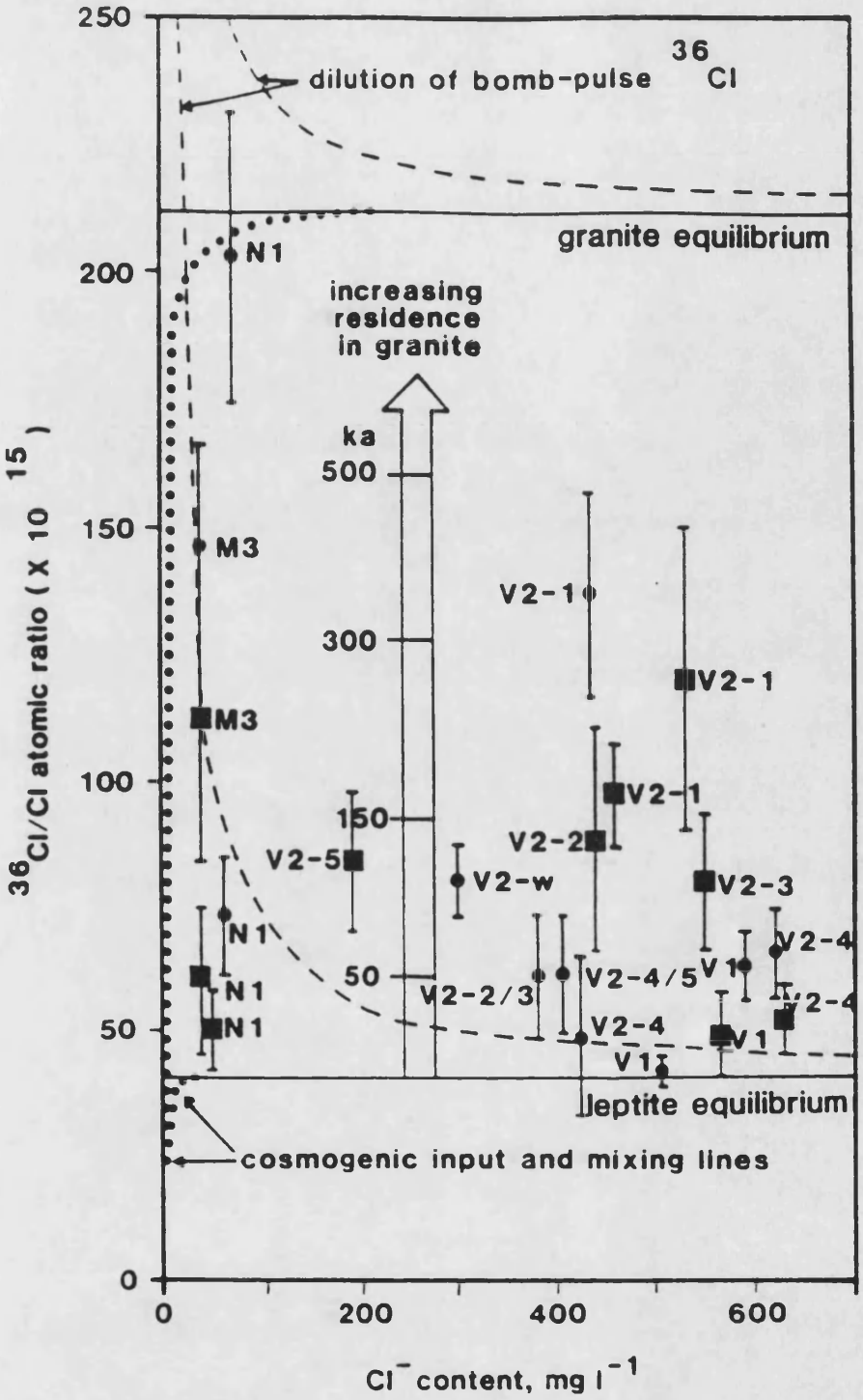

Fig. 5.5 The $^{36}Cl/Cl$ atomic ratio plotted against Cl^- content for the Stripa groundwaters. Dilution lines are shown for mixing of the atmospheric input of ^{36}Cl (cosmogenic and bomb-pulse) with chloride derived from the leptite and granite. These lines show that bomb-pulse and atmospheric inputs can have little influence on in-situ ratios at high chlorinities. The approximate depths (m) below ground for the various samples are: M3 (336-350); N1 (377-397); V1 (457-863); V2-5 (797-805); V2-3 (898-906); V2-2 (958-966); V2-1 (967-1230); V2-W (408-1230). Data points from ANDREWS et al (1986) are shown as circles, new points are indicated by squares.

6. IN-SITU NEUTRON PRODUCTION IN THE CARNMENELLIS GRANITE.

6.1. Introduction.

The Hercynian granites of South West England have, for a long period of time been one of the major metalliferous mining areas of the United Kingdom. The high metal contents are primarily due to large scale fluid circulation and ore emplacement which are consequences of high geothermal gradients (BROWN et al., 1980). This hydrothermal activity is still evident in hot (up to 55°C) high salinity waters which have entered mines for at least the last hundred years (EDMUNDS et al., 1987).

Interest in the thermal waters of the Carnmenellis granite has recently been re-awakened due to the development of the area as a source for geothermal energy. In the late 1970's Cambourne School of Mines developed the technology of circulating surface water through dry fractured granite at depth to produce electricity. Preliminary tests funded jointly by the Department of the Energy and the European Economic Community were successful and during the 1980's deeper circulation test were and are still being carried out. The major geochemical question in such a scheme is how, and at what rate will alteration of the granite effect the composition of fracture surfaces and circulating fluids. Alteration of fracture surfaces will effect the permeability of the system, and the fluids composition will alter both its corrosive and toxicological properties. Present day natural circulation systems within the granite could be used as an analogue to the long term use of such geothermal energy units. Their use could also yield alteration rates of mineral phases within the granite and information pertinent to assessing the effect of circulation waters entering the local water table.

To this end natural analogues of this process have been extensively studied (EDMUNDS et al., 1984, EDMUNDS et al., 1985 and EDMUNDS et al., 1987). As a result of these studies a number of areas have been identified in which the use of radiogenic isotopes such as ^{3}H, ^{3}He and ^{36}Cl may be helpful. These include the study of alteration rates and the origin of groundwater salinity, the possible mixing of modern meteoric water with older more saline water and the use of He isotopes to predict heat flow.

The objectives of the experimental and theoretical work

outlined in this Section were to :-

(a) Estimate the possible neutron flux distribution within the Carnmenellis granite (a granite enriched in Li and B) and surrounding Killas. These estimates were then used to compare calculated production rates of ^{3}H, ^{3}He and ^{36}Cl with measured concentrations of these isotopes within local groundwaters.

(b) Evaluate the possibility of using ^{36}Cl ratios to identify the source of chloride in local high chlorinity groundwaters.

(c) Compare measured neutron flux values for specific sites within the the Carnmenellis granite with the average neutron flux calculated in (a) above. The method and results of these site measurements have been discussed in Section 3.0 will only be briefly referred to in this Section.

6.1.1 Local Geology.

The Carnmenellis granite forms part of the South West England granites which were intruded into Devonian argillaceous sediments towards the end of the Variscan orogeny. The major rock types of the area are granite and killas (a local name for all bedded rocks). The South West England granites form six major plutons together with a number of minor stocks believed to be connected at depth (BOTT and SCOTT., 1964) (Fig 6.1). Recent gravity data (TOMBS., 1977) suggests that the continuous batholith lies at a depth of 10 to 15 Km below the present day level of exposure. All of the granites are anomalously rich in Cl, B, Li and F (EXLEY and STONE., 1964, FUGE and POWER., 1969) and were probably emplaced at a high crustal level, between 1.5 and 4 km (FLOYD., 1971). Present day topography is due to Tertiary erosion.

Two smaller granite bodies were emplaced just north of the main Carnmenellis mass (Fig 6.1). These are the Carn Brea and Carn Marth stocks. Davidson (1926) demonstrated that these were probably connected at shallow depth to the Carnmenellis granite, and there is little evidence to suggest that they are geochemically differentiated from the Carnmenellis granite (see Section 6.3).

The Carnmenellis granite is predominantly a micaceous adamellitic granite with quartz, plagioclase, orthoclase, biotite and/or muscovite and commonly carries accessory tourmaline, apatite and zircon (EXLEY and STONE., 1964). High Li and Cl contents together with moderately enriched U and Th

concentrations make the batholith a particularly interesting site for the study of neutron induced production of ^{3}H, ^{3}He, and ^{36}Cl.

6.1.2 Production of ^{3}H, ^{3}He and ^{36}Cl.

ANDREWS and KAY (1984) were the first to suggest the possibility of in-situ production occurring to a significant extent within the Carnmenellis granite. They concentrated on the production of ^{3}H, significant amounts of which had been measured in the high salinity fluids found in South Crofty mine. Their conclusion was that such levels of ^{3}H (>6 TU [equivalent to $4x10^{5}$ atoms cm^{-3} H_2O]) could not be produced by in-situ production and that they must be attributed to mixing with modern water. This hypothesis is tested later in this Section.

The study of ^{4}He and its rare isotope ^{3}He in the Carnmenellis granite has been carried out in parallel with that of ^{3}H. Measurements of $^{3}He/^{4}He$ ratios have shown that He contents of both natural and anthropogenic groundwaters from the Carnmenellis groundwaters are of radiogenic origin (HILTON et al., 1985). The decay of ^{3}H produced by the $^{6}Li(n,\alpha)^{3}H$ is expected to be the major source of ^{3}He in the groundwaters (ANDREWS and KAY., 1982 and MAMYRIN and TOLSTIKHIN et al ., 1984).

Measurements of He present in groundwaters from the Carnmenellis granite by HILTON (1985) give the $^{3}He/^{4}He$ ratio of circulation water from the Hot Dry Rock site as 3.5 ± 0.4 $x10^{-8}$. The same author quotes $^{3}He/^{4}He$ ratios of groundwater from saline sources at the 380 fathom level in South Crofty mine as $7.14\pm0.4x10^{-8}$ (actual sites sampled were not listed). A knowledge of the actual sampling sites used at this level would be useful as salinities of waters, at possible sampling sites, vary by an order of magnitude and may represent admixtures of a saline "end member" with "recent" meteoric water (EDMUNDS et al., 1984).

Differences between the ratio of this sample and that of the HDR circulation water cannot be attributed to experimental error (HILTON et al., 1985). This may signify differences between either the production of rates ^{3}He and ^{4}He or the evolution of He content of the fluids sampled at each site.

As to date ^{36}Cl has not been studied within the Carnmenellis granite due to the difficulty of measurement of

this rare isotope. Samples of AgCl prepared from Carnmenellis waters have been submitted to the Technische Universitat Munchen for ^{36}Cl analysis, but as of yet results have been not been reported.

All of the above studies require an estimate of the neutron flux produced within the Carnmenellis granite. Due to the ease of access to areas of granite below the influence of cosmic rays (through the use of mine shafts and boreholes) this area was selected to study the accuracy of the theoretical estimation of in-situ neutron flux. To do this a number of measurements were made of the neutron flux in different areas of the Carnmenellis granite (see Section 3, which also compares the measured and calculated fluxes for these specific sites). The following Sub-Section overviews the results of measurements made in the Carnmenellis granite.

6.2 Measurement of the in-situ neutron flux.

Neutron flux measurements were carried out as described in Appendix 4 and Section 3.0, near the surface at Rosemanowes quarry (NGR SW(343 759), and underground in South Crofty (NGR SW(413 669) and Pendarves (NGR (382 647) mines. They were made in areas of granite which were free from major alteration and sufficiently far away from lode structures to give a true measurement of the flux in bulk unaltered granite. Further measurements were made in the similar Lands End granite so as to investigate possible ranges in neutron flux over different areas of the South Western granites. These measurements were made at Rose Vale mine near Zennor (NGR SW(378 461)). Results of these measurements are shown in Table 6.1.

The magnitude of neutron flux measured near the surface (6m below the air/ground interface) in two 5m long boreholes that were drilled horizontally 6 m from the top of a rock face at Rosemanowes Quarry are clearly higher than any of those made at a much greater depth. These high flux values are more likely to be due to cosmic radiation than either localised high concentrations of Uranium and Thorium, or low concentrations of neutron absorbing materials. The enhanced flux may be due to leakage of cosmic radiation or cosmic ray produced radiation down the borehole used for these measurements, or to interaction of cosmic ray secondary particles such as protons, pions or negative muons with the rock matrix to produce neutrons at this depth (see Section 2.0). In the case of measurements taken at Rosemanowes the

latter process seems the most likely since the detector was placed at least 3m into 12.5 cm boreholes (which were perpendicular to the rock face (see Appendix 2)) and that the count-rate did not vary significantly with the distance that the detector was placed into the borehole.

Table 6.1 shows that total flux values measured at depth of greater than 25 metres fall into two groups :-
(a) Values of 6.3 to 3.9×10^{-5} neutrons $cm^{-2}s^{-1}$. These represent borehole and small chamber measurements.
(b) Values of $< 3.9 \times 10^{-5}$ neutrons $cm^{-2}s^{-1}$. These represent measurements taken in long passages.
Measured thermal neutron fluxes remain approximately constant (between 3.8 and 3.2×10^{-5} $cm^{-2}s^{-1}$).

There are significant differences in the thermal-epicadmium ratios (R_{Cd}) between borehole and non-borehole measurements. The epicadmium component being higher in boreholes this is the opposite effect to that than experienced at Stripa (ANDREWS et al., 1986a) where borehole measurements gave a smaller epicadmium component. These results suggest that the differences in the thermal/epicadmium ratios noted at Stripa may be due to variation in rock chemistry rather than surface area effects as suggested in ANDREWS et al (1986a).

The conclusion of Section 3.0 was that calculated thermal fluxes represent the total neutron flux better than the measured thermal flux which is generally 40 to 50% lower than the calculated value. This fact was also observed at the Stripa site (ANDREWS et al., 1986a) although at that site the measured thermal flux was > 80% of the calculated thermal flux. The large component of epi-cadmium neutrons measured in the Carnmenellis granite may be attributable to the presence of large concentrations of B which has a high resonance absorption cross-section. This effectively lowers F_{th} and increases the most probable neutron energy. Both of these effects lower the calculated thermal neutron flux (see Section 3). From experimental measurements carried out on the Carnmenellis granite in the course of this thesis $F_{th} = 0.65 \pm 0.07$ (This ignores the measurement made at Rosemanowes Quarry B/H C as this site has a high permeability and is often over saturated with meteoric water which is reflected in its high thermal/epicadmium ratio).
An F_{th} value of 0.65 is valid only for unaltered Carnmenellis granite and is likely to be higher for altered granite which has a higher water content as this would aid thermalisation.

The following sub-section attempts to calculate an average neutron flux for the Carnmenellis granite based on an appraisal of the geochemistry of the Carnmenellis area and results of measurements at specific sites. This "average" flux is then be used to estimate possible production of the radioisotopes ^{3}H, ^{3}He and ^{36}Cl.

6.3. Calculation of the average neutron flux.

The estimation of average neutron flux present in the Carnmenellis granite from geochemical data may be divided into 4 sections. The first section considers the analytical parameters which may be input into any model of the Carnmenellis granite and the second uses these parameters to estimate neutron production rates. The final two sections estimate the calculation of, and variation in the macroscopic thermal neutron absorption cross-section (Σ_m), and thence the neutron flux.

6.3.1 Geochemistry and chemical composition.

The calculation of an average neutron flux, which may be applied to a large rock mass such as the Carnmenellis granite, is required in order to asses the input of isotopes from large unsampled areas. Any model which attempts to estimate such an average requires a detailed knowledge of the geochemistry and chemical composition of the particular formation.

In calculating this average flux a major problem is what chemical composition accurately reflects such a large mass of granite. This problem is particularly accute for situations in which the neutron flux is controlled by the trace element rather than bulk element geochemistry. The flux in the Carnmenellis granite is controlled by the geochemistry of B, Li, U and Th (ANDREWS and KAY., 1982) all of which show considerable enrichment and inhomogeneity, hence the calculation of an average flux in this case is more difficult than for "relatively" homogeneous, low B/Li granites such as those found at Stripa.

6.3.1.1 Major elements. The major element geochemistry of the Carnmenellis granite was first studied in detail by GOSH who classified the granite into three distinct types, TYPE I, II and III (GOSH., 1934) see Fig 6.2. Further studies show that there is little geochemical difference between TYPE I and II granites whilst TYPE III granite is slightly differentiated with respect to Mg, Ca, Ti, Fe, Zn and Zr (Al-TURKI and STONE., 1978). Differences between the major element geochemistry of TYPE I/II and III granites are in elements which contribute <10 % to either the neutron production rate or absorption cross-section. Therefore the contribution to the above neutron production rate and absorption cross-section by major elements should be similar for all three types of granite. All of the sites studied are within TYPE I/II granites and the major element geochemistry would be expected to show little variation. This observation is consistent with the small variation observed in the calculated neutron yields (see Table 6.2) which have been based on analysis of rock samples from the Carnmenellis granite (see Appendix 2).

The geochemistry and distribution of Li, B, U and Th within the Carnmenellis granite is less well defined especially at depth and are discussed below.

6.3.1.2 Lithium. The geochemistry of Li in the Carnmenellis granite is complicated since Li can be found in a number of mineral phases some of which are strongly associated with secondary mineralisation and tourmalinisation. WILSON and LONG (1983) show that Li in the Carnmenellis granite is mainly associated with Micas such as Biotite where concentrations may reach 1% and that significant amounts may also be associated with Tourmaline and Quartz.

A number of average whole rock Li contents for the Carnmenellis granite have been interpolated from tabulated values for the granites of South West England made by BEER and EDMUNDS., (1978) (ANDREWS and KAY., 1982). These interpolations give an average concentration of 288 ppm with a range from 40 to 743 ppm. Average Li concentrations calculated directly from analysis of samples of Carnmenellis granite by Al-TURKI and STONE., 1978, KARIM., 1971 and WEBB et al., 1985 show that :-

(a) Lithium is not differentiated between TYPE I, II and III granites.

(b) The average Li concentration of Carnmenellis granite is 335 ± 150 ppm. This suggests that the Carnmenellis granite is slightly enriched in Li with respect to the other granites of the South West being higher than the average for all South West England granites.

(c) Results from AL-TURKI and STONE (1978) suggest that the range of Li concentrations found in TYPE III granites is greater than that found in TYPES I and II. (Although the mean value shows no differentiation.

Analysis of Li carried out on samples collected from sites within the Carnmenellis granite (see Appendix 2) fall within the range suggested above. The value suggested in (b) above (335 +/- 150 ppm) has been taken to reflect the average Li concentration of the Carnmenellis granite.

6.3.1.3 Boron. The Carnmenellis granite is enriched in B relative to the granites of South West England. Tourmaline is the principal B-bearing mineral and is present in both primary and secondary forms (EDMUNDS et al., 1985). ANDREWS and KAY (1982) estimated the average B content of the Carnmenellis granite to be 250 ppm. This is consistent with B analysis carried out on ten samples of Carnmenellis granite (see Appendix 2) which yield a value of 258 +/- 102 ppm. The variation in B content with depth is uncertain, analysis of material from the Rosemanowes borehole suggest that the B concentration at a depth of 1.75 Km (400 ppm) is greater than that nearer the surface (89 ppm) (see Appendix 2).

Enrichment of B within the Carnmenellis granite is due to transport of B from surrounding sediments in hydrothermal fluids during emplacement (J. PLANT pers comm) and localised high concentrations along major fluid flow paths may therefore be expected. Furthermore association of B with U is unlikely since U and Th are considered to have crystallised out during magmatic stages where as B enrichment (Tourmalinisation) is thought to have occurred during postmagmatic stages (STONE., 1984).

As of date little detailed investigation has been carried out by other workers on the variation of the B content of the Carnmenellis granite especially with depth, therefore the measured average concentration of 258 +/- 102 ppm has been used in calculations of neutron flux.

In view of the high dependence of both the magnitude and energy distribution of the neutron flux on the B content this variable warrents a more detailed study should more accurate estimates of the neutron flux be required.

6.3.1.4 Samarium and Gadolinium. The Carnmenellis granite is enriched in the light rare earths (Ce, La, Pr, Nd and Sm) with slight negative Eu anomalies (JEFFERIES., 1985 and ALDERTON et al., 1980). The rare earths of interest Sm and Gd are mainly associated with the minerals monazite and apatite, which in turn are associated with the radioactive mineral assemblage (monazite-xenotime-apatite-zircon) and uraninite (JEFFERIES., 1985). Tourmalinisation and other alteration mechanisms have been shown to markedly affect this distribution (ALDERTON et al., 1980). Average concentrations of Sm and Gd in bulk Carnmenellis granite are 6.0±1.3 and 3.7±0.7 respectively (JEFFERIES., 1985 and ALDERTON et al., 1980). These results show an average Sm:Gd ratio of 1.6 compared to a Sm:Gd ratio for "average granites" of 1 (PARKER., 1967). It was not possible to analyse the ten samples of Carnmenellis granite detailed in Appendix 2 for Gd and the displayed Gd concentrations have been calculated from measured Sm concentrations and a Sm/Gd ratio of 1.6. Concentrations so calculated (Appendix 2) are not inconsistent with the average range suggested above.

6.3.1.5 Uranium and Thorium. The Carnmenellis granite is enriched in the radioelements U and Th respect to average granites. Uranium occurs mainly as uraninite (UO_2) whilst Th is found in zircon and monazite where it substitutes for Ce and Zr. As mentioned above these minerals often occur in assemblages which have been shown to have crystallised prior to the crystalisation of feldspar/quartz/biotite (JEFFERIES et al., 1984) an observation which is consistent with both U and Th being of primary magmatic origin.

Whole rock analysis of U and Th carried out by a large number of authors (ANDREWS et al., 1986b, HILTON., 1985, JEFFERIES et al., 1985, WEBB et al., 1985 and TAMMEMAGI and WHEILDON., 1974) show a large variation in the concentrations of U and Th (5 to 20 ppm and 5 to 25 ppm respectively).

This wide range cannot be explained by differentiation between TYPE I, II and III granites (JEFFERIES et al., 1985) but a large proportion of it may be accounted for by sampling and analytical error. Some of the surface samples obtained from quarries may have lost U due to weathering whilst deeper "core samples" may in fact be drill chippings which can easily loose U into drilling fluids (WEBB et al., 1985). Analysis by α spectroscopy requires such a small sample that great care must be taken to insure that the sample is representative of the bulk. Analysis of U and Th by γ spectroscopy also has its inherent problems especially when carried out in-situ using borehole logging equipment.

Bearing the above in mind an average U and Th composition of 12ppm U and 18 ppm Th has been taken to represent the bulk of the Carnmenellis granite. This forms the median composition between that suggested by WEBB et al., 1985 and by JEFFERIES et al., 1985. These values are also consistent with analysis results carried out during the preparation of this thesis (see Appendix 2). A range of +/- 5ppm for both of these values is easily justified from the papers mentioned above.

6.3.1.6. Summary. From the above it is apparent that both the trace element and major element geochemistry of the Carnmenellis granite are well represented by the ten samples of Carnmenellis granite analysed in the course of this thesis (see Appendix 2). For this reason analysis of these samples have been used to calculate an average neutron flux.

6.3.2 Average neutron production rates (P_{tot}).

The total neutron yield g^{-1} a^{-1} (P_{tot}) may be calculated from the elemental composition of the rock using methods discussed in Section 2. The average neutron production rate for the Carnmenellis granite may best be estimated using average neutron yields per μg^{-1} U and Th respectively calculated for the ten samples of Carnmenellis granite given in Appendix 2 (see Table 6.3) and then multiplying the result by the average U and Th concentrations discussed above (along with associated propagation of standard deviations (1s)). The small deviation in neutron production rates a^{-1} ppm^{-1} U and Th between each of the ten samples shown in Table 6.3 is testament to the small variation in the concentration of major

elements discussed in Section 6.3.1. The calculated average total neutron production rate for the Carnmenellis granite is 17.4±7.7 $g^{-1}a^{-1}$. The large range in this final production rate is due to the high variation in U and Th concentrations. A similar calculation for the surrounding Killas (made using the chemical analysis for samples HF1 and HF2 given in Appendix 2) yields a total neutron production rate of 8.76 ± 0.58 $g^{-1}a^{-1}$ based on U and Th concentrations of 4.65 ± 0.35 and 5.25 ± 0.35 respectively. This production rate is significantly lower than that for the granite due to the lower U and Th content of the Killas.

6.3.3. Average thermal neutron absorption cross-sections.

As discussed in Sections 3 and Appendix 4 the thermal neutron absorption cross-section (Σ_m) may either be measured experimentally, or calculated based upon a chemical analysis.

An average value of Σ_m has been calculated from the individual absorption cross-sections of samples of Carnmenellis granite (see Appendix 2). Results of this calculation are given in Table 6.4. The resulting average thermal absorption cross-section is 0.017 ± 0.005 cm^2g^{-1}. A similar calculation for the Killas yields an absorption cross-section of 0.012 ± 0.001 cm^2g^{-1}. The large variation in the absorption cross-section of these granite samples is due to variation in the concentration of B which accounts for up to 60% of the absorption cross-section of these samples.

6.3.4 Average neutron flux in the Carnmenellis granite.

As discussed in Section 3 the thermal neutron flux (ϕ) may be calculated from the neutron production rate and absorption cross-section by the equation :-

$$\phi = \frac{P_{tot}\ F_{th}}{\Sigma_m} \qquad (cm^{-2}\ s^{-1}) \qquad \text{Eqn. 6.1}$$

Where P_{tot} is the total neutron production rate ($g^{-1}s^{-1}$), Σ_m is the thermal neutron absorption cross-section (cm^2g^{-1}) and F_{th} is the fraction of produced neutrons reaching thermal energy. Using the values calculated in Sections 6.3.2 and 6.3.3 above and assuming F_{th} is close to 1 yields average thermal neutron fluxes of :-

$0.47 \pm 0.20 \times 10^{-4}$ cm^2 s^{-1} for Carnmenellis granite

$0.23 \pm 0.02 \times 10^{-4}$ cm^2 s^{-1} for Killas.

If however F_{th} is 0.65 as suggested in Section 6.3 then the thermal neutron fluxes above would be reduced by that factor to give:-

$0.31 \pm 0.13 \times 10^{-4}$ cm^2s^{-1} for Carnmenellis granite.

$0.15 \pm 0.02 \times 10^{-4}$ cm^2s^{-1} for Killas.

These thermal fluxes are slightly lower than those calculated for each of the measurement sites used in the Carnmenellis granite (Section 3). However those sites had slightly enhanced U and Th concentrations relative to the average used above. The measured fluxes given in Section 3.0 lie within the range suggested for these average values even if F_{th} is assumed to be 0.65. The large range associated with these calculated average fluxes emphasises the wide variation in production rates and equilibrium concentrations of any isotopes produced by neutron reactions within the Carnmenellis granite. For instance even if the U, Th and B were assumed to be less variable than assumed above uncertainty in F_{th} could still cause large differences in isotope production rates, especially in areas of enhanced permeability.

Although the variation in thermal neutron flux discussed above means that accurate determination of the rate of production of ^3H, ^3He and ^{36}Cl is impossible, limits as to the possible production rates and equilibrium ratios may still be calculated. These limits are calculated in the following Section.

6.4. Levels of in-situ produced ^3H, ^3He and ^{36}Cl in the Carnmenellis granite.

The limits for in-situ production of each of these nuclides in the Carnmenellis granite are discussed in turn and compared to measured concentrations found in local natural and anthropogenic groundwaters. As discussed in Section 4.0 all of these nuclides may be produced by a number of reactions induced either by cosmic rays or neutrons. In this Section only the production of nuclides below the influence of cosmic rays is considered (depths > 30m for a granite) and hence all of the reactions are induced by neutrons from (α,n) and spontaneous fission.

6.4.1 Tritium.

The production of ^{3}H in the lithosphere has been reviewed in Section 4. In the Carnmenellis granite the $^{6}Li(n,\alpha)^{3}H$ reaction accounts for >99% of the total production. Production from the $^{10}B(n,2\alpha)^{3}H$ being small compared to the ^{6}Li reaction despite the high B concentration. Assuming a thermal neutron flux the ^{3}H production rate (N_{3H} $g^{-1}a^{-1}$) may calculated from the equation :-

$$N_{3H} = N_{Li}\ \sigma\ \phi\ K \qquad \text{Eqn 6.2}$$

Where N_{Li} is the number of ^{6}Li atoms (g^{-1}), σ is the (n,α) reaction cross-section (cm^{-2}), ϕ is the thermal neutron flux (cm^{-2} s^{-1}) and K is the number of seconds in a year. This equation simplifies to :-

$$N_{3H} = [Li]\ \phi\ 193 \qquad \text{Eqn 6.3}$$

Where the concentration of Li is in ppm. The concentration of ^{3}H (atoms g^{-1}) produced at secular equilibrium ($\tilde{N}_{3H}$) will be :-

$$\tilde{N}_{3H} = \frac{N_{3H}}{\lambda_{3H}} \qquad \text{Eqn. 6.4}$$

Where λ_{3H} is the decay constant of ^{3}H (a^{-1}). The error in $\tilde{N}_{3H}$ due to uncertainties in [Li] and ϕ may be calculated using standard error propagation procedures.

Results of calculations for the Carnmenellis granite and surrounding Killas are given in Table 6.5. These calculations have been based on granitic thermal fluxes calculated with F_{th}=1 as this yields maximum possible values for N_{3H} and $\tilde{N}_{3H}$.

From these results it may be seen that production of ^{3}H is much greater in the granite than the Killas. This is due to the higher flux and Li content of the granite. The large uncertainties both in production rate and equilibrium ratio reflect the large uncertainties in Li contents and to a smaller extent neutron flux.

The calculated concentration of ^{3}H produced at secular equilibrium within the Carnmenellis granite ($\tilde{N}_{3H}$) is approximately three times that calculated for the Stripa granite (18 g^{-1}) in Section 5.0 due to its enhanced Li

content. The movement of such produced ^{3}H from its production site and into fracture fluids should be similar in both granites. If nuclide migration models applied to the Stripa site are applied to the Carnmenellis granite and Killas (total transport into fracture fluids and transport from fracture walls) then resulting ^{3}H concentrations in fluids would be:-

(a) Total transport.

In this model all of the produced ^{3}H would be transported into fracture fluids. The Carnmenellis granite has a density of 2.64 gcm^{-3} (BATCHELOR., 1986) and a porosity of 1% (ANDREWS and KAY., 1982). The concentration of ^{3}H in fracture fluids would thus be 100 times greater than that in the rock if 100% transfer is assumed. The assumption of a similar porosity and density for the Killas would yield concentrations of 14000±8900 and 4200±1000 atoms ^{3}H cm^{-3} of fracture fluid for the Carnmenellis granite and Killas respectively. These concentrations correspond to 0.21±0.13 and 0.063±0.015 TU respectively.

(b) Transport from fracture walls.

A number of key parameters in this model such as average fracture width have not yet been determined for the natural groundwater flow paths of the Carnmenellis granite or Killas. If these are assumed to similar to the Stripa site then the resulting concentrations in fracture fluids would be approximately 560 and 170 atoms ^{3}H cm^{-3} (0.008 Tu and 0.002 TU) for the Carnmenellis granite and Killas respectively. These as expected are much lower that calculated from the total transport model.

The above calculated ^{3}H contents are upper limits and show that even under the most favourable circumstances labeling of groundwaters with in-situ levels of ^{3}H above 0.5 TU let alone 6 TU is unlikely. This finding is consistent with the conclusions of ANDREWS and KAY (1982).

6.4.2 ^{3}He and $^{3}He/^{4}He$ ratios.

Helium isotopes may be present in rock matrices as a "entrained" remnant of primordial helium or as the result of radiogenic production since crystalisation of the matrix (MAMYRIN and TOLSTIKHIN., 1984). In the case of the Carnmenellis granite and associated Killas He isotopes are said to be due to radiogenic production (HOOKER et al., 1985).

^{3}He is predominantly produced below the influence of cosmic rays in terrestrial rocks by the reaction of neutrons on ^{6}Li, the neutron flux being the result of (α,n) and spontaneous fission (MORRISON and PINE., 1955, MAMYRIN and TOLSTIKHIN., 1984, ANDREWS., 1985 and KURZ., 1986). ^{4}He is generated by the neutralisation of α particles emitted during the decay of U and Th series isotopes. These reactions may be summarised as:-

$$^{6}Li(n,\alpha) \longrightarrow {}^{3}H \longrightarrow \beta^{-} \longrightarrow {}^{3}He$$
$$^{238}U \longrightarrow {}^{206}Pb + 8\ {}^{4}He$$
$$^{235}U \longrightarrow {}^{207}Pb + 7\ {}^{4}He$$
$$^{232}Th \longrightarrow {}^{208}Pb + 6\ {}^{4}He$$

All groundwaters contain dissolved He which entered solution because of equilibrium with the atmosphere at recharge. ANDREWS and LEE (1979) and HEATON (1984) have demonstrated that additional radiogenic He accumulates in an amount which increases with groundwater age (as a consequence of radioactive decay in the aquifer and diffusion from surrounding formations). The $^{3}He/^{4}He$ ratio of He in these groundwaters thus decreases from that characteristic of atmospheric He sources to that characteristic of the surrounding formation. When the amount of radiogenic He greatly exceeds the amount of atmospheric He the $^{3}He/^{4}He$ ratio will reach a limiting value characteristic of the source rock for the radiogenic He.

Studies of the He isotopes present in both the anthropogenic circulation water at Rosemanowes Quarry and natural saline fluids have shown that measured $^{3}He/^{4}He$ ratios broadly reflect the $^{3}He/^{4}He$ ratios of the surrounding formations (HILTON et al., 1985 and ANDREWS et al., 1987). In the case of the Rosemanowes circulation waters this certainly means the granite, whilst the origin and flow paths of the natural saline fluids found at South Crofty mine are less certain although studies by EDMUNDS et al (1985) has strongly suggested a granitic origin.

6.4.2.1 Calculation of $^3He/^4He$ ratios for the Carnmenellis granite and Killas. The $^3He/^4He$ ratio (R_{He}) may be calculated from the ratio of the production rates of ^3He and ^4He. The production rate of ^3He (N_{3He} $g^{-1}a^{-1}$) is equal to the production rate of ^3H (N_{3H} $g^{-1}a^{-1}$ (see Section 6.4.1) once secular equilibrium has been achieved for the production of ^3H. This takes approximately 60 years which is short compared to the residence time of ^3H within the rock matrix. The ^4He production rate (N_{4He} $g^{-1}a^{-1}$) may be calculated from the number of α particles emitted by U and Th in secular equilibrium with their daughters per year.

The ^3He production rate N_{3He} may be calculated from :-

$$N_{3He} = N_{3H} = f\ N_{Li}\ \sigma \qquad (g^{-1}a^{-1}) \qquad \text{Eqn. 6.5}$$

Where σ is the $^6Li(n,\alpha)$ cross-section (cm^2), N_{Li} is the number of ^6Li atoms g^{-1} and f is the thermal neutron flux ($cm^{-2}a^{-1}$). This equation may be combined with equation 6.1 to give equation 6.6 provided that Σ_m does not vary greatly with Li concentration and that $F_{th} = 1$.

$$N_{3He} = \frac{([U]A + [Th]B)\ N_{Li}\ \sigma_{Li}}{\Sigma_m} \qquad \text{Eqn. 6.6}$$

Where A and B are the neutron yields due to (α,n) and spontaneous fission reactions per ppm of U and Th respectively ($ppm^{-1}g^{-1}a^{-1}$), [U] and [Th] are the U and Th concentrations in ppm, σ_{Li} is the (n,α) cross-section and Σ_m is the thermal neutron absorption cross-section. This equation further simplified becomes :-

$$N_{3He} = \frac{([U]A + [Th]B)\ [Li]\ f}{\Sigma_m} \qquad \text{Eqn 6.7}$$

Where f is a constant equal to 6.12×10^{-6}. The ^4He production rate $g^{-1}a^{-1}$ (N_{4He}) is equal to :-

$$N_{4He} = ([U]3.212x10^{6} + [Th]7.768x10^{5}) \qquad \text{Eqn. 6.8}$$

Where [U] and [Th] are the U and Th concentrations in ppm. This may be combined with equation 6.7 to give the $^{3}He/^{4}He$ ratio (R_{He}).

$$R_{He} = \frac{([U]A + [Th]B)\ [Li]\ f}{([U]3.21x10^{6} + [Th]7.76x10^{5})\ \Sigma_m} \qquad \text{Eqn 6.9}$$

Note that both the ^{3}He and ^{4}He production rates are dependent on the U and Th distribution within the matrix. Uncertainties in equation 6.9 may be evaluated by comparing contributions from the three component factors.

(a)

$$R_{He} = \frac{[U]A + [Th]B}{([U]3.21x10^{6} + [Th]7.76x10^{5})} \qquad \text{Eqn 6.10}$$

The uncertainty associated with equation 6.10 lies mainly in the concentration of U and Th. As discussed in Section 6.3 the U and Th concentrations within the Carnmenellis area have been taken to be 12±5 and 18±5 ppm respectively for granite and 4.65±0.35 and 5.25±0.35 respectively for Killas. Propagation of these uncertainties results in an uncertainty in equation 6.10 of 32% for the granite and 10% for Killas.

(b)

$$\frac{[Li]}{\Sigma_m} \qquad \text{Eqn 6.11}$$

The uncertainty associated with equation 6.11 lies in values of Σ_m and [Li]. As stated above equation 6.9 is only valid if variations in [Li] have little effect on Σ_m. Although Li has a high neutron absorption cross-section, variations in its concentration have little effect on Σ_m of the Carnmenellis granite as, Σ_m is strongly controlled by absorption due to B. For example a variation of one standard deviation in the Li content will change the average value of Σ_m by less than 5% in either the granite or Killas.

The uncertainty in equation 6.11 may be calculated using standard error propagation procedures given that :-

[Li] Carnmenellis granite = 335 ± 150 ppm

[Li] Killas = 201 ± 45 ppm

Σ_m Carnmenellis granite = 0.017 ± 0.005 cm^2g^{-1}.

Σ_m Killas = 0.012 ± 0.001 cm^2g^{-1}

The calculated uncertainty in equation 6.11 for granite and Killas are 54% and 24% respectively.

(c) The constant f .

Uncertainties associated with the constants that make up f are negligible compared to those associated with equations 6.10 and 6.11.

6.4.2.2 Results of $^3He/^4He$ ratio calculations. R_{He} and its associated uncertainty were calculated for the Carnmenellis granite and Killas assuming that the fraction of neutrons that reach thermal energies before absorption (F_{th}) = 1. The results (Table 6.6) show that R_{He} produced within the Killas is not significantly different from that produced within the granite. The value calculated for the granite is subject to a large degree of uncertainty which arises because of variations in the concentration of Li and variation in Σ_m (caused by variation in the B content of the granite). Calculations made assuming F_{th} = 0.65 (as is suggested by measurements of the thermal/epi-cadmium ratio in Section 3) yield lower R_{He} values ($3.8\pm2.4 \times 10^{-8}$ for the Carnmenellis granite).

Measured values of R_{He} ($3.5\pm0.4 \times 10^{-8}$ and $7.14\pm0.4 \times 10^{-8}$ for Rosemanowes circulation water and South Crofty water respectively see Section 6.4.) lie within uncertainty range for these calculations. The $^3He/^4He$ the ratios from these two locations are therefore indistinguishable.

The Rosemanowes circulation system is a recent phenomenon and circulation water must be stripping stored He from granite near the newly opened fracture flow paths. It would thus seem reasonable that the measured $^3He/^4He$ ratio at this site is representative of massive fresh granite, with a low water content, in which F_{th} would be low (resulting in a lower than average value of R_{He}). The waters at South Crofty however represents a more mature system than that at Rosemanowes. In such a mature system it is possible that stored He has been previously stripped from rock surrounding flow paths, and that

present He contents show $^3He/^4He$ ratios attained under conditions in which F_{th} is likely to be close to unity (ie/ higher porosity/water content). Under such conditions R_{He} would be higher than that at the Rosemanowes site, which is consistent with the measured data of HILTON (1985). It is also possible that in such mature systems the differentiation of chemical composition with depth and/or groundwater interaction has produced variation in R_{He} between these sites.

6.4.3 Chlorine-36.

The in-situ production of ^{36}Cl within the Carnmenellis granite and associated Killas would be expected to be much lower than levels produced in the Stripa granite due to its lower neutron flux. To carry out similar studies into the origin of chlorinity, differences between the neutron fluxes in the Carnmenellis granite and Killas should be as large as possible. Differences in the neutron fluxes produced within the granite and Killas are small and both fluxes are subject to large uncertainties (Section 6.3).

In both formations the production of ^{36}Cl at depths below the influence of cosmic rays is controlled by the $^{35}Cl(n,\gamma)$ reaction as the K/Cl ratio for both rock types is low (FUGE., 1979). The ^{36}Cl production rate (N_{Cl} g^{-1} a^{-1}) being equal to:-

$$N_{Cl} = N_{35Cl}\ \sigma\ f \qquad \text{Eqn. 6.13}$$

Where N_{35Cl} is the number of ^{35}Cl atoms g^{-1}, f is the thermal neutron flux ($cm^{-2}a^{-1}$) and σ is the thermal neutron cross-section for the (n,γ) reaction (cm^2). The $^{36}Cl/Cl$ ratio (R_{Cl}) attained at secular equilibrium (1.5 million years) may be calculated by dividing N_{Cl} by the total number of Cl atoms g^{-1} and the decay constant for ^{36}Cl (a^{-1}).

Thus $$R_{Cl} = f\ 4.56 \times 10^{-10} \qquad \text{Eqn. 6.14}$$

Note that the ratio R_{Cl} is independent of variation in the Cl concentration provided that the variation is small (changes in the chloride concentration will also have a marginal effect on the neutron flux by causing Σ_m to vary). Values of R_{Cl} calculated for the Carnmenellis granite and Killas (assuming $F_{th} = 1$) are given in Table 6.7 along with uncertainties due to variations in the neutron flux. From this it may be seen that

the equilibrium ratio formed within the granite is twice that formed within the Killas. However the ratio attained due to irradiation within the granite is only 21×10^{-15} thus to measure the difference between the granite and Killas a precision of better than 5×10^{-15} (24%) would be required even if the uncertainties in ratios were less than calculated. At present such precision is only available using accelerator mass spectrometry and samples of Cl^- from various saline groundwater sources in the Carnmenellis granite have been prepared for $^{36}Cl/Cl$ ratio measurement by this method. Samples were prepared by precipitation of SO_4^{2-} using $Ba(OH)_2$ to remove isobaric ^{36}S prior to collection of Cl^- as AgCl. These samples have been sent to the Technical University of Munich for measurement.

Until the results of such measurements are available it may be concluded that measurements of $^{36}Cl/Cl$ ratios may enable the source of Cl^- in natural saline groundwaters of the Carnmenellis granite to be identified, although this will be complicated by uncertainty in the neutron flux. The measured ratios may also give an indication as to the value of F_{th} in the region in which the water obtains its salinity.

6.5 Conclusions.

Principal conclusions of the present study on the Carnmenellis granite can be summarised as follows:-

(1) The average thermal neutron flux produced within the Carnmenellis granite lies within the range 0.3 to 0.6 $\times 10^{-4}$ $cm^{-2}s^{-1}$ and is controlled by the geochemistry of B, U and Th. Measured values at a number of sites lie within this range. Calculated values of neutron flux produced within the Killas yield values between 0.1 and 0.2 $\times 10^{-4}$ $cm^{-2}s^{-1}$ which is slightly lower than that expected in average clays and shales (See also Section 3).

(2) The calculated thermal neutron flux for individual sites within the Carnmenellis granite show good agreement with the measured fluxes at those sites (see also Section 3).

(3) It is likely that the fraction of neutrons that reach thermal energies (F_{th}) is controlled by the porosity and B content of the Carnmenellis granite.

(4) The levels of ^{3}H found in natural saline waters (6 TU) cannot be explained by in-situ production in either the Granite or Killas and hence must be attributed to mixing with recent meteoric water.

(5) The range in measured $^{3}He/^{4}He$ ratios within the Carnmenellis granite may be accounted for by variations in parameters which constrain the magnitude of the neutron flux.

(6) $^{36}Cl/Cl$ ratios generated within the Carnmenellis granite are predicted to be twice those generated within the Killas. Variations in the thermal neutron flux are likely to complicate the use of these ratios to define the origin of groundwater chlorinity in the natural circulation system.

(7) Further studies need to be carried out to investigate the B and Li distribution within the Carnmenellis granite if a more precise estimate of in-situ production rates are to be made.

Table 6.1. Calculated and measured total and thermal neutron flux for each of the sites described in Appendix 2.

Measurement and site	site depth (1) m	sample analysis	measured total neutron flux $x10^{-4}$ cm^{-2} s^{-1}	+/-	measured thermal neutron flux $x10^{-4}$ cm^{-2} s^{-1}	+/-
FM13 Rosemanowes B/H C FM14 average of 4 measure- FM15 ments between 3.8 and FM17 5.98 m into the face.	6	SA4	1.67	0.22	1.17	0.04
FM16 Rosemanowes B/H B 3.80 m into face.	6	SA4	1.47	0.04	----	----
FM20 South Crofty B/H A	560	SA1	0.61	0.01	0.37	0.02
FM21 South Crofty B/H B	560	SA1	0.63	0.02	0.38	0.02
FM24 Pendarves B/H A	100	SA2	0.53	0.02	0.32	0.03
FM22 South Crofty centre of chamber	560	SA1	0.51	0.02	0.34	0.02
FM23 South Crofty wall of chamber	560	SA1	0.49	0.02	0.35	0.03
FM25 Pendarves against wall of passage	100	SA2	0.30	0.03	0.22	0.02

Key :- (1) Depth below air/ground interface in metres.
(2) B/H = Borehole.

Table 6.2 Results of neutron production rate calculations showing variation in the calculated production rate between different samples. For details of samples see APPENDIX 2.

Site	Depth below surface	neutron production rate $g^{-1}a^{-1}\mu g^{-1}$ U	Th
Granites			
South Crofty	-560m	1.44	0.43
Pendarves	-100m	1.40	0.41
Penryn Quarry	Q	1.49	0.46
Rosemanowes	-1700m	1.53	0.48
Rosemanowes	-2000m	1.33	0.37
AM1	Q	1.46	0.44
AM13	Q	1.55	0.49
WJE	-340m	1.27	0.36
J11	-340m	1.53	0.48
AM30	Q	1.53	0.48
Mean granite		1.45±0.09	0.44±0.05
Killas			
HF1	-151m	1.42	0.43
HF2	-297m	1.40	0.41
Mean Killas		1.41±0.01	0.42±0.01

Q signifies sample taken from a quarry, therefore assumed to represent surface material.

Typical errors in individual neutron production rates are 4% and 6% for U and Th respectively.

Table 6.3 Results of neutron absorption cross-section calculations showing variation in the calculated cross-section between different samples. For details of samples see APPENDIX 2.

Site		Depth below surface	neutron absorption cross-section cm^2g^{-1}
Granites			
SA1	South Crofty	-560m	0.012
SA2	Pendarves	-100m	0.019
SA3	Penryn Quarry	Q	0.010
SA4	Rosemanowes	-1700m	0.024
SA13	Rosemanowes	-2000m	0.024
SA5	AM1	Q	0.019
SA6	AM13	Q	0.018
SA7	WJE	-340m	0.013
SA8	J11	-340m	0.017
SA10	AM30	Q	0.018
Mean granite			0.017±0.005
Killas			
SA11	HF1	-151m	0.011
SA12	HF2	-297m	0.012
Mean Killas			0.012±0.001

Q signifies sample taken from a quarry, therefore assumed to represent surface material.
Errors in individual absorption cross sections are in the range 5 to 7%.

Table 6.4 Production rates (N_{3H}) and equilibrium concentrations (N_{3H}) of ^{3}H produced in the Carnmenellis granite and Killas.

Site	N_{3H} $g^{-1}a^{-1}$	±	N_{3H} g^{-1}	±
Granite	3.0	1.9	54	34
Killas	0.89	0.22	16	3.9

Based on for the Carnmenellis granite :-

[Li] = 335±150 ppm

f = 4.7±2.0 x10^{-5} $cm^{-2}s^{-1}$ (F_{th} = 1)

and for the Killas :-

[Li] = 201±45 ppm

f = 2.3±0.23 x10^{-5} $cm^{-2}s^{-1}$ (F_{th} = 1)

Table 6.5 Calculated $^{3}He/^{4}He$ ratios for the Carnmenellis granite and Killas.

Site	$^{3}He/^{4}He$ ratio (R_{He}) x 10^{-8}
Granite	5.8 ± 3.7
Killas	4.9 ± 1.3

Table 6.6 Calculated $^{36}Cl/Cl$ ratios for the Carnmenellis granite and Killas.

Site	$^{36}Cl/Cl$ ratio (R_{Cl}) $x10^{-15}$
Granite	21.4 ± 9.1
Killas	10.5 ± 1.0

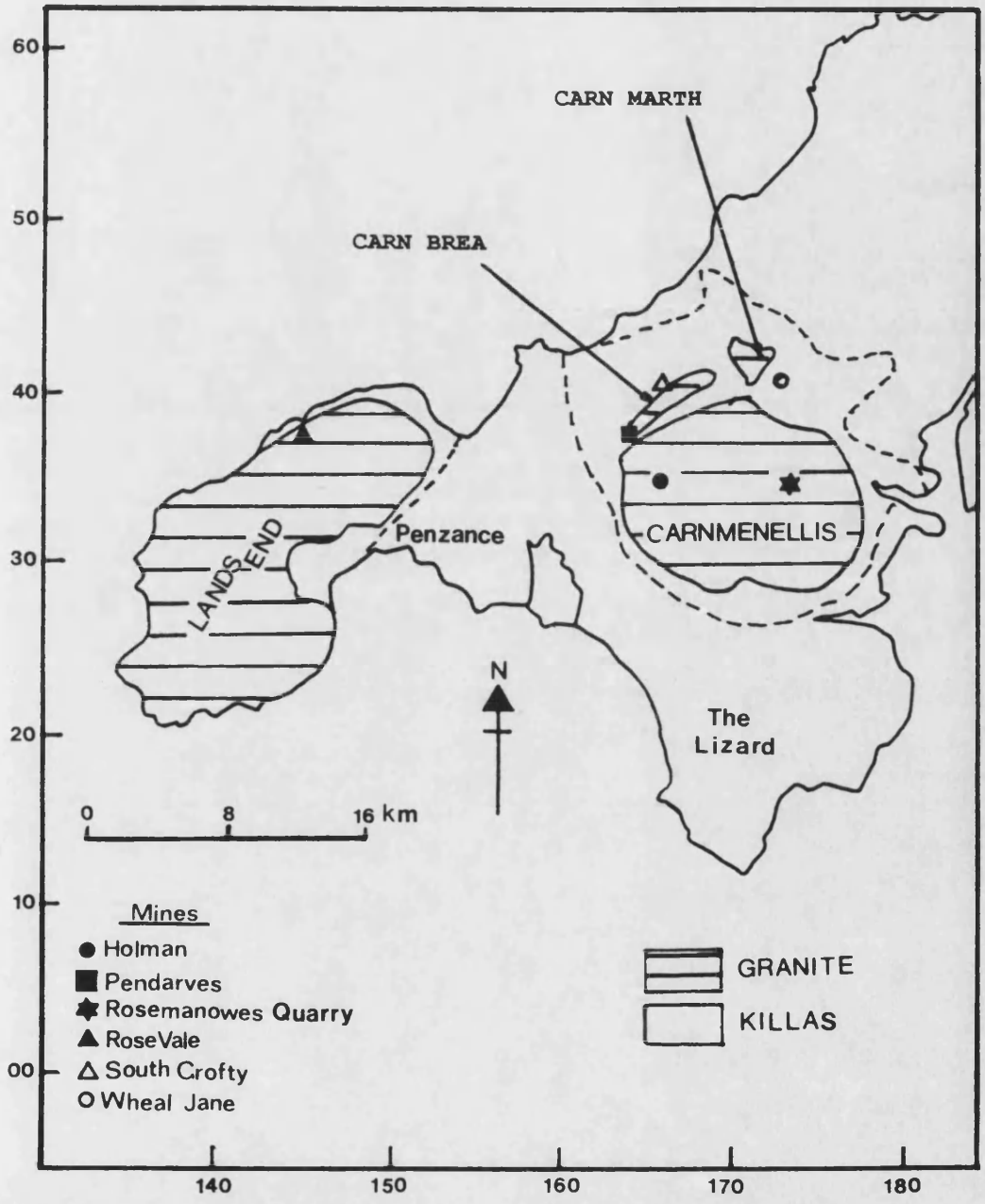

Fig. 6.1. Map showing the general geology of South West Cornwall and the location of important mines, and sites at which the neutron flux has been measured.

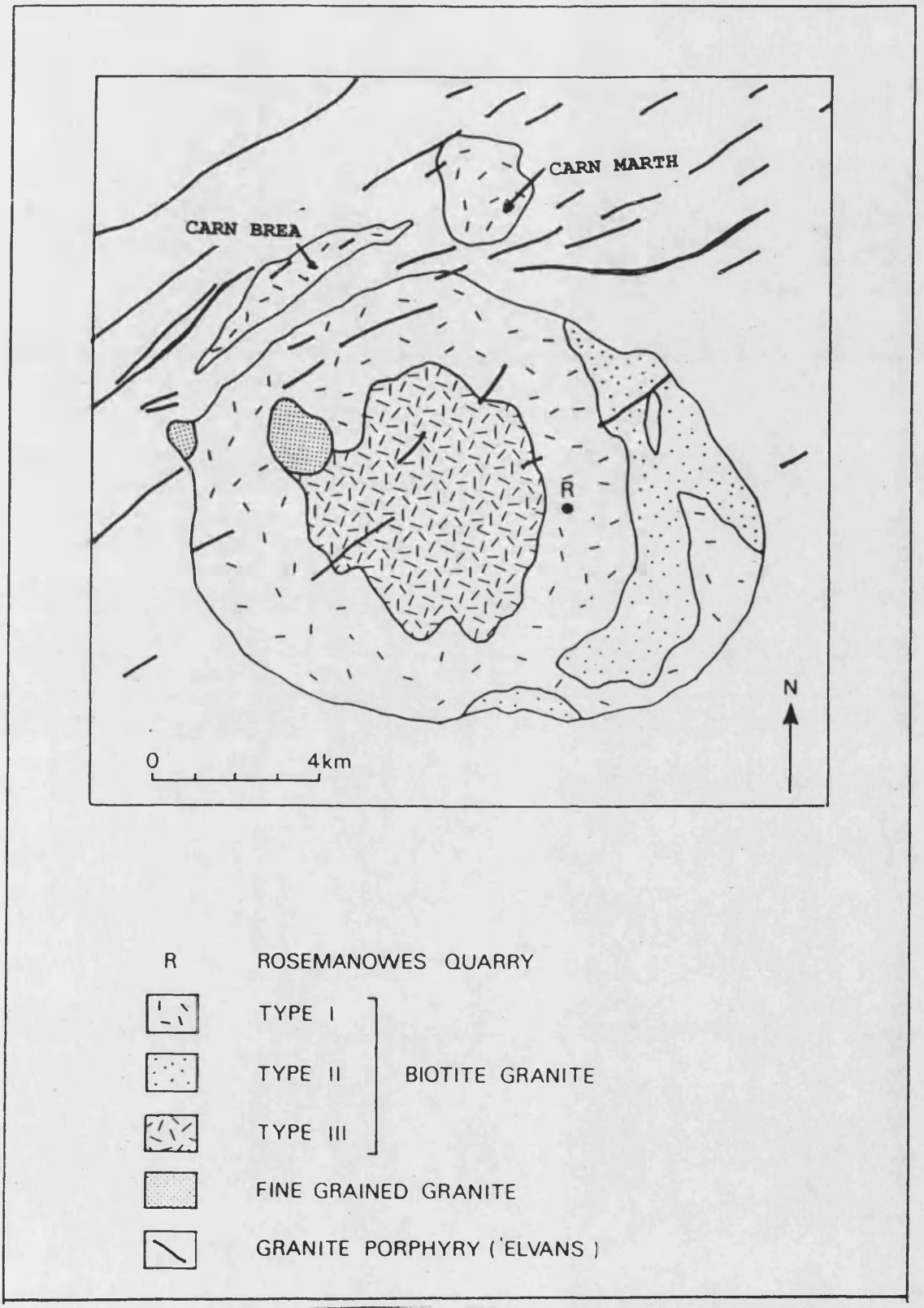

Fig. 6.2. Outline Geological map of the Carnmenellis granite (after GOSH, 1934).

7.0 FINAL ASSESSMENT.

7.2 Neutron flux calculations.

The estimation of neutron production rates and derived neutron flux is pre-requisite to assessing the impact of in-situ production on particular site investigations. Comparison of calculated and measured neutron flux (Section 3) and case studies on the Stripa and Carnmenellis granites (Sections 5 and 6), show that the total sub-surface neutron flux can either be determined experimentally or be calculated from the neutron production rate and neutron absorbing capacity of the rock. This result is of particular relevance to geochemical investigations where prediction of "average fluxes" that may be applied to particular formations must rely upon estimates based upon theoretical models.

The accurate prediction of neutron flux by such models requires a geochemical survey which must include rock analysis (major element analysis, trace element analysis (Li, B, Gd and Sm), radio element analysis (U and Th)) and mineralogical analysis. The requirement for the analysis of B, Gd and Sm may be reduced if sufficient sample is available to allow the experimental measurement of thermal neutron absorption cross-section (Appendix 3). It should be noted that the quality of such a geochemical survey has a direct influence on the reliability of any predicted flux and derived in-situ production rate. If such a survey is not possible then a reasonable approximation to the neutron flux may be made using neutron yields and cross-sections for the most appropriate average rock type (see Appendix 1) together with measured U and Th concentrations.

Comparison of calculated and measured thermal neutron flux have demonstrated that the calculated thermal neutron flux reflects the total measured flux rather than the measured thermal flux. From this it must be assumed that either, a higher proportion of neutrons are being absorbed prior to reaching thermal energies than predicted, or that the average energy of the thermal flux distribution is being shifted to higher energies by neutron absorption. Whilst a detailed analysis of these factors is not possible without the use of multi-group neutron transport theory it very likely that both factors contribute to the observed energy distribution.

Neutron production in the epigene zone by the interaction of protons, pions and muons is dependent upon geomagnetic latitude and height above sea level. Calculation of production rates and correction factors that may be universly applied to these reactions is extremely difficult due to the complex nature of such interactions, however an approximation may be made using the data discussed in Sections 2.3, 2.4 and 2.5. Relative production rates show that production from protons and pions dominate at depths < 4 meters below the Earth's surface. At greater depths production from muons dominate until attenuation of the muonic flux reduces muonic production rates to levels below that of (α,n) and spontaneous fission reactions.

Comparison of calculated and measured neutron flux (at depths < 60 m below the Earth's surface) show reasonable agreement (Section 3) given such the complexity of such calculations. At very shallow depths the calculated values seriously overestimate the flux (by up to 800 %) reasons for this departure are at present uncertain.

7.2 In-situ production of ^{3}H, ^{14}C, ^{36}Cl, ^{37}Ar and ^{39}Ar.

Conclusions drawn in Section 4 demonstrate that in-situ production of ^{3}H, ^{14}C, ^{36}Cl, ^{37}Ar and ^{39}Ar below the Earth's surface is dominated by neutron induced nuclear reactions. At relatively shallow depths (0 to 5m) the interaction of cosmic-rays with the rock matrix also produce these isotopes either directly or indirectly via neutrons produced during the interaction of such particles. The relative importance of a particular nuclear reaction, is dependant on the availability of a suitable target nuclide as well as the particle flux. For example in the case of ^{36}Cl if the concentration of Cl in the rock matrix is high, production via the $^{35}Cl(n,\gamma)$ reaction dominates. However if the concentration of Cl is low, production via the $^{39}K(n,\alpha)$ reaction becomes relatively more important. Such effects also increase the relative importance of low probability reactions especially those that have a highly abundant target nuclide such as Si or O.

The magnitude of other production reactions such as exotic decay of U and Th series isotopes, and (α,x) reactions, are generally low in average rock matrices compared to neutron induced reactions. However in areas of very high radioelement concentration, such as in uranium ores, their relative effect is likely to be enhanced since neutron production via (α,n)

reactions may be reduced by the high concentration of heavy elements.

It is clear from work discussed in Section 4 that a large number of reactions probabilities and cross-sections are either unavailable or have a high degrees of uncertainty. If better estimates of in-situ production rates are to be made it is essential that further work include the determination of such probabilities. This is especially true for reactions that emit charged particles following negative muon capture (e.g. production of ^{3}H Section 4.2).

7.3 In-situ production at the Stripa site.

There is good agreement between calculated and measured total neutron fluxes in the Stripa Granite and Leptite. There is also reasonable agreement between the measured and calculated thermal neutron fluxes. This indicates that at the Stripa site neutrons are well represented by a thermal neutron energy distribution. This is consistent with the the Stripa granite and Leptite having relatively low neutron absorption cross-sections together with low concentrations of 1/v absorbers such as B and Li.

The estimated groundwater contents of in-situ produced ^{3}H and ^{14}C are close to the present detection limits for these nuclides despite the high concentration of U and Th in the matrix. For ^{3}H, the production site is within the minerals of the rock matrix and the efficiency of its transfer to the fluids is probably low. The most significant n-induced ^{14}C production probably occurs within the fracture fluids of a granite matrix. The emission of ^{14}C by exotic decay of Ra and other natural radioelements may also be an important source of in-situ produced ^{14}C.

In groundwaters of Stripa granite, in-situ production of ^{36}Cl dominates over atmospheric inputs due to both cosmogenic production and nuclear weapon testing. Calculated $^{36}Cl/Cl$ ratios for the Stripa granite are not inconsistent with measured values obtained from extracted rock Cl^{-}. Further analytical data ($^{36}Cl/Cl$ ratios) confirm the earlier conclusions of ANDREWS et al., (1986) that such data may be used for determining the origin of groundwater salinity in the Stripa granite/Leptite system.

In-situ production of ^{39}Ar occurs mainly within the feldspars and micas of a granitic matrix, that is, at the natural K sites. ^{37}Ar production occurs mainly within the fracture minerals within the Stripa granite, that is, at the high concentration of Ca target within the calcite of the fracture infill. ^{85}Kr production occurs at U sites and is controlled by the micro-distribution of U. Fracture infill minerals and microfractures within the matrix minerals are potentially important production sites.

7.4 In-situ production in the Carnmenellis granite.

The calculated average thermal neutron flux produced within the Carnmenellis granite lies within the range 0.3 to 0.6 $x10^{-4}$ $cm^{-2}s^{-1}$ and is controlled by the geochemistry of B, U and Th. These values are consistent with measured neutron fluxes at Rosemanowes Quarry, South Crofty Mine and Pendarves Mine. Calculated values of neutron flux produced within the surrounding Killas yield values between 0.1 and 0.2 $x10^{-4}$ $cm^{-2}s^{-1}$ which is slightly lower than that expected similar rock types (ie. average clays and shales). The large number of epi-thermal neutrons measured at sites within the Carnmenellis granite is consistent with the granites higher than average B concentration.

Levels of ^{3}H found in natural saline waters (6 TU) cannot be explained by in-situ production in either the Granite or Killas and hence must be attributed to mixing with recent meteoric water. This supports the conclusions of ANDREWS and KAY., (1982).

The range in measured $^{3}He/^{4}He$ ratios within the Carnmenellis granite can be accounted for by variations in parameters which constrain the magnitude of the thermal neutron flux and the ^{3}H production rate. Results suggest that ratios measured for Rosmanowes circulation water represent He produced in an environment where the neutron flux is less well thermalised than in natural well evolved flow paths. This is consistent with the stripping of stored He from granite near newly opened fracture flow paths.

$^{36}Cl/Cl$ ratios generated within the Carnmenellis granite are predicted to be twice those generated within the Killas. Variations in the thermal neutron flux produced within the granite will complicate the use of these ratios to define the origin of groundwater chlorinity in the natural hydrothermal

system.

The further study of in-situ production within the Carnmenellis granite requires a more detailed investigation of the B and Li distribution within the Carnmenellis granite. Only when the effect of variations in the concentration of these elements on the neutron energy distribution is studied will a more precise estimate of in-situ production rates be possible.

7.4 Conclusions.

Using methods discussed in this thesis it is possible to estimate the relative magnitude of various nuclear reactions that lead to the in-situ production of ^{3}H, ^{14}C, ^{36}Cl, ^{37}Ar and ^{39}Ar. As discussed in Section 1 these isotopes have been extensively used for radiochemical dating of geological events and studying groundwater evolution. The effect of in-situ production on the use of ^{3}H and ^{14}C for these purposes is small since the magnitude of in-situ production for these isotopes represents levels at or below the detection limits achievable using present sampling techniques. Furthermore for these isotopes chemical effects will generally be a more important source of error. For ^{36}Cl, ^{37}Ar and ^{39}Ar levels of in-situ produced isotopes exceed cosmogenic input under favorable circumstances and hence greatly limit the use of these isotopes for groundwater dating. Alternatively if in-situ production levels can be accurately calculated these isotopes will be particularly useful in the study of rock water interactions. The major uncertainties in assessing the magnitude of such effects lie in assuming the energy distribution of reacting particles and the sampling of material that accurately reflects the composition of rock in which the particular groundwater has evolved.

8.0 REFERENCES.

AHMED AWAD KARIM M.A. (1971). The distribution of some major and trace elements in the granites of West Cornwall. *Unpublished MSc Thesis Camborne School of Mines* , Camborne.

ALEXANDER J., HALL D.H. and STOREY B.C. (1981) Porosity measurements of crystalline rocks by laboratory and geophysical methods. *Report ENPU 81-10* , British Geological Survey Keyworth U.K.

ALDERTON D.H.M., PEARCE J.A. and POTTS P.J. (1980) Rare earth element mobility during granite alteration evidence from south west England. *Earth Planet. Sci. Lett.* **49**, 149-165

ALLEN W.D. (1960) *Neutron detection* . George Newnes Ltd, London. 260p.

AL-TURKI K.I.S. and STONE M. (1978) Petrographic and chemical distinction between the megacrystic members of the Carnmenellis granite, Cornwall. *Proc. Ussher Soc.* **4**, 182-189.

ANDERSON E.C. and LIBBY W.F. (1951) Worldwide distribution of natural radiocarbon. *Phys. Rev.* **81**, 64-69.

ANDREWS J.N. (1985) The isotopic composition of radiogenic helium and its use to study ground water movement in confined aquifers. *Chemical Geology* . **49**, 339-351.

ANDREWS J.N., DAVIS S., FABRYKA-MARTIN J. FONTES J-C., FRITZ P., LEHMANN B., LOOSLI H.H., MICHELOT J-L., MOSER H., SMITH B. and WOLF M. (1989). The insitu production of radioisotopes in rock matrices with particular reference to the Stripa granite. *Geochimica et Cosmochimica Acta* (in press).

ANDREWS J.N., FONTES J-Ch., MICHELOT J-L. and ELMORE D. (1986) In-situ ^{36}Cl production and groundwater evolution in crystalline rocks at Stripa Sweden. *Earth Planet. Sci. Lett* . **77**, 49-58.

ANDREWS J.N. and LEE D.J. (1979). Inert gases in groundwater from the bunter sandstone of England as indicators of age and palaeoclimatic trends. *Journal of Hydrologyp.* ***41***, 233-252.

ANDREWS J.N., HUSSAIN N., BATCHELOR A.S. and KWAKWA K. (1986b) ^{222}Rn solution by the circulating fluid in a hot dry rock geothermal reservoir. *Applied Geochem* . **1**, 647-657.

ANDREWS J.N., HUSSAIN N., FORD D. SMITH B. and YOUNGMAN M.T. (1987) Radio element and inert gas studies . In: Granite-water interactions in relation to Hot Dry Rock geothermal development. Investigation of the geothermal potential of the UK, British Geological Survey . 116p.

ANDREWS J.N. and KAY R.L.F. (1982) Natural production of tritium in permeable rocks. *Nature.* **298**, 361-363.

ANTONOV A.V., GRANATKIN B.V., MERKULEV A.Yu., MILLER V.V. and SHIMELEVICH Yu.S. (1966). *Radioisotope Instruments in Industry and Geophysics.* Vol. 2, p139 . I.A.E.A., Vienna.

ATTREP. M., LEDBETTER. W.B. and RIDDLE. D.K. (1979) The effects of boron and lithium on the ratio of spontaneous fission in natural uranium. *J. Inor. Nucl. Chem .* **41**, 1-3.

BAIR J.K. and GOMEZ del CAMPO J. (1979) Neutron yields from alpha-particle bombardment. *Nuclear Science and Engineering .* **71**, 18-28.

BARKER D., JULL A.J.T. and DONAHUE D.J. (1985) Excess carbon-14 abundances in uranium ores: possible evidence for emission from uranium-series isotopes. *Geophys. Res. Lett .* **12**, 737-740.

BARWICK S.W., PRICE P.B., RAVN H.L., HOURANI E. and HUSSONNOIS M.(1986) Systematics of spontaneous emission of intermediate mass fragments from heavy nuclei. *Phys. Rev. C.*, Rapid Commun. **34**, 362-365.

BASS R., FANGER U. and SALEH F.M. (1964) Cross sections for the reactions $^{39}K(n,p)^{39}Ar$ and $^{39}K(n,\alpha)^{36}Cl$. *Nuclear Physics.* **56**, 569-576.

BEER K.H. and EDMUNDS W.M. (1978) A preliminary look at lithium in the United Kingdom. *Energy.* **3**, 281-292.

BENTLEY H., BRISSAUD I., ELMORE D., GOVE H. and MA X.A. (1983) Search for ^{36}Cl in Stripa site groundwaters. *Z.Phys.A Atoms & Nucli.* **313**, 243-244.

BENTLEY H.W., PHILLIPS F.M. and DAVIS S.N. (1986) Chlorine-36 in the terrestrial environment. In *Handbook of Environmental Isotope Geochemistry* (eds P. Fritz and J.-Ch. Fontes) Vol. 2 *The terrestrial environment,* Elsevier, Amsterdam. pp. 427-480.

BENTLEY H.W., PHILLIPS F.M., DAVIS S.N., GIFFORD S., ELMORE D., TUBBS L.E. and GOVE H.E. (1982) Thermonuclear ^{36}Cl pulse in natural water. *Nature.* **300**, 737-740.

BENTLEY H.W., PHILLIPS F.M., DAVIS S.N., HABERMEHL M.A., AIREY P.L., CALF G.E., ELMORE D., GOVE H.E. and TORGERSEN T. (1986b) Chlorine-36 dating of very old groundwater: 1. The great Artesian basin Australia. *Water Resources Research.* **22**, 1991-2001.

BEVINGTON P.R. (1969) *Data reduction and error analysis for the physical sciences.* McGraw-Hill, New York. 336p.

BLAND C.J. and CIONI G. (1968) Geomagnetic cutoff rigidities in non-vertical directions. *Earth Planet Sci. Lett.* **4**, 339.

BOBODYANOV I.B. (1970) Average multiplicity of the formation of neutrons in μ capture. Acta. Phys. Acad. Sci. Hung. **29**, Supple. 4, 151.

BOHR N., and WHEELER J.A. (1939) The Mechanism of nuclear fission. *Phys. Rev.* **5**, 426-450

BOTT M.H.P., and SCOTT P (1964) Recent Geophysical studies in S.W. England. In: *Present views on some aspects of the geology of Cornwall and Devon* (eds Hosking K.F.G. and Shrimpton G.J.). 150th Anniversary Volume. *R. Geol. Soc. Cornwall.* pp.25-44.

BROWN G.C., CASSIDY J., OXBURGH E.R., PLANT J., SABINE P.A. and WATSON J.V. (1980). Basement heat flow and metalliferous mineralisation in England and Wales. *Nature*. **288**, 657-659.

CARTER G. and COLLIGON J.S. (1969) *Ion bombardment of solids* . Elsevier, New York. 464p.

CENTRONICS (1986) Centronics Nuclear Products data sheet. Centronic ltd., Centronic House, King Henry's Drive, New Addington, Croydon, Surrey.

CHARALAMBUS S. (1971) Nuclear transmutation by negative stopped muons and the activity induced by the cosmic-ray muons. *Nuclear Physics.* **A166**, 145-161.

CHOPPIN G.R. and RYDBERG J. (1980) *Nuclear Chemistry, Theory and Applications.* Pergamon Press, Oxford. 667p.

CLOSE. F., MARTEN M. and SUTTON C. (1987) *The Particle explosion*. Oxford Univerity press, New York. 239p .

COCCONI G and COCCONI TONGIORGI V. (1951) Nuclear disintegrations induced by μ-mesons. *Physical Review*. **84**, 29-36.

CONVERSI M. (1950) Flux of Slow μ-Mesons near the equator. *Phys. Rev*. **79**, 749.

CRAIG H. and LAL D. (1961) The production rate of natural tritium. *Tellus*. **13**, 85-105.

CZUBEC J.A., DROZKOWREZ K., KRYNICKA DROZDOWIEZ E., IGIELSKI A., SOBCZYNSKI Z. and WOZNICKA U. (1981) How to measure the neutron absorption cross-section of rock samples. *J. Phys.* **D: 14**, 977.

CURRIE L. A. (1982) *Nuclear and Chemical dating techniques :- interpreting the environmental record* . American Chemical Society, Washington D.C. 516p.

CZUBEK J.A., DROZDOWICZ K., KRYNICA-DROZDOWICZ E. IGIELSKI A., and WOZNICA V. (1983) Measurement of the thermal neutron absorption cross section of rock samples. *Int. J. Applied Radiation & Isotopes*. **34**, 143-151.

DAVIS S.N. and DeWIEST R.J.M. (1966) *Hydrogeology*. John Wiley & Sons, New York. 463p.

DAVIS R. and SCHAEFFER O.,W. (1955) Chlorine-36 in Nature. *Annals of the New York Academy of Sciences*. **62**, 105-122.

DAVIS S.N., and BENTLEY H.W. (1982) Dating groundwater (A short review) In *Nuclear & Chemical Dating Techniques :- Interpreting the environmental record* (ed. L.A. Currie). A.C.S. Symposium Series. **176**, pp.187-222.

DeCARVALHO H.H., MARTINS J.B., MEDEIROS E.L. and TAVARES O.A.P. (1982) Decay constant for the spontaneous fission process in ^{238}U. *Nucl. Instr. Meth*. **197**, 417-426.

EDMUNDS W.M. ANDREWS J.N., BURGESS W.G., KAY R.L.F., and LEE D.J. (1984) The evolution of saline and thermal groundwater in the Carnmenellis granite. *Mineralogical Magazine*. **48**, 407-424.

EDMUNDS W.M., KAY R.L.F. and McCartney R.A. (1985). Origin of saline groundwaters in the Carnmenellis granite: natural processes and reaction during Hot Dry Rock reservoir circulation: *Chemical Geology* . **49**, 287-301.

EDMUNDS W.M., KAY R.L.F., MILES D.L. and COOK J.M. (1987)The origin of saline groundwaters in the Carnmenellis granite Cornwall (U.K.): Further evidence from minor and trace elements. In *Saline Waters and Gases in Crystaline rocks* (eds. Fritz P. and Frape S.K.). *Geochemical Association of Canada Special Paper* **33**.

EINSTEIN A.E. (1907) The inertia of energy, as demanded by the principal of relativity. *Ann. der Phys.* **23**, 371-384.

ELMORE D., FULTON B.R., CLOVER M.R., MARSDEN J.R., GOVE H.E., NAYLOR H., PURSER K.H. KILLIUS L.R., BEUKENS R.P. and LITHERLAND A.E. (1979) Analysis of ^{36}Cl in environmental water samples using an electrostatic accelerator. *Nature.* **277**, 22-25.

ELMORE D., TUBBS L.E., NEWMAN D., MA X.Z., FINKEL R., NISHIIZUMI K., BEER J., OESCHGER H. and ANDREE M. (1982) The ^{36}Cl bomb pulse measured in a shallow ice core from Dye 3 Greenland. *Nature.* **300**, 735-737.

ERIKSSON E. (1960) The yearly circulation of chloride and sulphur in nature; meteorological geochemical and pedological implcations. Part II. *Tellus.* **12**, 63-109.

EVANS G.V., OTLET R.L., WASSELL L.L. and BATH A.H. (1984) Verification of the presence of carbon-14 in secondary carbonates within a sandstone aquifer and its hydrological implications. In: *Isotope Hydrology* 1983 577-590 I.A.E.A., Vienna.

EXLEY C.S. and STONE M. (1964) The granitic rocks of south west England. In: *Present views on some aspects of the geology of Cornwall and Devon* (eds Hosking K.F.G. and Shrimpton G.J.). 150th Anniversary Volume. *R. Geol. Soc. Cornwall.* pp.131-184.

FAURE G. (1986). *Principals of isotope geology* , 2^{nd} edition John Wiley and Sons. 358p.

FERMI E. (1934). Versuch einer theorie der β-strahlen. *Z. Phys.* **88**, 161.

FEIGE Y., OLTMAN B.G. and KASTNER J. (1968) Production rates of neutrons in soils due to natural radoactivity. *J. Geophys. Res.* **73**, 3135-3142.

FETH J.H (1981) *Chloride in natural continental water: a review*. U.S.G.S. Water Supply Paper 2176, 36p

FINK D., MEIRAV O., PAUL M., ERNST H., HENNING W., KUTSCHERA W., KAIM R., KAUFMAN A. and MAGARITZ M. (1982) Accelerator mass spectrometry at the Rehovot pelletron tandem: measurements of abundances of cosmogenic radioisotopes and future prospects. *Nucl. Inst. and Meth. in Phys. Res.* **B5**, 123-128.

FINKEL R.C., NISHIIZUMI K., ELMORE D., FERRARO R.D. and GOVE H.E. (1980) ^{36}Cl in polar ice, rainwater and seawater. *Geophysical Res. Lett.* **7**, 983-986.

FLEROV G.N., and PETRZHAK K.A. (1940) Spontaneous fission of uranium *J. Phys. (U.S.S.R.)* . **3**, 275-280.

FLOYD P.A. (1971) Temperature distribution in the Lands End aureole Cornwall. *Proc. USSHER. Soc* . **2**, 335-351.

FONTES J-Ch., BRISSAUD I and MICHELOT J.L. (1984) Hydrological implications of deep production of chlorine-36. *Nucl. Inst. and Methods in Physics Res* . **233**, 303-307.

FRIEDLANDER G., KENNEDY J.W., MACIAS E.S. and MILLER J.M. (1981). *Nuclear and radiochemistry* 3rd edition. Wiley-Interscience Canada. 684p.

FRISCH O.R. (1958) *The Nuclear Handbook.* George Newnes Ltd, London. 350p.

Fritz P. and Fontes J.-Ch. (1980) *Handbook of Environmental Isotope Geochemistry* Vol. 1 *The terrestrial environment, A,* Elsevier, Amsterdam. 600p.

Fritz P. and Fontes J.-Ch. (1986) *Handbook of Environmental Isotope Geochemistry* Vol. 2 *The terrestrial environment, B,* Elsevier, Amsterdam. p545.

FUGE R. (1979) Water soluble chlorine in granitic rocks. Chem. *Geology.* **25**, 169-174.

FUGE R., and POWER G.M. (1969) Chlorine and fluorine in granitic rocks from S.W. England. *Geochim. et cosmochim. Acta* . **33**, 888-893.

FYFE W.S. PRICE N.J. and THOMPSON A.B. (1978) *Fluids in the Earth's crust* . Elsevier, Amsterdam. 383p.

GAMOW. G. (1928). Zur quantentheorie des atomkernes. *Z. Phys* . **51**, 204.

GAT J.R. (1980) The isotopes of hydrogen and oxygen in precipitation. In *Handbook of Environmental Isotope Geochemistry* (eds P. Fritz and J.-Ch. Fontes) Vol. 1 , Elsevier, Amsterdam. pp.21-47.

GALES S., HOURANI E., HUSSONNOIS M., SCHAPIRA J.P., STAB L. and VERGNES M.(1984) Exotic nuclear decay of ^{223}Rn by Emission of ^{14}C nuclei. *Phys. Rev. Lett* . **53**, 759-762.

GALE J.E. and WITHERSPOON P.A. (1979) An approach to the fracture hydrology st Stripa: preliminary results. *Technical report 7079 (SAC-15), Lawrence Berkeley Laboratory, University of California.*

GEORGE E.P. (1957) Observations of cosmic rays underground and their interpretation. In *Progress in Cosmic Ray Physics* (ed. Wilson J.G). North Holland, Amsterdam 200p.

GIBSON W.M. (1971) *Nuclear reactions* . Penguin libary of physical sciences: Physics, Penguine books, London. 286p

GORSHKOV G.V., ZYABKIN V.A., and TSVETKOV O.S. (1962) Neutron yield from the reaction (α,n) in standards and granite irradiated with polonium particles. *Atomnaya Energiya.* **13**, 654-657.

GOSH P.K. (1934) The carnmenellis granite: its petrology metamorphism and tectonics. *Q. J. Geol. Soc* . **90**, 240-76.

GURNEY. R.W. and CONDON. E.U. (1928) Quantum mechanics and radioactive disintegration. *Nature*. **122**, 439.

HAMPLE W. and KIRSTEN. T. (1975) Measurement of cosmic ray muon-induced radioisotopes ^{57}Co ^{58}Co and ^{60}Co in nickel. *Proc. 14th Int. Cosmic. Ray. Conf* . pp1895-1899.

HEATON T.H.E. (1984) Rates amd sources of ^{4}He accumulation. *Journal of Hydrological Sciences.* **29**, 29-47.

HENDRICK L.D., and EDGE R.D. (1966) Cosmic ray neutrons near the earth. *Physical Review.* **145**, 1023-1025.

HILTON D.R., OXBURGH E.R., AND O'NIONS R.K. (1985) Fluid flow through a high heat flow granite: constraints imposed by He and RN data. In: High heat production (HHP) granites, hydrothermal circulation and ore genesis. *Inst. Mining. Met .*, London, 135-142.

HOOKER P.J., O'NIONS R.K., AND OXBURGH E.R. (1985) Helium isotopes in North Sea gas fields and the Rhine Rift. *Nature.* **318**, 273-275.

HOUTERMANS F.G., and OESCHGER H. (1958) Proportional counter for measurement of weak activity of soft beta-decay. *Helv. Phys. Acta*. **31**, 117-26.

HUGHES D.J. and SCHWARTZ R.B. (1958) Neutron Cross-sections. *Brookhaven National Laboratory Report BNL-325.*

IAEA (1973) *Nuclear Techniques in groundwater hydrology.* In: Groundwater studies, UNESCO, Paris, Sections 10.1 to 10.4. 38p.

ICRU (1969) *Neutron Fluence, Neutron Spectra and Kerma.* International Commission on Radiation units and Measurements Report 13, Washington D.C. 55p.

IAEA (1970) *Neutron Fluence Measurements.* International Atomic Energy Agency, Technical Report series No.107, Vienna. 184p.

IAEA (1987) Evaluation of data obtained for the absoption cross-section of the MCS-1, MCS-2 and MCS-3 rock samples. Interim report by J.A. Czubek to the International Atomic Energy Agency (April 1987). 8p.

INTHOFF W. (1955) Fission neutron reaction cross-sections. *Nucleonics*. **13**, 67.

JEFFERIES N.L. (1984) The radioactive accessory mineral assemblage of the Carnmenellis granite Cornwall. *Proc. Ussher Soc*. **6**, 35-40.

JEFFERIES N.L. (1985) The distribution of the rare earth elements within the carnmenellis pluton Cornwall. *Minerological Magazine.* **49**, 495-504.

JULL A.J.T., BARKER D.L. and DONAHUE D.J. (1988) On the ^{14}C content in radioactive ores. *Chemical Geology, Isotope Geoscience Section*. **66**, 35-40.

KAPLAN I. (1955) *Nuclear Physics.* Addison-Wesley, Reading Mass. 609p.

KAYE G.W.C. and LABY T.H. (1986) *Tables of Physical and Chemical constants, 15th Edition,* Longman Group ltd., Essex. 477p.

KOZCOWSKI. T., BERTL. W., POVEL. H.P., SENNHAUSER. U., WALTER. H.K., ZGLINSKI. A., ENGFER. C.H., GRAB. C.H., HERMES. H.A., ISAAK H.P., VAN DER PLUYM. J. and HESSELINK. W.H.A. (1985) Energy spectra and asymmetries of neutrons emitted after muon capture. *Nuclear Physics* . **A436**, 717-732.

KREFT A. (1973) The question of fast neutron absorption in moisture measurements by the fast neutron method. *Nukleonika* **18**, 615-623.

KUBIC P.W., KORSCHINEK G. and NOLTE E. (1984) Accelerator mass spectrometry with completely stripped Cl-36 ions at the Munich post-accelerator. *Nucl. Instr. Meth. in Phys. Res.* **B1**, 51-59.

KUHN M.W., DAVIS S.N., BENTLEY H. and ZITO R. (1984) Measurement of thermal neutrons in the subsurface. *Geophys. Res. Lett.* **11**, 607-610.

KURZ M.D. (1986) Cosmogenic helium in a terrestrial igneous rock. *Nature.* **320**, 435-439.

LAL D. (1963) Isotopic changes induced by neutrinos. *Proc. of the 6th Int. Conf. on Cosmic Rays,* Jaipur, India. pp. 190-208.

LAL D. (1987) Production of ^{3}He in terrestrial rocks. *Chemical Geology (isotope Geoscience Section).* **66**, 89-98.

LAL D. and PETERS S. (1967) Cosmic ray produced radioactivity on the earth. In: *Handbuch der Physik 46/2* (ed. K. Sitte) Springer-Verlag, Berlin. pp.512-612.

LEDERER C.M. and SHIRLEY V.S. (1978) *Table of the isotopes, seventh edition.* Wiley-Interscience, New York. 1523p.

LIBBY W.F. (1946) Atmospheric helium three and radiocarbon from cosmic radiation. *Phys. Rev.* **69**, 671.

LIBBY W.F. (1955) *Radiocarbon Dating* , 2nd edition. University of Chicago Press Chicago. 175p.

LISKIEN. H. and PAULSEN. A. (1977) Neutron yields of light elements under α-bombardment. *Atomkernenergie* . **30**, 59-61.

LOOSLI H.H., LEHMANN B.E. BALDERER W. (1989) Argon-39, argon-37 and krypton-85 isotopes in Stripa groundwaters. *Geochim. Cosmochim. Acta.* (in press).

LOOSLI H.H. (1983) A dating method with ^{39}Ar. *Earth Planet. Sci. Lett.* **63**, 51-62.

LOOSLI H.H. and OESCHGER H. (1968). *Earth Planet. Sci. Lett.***5**, 191.

LOOSLI H.H. and OESCHGER H. (1969). *Earth Planet. Sci. Lett.***7**, 67.

LOOSLI H.H. and OESCHGER H. (1978) Argon-39, carbon-14 and krypton-85 measurements in groundwater samples. *Isotope Hydrology*. I.A.E.A., Vienna. pp.931-945.

LOOSLI H.H. and OESCHGER H. (1980) Use of ^{39}Ar and ^{14}C for groundwater dating. *Radiocarbon* **22**, 863-870.

MATERCZYK J. and ZUBER A. (1966) . *Radioisotope instruments in industry and geophysics,* Vol 2, IAEA, Vienna. 383p.

MAMYRIN B.A., and TOLSTIKHIN I.N. (1984) *Helium Isotopes in nature*. Elsevier, Amsterdam. 300p.

MARSHAK R.E., RIAZUDDIN RYAN C.P. (1969) Theory of weak interactions in particle physics. In: *Monographs and Texts in Physics and Astronomy 24* (ed. R.E. Marshak). Wiley Interscience, London. 761p.

MARSHALL W. (1983) *Nuclear power technology :- Volume 3 Nuclear radiation*. Clarendon Press, Oxford. 363p.

McDONALD. B., JUSTO. A.D., SELIG. N., KAPLAN. S.N. and PYLE. V.P. (1965) Neutrons from negative-muon capture. *Physical Review* **139**, 1253-1263.

MICHELOT J.L., BENTLEY H.E., BRISAUD I., ELMORE D. and FONTES J.-Ch. (1984). Progress in environmental isotopes studies (^{36}Cl 34S ^{18}O) at the Stripa site. *Isotope Hydrology,* I.A.E.A., Vienna. pp.207-229.

MIDDLETON G.V. (1963) *Statistical inference in geochemistry* In: Studies in analytical geochemistry (ed. D.M.Shaw), The Royal Society of Canada, special publication series, No 6, 140p.

MOOK W.G. (1980) Carbon-14 in hydrological studies. In *Handbook of Environmental Isotope Geochemistry* (eds P. Fritz and J.-Ch. Fontes) Vol. 1 , Elsevier, Amsterdam. pp.49-74.

MORRISON P. and PINE J. (1955) Radiogenic origin of the helium isotopes in rocks. *Annals of the New York Academy of Sciences*. **62**, 69-72.

MOSER H., WOLF M., FRITZ P., FONTES J.-Ch., FLORKOWSKI T. and PAYNE B.R.(1989) ^{18}O ^{2}H and ^{3}H measurements of the Stripa groundwaters. *Geochim. Cosmochim. Acta.* In Press.

MUKHOPADHYAY (1977) relationship between no of emitted neutrons and atomic mass review article

MUNNICH K.O. (1957) Messungen des ^{14}C Gehaltes von hartem Grundwasser. *Naturwiss*. **44**, 32-34.

MUENNICH F. (1958) Untersuchung der energietonung und des Wirkungsquerschnitts einiger durch thermische Neutronen ausgeloster (n, α)-Prozesse. *Zeitschrift fur Physik* **153**, 106-123.

MUGHABGHAB S.F., DIVADEENAM M. and HOLDEN N.E. (1981) *Neutron cross sections Vol. 1 :- Neutron resonance parameters and thermal cross sections.* National Nuclear Data Center Brookhaven National Laboratory, Upton, New York.

MYERS W.D. and SWIATECKI W.J. (1966). Nuclear masses and deformations. *Nuclear. Physics* . **81**, 1.

NAKASIMA. R. (1982). Neutron yields from bombardment of α-particles. *J.A.E.R.I-M.* **82-117**, 66p.

NCRP (1979) *Tritium Report* 62. National Council on Radiation Protection and Measurement, Washington D.C.

NELSON P., PAULSSON B., RACHIELE R. and ANDERSSON L. (1979) Preliminary report on geophysical and mechanical borehole measurements at Stripa. Lawrence Berkeley Laboratory Report. LBL-8280, California, 1979.

NISHIIZUMI K., ARNOLD J.R., ELMORE D., Ma X., NEWMAN D. and GOVE H.E. (1983). ^{36}Cl and ^{53}Mn in Antartic meteorites and ^{10}Be-^{36}Cl dating of Antartic ice. *Earth Planet. Sci. Letters.* **62**, 407-417.

NISHIIZUMI K., ELMORE D., Ma X.A. and ARNOLD J.R. (1984). ^{10}B and ^{36}Cl depth profiles in an Apollo 15 drill core. *Earth Planet. Sci. Letters* . **70**, 157.

NORDSTROM D.K., ANDREWS J.N., CARLSSON L., FONTES J.-Ch., FRITZ P., MOSER H. and OLSSON T., (1985) Hydrochemical investigations in boreholes: geochemical and isotope characterisation of the Stripa groundswaters. Stripa Report KBS Stockholm 1985.

NORDSTROM D.K. and OLSSON T. (1987) Fluid inclusions as a source o dissolved salts in dep granitic groundwaters. In *Saline Waters and Gases in Crystaline rocks* (eds. Fritz P. and Frape S.K.). *Geochemical Association of Canada Special Paper* **33**, 111-119.

NUCLEAR ENTERPRISES Ltd. (1969) Thermal neutron detector NE 422. Bulletin No. 250 (Nov. 1969).

NUCLEAR ENTERPRISES (1980) Scintillators for the physical sciences nuclear enterprises data book. Brochure No. 126 (1980).

O'BRIEN K., SANDMEIER H.A., HANSEN G.E. and CAMPBELL J.E. (1978) Cosmic ray induced neutron background sources and fluxes for geometries of air over water ground iron aluminium. *J. Geophys. Res.* **83**, 114-120.

OESCHGER H., GUGELMANN L.H., SCHOTTERER U., SIEGENFHALER U. and WIEST A. (1974). Ar dating of groundwater In: *Isotope Techniques in Groundwater Hydrology* . I.A.E.A., Vienna pp.179-189.

OESCHGER H. (1982). The contribution of radioactive and chemical dating to the understanding of the environmental system. In *Nuclear & Chemical Dating Techniques:- Interpreting the environmental record* (ed. L.A. Currie). ACS Symposium Series 176 pp.5-42.

PAL P. and BHATTACHARYYA D.P. (1985) Derivation of nuon range spectrum under rock from recent primary spectrum. *Can. J. Phys.* **63**, 1050.

PARKER R.L., (1967) Composition of the earth's crust. In *Data of Geochemistry* (Ed. M. Fleischer). U.S. Geol. Survey Professional Paper 440-D.

PAUL M. KAUFMAN A., MAGARITZ M., FINK D., HENNING W., KAIM R., KUTSCHERA W. MEIRAU O. (1986) A new ^{36}Cl hydrological model and ^{36}Cl systematics in the Jordan River/Dead Sea System. *Nature*. **321**, 511-515.

PHILLIPS F.M. SMITH G.I., BENTLEY H.W. ELMORE D., and GOVE H.E. (1983) ^{36}Cl dating of saline sediments: Preliminary results from Searles Lake California. *Science*. **222**, 925-927.

PHILLIPS F.M., GOFF. F., VUATAZ F., BENTLEY H.W., ELMORE D. and GOVE H.E. (1984) ^{36}Cl as a tracer in geothermal systems: examples from Valles Caldera New Mexico. *Geophys. Res. Lett.* **11**, 1227-1230.

PHILLIPS F.M., LEAVY B.D., JANNICK N.O., ELMORE D. and KUBIC P. (1986). The accumulation of cosmogenic Cl-36 in rocks: amethod for surface exposure dating. *Science*. **231**, 41-43.

PRICE W.J. (1964) *McGraw-Hill series in nuclear engineering :- nuclear radiation detection* second edition. McGraw-Hill Inc, New York. 430p.

PRICE P.B., STEVENSON J.D., BARWICK S.W. and RAUN H.L. (1985) Discovery of radioactive decay of ^{222}Ra and ^{224}Ra by ^{14}C emission. *Physical Review Lett* . **54**, 297-299.

PRICE P.B. and WALKER R.M. (1963) Fossil tracks of charged particles in mica and the age of minerals. *J. Geophys. Res.* **68**, 4847-4862.

PURSER K.H., RUSSO C.J., LIEBERT R.B., GOVE H.E., ELMORE D., FERRARO R., LITHERLAND A.E., BEUKENS R.P., CHANG H.K. KILIUS L.R. and LEE H.W. (1982) The application of electrostatic tandems to ulstrasensitive mass spectrometry and nuclear dating. *In Nuclear and Chemical dating Techniques:- Interpreting the Environmental Record* (Ed. L.A. Currie). ACS Symposium Series 176, pp.45-75.

QUENBY J.J. (1967) The time variations of the cosmic ray intensity In *Encyclopedia of physics* Vol. XLV1/2 Cosmic Rays (II) (ed S. Fugle) Springer-Verlag, Berlin.

RALPH E.K., (1971) Carbon-14 dating. In *Dating techniques for the archaeologist* (eds H.N. Michael and E.K.Ralph). M.I.T. Press, Cambridge Mass. pp1-48.

RAMA and HONDA M. (1961) Cosmic-ray-induced radioactivity in terrestrial materials. *Journal of Geophysical Res.* **66,** 3533-3539

REEDY R.C. and ARNOLD J.R. (1972). Interaction of solar and galactic cosmic ray particles with the moon. *Journal of Geophysical Res.* **77,** 537-555.

REGNIER S., BAKLOUTI M., SIMONOFF-LAGARDE M. and SIMONOFF G.N. (1977). Production of Cl-36 by high energy spallation. *Phys. Lett.* **68B,** 202-204.

REINES F. (1975) The early days of experimental neutrino physics. *Science*. **203,** 11-16.

ROBERTS J.H. (1947) Neutron yields for several light elements bombarded with polonium alpha particles. *Los Alamos Lab. Report* MDDDC-731. 1944.

ROMAN D., and AIREY P.L. (1981) The Application of environmental ^{36}Cl to hydrology - 1. Liquid scintillation counting. *Int. Journal of Applied Radiation and Isotopes.* **32,** 287-290.

RONZANI C. and TAMERS M.A. (1966) Low level ^{36}Cl detection with liquid scintillation techniques. *Radio Chimica Acta* . **6,** 206-210.

ROSE H.J. and JONES G.A. (1984) A new kind of natural radioactivity. *Nature.* **307,** 245-247.

ROSSI B. (1948) Cosmic ray phenomena. *Rev. Mod. Phys.* **20,** 537-583.

ROZANSKI K. and FLORKOWSKI T. (1979) Krypton-85 dating of groundwater In: *Isotope Hydrology 1978* , 949-961 I.A.E.A., Vienna 1979.

SATCHLER G.R. (1980) *An introduction to nuclear reactions.* MacMillian Press ltd, London. 190p.

SCHAEFFER D.A., THOMPSON S.O. and LARK N.L. (1960) Chlorine-36 Radioactivity in rain. *Journal of Geophysical Research* **65,** 4013-4016

SIMPSON J.A. (1951) Neutrons produced in the atmosphere by the cosmic radiations. *Phys. Rev.* **83,** 1175-1188.

SIMPSON J.A. and FAGOT W.C.(1953) Properties of the low energy nucleonic component at large atmospheric depths. *Phys. Rev.* **90**, 1068-1072.

SINGER P. (1974) Emission of particles following muon capture in intermediate and heavy nuclei. *Springer Tracts in Mod. Phys*. **71**, 39-87

STONE M. (1984) Textural evolution of lithium mica granites in the Cornubian batholith. *Proc. Geol. Ass.* **95**, 28-41.

SUBRAMANIAN. A., NARANAN. S., RAMANAMURPHY. P.V., SAHIAR. A.B. and SIDDHESHWAR LAL. (1958) Flux of slow u-mesons and protons near the geomagnetic equator. *Nuovo Cimento.* **7**, 110-113.

SUESS H.E. (1955). Radiocarbon concentration in modern wood. *Science*. **120**, 1-3.

SWINSON D.B. and KANANEU H. (1982) Reversal of the cosmic ray density gradient perpendicular to the ecliptic plane. *J. Geophys. Res.* **87**, 1685-1687

TAGAKI. J. and TANAKA. S. (1968) Calculation of the production rate of radioactivity by cosmic rays at sea level. I.N.S.J. Report 110, 24p.

TAMERS M.A., RONZANI C. and SCHARPENSEEL H.W. (1969) Naturally occuring chlorine-36. *Atompraxis.* **15**, 433-437.

TAMMEMAGI H.Y. and WHEILDON J (1974) Terrestrial heat flow and heat generation in south-west England. *Geophys. J.R. Astr. Soc.* **38**, 83-94.

TITTLE C.W. and CRAWFORD G.W. (1983) Measuring the thermal neutron absorption cross section of rocks. *The Log Analyst* May/June 1983, 12-15

TOMBS J.M.C. (1977) Concealed granites in Cornwall: Its shape from its gravitational effect. *Trans. Inst. Min. Met.* **86**, B93-B95

U.E.A.E.C., (1963) Reactor Physics Constants Argonne National Laboratory Report ANL-5800 850 U.S.A.E.C 1963

VON BUTTLAR H. and LIBBY W.F. (1955) Natural distribution of cosmic-ray-produced tritium. *J. Inorg. Nucl. Chem.* **1**, 75-91.

VON EGIDY T. and HARTMANN F.J. (1982) Average muonic coulomb capture probabilities for 65 elements. *Phys. Rev.* **A26**, 2355-2360.

WEISS W. and ROETHER W. (1975) Der Tritiumabfluss des Rheins 1961-1973. *Deutsche Gewaesserkundliche Mitteilungen.* **19**, 1-5.

WEST D. (1979) The calculation of neutron yields in mixtures and compounds from the thick target (α,n) yields in the separate constituents. *Journals of Nuclear Energy.* **6**, 549-552.

WEST D., and SHERWOOD A.C.(1982) Measurements of thick-target (α,n) yields from light elements. *Ann. nucl. Energy.* **9**, 551-577.

WILSON G.C. and LONG J.V.P. (1983) The distribution of lithium in some Cornish minerals: ion microprobe measurements. *Min. Mag.* **47**, 191-1990

WILLIAMSON. C.F., BOUJOT. J-P. and PICARD. J. (1966). C.E.A. Report 3042.

WOLF M., RAUERT W. and WEIGEL F. (1981) Low-level measurement of tritium by hyhdrogenation of propadiene and gas counting of propane. *Int. J. Appl. Rad. Isot.* **32**, 919-928.

WOLLENBERG H., FLEXER S., and ANDERSON L. (1980) Petrology and radiology of the Stripa pluton Lawrence Berkeley Laboratory Report LBL-11654 SAC-36 73 pp Berkeley California.

WYTTENBACH. A., BAERTSCHI P., BAJO S., HADERMANN J., JUNKER K., KATCOFF S., HERMES E.A. and PRUYS H.S. (1978). Probabilities of muon induced nuclear reactions involving charged particle emission. *Nuclear Physics.* **A294**, 278-292.

YAMASHITA M., STEPHENS L.D.,and WADE-PATTERSON H. (1966) Cosmic ray produced neutrons at ground level neutron production rate and flux distribution. *J. of Geophysical Research.* **71**, 3817-3834.

YOKOYAMA Y., REYSS J-L. and GUICHARD F. (1977). Production of radionuclides by cosmic rays at mountain altitudes. *Earth Planet. Sci. Lett.* **36**, 44-50.

ZIEGLER. J.F. (1980) *The stopping and ranges of ions in matter*. Pergamon Press, Oxford. 400p.

ZITO R., DONAHUE D.J., DAVIS S.N., BENTLEY H.W. and FRITZ P. (1980) Possible subsurface production of carbon-14. *Geophys. Res. Lett.* **7**, 235-238.

APPENDIX 1

The composition and physical properties of six average rock types as defined by PARKER (1967). Σ_m, P_{tot} and ϕ are calculated for each rock type as described in Sections 2 and 3.

Element	Granite	Basalt	Sandstone
H	-	-	-
He	-	-	-
Li	40	17	15
Be	5.5	1.0	0.1
B	15	5	35
C	300	-	-
N	20	20	10
O	487000	441000	535000
F	800	400	270
Ne	-	-	-
Na	27700	18000	3300
Mg	5600	46000	7000
Al	77000	78000	25000
Si	323000	230000	368000
P	700	1100	170
S	400	300	240
Cl	240	60	10
K	33400	8300	10700
Ca	1580	76000	39100
Sc	3	30	1
Ti	2300	13800	1500
V	40	250	20
Cr	25	170	35
Mn	600	1500	50
Fe	27000	86500	9800
Co	5	48	0.3
Ni	8	130	2.0
Cu	20	87	5
Zn	60	105	16
Ga	20	17	12
Ge	1.4	1.3	0.8
As	1.5	2.0	1.0
Se	0.05	0.05	0.05
Br	1.7	3.6	1.0
Kr	-	-	-
Rb	200	30	60
Sr	300	465	20
Y	34	21	40
Zr	200	140	220
Nb	20	19	0.05
Mo	1.0	1.5	0.2
Tc	-	-	-
Ru	-	-	-
Rh	-	-	-
Pd	0.1	0.2	-
Ag	0.05	0.11	0.05
Cd	0.1	0.22	0.05
In	0.26	0.22	0.05

cont'd

Element	Granite	Basalt	Sandstone
Sn	3.0	1.5	0.5
Sb	0.26	0.2	0.05
Te	0.001	-	-
I	0.4	0.5	1.7
Xe	-	-	-
Cs	0.5	1.5	0.5
Ba	830	330	50
La	60	15	30
Ce	100	48	92
Pr	12	4.6	8.8
Nd	46	20	37
Pm	-	-	-
Sm	9	5.3	10
Eu	1.5	0.8	1.6
Gd	9	5.3	10
Tb	2.5	0.8	1.6
Dy	6.7	3.8	7.2
Ho	2.0	1.1	2.0
Er	4.0	2.1	4.0
Tm	0.3	0.2	0.3
Yb	4.0	2.1	4.0
Lu	1.0	0.6	1.2
Hf	1.0	2.0	3.9
Ta	3.5	1.1	0.05
W	1.5	0.7	1.5
Re	0.00067	-	-
Os	-	-	-
Ir	0.0063	-	-
Pt	-	-	-
Au	0.0045	0.004	0.005
Hg	0.08	0.09	0.03
Tl	1.5	0.21	0.82
Pb	20	6.0	7.0
Bi	0.01	0.007	-
Po	-	-	-
At	-	-	-
Rn	-	-	-
Fr	-	-	-
Ra	-	-	-
Ac	-	-	-
Th	18	4	1.7
Pa	-	-	-
U	3.5	1	0.45
Density ($g\ cm^{-3}$)	2.62	2.82	2.24
P_{tot} ($g^{-1}a^{-1}$)	14.1+/-0.7	3.62+/-0.17	0.88+/-0.04
Σ_m (cm^2g^{-1})	.0068+/-.0003	.0073+/-.0003	.0060+/-.0003
ϕ $x10^{-5}$ ($cm^{-2}s^{-1}$)	6.6+/-0.4	1.6+/-0.1	0.46+/-0.03

Element	Ultramafic	Clays & Shales	Limestones
H	-	-	-
He	-	-	-
Li	0.5	60	5
Be	0.5	3.0	0.5
B	3.0	100	20
C	-	10000	120000
N	6	600	10
O	445000	528000	494000
F	100	500	330
Ne	-	-	-
Na	4200	6600	400
Mg	204000	13400	47000
Al	20000	104500	4200
Si	205000	238000	24000
P	220	700	400
S	300	3000	330
Cl	85	160	150
K	40	22800	2700
Ca	25000	25300	302300
Sc	15	10	1
Ti	300	4500	400
V	40	130	20
Cr	1600	100	11
Mn	1620	670	1100
Fe	94300	33300	3800
Co	150	20	0.1
Ni	2000	95	20.0
Cu	10	57	4
Zn	50	80	20
Ga	1.5	30	4
Ge	1.5	2.0	0.2
As	1	6.6	1.0
Se	0.05	0.6	0.08
Br	1	6.0	6.2
Kr	-	-	-
Rb	0.2	200	3
Sr	1	450	610
Y	0.5	30	30
Zr	45	200	19
Nb	16	20	0.3
Mo	0.3	2.0	0.4
Tc	-	-	-
Ru	-	-	-
Rh	-	-	-
Pd	0.12	-	-
Ag	0.06	0.1	0.05
Cd	0.5	0.3	0.035
In	0.01	0.05	0.05
Sn	0.5	10	0.5
Sb	0.1	2	0.2
Te	-	0.01	-
I	0.5	1.0	1.2
Xe	-	-	-
Cs	0.5	12	0.5
Ba	0.4	800	10
La	0.5	40	5.0

Cont'd

Element	Ultramafic	Clays & Shales	Limestones
Ce	0.5	50	11.5
Pr	0.5	5	1.1
Nd	0.5	23	4.7
Pm	-	-	-
Sm	0.5	6.5	1.3
Eu	0.5	1.0	0.2
Gd	0.5	6.5	1.3
Tb	0.5	0.9	0.2
Dy	0.5	4.5	0.9
Ho	0.5	1.1	0.3
Er	0.5	2.5	0.5
Tm	0.5	0.25	0.04
Yb	0.5	3.0	0.5
Lu	0.5	0.7	0.2
Hf	0.6	6.0	0.3
Ta	1.0	3.5	0.05
W	0.77	2.0	0.6
Re	-	-	-
Os	-	-	-
Ir	-	-	-
Pt	-	-	-
Au	0.006	0.001	0.005
Hg	0.05	0.4	0.04
Tl	0.06	1.0	0.05
Pb	1	20.	9.0
Bi	-	0.01	-
Po	-	-	-
At	-	-	-
Rn	-	-	-
Fr	-	-	-
Ra	-	-	-
Ac	-	-	-
Th	0.004	11	1.7
Pa	-	-	-
U	0.001	3.2	2.2
Density ($g\ cm^{-3}$)	2.97	1.90	2.21
P_{tot} ($g^{-1}a^{-1}$)	0.0045+/-0.0003	9.26+/-0.46	2.45+/-0.15
Σ_m (cm^2g^{-1})	.0047+/-.0003	.0097+/-.0005	.0045+/-.0002
ϕ $x10^{-5}$ ($cm^{-2}s^{-1}$)	0.003+/-0.0003	3.0+/-0.2	1.7+/-0.13

APPENDIX 2

A2.1 Descriptions of sites and rock samples used in the course of this thesis to measure neutron flux and calibrate the neutron absorptiometer.

Site:- Nottingham Castle NGR SK 569 396.
Neutron flux measured at the surface (FM1) and in a man made chamber 17 m below the surface, 0.5 m from the chamber wall (FM2), close to the chamber wall (FM3) and in the center of the chamber (FM4). The rock consisted of loosely cemented Bunter sandstone which had a density of 1.946 gcm^{-3} (CROOKES pers comm). The analysed sample (SA16) was collected from the wall of the chamber adjacent to measurement site.

Site:- Bath University NGR ST 774 643.
Surface neutron flux measurements were made on floor of wooden meterological hut (FM5). Near surface measurements were made at different depths in a pit of sand (at the surface (FM6), 0.50 m below the surface (FM7) and 1.2 m below the surface (FM8)). The sand was homogeneous "Bristol Grit" and had a bulk density of 1.6 gcm^{-3}. The thermal neutron absorption cross section and density of the sand were measured on a sample removed from the pit prior to neutron flux measurements.

Site:- Corsham stone mine NGR ST 885 676.
Neutron flux was measured in a mined chamber in a "Bath Stone" mine at Corsham near Bath. Measurements were made in a saw slot approximately 50 cm deep and 6 cm high (FM9) and in the center of the chamber (FM10). The chamber was 30m below the surface and overlying strata had an estimated density of 2.2 gcm^{-3}. The formation in which measurements were made consisted of homogeneous Oolitic limestone. A sample (SA15) was collected from a slot in which measurements were made.

Site:- Rosemanowes Quarry NGR SW 735 346.
Neutron flux measurements were made at the surface (FM11), in boreholes B (FM16) and C (FM12, FM13, FM14, FM15, FM17 and FM18) and at 50 m below the surface in a vertical borehole (FM19). Boreholes B and C were horizontal boreholes drilled into a vertical granite face 6 m from the top (See Fig A2.1).

The granite surrounding boreholes B and C is classed as Type 1 megacrystic granite and had a density of 2.62 gcm^{-3}. Samples of rock were collected from the nearby Penryn quarry (SA3) (which was said to be of a similar composition to the surface material) and from core material (SA4 and SA13).

Site:- South Crofty mine NGR SW 665 413.
Neutron flux measurements were made in two boreholes (FM20 and FM21), in the centre of the passage (FM22) and against the passage wall (FM23) (See Fig A2). The boreholes were freshly drilled for these measurements and were 7 cm in diameter and 4 m deep. The site was in Type 1 granite which appeared to be free from any alteration in the vicinity of measurement. The site formed part of the "3b School" 560m below the surface. Samples of granite (SA1) (approx 5 Kg) were collected from material mined to make the passage.

Site:- Pendarves mine NGR SW 647 382.
Neutron flux measurements were made in a borehole (FM24) and in the centre of a passage (FM25). The borehole was freshly drilled for these measurements and was 7 cm in diameter and 4m deep. The site was in Type 1 granite approximately 100m below the surface and approximately 50m from the Granite/killas contact. The granite surrounding the borehole appeared to be free from any alteration. Samples of granite (SA2) (approx 4Kg) were collected from material removed from the wall of the passage in the process of drilling the borehole.

Site:- Wookey Hole cave NGR ST 512 453.
Neutron flux measurements were made in a small chamber approximately 10m above the entrance level of the cave (FM26). The walls of the chamber were made of solid limestone and were sited approximately 50m below the surface.

Site:- Rosevale mine, Zennor. NGR SW 459 380.
Neutron flux measurements were made in a small chamber approximately 40m below surface (FM27). The walls of the chamber were made of solid granite.

A2.2 Geographic data for measurement sites.

Site	Latitude degrees	Longitude	Altitude m above M.S.L*	Geomagnetic Latitude m
Nottingham Castle	53.0 N	1.1 W	20	55.9
Bath University + Corsham stone mine	51.4 N	2.3 W	180	54.6
Cornwall Rosmanowes quarry South Crofty mine Pendarves mine	50.1 N	5.2 W	150	53.9
Stripa mine	59.7 N	15.1 E	85	64.9
Wookey Hole	51.2 N	2.6 W	100	54.5

* M.S.L = mean sea level.

A2.3 Physical data and correction factors for measurement sites.

Site	proton Latitude correction factor	proton Altitude correction factor	muon Altitude correction factor	muon Latitude correction factor
Nottingham Castle	0.97	1.00	1.00	1.00
Bath University Corsham stone mine	0.96	1.14	1.03	1.00
Cornwall	0.95	1.11	1.02	1.00
Stripa	1.00	1.06	1.00	1.00
Wookey Hole	0.95	1.07	1.01	1.00

Factors are relative to a site at a geomagnetic latitude > 40°N

and at sea level.

A2.4 Chemical analysis of samples collected from measurement sites.

A2.4.1 Samples collected from Cornwall (1)

Element	(SA1) South Crofty	(SA2) Pendarves	(SA3) Penryn	(SA4) Rosemanowes
Li	110.	136.	325.	463.+
B	140.	295.	89.	400.+
O	492000.	487000.	491000.	491000.+
Na	19510.	13650.	23070.	26100.+
Mg	2710.	2960.	2530.	1330.+
Al	75570.	78590.	79540.	81020.+
Si	348000.	337000.	342000.	344000.+
Cl	240.*	240.*	240.*	240.*
K	41700.	50600.	40800.	40900.+
Ca	6430.	4650.	7080.	6217.+
Ti	1370.	1560.	1500.	874.+
Cr	25.*	25.*	25.*	8.+
Mn	310.	542.	387.	310.+
Fe	12800.	23100.	12200.	7830.+
Co	21.	33.	21.	57.+
Ni	8.	10.	8.	8.+
Sm	9.8	6.7	5.5	6.2
Gd	6.1++	4.2++	3.4++	3.9++
Th	16.9	25.3	16.9	19.0
U	16.2	13.1	11.7	14.7
Σ_m x10^{-3} (cm^2g^{-1})	12+/-0.7	19+/-1.3	10+/-0.5	24+/-0.8
Σ_n (cm^2g^{-1})	0.122	0.122	0.122	0.122
P_{tot}($g^{-1}a^{-1}$)	30.5+/-1.4	28.8+/-1.3	25.3+/-1.1	31.8+/-1.4

(SA1) Sampled from South Crofty Mine (NGR:SW 665 413);
3b School 310-level (-560m).
(SA2) Sampled from Pendarves Mine (NGR:SW 647 382) (-100 m).
(SA3) Sampled from Penryn Quarry (NGR:SW 760 342).
(SA4) Sampled from Rosemanowes Geothermal Site (NGR:SW 735 346);
core sample from borehole RH11 (-1700m).

A2.4.2 Samples collected from Cornwall (2)

	(SA5) AM1	(SA6) AM13	(SA7) WJE	(SA8) J11
Li	163.	427.	127.	385.
B	294.	250.	201.	234.
O	490000.	486000.	508000.	488000.
Na	19510.	24500.	594.	23700.
Mg	2410.	3200.	1200.	3260.
Al	79100.	86700.	86200.	83300.
Si	344000.	337000.	364000.	335000.
Cl	240.*	240.*	240.*	240.*
K	46200.	44900.	23200.	43700.
Ca	4500.	7720.	3360.	7200.
Ti	1190.	1810.	500.	1700.
Cr	25.*	25.*	25.*	25.*
Mn	310.	387.	470.	387.
Fe	12700.	14600.	11960.	13428.
Co	25.	23.	35.	30.
Ni	13.	9.	4.	11.
Sm	8.3	5.9	2.9	6.3
Gd	5.2++	3.7++	1.8++	3.9++
Th	n.m	n.m	n.m	n.m
U	n.m	n.m	n.m	n.m
Σ_m x10^{-3} (cm^2g^{-1})	19+/-1.3	18+/-1.1	13+/-0.9	17+/-1.0
Σ_n (cm^2g^{-1})	0.122	0.122	0.122	0.122
P_{tot} ($g^{-1}a^{-1}$)	n.c	n.c	n.c	n.c

(SA5) Sampled from NGR:SW 657-367 surface quarry (Type 1 granite).

(SA6) Sampled from NGR:SW 730-311 surface quarry (Type 1 granite).

(SA7) Sampled from NGR:SW 775-426 Wheal Jane mine, -340 (ELVENS).

(SA8) Sampled from NGR:SW 775 426 Wheal Jane mine, -340 (ELVENS).

A2.4.3 Samples collected from Cornwall (3)

	(SA9) AM22	(SA10) AM30	(SA11) HF1	(SA12) HF2	(SA13) Rosemanowes
Li	157.	306.	169.	233.	450.
B	209.	260.	87.	82.	414.
O	489000.	485000.	501000.	475000.	595000.
Na	11800.	23100.	6600.*	6600.*	20100.
Mg	1630.	4050.	15400.	28160.	1090.
Al	84300.	84400.	95200.	74600.	50800.
Si	343000.	328000.	262000.	257000.	277000.
Cl	240.*	240.*	160.*	160.*	240.*
K	60000.	46400.	37300.	30000.	42300.
Ca	2500.	6860.	0.	18300.	5150.
Ti	690.	2310.	4380.	9240.	840.
Cr	25.*	25.*	125.	170.	29.
Mn	155.	387.	1040.	1230.	300.
Fe	9510.	19800.	76600.	98900.	6510.
Co	66.	34.	28.	40.	6.
Ni	6.	10.	86.	109.	6.
Sm	5.2	8.0	6.5*	6.5*	6.2*
Gd	3.3++	5.0++	6.5*	6.5*	3.9++
Th	n.m	n.m	5.5	5.0	17.1
U	n.m	n.m	4.9	4.4	15.6
Σ_m x10^{-3} (cm^2g^{-1})	15+/-0.9	18+/-1.1	11+/-0.4	12+/-0.7	24+/-0.7
Σ_n (cm^2g^{-1})	0.121	0.122	n.c	n.c	n.c
P_{tot} ($g^{-1}a^{-1}$)	n.c	n.c	9.3+/-0.4	8.2+/-0.4	28.5+/-1.3

(SA9) Sampled from NGR:SW 439-345 Lands End Quarry (finegrain).

(SA10) Sampled from NGR:SW 730-311 Surface Quarry (porphorytic).

(SA11) Sampled Treago Farm NGR:SW 782-602 Killas borehole -151m.

(SA12) Sampled Gwinear NGR:SW 804-575 Killas borehole -297m.

(SA13) Sampled from Rosemanowes Quarry borehole RH11 1689m.

A2.4.4 Samples collected from miscellaneous sites (1)

Element	(SA14) Stripa Granite	(SA15) Oolitic Limestone	(SA16) Bunter Sandstone	(SA17) Bunter Sandstone
Li	9.0	6.0	27.	14.
B	8.+	47.	37.	50.
O	491000.	515000.	509000.	488000.
Na	28340.	148.	1560.	9200.
Mg	1270.	2710.	5200.	4703.
Al	74250.	1270.	41650.	52700.
Si	349000.	1000.	399000.	358000.
Cl	240.*	150.*	10.*	10.*
K	38800.	332.	30200.	54900.
Ca	6220.	366000.	5360.	14500.
Ti	437.	250.	1120.	2120.
Cr	25.*	11.*	35.*	35.*
Mn	310.	310.	230.	310.
Fe	10200.	4200.	7400.	15400.
Co	15.	0.	36.	18.
Ni	3.	0.	12.	13.
Sm	9.8	1.3	3.9	4.5
Gd	9.8**	1.3**	3.9**	4.5**
Th	33.0	0.50***	4.60	14.0
U	44.1	1.23***	1.31	3.6
Σ_m x10^{-3} (cm^2g^{-1})	6.0+/-0.3	5.0+/-0.2	5.5+/-0.3	7.2+/-0.6
Σ_n (cm^2g^{-1})	0.123	0.125	0.123	0.121
P_{tot} ($g^{-1}a^{-1}$)	82+/-3.9	0.87+/-0.04	2.7+/-0.13	9.0+/-0.4

(SA14) Sampled from V2-borehole, Stripa granite.
(SA15) Sampled from Corsham Stone mine, NGR:ST 885 676, -30m.
(SA16) Sampled Nottingham castle chamber NGR:SK 569 396, -20m.
(SA17) Sampled Winterbourne Kingston borehole NGR:SY 847 980.

A2.4.5 Samples collected from miscellaneous sites (2)

Element	(SA18) Triassic Sandstone	(SA19) Triassic Sandstone	(SA20) Old Red Sandstone	(SA21) Basaltic Tuff
Li	32.	23.	40.	25.
B	79.	16.+	42.	94.
O	511000.	519000.	465000.	480000.
Na	3640.	1410.	1340.	6970.
Mg	4820.	4220.	29300.	49000.
Al	33400.	17500.	82000.	57400.
Si	405000.	430500.	283000.	308000.
Cl	10.*	10.*	10.*	50.*
K	16700.	12300.	52900.	11200.
Ca	1860.	4500.	25400.	28400.
Ti	2190.	562.	4250.	6200.
Cr	35.*	35.*	35.*	200.*
Mn	155.	232.	697.	1000.
Fe	21300.	9500.	56600.	52500.
Co	26.	15.	20.	33.
Ni	25.	12.	50.	293.
Sm	4.1	1.7	6.0	5.9
Gd	4.1**	1.7**	6.0**	5.0**
Th	n.m	n.m	10.2	7.4
U	n.m	n.m	2.7	1.5
Σ_m x10^{-3} (cm^2g^{-1})	7.3+/-0.4	3.6+/-0.9	8.5+/-0.3	9.3+/-0.4
Σ_n (cm^2g^{-1})	0.125	0.126	0.123	0.127
P_{tot} ($g^{-1}a^{-1}$)	n.c	n.c	7.7+/-0.4	5.2+/-0.3

(SA18) Sampled from Southampton borehole NGR:SU 442 112.
(SA19) Sampled from Kempsey borehole -920m NGR:SO 861 493.
(SA20) Sampled from Burrington Combe addit NGR:SW 475 583.
(SA21) Sampled from surface at Kaphenstein.

A2.4.6 Samples collected from miscellaneous sites (3)

Element	(SA22) Trachy Andesite	(SA23) Basalt
Li	10.	13.
B	22.+	5.+
O	511000.	354000.
Na	17700.	32100.
Mg	2500.	49600.
Al	66500.	77800.
Si	341000.	243000.
Cl	100.*	50.*
K	30300.	20000.
Ca	17900.	70300.
Ti	4180.	13239.
Cr	50.*	200.*
Mn	697.	1162.
Fe	30100.	67400.
Co	18.	38.
Ni	17.	142.
Sm	4.6	8.3
Gd	n.m	n.m
Th	n.m	n.m
U	n.m	n.m
Σ_m x10^{-3} (cm^2g^{-1})	6.0+/-0.4	7.2+/-0.4
Σ_n (cm^2g^{-1})	0.127	0.128
P_{tot} ($g^{-1}a^{-1}$)	18+/-0.8	12+/-0.6

(SA22) Sampled from surface at Gleichenberg Austria.
(SA23) Sampled from surface at Kloch Austria.

KEY TO A2.4.N

* Estimated analysis based on PARKER (1967).
** Estimated analysis based on Sm:Gd ratio = 1.
*** Analysis by alpha spectrometry.
\+ Analysis by DC arc emission.
++ Estimated from Sm:Gd ratio = 1.6 (JEFFERIES., 1985).
n.m Value not measured.
n.c Value not calculated.
Unless otherwise stated major element analysis by inductively coupled plasma atomic emission spectroscopy (ICPAES) and U and Th analysis by gamma spectroscopy (200g sample).

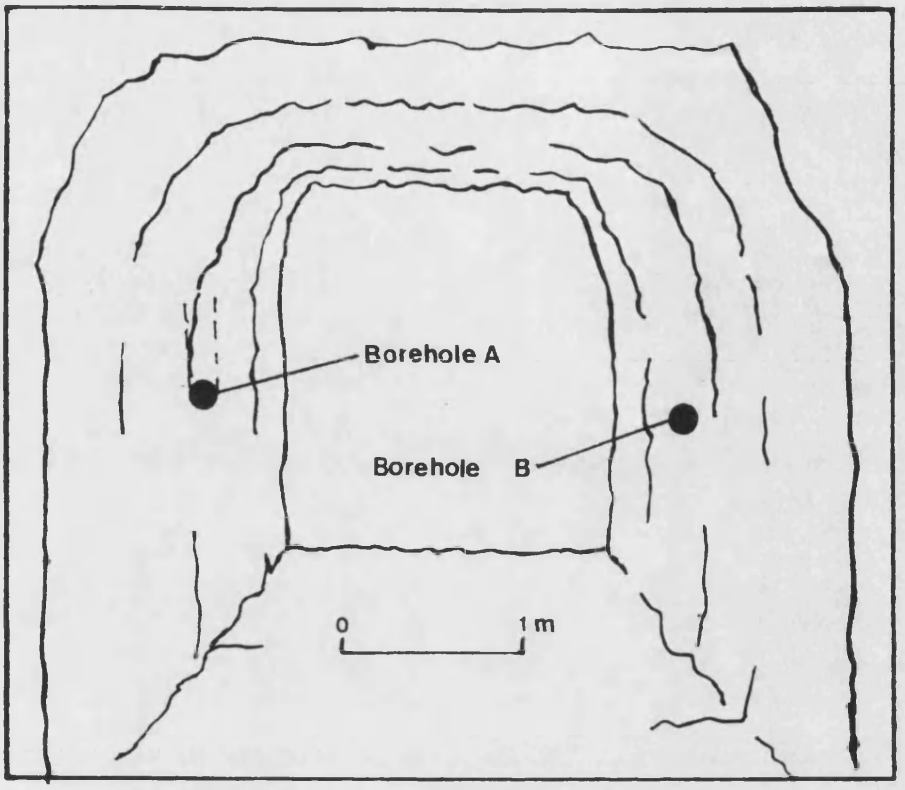

Fig A2.1 Diagrammatic representation of the chamber used in South Crofty mine for neutron flux measurements.

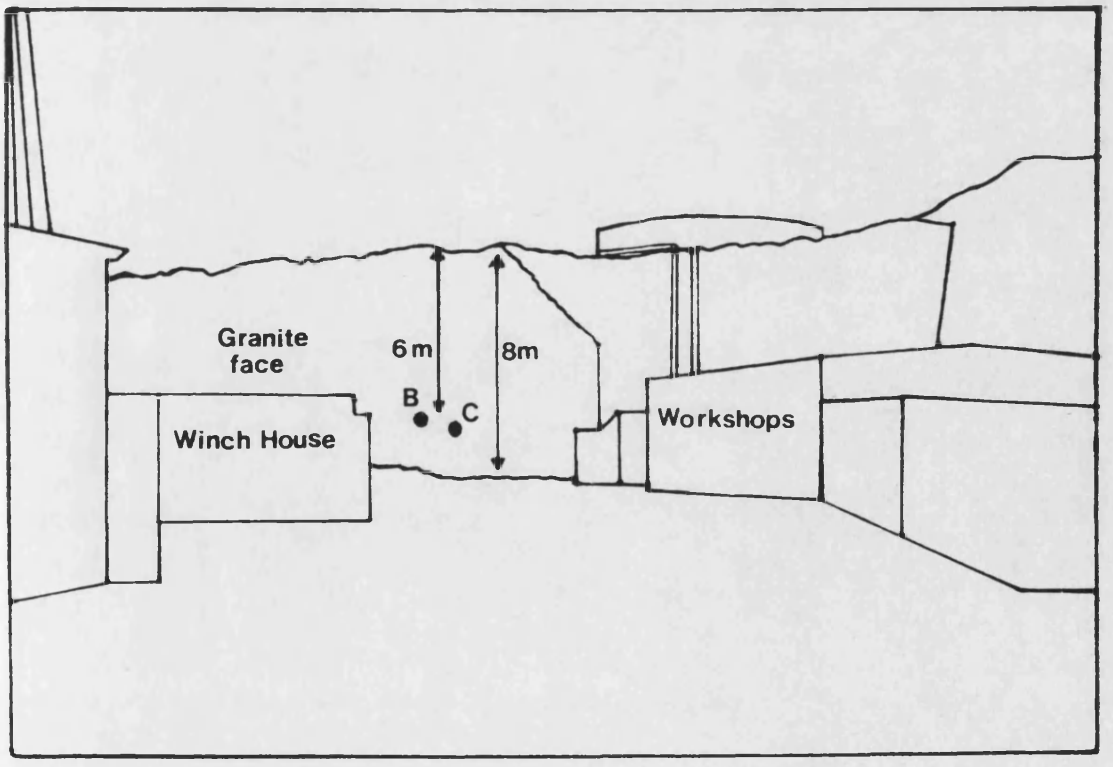

Fig A2.2 Diagram showing locations of boreholes used for neutron flux measurements at the Rosemanowes geothermal site.

APPENDIX 3.LABORATORY MEASUREMENT OF ABSORPTION CROSS-SECTION.

As discussed in the section 3 the thermal neutron mass absorption cross-section (Σ_m (cm^2 g^{-1})) for geological material depends strongly on the concentration of boron and lanthanides in the medium. The analysis of rock samples for these and the other elements which contribute to Σ_m is both time consuming and technically difficult. In view of this a method by which Σ_m could be directly determined on geological samples would greatly increase the ease by which the variability of this parameter in geological formations could be investigated.

As well as being used in in-situ production calculations, Σ_m is also an important parameter in the interpretation of many neutron logs based on the detection of artificially induced thermal neutron flux in boreholes (CZUBEK et al., 1981) and in soil moisture measurements (MAJERCZYK and ZUBER., 1966). It has principally been interest in these fields that has prompted a number of authors (ANTONOV et al., 1966, CZUBEK et al., 1981 and 1983, KREFT et al., 1983 and TITTLE and CRAWFORD., 1983) to develop methods of experimentally measuring Σ_m.

The experimental determination of the absorption cross-section is complicated by neutron scattering effects which are at least an order of magnitude greater than any absorption effects. Early methods required relatively large samples and/or the use of expensive equipment to overcome this, for instance the method of CZUBEK et al (1981) requires 1 to 2 kg of rock material and a pulsed neutron source. The more recent methods of TITTLE and CRAWFORD (1983) and KREFT et al (1983) use a simpler approach. The main disadvantage with the method of TITTLE and CRAWFORD (1983) is that the sample (500 g) preparation and standardisation procedures are cumbersome, especially for rock matrices of low porosity such as granites (which as discussed previously are of special interest in the study of in-situ production due to their high neutron production rate). The method described by KREFT et al (1983) would appear to be suitable for many different rock types and gives precise (+/- 10% (1σ)) and accurate results provided that samples of 1.5 to 2 kg are available. However it was not published until after equipment had been purchased and initial development had been carried out on the method described in Sections A3.1 to A3.3.

The performance of the method described below was tested by comparing experimentally determined Σ_m values with those:-
(1) Calculated from a full chemical analysis of the respective samples (Appendix 2).
(2) Determined by other authors during the course of an International Atomic Energy

A3.1 Experimental

Work was carried out between 1984 and 1986 to enable the measurement of Σ_m on small rock samples.

A3.1.1 Experimental apparatus.

The physical dimensions of the "Absorptometer" are shown to scale in Fig. A3.1. It was constructed using 2.7 cm thick polyethylene sheets which had been machined to the correct dimensions. The cylindrical sample cell was constructed out of thin sheet metal and had an outside diameter of 11.0 cm, and height of 7 cm. This gave the cell an internal volume of 665.0 cm^3 which enabled it to hold approximately 1 kg of ground rock at a density of 1.55 gcm^{-3}. The sample cell was incorporated into a draw in the polyethylene to enable the sample to be changed. A number of 1 cm diameter holes extending into the centre of the moderator material below the sample cell were drilled to allow the placement of a ^{252}Cf neutron source. This source consisted of 0.5 μg of ^{252}Cf encapsulated in a stainless steel pellet mounted at the end of a 0.5 m steel rod. An NE222 neutron detector and photomultiplier tube were mounted above the sample cell to enable measurement of the neutrons transmitted by the sample. It was found necessary to place a neutron absorbing "mask" along a plane level with the bottom of the sample container to reduce the number of scattered neutrons entering the detector without passing through the sample. This "mask" was made out of 1 mm thick Cd and had a 10 cm diameter hole cut in the middle to allow thermal neutrons to pass from the source and into the sample.

A schematic diagram of the experimental apparatus is shown in Fig. A3.2, encompassing three distinct units which are described below.

A3.1.1.1 The neutron source. As stated above the neutron source is ^{252}Cf which decays by alpha particle emission and spontaneous fission, with an effective half-life of 2.646 years. In ^{252}Cf spontaneous fission decay has a probability of 3.1% and emits 3.76 neutrons per fission. Thus the 0.5 μg source has a neutron emission rate of 1.16×10^{6} s^{-1}. Gamma rays are also emitted and their emission rate is quoted by CHOPPIN and RYDBERG (1980) to be 1.3×10^{13} photons $g^{-1}s^{-1}$. These gamma rays have a broad energy spectrum since they are due to both fission products and prompt emission. An energy spectrum of neutrons emitted from ^{252}Cf is shown in Fig. A3.3.

The neutrons emitted from the above source have an average energy of 2.35 Mev and must be slowed down to thermal energies before measurements of Σ_m may be made. This is accomplished by the use of a polyethylene moderator (Density 0.9 g cm^{-3}). The overall dimensions of the moderator that are required for thermalisation to take place may be estimated using Neutron Diffusion Theory (FRISCH., 1958). This facilitates the calculation of the average distance (Slowing Down Length (L_s)) that an emitted neutron travels before reaching thermal energies in a given medium. FRISCH (1958) has calculated this distance to be approximately 5cm in polyethylene. Thus in the absorptometer described above neutrons at least 5 cm from the source will be at or near thermal energies. The position of the source relative to the detector was selected to give good moderation whilst maintaining an adequate count rate due to neutrons.

A3.1.1.2 The sample. Samples consisted either of crushed rock or in some cases aqueous solutions containing boron. A standard sample size of 800g was selected in order to maximise absorption, whilst not overfilling the sample cell. Initially the samples consisted of crushed material (particle size less than 2mm). However in the case of samples to which standard additions were made the particle size was reduced to that of the standard additive to ensure even mixing. It was also decided to reduce the particle size of the measured samples to that of the standard to avoid any effects due to different particle size distributions, to enable representative sampling of the crushed material and to make drying the material easier. A large agate mortar mill was used to grind the crushed samples.

After grinding samples were dried at 105°C, which facilitated better replicate measurements, and comparison with the analysed standards was made easier as these were analysed on a dry weight basis.

A3.1.1.3 The neutron detector assembly. The neutron detector was a Nuclear Enterprises NE422 Thermal Neutron Detector which utilises the reaction of thermal neutrons with ^{6}Li. Neutrons react with ^{6}Li according to the reaction scheme shown in Fig. A3.4. This reaction has a thermal neutron cross-section of 910×10^{-24} cm^2. The produced triton and α particle are stopped in a ZnS(Ag) scintillator and the resulting light pulses are amplified and counted using a single channel analyser. The detector efficiency is energy dependent due to the variation in the $^{6}Li(n,\alpha)$ reaction cross-section. NUCLEAR ENTERPRISES (1980) quote an efficiency of 30% at 0.1 Mev and 60% at 0.01 Mev. The ZnS scintillator is also sensitive to γ rays, although Nuclear Enterprises (1980) quote that the detector can discriminate against γ rays in γ fluxes of 1×10^{7} photons s^{-1}. The ^{252}Cf source produces a γ flux of 6.5×10^{6} photons s^{-1} so discrimination between neutron and γ events should be possible.

The photomultiplier tube was connected to the following standard Canberra BIN units:-

Canberra ---- Preamplifier Discriminator (PAD) fitted with 47 k load resistor.

Canberra ---- Dual channel counter fitted with a "daisy chain" interface.

Canberra ---- Data logger/printer fitted with a "daisy chain" interface.

Canberra ---- High voltage power supply.

Instrumental settings used with the above apparatus were optimised and then adopted as standard operating conditions. The conditions given in Table A3.1 were used to collect all the experimental data given in this section. The setting of the low level discriminator was carried out using a Tracor TN1705 multichannel analyser and a ^{60}Co γ source. Pulse height spectra were obtained by connecting the input of the Tracor to the Amplifier OUT connection on the PAD. The pulse height spectra obtained are shown in Figs A3.5a, b and c.

Fig A3.5a shows the spectra obtained with the ^{252}Cf neutron source in position. Two peaks are identifiable (A and B) both are quite broad due to the poor energy resolution of the ZnS(Ag) scintillator. Fig A3.5b shows the spectra obtained when a ^{60}Co (γ) source is placed in the moderator instead of ^{252}Cf. This source emitted about $3x10^7$ photons s^{-1} and it may be seen that this produces a peak which occurs at a similar amplitude to peak A in Fig A3.5a. This is consistent with the assumption that peak A is due to γ rays from ^{252}Cf and indicates that the low level discriminator should be set to 0.150 V to eliminate pulses due to gamma rays. Fig A3.5c shows the spectra obtained with no source in position. From this it is evident that neither peak A or B in Fig A3.5a or Fig A3.5b is due to electronic noise, which is only present at very low amplitudes.

Once the low level discriminator had been set the variation in count rate with high voltage (Fig A3.6) was investigated. This investigation indicated that 1200 V was the optimum high voltage setting, maintaining stable amplification without sacrificing the lifetime of the photomultiplier tube.

A3.1.2 Theory of method.

The thermal neutron mass absorption cross-section (Σ_m) for a given material is defined as the sum of the elemental absorption cross-sections (σ_a cm^2) weighted by the atomic abundance of each element present. The elemental neutron absorption cross-section (σ_a) may be defined as:-

$$\sigma_a = \sigma_T + \sigma_n \qquad \text{Eqn. A3.1}$$

where σ_T (cm^2), is the total transport cross-section and σ_n (cm^2) is the total elastic and inelastic scattering cross-section of an element. In the described method the reduction in the number of neutrons passing through a sample due to absorption is used to experimentally evaluate Σ_m.

The attenuation of a neutron beam in a target material is an example of a random process which is analogous to the radioactive decay of nuclei. Thus the probability P(x) that a neutron will interact in a small distance X is :-

$$P(x) = \frac{x}{\lambda} \qquad \text{Eqn.A3.2}$$

where λ (cm) is the mean free path for neutron interaction in the target material and λ is related to σ_T by :-

$$\lambda = \frac{1}{N\ \sigma_T} \qquad \text{Eqn.A3.3}$$

where N is the number of atoms cm^{-3} in the material. In a similar way to radioactive decay the probability that a neutron will traverse the target material is given by :-

$$e^{\frac{-x}{\lambda}} = e^{-\sigma_T NX} \qquad \text{Eqn A3.4}$$

Provided that the neutrons all have a similar velocity and are essentially collimated then equation A3.4 becomes.

$$I = I_0\ e^{-\sigma_T NX} \qquad \text{Eqn. A3.5}$$

On taking logarithms :-

$$\ln \frac{I}{I_0} = -\sigma_T NX \qquad \text{Eqn. A3.6}$$

where I_O is the initial intensity of the neutron source prior to entering the sample, I is the intensity of the neutrons emerging from the sample, and X is the thickness of the sample in cm. For a multi-isotope element or multielement compound equation A3.6 becomes:-

$$\ln \frac{I}{I_0} = -\Sigma_T\ o\ X \qquad \text{Eqn. A3.7}$$

where o (gcm^{-3}) is the density of the sample and Σ_T ($cm^2\ g^{-1}$)

is the total transport cross-section of the sample material which is equal to:-

$$\Sigma_T = \Sigma_m + \Sigma_n \qquad \text{Eqn. A3.8}$$

Equation A3.7 may be further modified to relate ln I/I_o to the weight of sample (W (g)) placed in a sample cell of constant cross-sectional area (C_s cm^2) :-

$$\ln \frac{I}{I_0} = -\Sigma_T W C_s \qquad \text{Eqn A3.9}$$

From equations A3.8 and A3.9 it may be seen that Σ_m may be found by measuring I, I_o and W provided that either Σ_n is known or is $<< \Sigma_m$. Unfortunately rock matrices contain large amounts of oxygen which has a very high scattering cross-section (σ_n), which coupled with the low value of Σ_m of many rock matrices means that the above requirements are not generally fulfilled.

The method described attempts to overcome these shortcomings by assuming that differences in Σ_n between similar rock matrices are small and assuming a standard geometry for the sample/neutron source/detector arrangement. The validity of this assumption may be tested by calculating Σ_n in a similar way to Σ_m which is described in Section 3. In the case of Σ_n, σ_n rather than σ_a was summed and weighted according to the atomic abundance of each element. This summation process was carried out on all elements that have either appreciable Σ_n or were very abundant in the matrix under study. The most important elements, accounting for generally > 90% of Σ_n were H, O and Si in silicates and H, O and Ca in carbonates, H being present as bound or intergranular water (taken to be 1% on average) since the samples were dried prior to analysis. Iron, Mg and Ni may also be important for matrices which contain large amounts of these elements. The results of these calculations for a number of both theoretical, and analysed rock matrices are given in Table A3.2. From this table it may be seen that overall Σ_n ranges by 0.040 cm^2g^{-1} from 0.107 cm^2g^{-1} for an average analysis of Stripa granite to 0.150 cm^2g^{-1} for MCS3 which is an ultramafic sand high in Mg. If MCS3 is ignored due to its unusually high Mg concentration Σ_n varies by 0.010

cm^2g^{-1} between different silicate matrices. This represents an 8% variation which is much smaller than the variation in Σ_m which is over an order of magnitude. The variation in Σ_n is even smaller between samples of a similar formation. For instance the variation in Σ_n between the nine Cornish granite samples given in Table A3.2 is less than 0.001 cm^2g^{-1}. This suggests that even if an absolute determination based on a selected standard matrix cannot be made, relative values of Σ_m measured to determine its variation within a given formation should be reliable. It is thus possible to measure differences in Σ_m between samples of a similar matrix to a selected standard by a method that maintains a standard sample/neutron source/detector geometry.

A3.2 Method development.

The method of measuring Σ_m was developed at intervals over a two year period. Initially the precision with which I and I_o could be measured was investigated, which is particularly important since a logarithmic relationship was to be used between the measured property and Σ_m. Then variation in $\ln I/I_o$ with sample weight was investigated to qualify the prediction of equation 4.9. This lead to the development of the proposed experimental method of determining Σ_m, which was tested using a wide range of analysed materials including a number of intercomparison samples supplied by the I.A.E.A. As a result of these initial measurements the precision by which I and I_o could be measured was further investigated, which resulted in a reappraisal of the overall precision of the method, and a number of suggested improvements.

A3.2.1 Uncertainties in the measurement of Σ_m.

A3.2.1.1 The effect of measurement procedures on the precision of incident and transmitted intensity. The precision by which the transmitted (I) and incident (I_o) intensities may be measured is dependent on errors associated with two major factors. These are :-

(1) The randomness of nuclear decay processes that produce, transport, and detect the emitted neutrons.

(2) Fluctuations and variations in the physical properties of the sampling system and electronics.

The effect of these factors on the measurement of I and I_o is discussed below using the coefficient of variation (S) which is defined as :-

$$S = \frac{\text{standard deviation of } x}{x} \times 100\ \%$$

Errors caused by factor (1) are generally termed "counting errors" and in the case of the described method are small as the standard counting time (1600 s) gave at least 100,000 counts for all the measured samples. If standard counting errors are assumed this gives a theoretical coefficient of variation (S) in I or I_o of < 0.31%. An assumption that the precision of I or I_o measurements was due only to factor (1) errors was tested by calculating x (the mean number of counts) and S for 140 discrete I_o measurements (which were not sensitive to packing errors) made over a weekend. These gave a value for S of 1.35% which is approximately four times the theoretical variation (of 0.31%). The system parameters were re-calibrated and the values for x and S were recalculated on a further set of measurements made during the working week. The results of this second trial confirmed the above statistics giving S = 1.32%. The conclusion from these measurements was that the observed uncertainty in I_o could not be accounted for by factor (1) errors, and errors which limit the observed precision must be due to factor (2).

The time dependence of I_o was investigated by plotting the time at which a measurement was taken against the total number of counts measured during the counting period. Results for weekend and weekday measurements are shown in Figs A3.7 and A3.8 respectively. Both of these figures show that the magnitude of I_o varies sinusoidally with a wavelength of about 24 hours. The amplitude of this variation (Approximately 5% of the overall mean I_o value) was much larger than could be accounted for by factor (1) errors. Daily fluctuations in the laboratory temperature, which may effect the gain of the photomultiplier tube and associated electronics, was the most likely factor (2) error, and was the first to be investigated. Fig A3.9 shows a plot of temperature (measured with a thermocouple) adjacent to the photomultiplier tube against time and a plot of I_o measurements against time made on the same day.

The correlation between temperature and I_o measurement is good and indicates that temperature variations are the probable cause of the daily variation in I_o measurements.

The effect of temperature was further investigated by heating the photomultiplier tube over a known temperature range and making I_o measurements whilst the tube was held at a specific temperature. The dependence of I_o with respect to temperature is shown in Fig A3.10. This relationship is almost linear near room temperatures and shows that I_o decreases by about 1% for a temperature rise of one degree centigrade. A variation of this magnitude can account for the observed variations in I_o. However, according to Fig. A3.9 the count-rate decreases with rising temperature which suggests that changes in the temperature of the counting electronics rather than the photomultiplier tube are responsible for this effect. The precision of I_o and I determinations are therefore unlikly to be improved by thermostatically controlling the temperature of the photomultiplier tube. However, the use of a detection system (such as a BF_3 proportional counter) that gives better discrimination against gamma radiation and has a lower temperature dependence may reduce the observed variation.

Variation in I_o over shorter periods (1-2 hours) is much smaller than the the long term variation (about .27%) therefore any variation in I/I_o due to counting errors may be minimised by taking I_o values either immediately before or after measurements of I.

To summarise, two measurement techniques may be envisaged by which I/I_o is estimated :-

(1) An average value of I_o is found by taking I_o measurements over a number of days, and using this value, I/I_o is calculated from averaged I values taken over a smaller time period. This method produces the greatest uncertainty in I/I_o due to the large variation in I_o caused by the effects discussed above. This is referred to as the Case A method.

(2) The value of I_o is determined by a single measurement directly before a measurement of I is made. This procedure may be repeated if time permits with repacking of the sample and an average value of I/I_o taken. This method produces a much smaller uncertainty in I/I_o than that described in case A since the measurements are made over a much smaller temperature range.

This method is referred to as the Case B method, and the major cause of uncertainty is due to packing effects in the sample cell, which are discussed in greater detail below.

A3.2.1.2 The effect of packing density on transmitted intensity. Errors which effect the precision of transmitted neutron intensity (I) were expected to be predominantly caused by the packing of the sample into the sample cell. These were investigated by repeatedly measuring I for the same sample after repacking. The results for a sample of granite from Penryn quarry are shown in Table A3.3. From these a coefficient of variation for I (S_I) of 0.62% was obtained. This is greater than the coefficient expected from purely counting statistics (S_I < 0.31%). As discussed in section 4.2.1.1 this may be due to drift in the counting system over the period in which the samples were counted rather than being due to sample packing.

The variation in I with repacking was investigated further using the Case B method described above to determine the uncertainty associated purely with sample packing. This was carried out by measuring I/I_o (I measured directly after I_o) after repacking the sample. A second experiment was carried out to investigate the effects of :-

(1) packing the same sample into the cell using a large range of packing densities.

(2) different geometries between the detector and sample.

These two effects were investigated in one experiment by compressing the sample between measurements of I with a piston. The results from these experiments are shown in Tables A3.4 and A3.5.

Table A3.4 shows that the coefficient of variation in I/I_o ($S_{I/Io}$) = 0.97% for repeated measurements by the Case B method of the Penryn quarry sample with repacking. This is consistent with the uncertainty predicted by error propagation analysis. The value of $S_{I/Io}$ determined from the experimental results (0.97%) lying in between the values for Case B method $S_{I/Io}$ = 0.68% (S_I = 0.62% (packing errors) and S_{Io} = 0.27% (counting statistics)) in which measurements are made directly after each other and the Case A method $S_{I/Io}$=1.5% (S_I=0.62% (packing errors) and S_{Io}=1.35% (counting statistics and uncertainties due to temperature drift)) in which an average I_o value is used to calculate I/I_o from I values obtained on

different days. From this data and that of section 4.2.1.1 it may be concluded that where measurements of I and I_o are made directly after each other, provided that the number of counts amassed in a standard counting period (1600 s) is between 100,000 and 200,000 counts that the uncertainty in I/I_o is < 1%.

The results of Table A3.5 were obtained by placing a constant weight (800 g) of sample into the sample cell and compressing it to different densities using a Perspex piston. Densities (o) were calculated according to equation A3.10

$$o = \frac{800}{V-(dxC_s)} \qquad \text{Eqn. A3.10}$$

where C_s is the cross sectional area of the sample cell (95 cm^2), d is the distance of the sample surface from the top of the cell (cm) and V is the total internal volume of sample cell (646 cm^3). The results in Table A3.5 are plotted in Fig A3.11 with error bars drawn to represent the uncertainties discussed in the above section ($S_{I/Io}$ = 1%) and show that there is no significant difference in I/I_o obtained over the density range 1.4 to 1.8 gcm^{-3}. Similarly there must also be no significant effect due to differences in the detector/sample surface geometry. This is a great improvement on a number of the existing methods for the determination of Σ_m (KREFT et al., 1984 and TITTLE and CRAWFORD., 1983) which are very dependent on sample volume and detector geometry and hence simplifies sample preparation.

A3.2.1.3 Summary of measurement errors. Evaluation of equation A3.9 requires the measurement of Y where :-

$$Y = \ln \frac{I}{I_0} \qquad \text{Eqn. A3.11}$$

The associated uncertainty (standard deviation) in this measured parameter (σ_Y) is dependent upon the various errors discussed in sections 4.2.1.1, 4.2.1.2 and on the error propagated during the evaluation of the natural logarithm. According to error propagation analysis the error propagated

(σ_X) when taking a natural logarithm of a ratio X is equal to:-

$$\sigma_{lnX} = \frac{\sigma_X}{X} \qquad \text{Eqn. A3.12}$$

Thus σ_Y may be calculated from equation A3.13

$$\sigma_Y = \left(\left(\frac{\sigma_I}{I}\right)^2 + \left(\frac{\sigma_{I0}}{I_0}\right)^2 \right)^{0.5} \qquad \text{Eqn. A3.13}$$

This may be rewritten in terms of the coefficient of variability ($S_{I/Io}$) discussed in the previous sections as:-

$$\sigma_Y = \frac{S_{I/Io}}{100} \qquad \text{Eqn. A3.14}$$

Since $S_{I/Io}$ is taken to be constant at 1% the corresponding value of σ_Y is also constant at 0.01.

A3.2.2 The variation in neutron absorption with sample weight.

Equation 4.9 stated that :-

$$Y = - \Sigma_T \, W \, C_S \qquad \text{Eqn. A3.15}$$

Where Y is ln I/I_O, Σ_T is the is the total transport cross-section of the sample (cm^2g^{-1}), W is the weight of the sample (g) and C_s is the cross sectional area of the sample cell (cm^2). This relationship was investigated experimentally to determine if predicted theory was correct before attempting to develop calibration procedures. The relationship was investigated by placing varying weights of different absorbers in the sample cell and determining Y from I and I_O measurements. When Y was then plotted against sample weight (W), a straight line was obtained indicating that the relationship was obeyed. The results of experiments carried out using acid-washed silica sand, distilled water, granite from Penryn quarry, and acid-washed sand to which boron had

been added are shown in Fig A3.12. All of the experiments show a good linear correlation as predicted by equation A3.15, even though the mass of each material occupies a different volume of the sample cell and hence slightly alters the sample geometry. The slopes of the lines reflect Σ_T for each of the absorbers since C_s is constant. The magnitude of the slopes were in agreement with theory which predicted that:-

$$\Sigma_T\ H_2O > \Sigma_T\ SiO_2{+}B > \Sigma_T\ \text{Penryn granite} > \Sigma_T\ SiO_2$$

A3.3 Standardisation.

The above results show that Σ_T for a given matrix may be found by measuring Y for a known weight of material. The problem is how to separate Σ_T into its two components, the total scattering cross-section (Σ_n) and macroscopic absorption cross-section (Σ_m). The approach used in this method is described below.

It must first be assumed that Σ_n is constant for a particular matrix type ie/a silicate, limestone, ultramafic as is shown in Section 4.1. A suitable standard matrix may then be used to calibrate the system and estimate the value of Σ_n to be subtracted from each measurement of Σ_T to yield Σ_m. Unfortunately such standards were not and are still not available (CZUBEK., 1987). This problem was circumvented by adding small known amounts of a standard material which had a high well known absorption cross-section and low scattering cross-section sequentially to each of three matrices. Between each of these additions I/I_o was measured and Y calculated. Materials selected as standard matrices were acid-washed sand to represent silicates, laboratory grade $CaCO_3$ to represent limestones and a 50:50 mix of $CaCO_3$/MgO to represent dolomites. These matrices were selected because of their purity and similarity with respect to Σ_n to rock matrices of interest (See Table A3.2).

Boron was selected as the standard additive due to its availability and large σ_a:σ_n ratio (of 153). The additive was prepared by adding known weights of Analar Borax ($Na_2B_4O_7$) to 80 grams of the appropriate matrix prepared as discussed in Section 4.1.2 to form an "additive mix". The borax was thoroughly dispersed in the "additive mix" by grinding in an agate mill. Known weights (5, 10, 20, 40 and 80g) of the "additive mix" were then added sequentially to the standard matrix to give a total weight of 800 +/- 1g. After each

addition of "additive" the contents of the sample cell were well mixed prior to measurement of I and I_o.

Between each addition a known amount of material was removed at random to enable the total sample weight to be kept constant. During the calculation of total Σ_m added, a small proportion of the added Σ_m had to be subtracted from the calculated total Σ_m to correct for the proportion removed in the course of keeping the sample weight constant. To ensure the accuracy of Σ_m added the B content of each "additive mix" was assayed and results were consistent with that calculated based on the weight of borax added.

Results of standard addition experiments on the three standard matrices described above and on distilled water are given in Tables 4.6 to 4.8 together with linear fitting parameters. All of the experiments show a good linear correlation (>0.99) between Σ_m added and Y. The results are also displayed graphically in Figs A3.13 to A3.16. Errors in Y for the H_2O/B system given in Table A3.8 are lower than those for the rest of the tables since packing errors should be negligible for water. The parameters A' and B obtained during the linear fitting process represent the slope and intercept of the linear fit. A' represents the reduction in Y per cm^2g^{-1} of absorber added to 800g of sample which may be corrected to give the reduction in Y per cm^2g^{-1} of absorber (A) where:-

$$A = A' \times 800 \qquad \text{Eqn. A3.16}$$

B is a constant which is a combination of Σ_T and effects due to geometry. Values of A and B for each of the standard matrices are given in Table A3.9.

A full analysis of each of the three standard matrices (acid-washed sand, $CaCO_3$ and 50/50 $CaCO_3$/MgO) was then carried out to enable the macroscopic cross-section of each of the standards (Σ_{ms}) to be calculated as described in Section 3. The analysis and calculated cross-sections for these standards are given in Table A3.10. The resulting Σ_{ms} values are given in Table A3.11 together with a brief description of the applicability of each standard to different rock matrices.

The major uncertainty associated with each calculated Σ_{ms} value is due to the lack of Gd and Sm analyses on these samples. These analyses are at present being carried out at the Royal Holloway College, University of London and until these results are known a concentration of 1 ppm for each of

these elements in the standard materials has been assumed. This is justifiable since Gd and Sm compounds (including their oxides) are soluble in acids and should be removed in the preparation of each of these compounds. For the purpose of the calculation of Σ_m an error of 10% on calculated values of Σ_{ms} has been assumed.

A3.4 Calculation of Σ_m and its associated error.

The macroscopic thermal absorption cross-section (Σ_m) and its associated error may be calculated from measured I/I_o values, linear fit parameters (A and B) derived from standardisation procedure described above and Σ_m for the respective standard matrix (Σ_{ms}) calculated from its composition using equation A3.17.

$$\Sigma_m = \Sigma_{ms} + \frac{Y-B}{A} \qquad \text{Eqn. A3.17}$$

The associated error in Σ_m ($\sigma_{\Sigma m}$) is :-

$$\sigma_{\Sigma m} = \left[\left[\left(\frac{\sigma_Y^2 + \sigma_B^2}{(Y-B)^2} \right) + \left(\frac{\sigma_A}{A} \right)^2 \right] \left(\frac{Y-B}{A} \right)^2 + \sigma_{\Sigma ms}^2 \right]^{0.5} \qquad \text{Eqn. A3.18}$$

where :-

Σ_m = Mass absorption cross-section of the sample ($cm^2\ g^{-1}$).

Σ_{ms} = Mass absorption cross-section of the standard matrix ($cm^2\ g^{-1}$).

$Y = \ln I/I_o$ σ_m = The standard deviation of the absorption cross-section for the sample.

σ_{ms} = The standard deviation of the absorption cross-section for the standard matrix.

σ_Y = The standard deviation due to errors described in section 4.4.1.

σ_A = The standard deviation of the slope of the calibration plot.

σ_B = The standard deviation of the intercept of the calibration plot.

A3.5 Results of Σ_m measurements on rock matrices.

Samples of rocks selected to represent a wide range of

compositions were prepared as described in Section 4.1.2. I/I_o was then measured for each of these samples using the Case B method Section 4.2. Results of these measurements and subsequently calculated values of Y are given in Table A3.12. Calculated values of Σ_m based on these experimental measurements and equations A3.17 and A3.18 are given in Table A3.13 together with those calculated from a 19 element rock analysis of each matrix.

A3.6 Conclusions based on experimental results.

From the results given in Table A3.13 Fig A3.17 was constructed to show the degree of correlation between the calculated and measured values of Σ_m. From this figure it may be concluded that :-

(a) There is good agreement with no apparent bias between the measured macroscopic thermal absorption cross-sections and those calculated from a rock analysis. In most cases this agreement is within 5%.

(b) The percentage error in Σ_m is greater for matrices with a low absorption cross-section, which is due to the logarithmic nature of the relationship between I, I_o and Y.

(c) Given the agreement described above this method may be used to estimate Σ_m for an unknown rock sample provided that it has a similar matrix to a selected standard matrix.

A3.5 Discussion and further work.

A3.5.1 Results of the I.A.E.A intercomparison study.

As discussed in the introduction to this section three of the samples given in Table A3.13 (MCS1,MCS2,MCS3) were interlaboratory comparison samples supplied by the I.A.E.A. The objective of this interlaboratory exercise was firstly to validate a set of rocks as international standards, and secondly to compare the relative precision and accuracy of differing methods of measuring Σ_m. Table A3.14 compares our measured values of Σ_m with the mean of those determined by the other laboratories which took part in the study. From this table it may be seen that measurements carried out by the method described above are in good agreement with the mean of those made by the other laboratories. The overall error associated with our estimates of Σ_m is generally larger than that estimated for the other methods used in the intercomparison study (ie/ about +/- 20% (1σ) compared to about +/- 10% (1σ)). This situation could be improved by

increasing the precision with which I and I_o are measured. This may be achieved by either thermostating the counting electronics or by using another neutron detection device such as a BF_3 counter which is less sensitive to temperature and the settings of discriminator levels. The overall conclusion of the intercomparison study (I.E.A.E. report 1987) was that further work was required before an internationally agreed standard could be distributed for the measurement of Σ_m. It was suggested that the overall precision and hence accuracy of the results from different laboratories could be improved by using standard calibration samples consisting of samples of heavy water for which the scattering cross-section and absorption cross-section were accurately known.

A3.5.2 Experimental measurement of Σ_m using the absorptometer.

The described method is clearly capable of measuring Σ_m in rock samples to a level of accuracy which makes it suitable for estimating the relative neutron fluxes produced within rock formations. Further work to improve the accuracy of the method would be worth while if the method was to be used for measuring low cross-section materials for borehole logging studies.

Table A3.1 Standard operating conditions for the neutron absorptometer.

High voltage	= +1200 Volts
Gain	= 8 * 1
Low level discriminator	= 0.150 Volts
Preamplifier	= ON
Amplifier	= ON
Distance of source from detector	= 22 cm
Counting time	= 1600 Seconds

Table A3.2 Calculated total scattering cross-sections (Σ_n) for selected rock matrices with 1% bound or inter-granular water.

Sample	Σ_n (cm^2g^{-1})
Average Rocks (1)	
Ultramafic	0.135
Sandstone	0.128
Basalt	0.126
Carbonate	0.142
Clays and Shales	0.128
Cornish Granites (2)	
South Crofty (-310m)	0.122
Pendarves (-100m)	0.122
Penryn (surface)	0.122
Rosemanowes RH11 B/H (-1700m)	0.122
AM1 (Surface)	0.122
AM13 (Surface)	0.122
WJE Wheal Jane Elvens (-340m)	0.122
J11 Wheal Jane Elvens (-340m)	0.122
AM22 Lands End (Surface)	0.121
AM30 Lands End (Surface)	0.122
Stripa Samples (2)	
Granite Average Analysis (3)	0.107
Granite Composite from V2 B/H	0.123
Leptite	0.107
Miscellaneous Silicates (2)	
Bunter Sandstone Nottingham Castle	0.123
Bunter Sandstone Kingston B/H	0.121
Triassic Sandstone Southampton B/H	0.125
Triassic Sandstone Kempsey B/H	0.126
Old Red Sandstone	0.123
Acid Washed Silica Sand	0.128
MCS1 Ottawa Sand (4)	0.124
Basaltic Tuff Kaphenstien	0.127
Trachy Andesite	0.127
Basalt Kloch	0.128
MCS3 Dunite "Sand" 28% Mg (4)	0.150
Miscellaneous Carbonates (2)	
MCS3 Royer Dolomite (4)	0.148
Oolitic Limestone	0.125
Laboratory Grade $CaCO_3$	0.134

(1) Analysis of Parker (1967)
(2) See Appendix 2 for analytical results.
(3) Analysis from Andrews et al (1988).
(4) Analysis from I.A.E.A. (1987).

Table A3.3 Variation in transmitted intensity (I) between repacked samples counted on the same day

I	800 g Penryn granite 1600 s counting time
168496	
167306	
166880	
167138	X = 167779
169098	σ = 1047
168894	S = 0.62 %
167590	
166442	
169200	
166742	

Table A3.4 Variation in the ratio of transmitted to incident neutron intensity (I/I_o) for repacked Penryn Quarry samples (800g). Transmitted intensity (I) has been determined directly after incident intensity (I_o).

Date	I_o	I	I/I_o
16/6/87	181718	132291	0.728
17/6/87	182748	132130	0.723
18/6/87	179778	127867	0.711
21/6/87	181178	130985	0.723
30/6/87	177447	130213	0.734
1/7/87	179653	130567	0.723
2/7/87	176204	128757	0.731
18/9/87	168413	122846	0.729

X = 0.725
σ = 0.007
S = 0.97 %

Table A3.5 The variation in the natural logerithium of the ratio of transmitted to incident neutron intensity (ln I/I_o) for different densities of packing (constant weight (800g)).

Density g cm^{-3}	I_o	I	I/I_o	+/-
1.40	179778	127867	0.7112	0.0007
1.50	179778	128506	0.7148	0.0007
1.59	179778	128862	0.7168	0.0007
1.75	179778	128204	0.7131	0.0007

nb/ Sample volume varies.

Table A3.6 ln I/I_o values for a silicate (SiO_2) matrix (800g).

Σ_m added cm^2g^{-1}	ln I/I_o	+/-
0.000	-0.121	0.01
0.513	-0.138	0.01
1.026	-0.163	0.01
2.052	-0.203	0.01
4.051	-0.264	0.01
8.003	-0.394	0.01

Linear fitting parameters :-
Correlation coefficient = -0.998
Intercept = -0.125 +/- 0.0039
Slope --- = -0.0339 +/- 0.0010

Table A3.7 ln I/I_o values for limestone ($CaCO_3$) and dolimite ($Ca/MgCO_3$) matrices.

Σ_m added cm^2g^{-1}	Carbonate (800g) ln I/I_o	+/-	Dolomite (800g) ln I/I_o	+/-
0.0	-0.188	0.01	-0.163	0.01
0.423	-0.195	0.01	-0.180	0.01
1.266	-0.232	0.01	-0.214	0.01
2.928	-0.300	0.01	-0.279	0.01
6.153	-0.435	0.01	-0.412	0.01

Linear fitting parameters :-

	$CaCO_3$		$Ca/MgCO_3$	
Correlation coefficient =	-0.998		-0.999	
Intercept - =	-0.182	+/- 0.004	-0.163	+/- 0.004
Slope ----- =	-0.041	+/- 0.001	-0.040	+/- 0.001

Table A3.8 ln I/I_o values for water (H_2O) matrices (800g).

Σ_m added cm^2g^{-1}	ln I/I_o	+/-
0.00	-1.086	0.004
4.79	-1.285	0.004
9.57	-1.454	0.004
14.4	-1.582	0.004
19.1	-1.725	0.004

Linear fitting parameters :-
Correlation coefficient = -0.996
Intercept = -1.111 +/- 0.003
Slope --- = -0.033 +/- 0.0003

Table A3.9 Constants and uncertainties used in equations A3.16 to A3.18.

	Standard Matrix		
Quantity	SiO_2 sand(1)	$Ca/MgCO_3$(1)	$CaCO_3$(1)
A	-27.1 +/- 0.8	-31.8 +/- 0.8	-32.5 +/- 0.8
B ($*10^{-3}$)	-125 +/- 4	-163 +/- 4	-182 +/- 4
Σ_{ms} (cm^2g^{-1})	0.0018 +/- (2)	0.0026 +/- (2)	0.0037 +/-(2)
Weight (g)	800 +/- 1	800 +/- 1	800 +/- 1

(1) Values based on B analysis of standard additives.
(2) Uncertain error due to lack of Gd and Sm analyses.

Tables A3.10a to A3.10c Calculated macroscopic absorption cross-sections for standard rock matrices (Σ_{ms}).

Table A3.10a Silicate Matrix (Acid washed sand).

Element	Concentration (ppm)	Σ_m cm^2g^{-1} $*10^{-3}$
Li	<1	<0.001
B	<1	<0.001
Na	55	0.001
Mg	29	<0.001
Al	200	<0.001
Si	465100	1.591
Cl	10	0.005
K	57	0.002
Ca	34	<0.001
Ti	240	0.018
Cs	0.5	<0.001
Mn	0.5	<0.001
Fe	24	0.001
Co	<1	<0.001
Ni	0.5	<0.001
Sm	<1.0	<0.022
Gd	<1.0	<0.175
	Total (Σ_{ms}):	1.825

Table A3.10b Limestone matrix ($CaCO_3$).

Element	Concentration (ppm)	Σ_m cm^2g^{-1} $*10^{-3}$
Li	2	0.012
B	19	0.801
Na	127	<0.001
Mg	10	<0.001
Al	0.1	<0.001
Si	10	<0.001
Cl	10	0.006
K	8	<0.001
Ca	400000	2.644
Ti	<1	<0.001
Cs	<1	<0.001
Mn	6	<0.001
Fe	33	<0.001
Co	16	0.006
Ni	10	<0.001
Sm	1.0*	0.022
Gd	1.0*	0.175
	Total (Σ_{ms}):	3.674

Table A3.10c Dolomite matrix ($CaCO_3$ and MgO).

Element	Concentration (ppm)	Σ_m cm^2g^{-1} $*10^{-3}$
Li	3.1	0.019
B	20	0.841
Na	96	0.001
Mg	144130	0.225
Al	<1	<0.001
Si	1	<0.001
Cl	10	0.005
K	8	<0.001
Ca	200000	1.322
Ti	<1	<0.001
Cs	<1	<0.001
Mn	6	0.001
Fe	26	0.001
Co	13	0.005
Ni	5	<0.001
Sm	1*	0.022
Gd	1*	0.175
	Total (Σ_{ms}):	2.617

* see text for derivation of these concentrations.

Table A3.11. Standard rock matrices for different rock types

Standard rock matrix	Mass absorption cross-section for neutrons Σ_{ms} (cm^2g^{-1})	Rock type
SiO_2 sand	0.0018	silicate rocks (granites and sandstones)
$CaCO_3$ + MgO	0.0026	dolomites
$CaCO_3$	0.0037	carbonate rocks (limestones and chalks)

Table A3.12 ln I/I_o values for measured rock matrices

Sample no	Sample	I_o	I	$\ln_b$ I/Ø/-	+/-	%
SA1	South Crofty mine	179653	126220	-0.353	0.011	3.1
SA2	Pendarves mine	175146	95956	-0.602	0.011	1.8
SA3	Penryn quarry	179778	128862	-0.333	0.011	3.3
SA14	Stripa mine	169658	138957	-0.200	0.011	5.5
SA11	Borehole HF1 -150m	167855	113623	-0.390	0.011	2.8
SA12	Borehole HF2 -150m	167855	114442	-0.383	0.011	2.9
SA16	Bunter Notts	176204	141906	-0.216	0.011	5.1
SA17	Bunter W/B	169658	130695	-0.261	0.011	4.2
SA18	Triassic Southampton	169658	132923	-0.244	0.011	4.5
SA19	Triassic Kempsey	169658	141461	-0.182	0.011	6.0
SA20	Old Red Sandstone	169658	116810	-0.373	0.011	2.9
SA22	Trachy Andesite	169801	130533	-0.263	0.011	4.2
SA23	Basalt Kloch	169658	133457	-0.240	0.011	4.6
SA28	Bristol Grit	177447	147949	-0.174	0.011	6.3
SA29	MCS1	168106	147466	-0.131	0.011	8.4
SA30	MCS3	168893	143203	-0.165	0.011	6.6
SA15	Oolitic Limestone	180558	154954	-0.173	0.011	6.4
SA31	MCS2	175012	148392	-0.165	0.011	6.7

Table A3.13 Measured and calculated neutron absorption cross-sections. (Σ_m).

Sample no	Sample	measured values $_m\Sigma$ +/- (1Å)		calculated values Σ_m +/- (1Å)	
SA1	South Crofty mine	0.0102	0.0004	0.0124	0.0007
SA2	Pendarves mine	0.0194	0.0007	0.0189	0.0013
SA3	Penryn Quarry	0.0095	0.0005	0.0107	0.0005
SA14	Stripa mine	0.0046	0.0005	0.0060	0.0003
SA11	HF1 150m	0.0116	0.0006	0.0114	0.0004
SA12	HF2 297m	0.0113	0.0006	0.0124	0.0007
SA16	Bunter Notts	0.0052	0.0005	0.0055	0.0003
SA17	Bunter W/B	0.0068	0.0005	0.0072	0.0006
SA18	Triassic Southampton	0.0062	0.0005	0.0073	0.0004
SA19	Triassic Kempsey	0.0039	0.0005	0.0036	0.0009
SA20	Old Red Sandstone	0.0110	0.0005	0.0085	0.0003
SA22	Trachy Andesite	0.0069	0.0005	0.0060	0.0004
SA23	Basalt Kloch	0.0061	0.0005	0.0072	0.0004
SA28	Bristol Grit	0.0036	0.0005	------	------
SA29	MCS1	0.0021	0.0005	0.0019	0.0003
SA30	MCS3	0.0033	0.0005	0.0035	0.0006
SA15	Oolitic Limestone	0.0034	0.0004	0.0050	0.0002
SA31	MCS2	0.0027	0.0004	0.0024	0.0003

Table A3.14. Comparison of Σ_m for MCS1, MCS2 and MCS3 measured at Bath by the method described above with Σ_m determined by other laboratories in the I.A.E.A intercomparison study.

Method of measurement	Sample					
	$\Sigma_m * 10^{-3}$ cm^2 g^{-1}					
	MCS1	+/-	MCS2	+/-	MCS3	+/-
Measured by the above method *	2.10	0.25	2.70	0.16	3.30	0.25
Mean of other I.E.A.E methods **	1.87	0.32	2.30	0.25	3.46	0.13
Calculated from rock analysis ***	1.90	0.30	2.40	0.30	3.50	0.60

* Mean of six measurements.

** Mean of five laboratories neglecting initial measurements made by the method described above.

*** For method of calculation see Section 3.

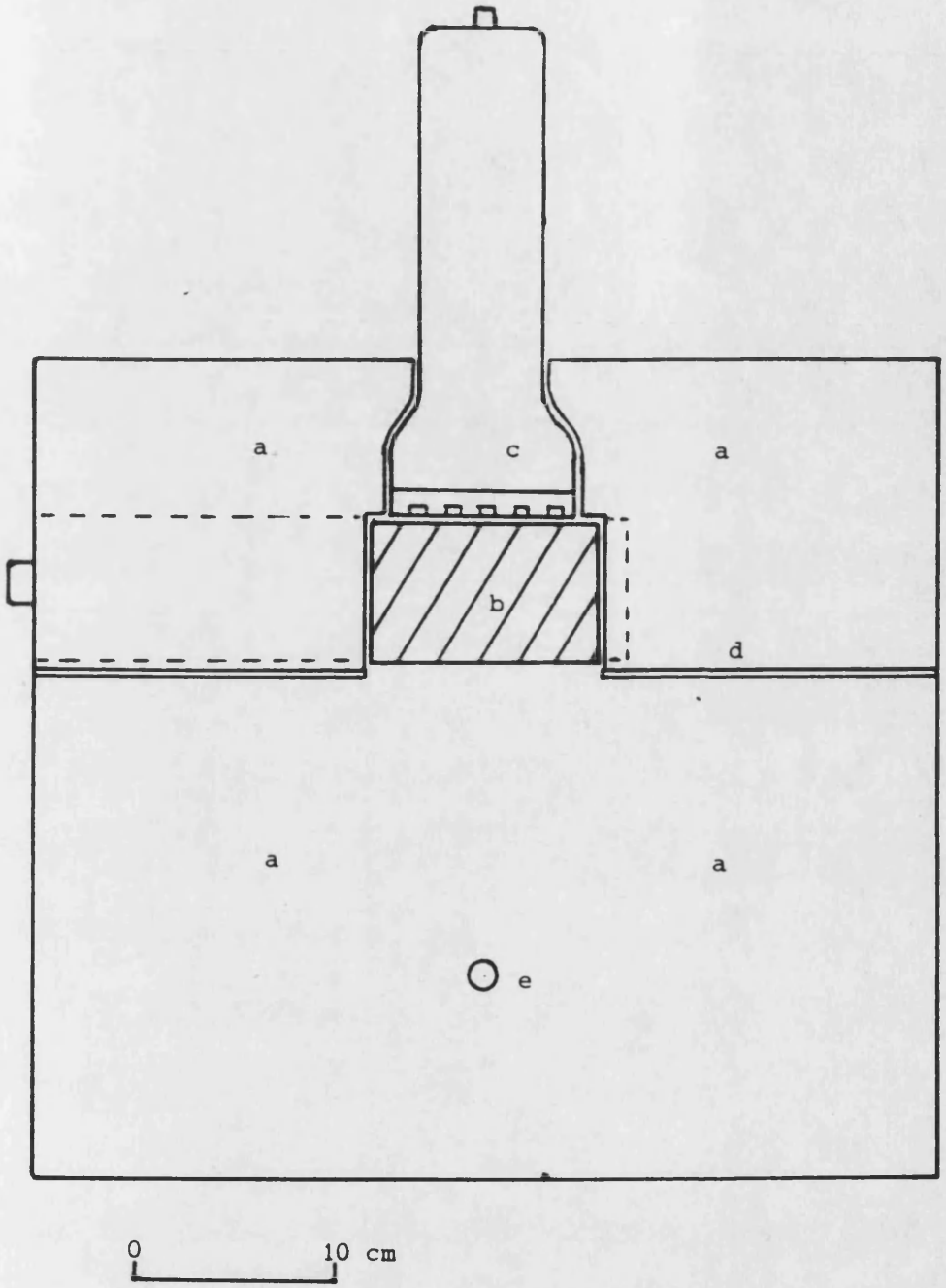

Fig. A3.1. Apparatus for neutron absorption measurements.

a. polythene moderator

b. sample cell

c. NE222 neutron detector with photomultiplier

d. cadmium absorber

e. 0.5 μg ^{252}Cf neutron source

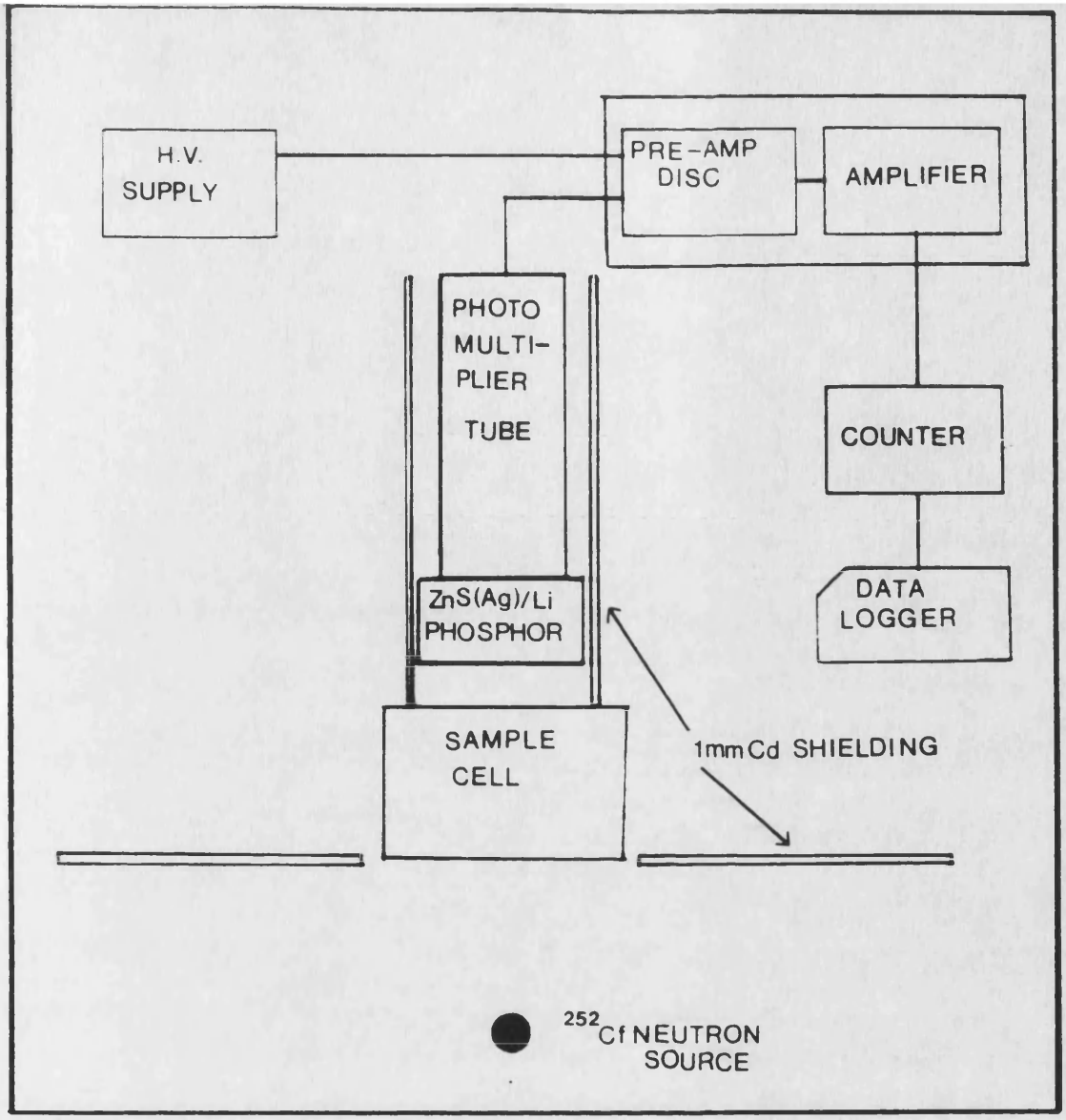

Fig. A3.2. Schematic diagram of the system used for neutron absorption measurements.

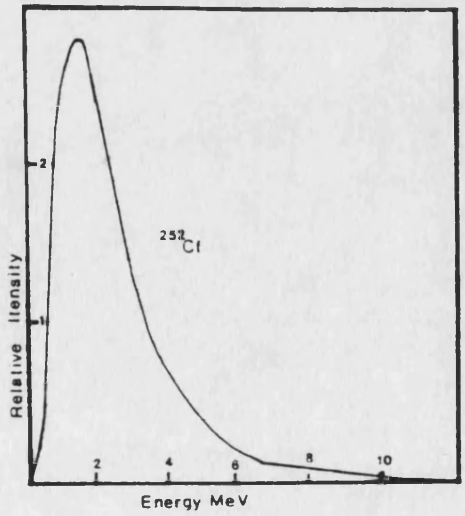

Fig. A3.3. The differential energy spectrum of neutrons emmitted during spontaneous fisson of ^{252}Cf.

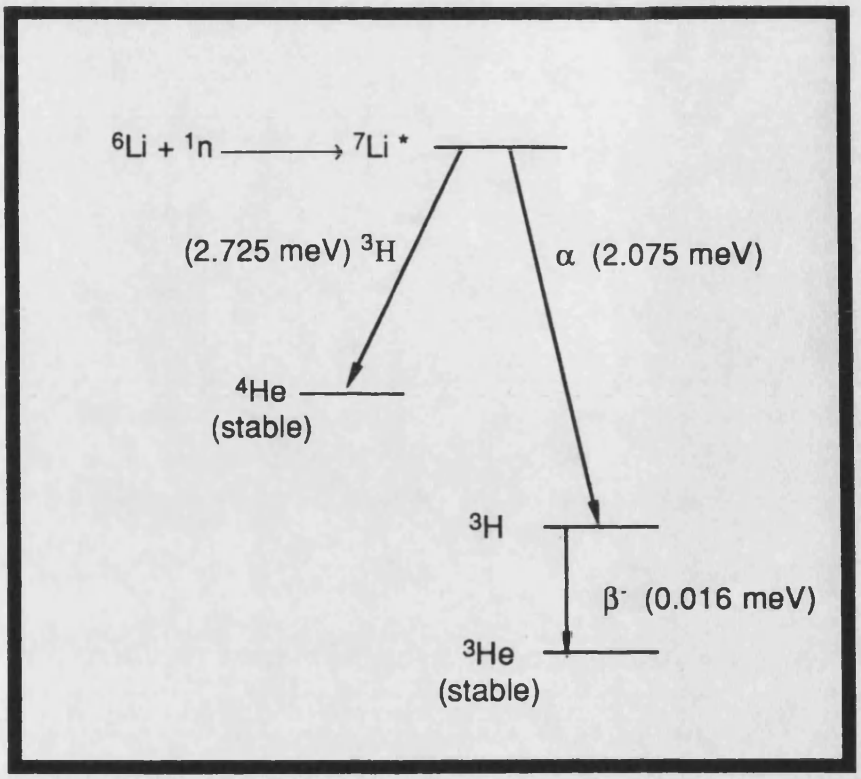

Fig. A3.4. Reaction scheme for the interaction of thermal neutrons with ^{6}Li.

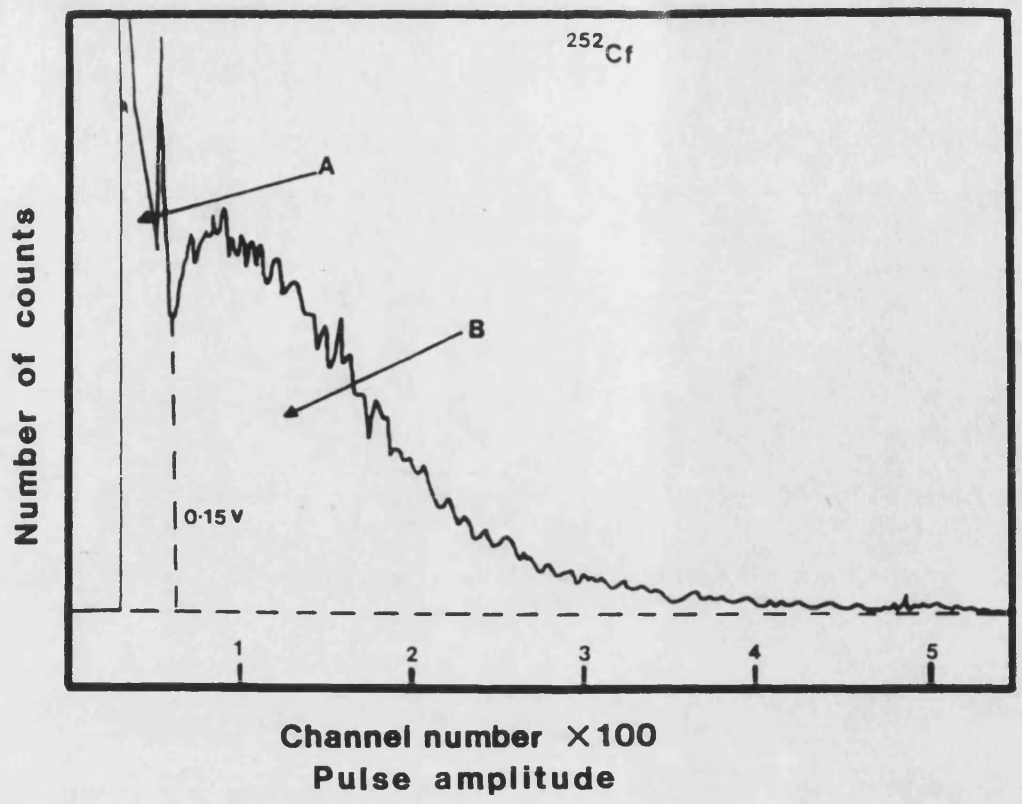

Fig. A3.5a. Pulse height spectrum obtained from the NE222 detector with the ^{252}Cf neutron source in position.

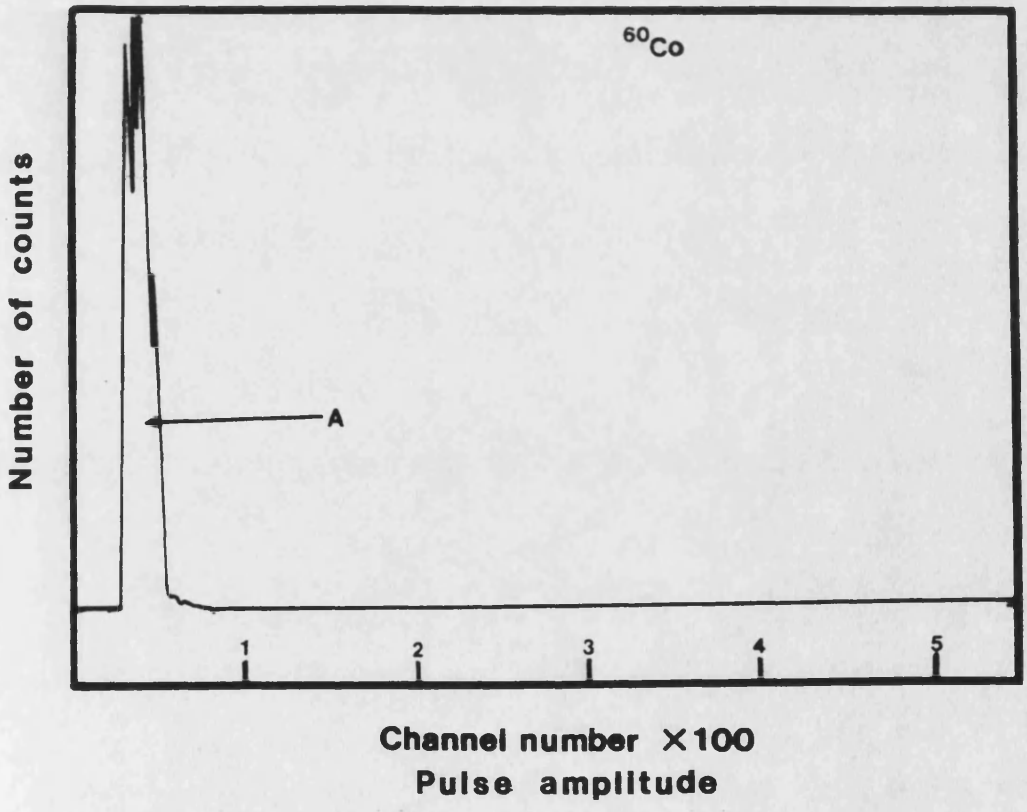

Fig. A3.5b. Pulse height spectrum obtained from the NE222 detector with a ^{60}Co γ source in position.

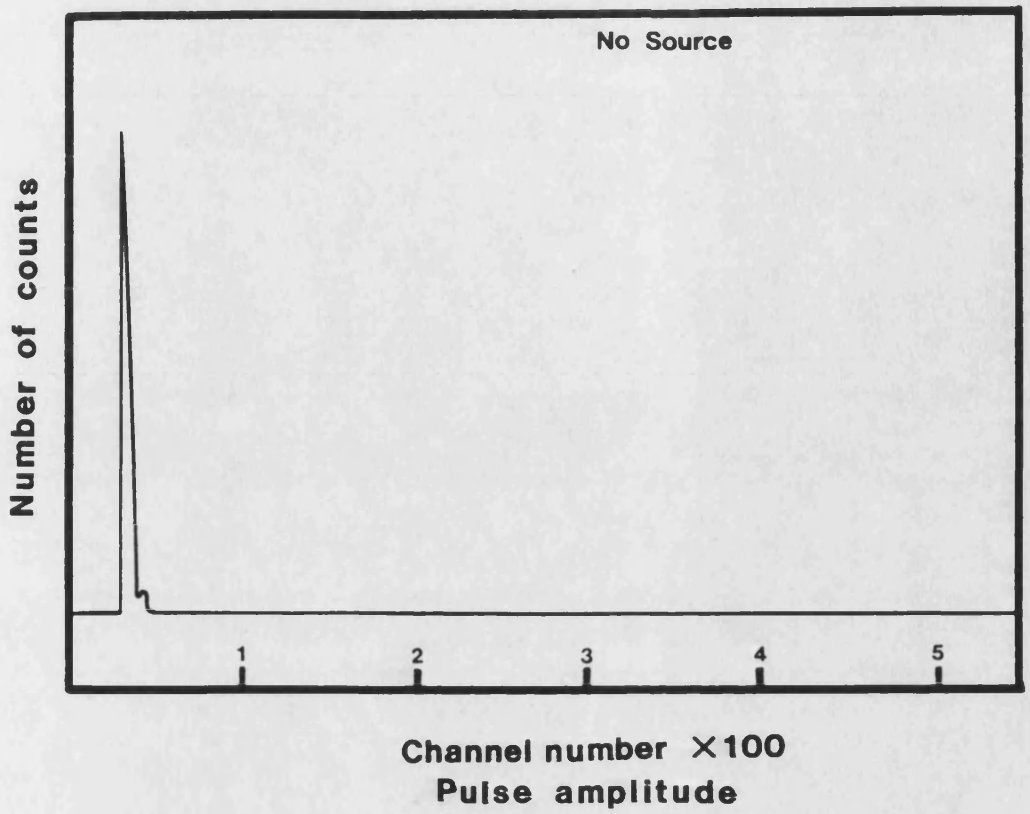

Fig. A3.5c. Pulse height spectrum obtained from the NE222 detector with no source in position.

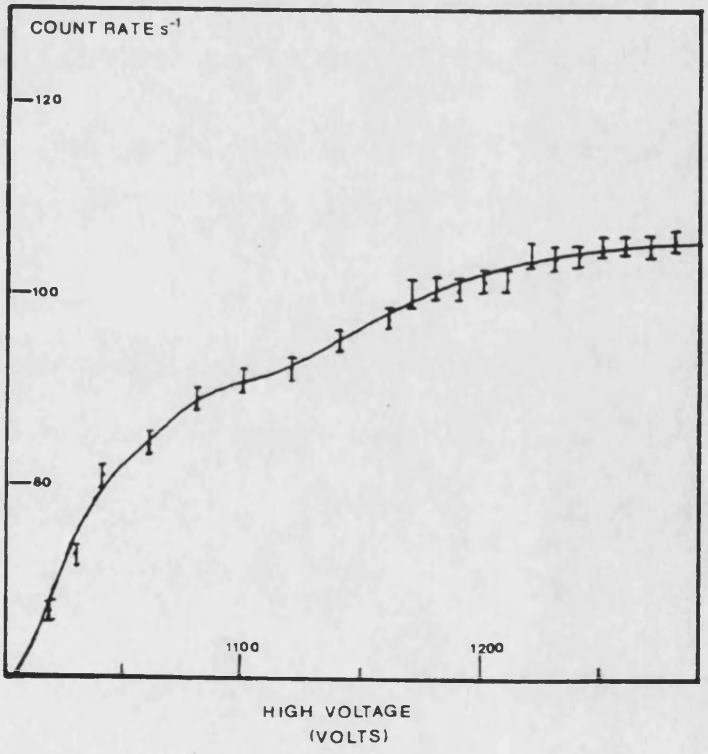

Fig. A3.6. Variation in count rate with photomultiplier tube voltage (^{252}Cf source in position and a gain of 4).

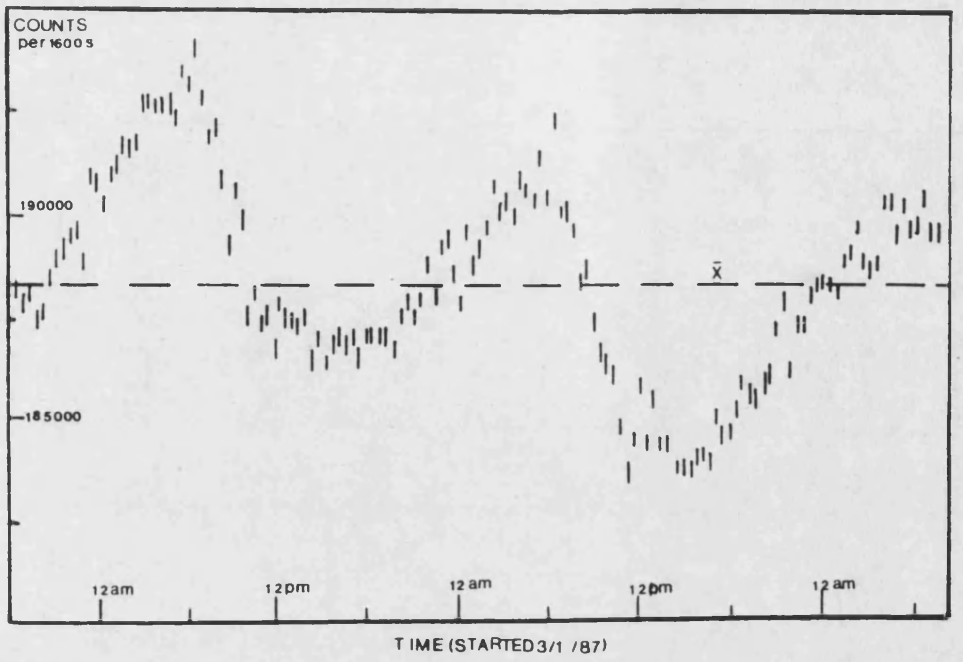

Fig. A3.7. Variation in counts amassed during 1600 s periods against time of day over a weekend period (3/1/87 ^{252}Cf source in position)

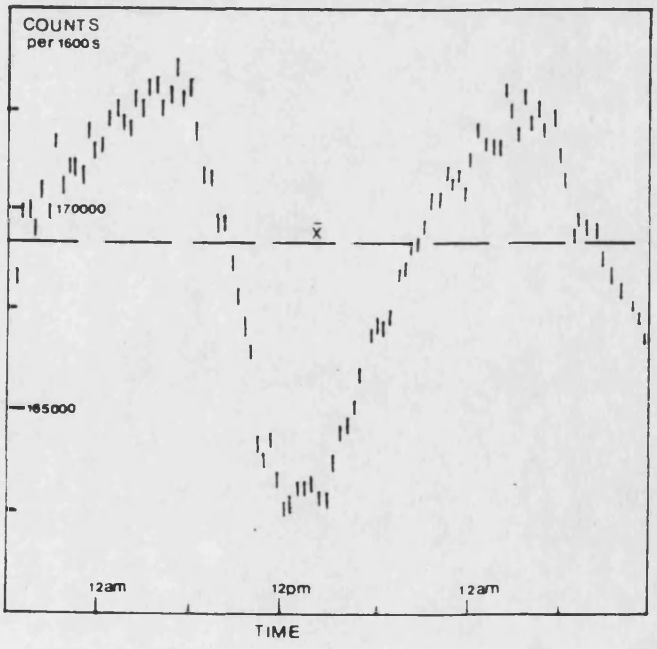

Fig. A3.8. Variation in countrate amassed during 1600 s periods against time of day during a weekday (^{252}Cf source in position).

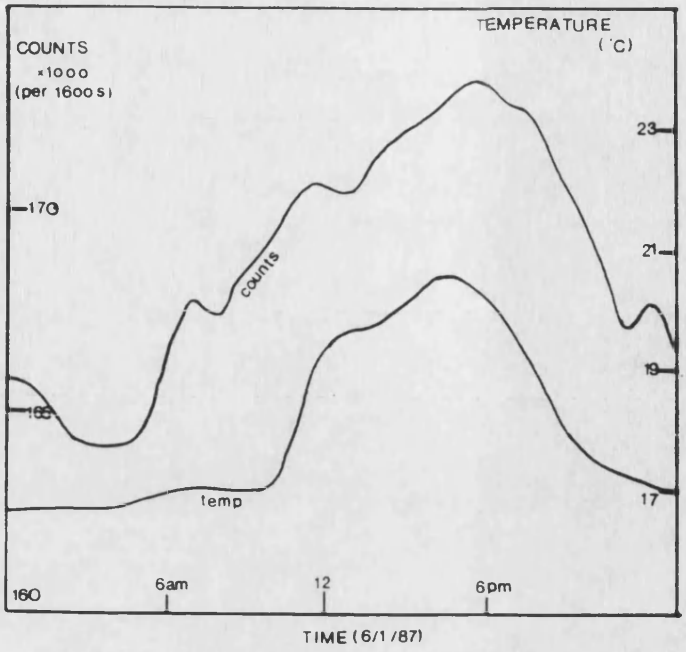

Fig. A3.9. Variation in counts amassed during 1600 s periods, and photomultiplier tube voltage against time of day over a weekday period (^{252}Cf source in position).

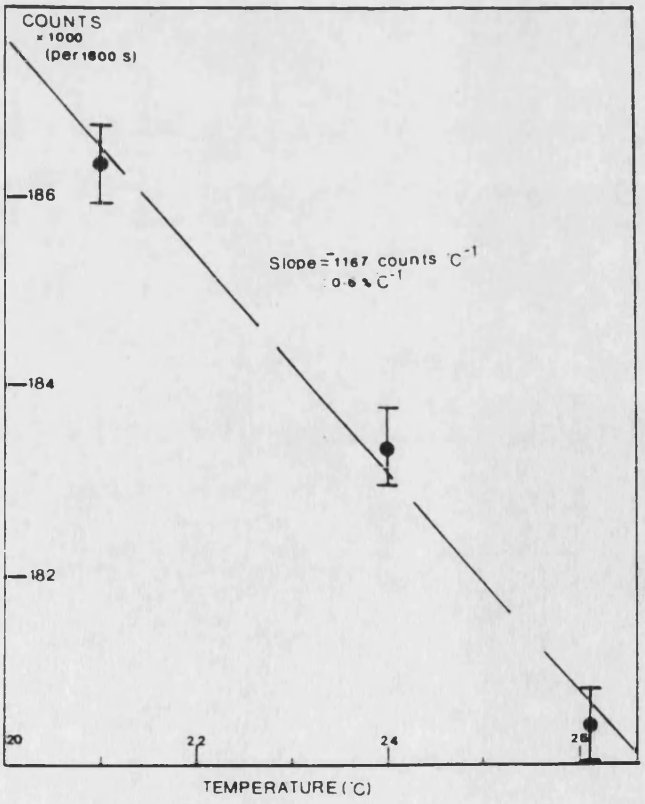

Fig. A3.10. Variation in counts amassed during 1600 s periods with photmultiplier tube temperature (^{252}Cf source in position).

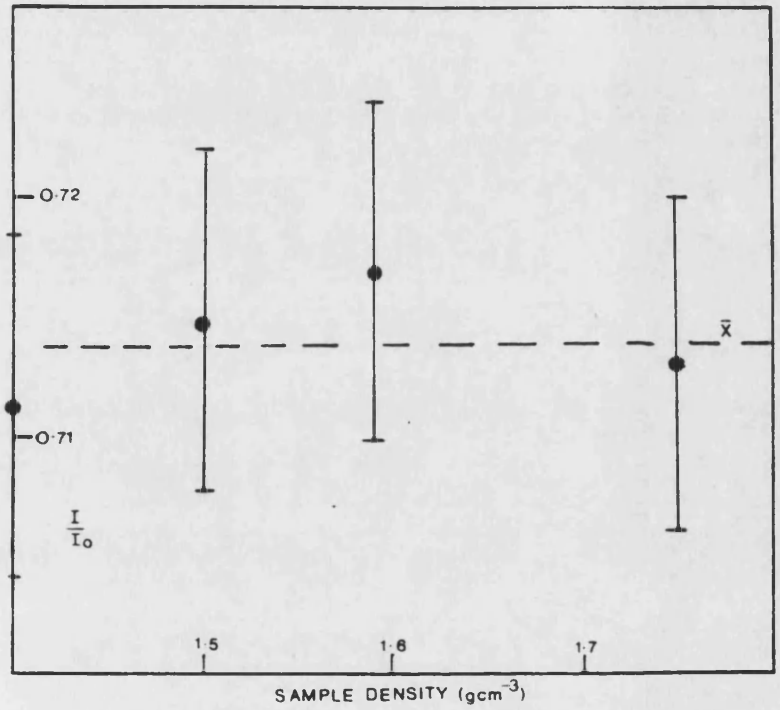

Fig. A3.11. Variation in the measured ratio of transmitted intensity to incident intensity (I/I_O) with sample density.

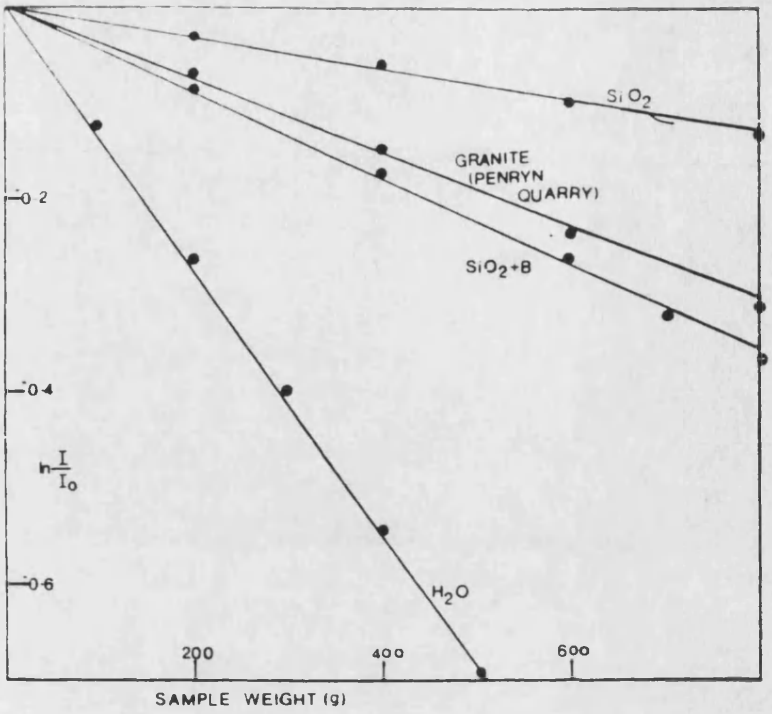

Fig. A3.12. Variation in the natural logerithium of measured I/I_o ratios with sample weight. A linear correlation supports the relationship described in equation A3.15.

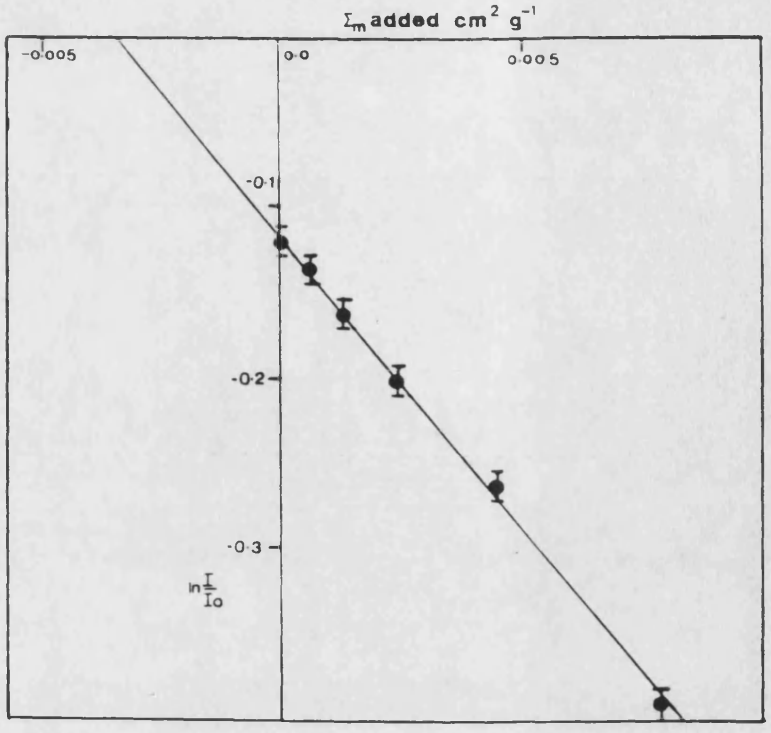

Fig. A3.13. The relationship between measured ln I/I_o values and the amount of absorption cross-section (Σ_m) added to silica sand.

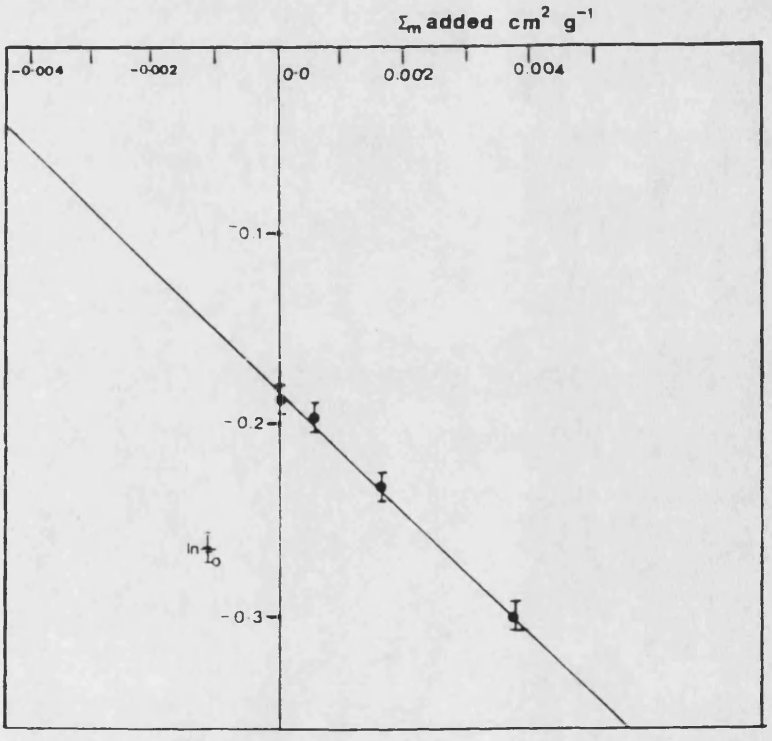

Fig. A3.14. The relationship between measured ln I/I_o values and the amount of absorption cross-section (Σ_m) added to $CaCO_3$.

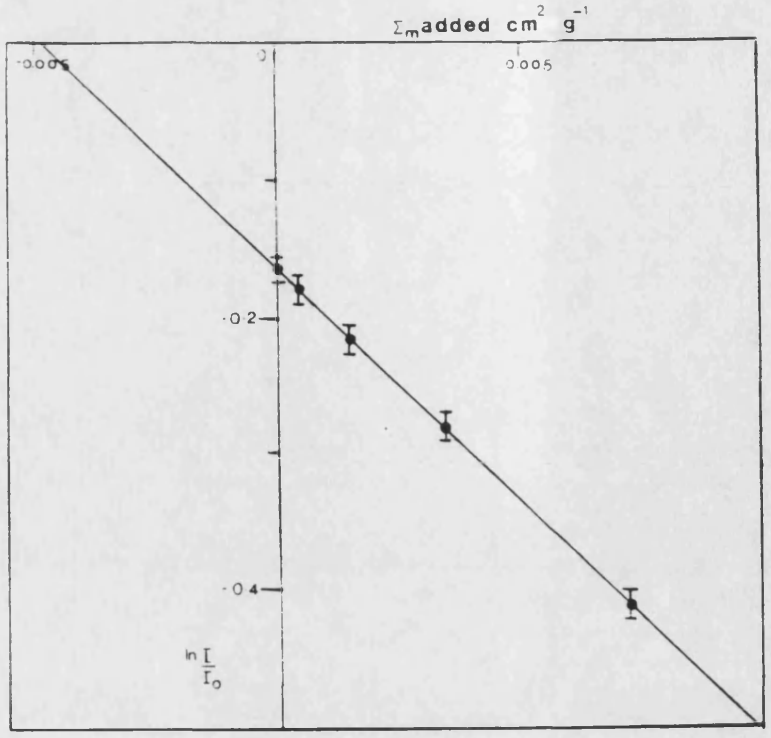

Fig. A3.15. The relationship between measured ln I/I_o values and the amount of absorption cross-section (Σ_m) added to $CaCO_3/MgCO_3$.

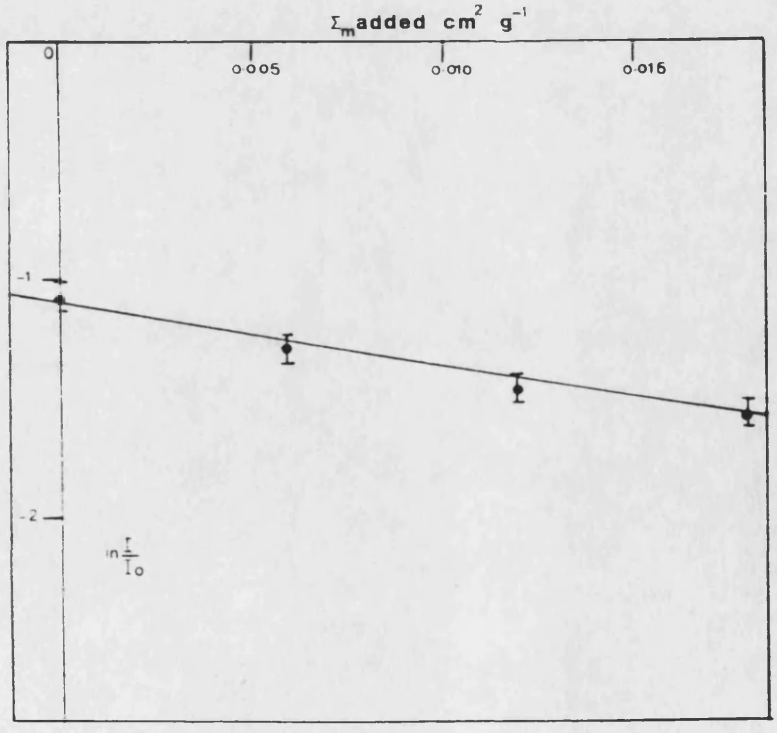

Fig. A3.16. The relationship between measured ln I/I_o values and the amount of absorption cross-section (Σ_m) added to distilled water.

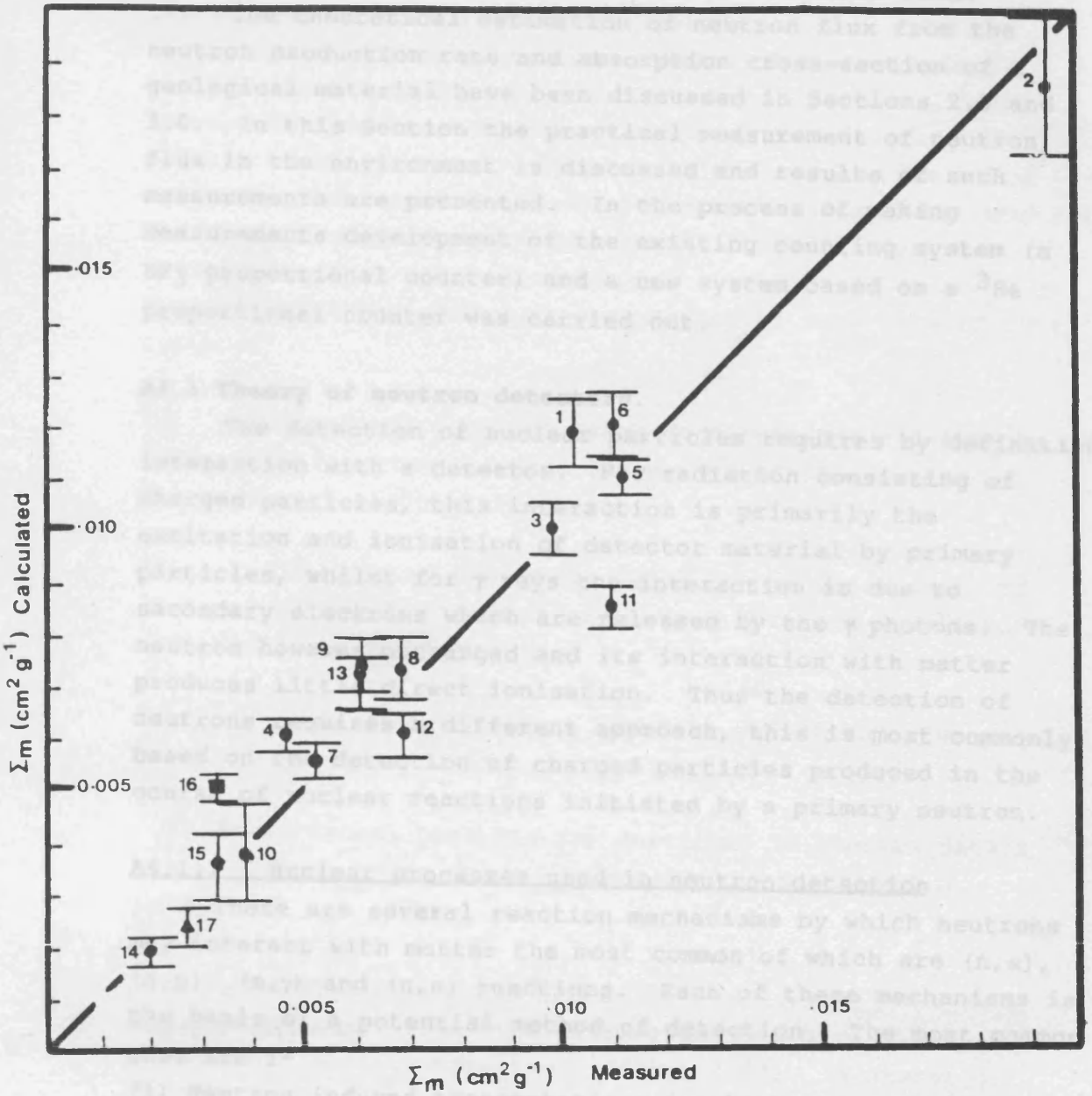

Fig. A3.17. The correlation between Σ_m measured using the method described in this section and Σ_m calculated from a chemical analysis of the same samples (see Appendix 2).

1. SA1 South Crofty mine
2. SA2 Pendarves Mine
3. SA3 Penryn Quarry
4. SA14 Stripa Mine
5. SA11 HF1 -150m
6. SA12 HF2 -297m
7. SA16 Bunter Notts.
8. SA17 Bunter W.B.
9. SA18 Triassic SSt.
10. SA19 Triassic Kempse
11. SA20 Old Red SSt.
12. SA24 Trachy Andesite
13. SA23 Basalt Kloch
14. SA29 MCS1
15. SA30 MCS3
16. SA15 Oolitic LSt.
17. SA31 MCS2

APPENDIX 4. FIELD MEASUREMENT OF IN-SITU NEUTRON FLUX.

The theoretical estimation of neutron flux from the neutron production rate and absorption cross-section of a geological material have been discussed in Sections 2.0 and 3.0. In this Section the practical measurement of neutron flux in the environment is discussed and results of such measurements are presented. In the process of making measurements development of the existing counting system (a BF_3 proportional counter) and a new system based on a ^3He proportional counter was carried out.

A4.1 Theory of neutron detectors.

The detection of nuclear particles requires by definition interaction with a detector. For radiation consisting of charged particles, this interaction is primarily the excitation and ionisation of detector material by primary particles, whilst for γ rays the interaction is due to secondary electrons which are released by the γ photons. The neutron however uncharged and its interaction with matter produces little direct ionisation. Thus the detection of neutrons requires a different approach, this is most commonly based on the detection of charged particles produced in the course of nuclear reactions initiated by a primary neutron.

A4.1.1 Nuclear processes used in neutron detection

There are several reaction mechanisms by which neutrons may interact with matter the most common of which are (n,α), (n,p), (n,γ) and (n,n) reactions. Each of these mechanisms is the basis of a potential method of detection. The most common ones are :-

(1) Neutron induced transmutations in which the product particles make possible the detection; ie/ (n,α), (n,p) and (n,γ). In these cases the proton or a particle give instantaneous information concerning the neutron.

(2) Neutron-induced transmutations which result in the formation of a radioactive nuclei. The subsequent decay of these nuclei yields information on the neutron flux that caused the transformation.

(3) Elastic scattering of neutrons in which the recoil particle is capable of being detected.

Neutron detection systems consist of the material required to bring about one of the nuclear process listed above, along with a means for measuring or indicating the results of the process. This latter part of the detection system may be one of the several conventional systems used for the detection of charged particles or photons (ie/ scintillation or gas ionisation).
Neutron detectors used during experimental work were of three types :-

(1) Proportional counters based on either the $^{10}B(n,\alpha)^{7}Li$ or $^{3}He(n,p)^{3}H$ reaction in which either ^{10}B or ^{3}He form an integral part of the filling gas.

(2) Radio-chemical detectors based on the measurement of isotopic ratios for elements that have attained equilibrium with the local neutron flux.

(3) Scintillation detectors based on the $^{6}Li(n,\alpha)^{3}He$ reaction.

Proportional counters are described in greater detail below, whilst scintillation detectors are described in APPENDIX 3.

A4.1.2 The BF_3 proportional counter.

A4.1.2.1 Theory. The $^{10}B(n,\alpha)$ reaction has been widely used for thermal neutron detection (ICRU., 1969). A number of factors make it highly satisfactory for this purpose:-

(a) The cross-section of the reaction is large and has a simple energy dependence over a wide energy range.

(b) The reaction is easy to detect even in the presence of large gamma fluxes because of the high specific ionisation and energy of the charged particles which are released.

(c) The target material ^{10}B is available in its isotopic form and has chemical properties which enable it to be easily incorporated into a detector.

The reaction is exothermic, with an energy release of 2.78 MeV. For the capture of a neutron of energy E, the kinetic energy E_{ke} is shared by the a particle and the lithium recoil nucleus. If the captured neutron is thermalised, E is approximately zero, and the energies of the lithium nucleus (E_{Li}) and the a particle (E_α) are:-

$$E_{Li} = \frac{E_{Ke}\ M_\alpha}{M_\alpha + M_{Li}} = 0.88 \text{ MeV} \qquad \text{Eqn A4.1}$$

$$E_\alpha = \frac{E_{Ke}\ M_{Li}}{M_\alpha + M_{Li}} = 1.47 \text{ MeV} \qquad \text{Eqn A4.2}$$

The ground state of the ^7Li product nucleus may either be formed directly, with the entire energy being shared by the ^7Li and the alpha particle; or alternatively, via an intermediate excited state of ^7Li, followed by the emission of a 0.48 MeV gamma. The probability of reaching the ground state directly is only 0.064 for reactions induced by thermal neutrons (PRICE., 1964); thus in thermal fluxes a 1.47 MeV α and 0.88 MeV Li recoil nucleus are the predominantly detected particles. This produces a maximum in the pulse amplitude frequency plot at corresponding to 2.35 MeV. The overall bimodal decay process is summarised in Fig A4.1. The maximum primary ionisation occurs within the counter when an alpha particle and its associated recoil nucleus dissipate all of their energy in the filling gas. This primary ionisation is reduced when one of the particles strikes the counter wall before giving up all of its kinetic energy. Fig A4.2 shows a theoretical pulse amplitude spectrum for a 0.05 m diameter BF_3 counter.

A4.1.2.2 Construction of the BF_3 counter. The BF_3 proportional counter used for the measurements described in this chapter was a 150EB counter manufactured by Centronics Nuclear Products. It consisted of a 1.5m by 0.050m copper tube filled to a pressure of 70 cm Hg with BF_3 gas enriched to 90% ^{10}B. The copper tube acted as a cathode whilst a tungsten wire which passed through the tubes centre acted as an anode. A schematic diagram of a BF_3 proportional counter is shown in Fig A4.3. As supplied this detector had a quoted sensitivity of 242.0 counts per second per unit neutron flux. A Canberra 2006 charge sensitive spectroscopy amplifier was attached to the counters output. This converted the current pulses produced by ionisation within the tube into suitably shaped voltage pulses which were either fed into an amplifier and single channel analyser or a multichannel analyser. The operating parameters selected for routine operation and characteristics of the tube are described later in this section.

A4.1.3 The ^3He proportional counter.

A4.1.3.1 Theory The $^3He(n,p)$ reaction has also been widely used for thermal neutron detection (ICRU., 1969). Factors which make it satisfactory for the detection of thermal neutrons are similar to those of BF_3 counters for example:-

(a) The cross-section of the reaction is large and has a simple energy dependence over a wide range of energy values.

(b) The target material ^3He although more expensive than BF_3 is available isotopically pure and its chemical properties are such that it may be incorporated in the detector.

However differences in the energetics of the reaction mean that the ^3He proportional counter is more sensitive to gamma rays which is a disadvantage, and that neutron spectroscopy is theoretically possible which is an advantage over the BF_3 proportional counter.

The reaction is exothermic, with an energy release of only 0.765 MeV compared to 2.78 MeV for the $^{10}B(n,\alpha)$ reaction. For the capture of a neutron of energy E, the kinetic energy of 0.765 MeV is shared by the proton and the tritium recoil nucleus. If the captured neutron is thermalised, E is approximately zero, and the total energy carried away by tritium nucleus and the proton is 0.765 MeV, however if E is

greater than zero then the total energy carried away is E+0.765 MeV. The overall decay process is summarised in Fig A4.4. As for the BF_3 counter maximum primary ionisation occurs within the counter when a proton and its associated recoil triton dissipate all of their energy in the filling gas. This primary ionisation is reduced when one or more of the particles strikes the counter wall before giving up all of its kinetic energy. However the characteristic pulse spectrum of the ^3He proportional counter is much simpler than that of BF_3 counter due to the mono-modal decay process of the intermediate $^4He^*$ nuclei. Note that to be used as an effective neutron spectrometer the energies of the neutrons should be spread over as wide a range as possible, this giving as large a shift in pulse height as possible (ICRU., 1971).

A4.1.3.2 Construction. The ^3He proportional counter used for the measurements described in this chapter was a H3-8-205/4 detector manufactured by Harshaw. It consisted of a 0.51m by 0.025m type 304 stainless steel tube filled to a pressure of 4 atm with ^3He gas. The steel tube acted as a cathode whilst a tungsten wire which passed through the tubes centre acted as an anode. Schematically the ^3He counter is similar to the BF_3 proportional counter shown in Fig A4.3. This detector was supplied without a quoted sensitivity and was standardised against the BF_3 described above. The electronics used to shape, amplify and analyse the data from this tube were similar to that described in previous sections above for the BF_3 tube, except that a higher amplification was required to counter the low charge pulses produced by the ^3He counter during operation.

A4.1.4 Energy dependence of reaction rates and thence detector sensitivity.

As discussed in the above sections both types of detectors register the ionisation caused by neutron induced reaction products. Thus the sensitivity of the detection system may be discussed in terms of the reaction rate (R (reactions s^{-1}) for a particular neutron energy distribution.

R_v the reaction rate for neutrons of velocity v is defined as (PRICE., 1964) :-

$$R_v = \sigma_v n_v \, v \, N = \sigma_v \phi_v N \qquad \text{Eqn A4.3}$$

Where σ_v and n_v are the cross-section (cm^2) and neutron density (cm^{-3}) for neutrons of velocity v, ϕ is the corresponding neutron flux (see section 3) for neutrons of velocity v and N is the atomic density of ^{10}B or ^{3}He atoms (cm^{-3}). The energy dependence of the $^{10}B(n,\alpha)$ and $^{3}He(n,p)$ reaction cross-sections for both have a 1/v dependence up to 30 keV (see Fig A4.5) and :-

$$\sigma_v = \frac{\sigma_0 v_0}{v} \qquad \text{Eqn A4.4}$$

Where v is the neutron velocity, v_0 and σ_0 are the reference neutron velocity and corresponding reference cross-section. These may be taken as the thermal neutron velocity at 25°C (2200 ms^{-1} (0.0253 eV) ICRU., 1969) and the corresponding reaction cross-sections of $3,838 \times 10^{-24}$ cm^2 for $^{10}B(n,\alpha)^{7}Li$ and 5330×10^{-24} cm^2 for $^{3}He(n,p)^{3}H$ (KAYE and LABY., 1986).

The reaction rate (R) for a "perfect" detector placed in an isotropic flux of neutrons with energies between 0 and 30 KeV is therfore equal to :-

$$R = \frac{\sigma_0 \, v_0}{v} \, n_v \, N \, v \, dv \qquad \text{Eqn A4.5}$$

simplification of which gives :-

$$R = \sigma_0 \, v_0 \, n_v \, N \, dv \qquad \text{Eqn A4.6}$$

which may be integrated over all neutron velocities up to 30 keV :-

$$R = \sigma_0 \, v_0 \, N \int_{n_{v_0}}^{30\ \text{KeV}} n_v \, dv \qquad \text{Eqn A4.7}$$

given that the neutron flux (ϕ) equals :-

$$\phi = n v_0 \qquad \text{Eqn A4.8}$$

where n is the total neutron density and v_0 is the standard neutron velocity. The reaction rate (R) in the energy range 0 to 30 KeV therfore equals :-

$$R = \sigma_0 \, \phi \, N \qquad \text{Eqn A4.9}$$

Thus the reaction rate R is independent of neutron energy provided that a significant proportion of neutrons do not exceed 30 keV. The validity of this condition in rock matrices where the average neutron energy is not known exactly (due to the experimental difficulties in neutron spectroscopy at such low fluxes) may only be confirmed by theoretical multi group neutron transport calculations (see Section 3). As discussed in that section these show that the probability of neutrons reaching thermal energies in rock matrices generally exceeds 90% and thus the above condition may be said to hold.

The consequence of this is that the above described BF_3 counter which has been calibrated at thermal neutron energies may be accurately used to measure the flux of neutrons in rock matrices provided that a significant portion of those neutrons do not exceed 30 KeV. It also implies that the ^3He counter may also be used in the above energy range once calibrated against the BF_3 counter.

A4.1.5 The use of Cadmium as a neutron filter.

As stated in section A4.1.1 neutron spectroscopy is not possible with BF_3 proportional counters, since the energy of reaction products are virtually invariant with incident neutron energy. However a crude form of neutron spectroscopy may carried out if the counter is covered with metal foils

which may be used to filter neutrons of known energies through absorption (I.A.E.A., 1970). These "filter foils" should have a well characterised cross-section/energy dependence and exhibit a sharp cutoff in neutron absorbance. The most commonly used filter foil is Cd, the cross-section/energy dependence of which is shown in Fig A4.6. From this it may be seen that below 0.3 eV Cd has an absorption cross-section of about $2{,}000 \times 10^{-24}$ cm^2 whilst above 1 eV this drops to less than 10×10^{-24} cm^2. The intensity I_x of neutrons transmitted through an absorber of thickness x cm, is related to the incident neutron intensity I_o by :-

$$I_x = I_o \, e^{-\sigma_E N \, x} \qquad \text{Eqn A4.10}$$

Where σ_E is the absorption cross-section (cm^2) at an energy E and N is the number of absorbing nuclei cm^{-3}. For the Cd sheet used in these experiments x = 0.05 cm and $N = 4.6 \times 10^{22}$ atoms cm^{-3}. From equation A4.10 it may be calculated that :-

(1) At thermal neutron energies (0.025 eV) less than 0.3% of incident neutrons pass through the Cd shielding and into the counter.

(2) At neutron energies of 0.3 eV 10% of incident neutrons pass through the Cd shielding and into the counter.

(3) At neutron energies of >1 eV more than 98% of incident neutrons pass through the Cd shielding and into the counter.

Using the cutoff limits summarised in Fig A4.6 it is possible to state that where 0.5 mm Cd shielding is used as a neutron filter counts measured with the filter in place represent events due to neutrons in excess of 0.3 eV. The cylindrical Cd filters used in these experiments were manufactured by rolling 0.5 mm Cd sheets into diameters suitable for sliding over the respective detector assemble. The cylinders were spot welded to retain their shape and sprayed with a plastic compound to prevent corrosion and to enable the shielding to be safely handled (Cd metal is poisonous).

A4.2 Selection criteria for high sensitivity neutron detectors.

The main criterion for the choice of neutron detectors

which may be used in the natural environment are sensitivity and ruggedness. This criteria is met by both detectors discussed above however each of these detectors have their advantages and disadvantages. The major advantage of the ^{10}B detector is cost which is approximately a quarter of that of a ^{3}He counter of similar sensitivity. The advantage of the ^{3}He counter is greater sensitivity per unit volume and its ability to perform neutron spectroscopy. A disadvantage with the BF_3 is that because of the chemical reactivity of the filling gas it cannot be carried on aircraft.

Experience in the field has shown that BF_3 counters are to be preferred where size is unimportant because of their inherently large pulse amplitude. This reduces the possibility of electronic noise entering the counting system during amplification. The following sections discuss aspects to be considered when carrying out field measurements of the neutron flux in mines and boreholes.

A4.2.1 Neutron detection in mines.

Mines in which there is a risk of explosion from natural gases require that instruments are certified as being "intrinsically safe" before they may be used underground. Because of the high voltages used in either proportional counter neither are likely to meet the above criteria of being "intrinsically safe" and hence the above systems may not be used where the above requirement is enforced. This generally excludes measurements being made in coal mines. Other mines for example tin mines do not have such a requirement and hence the above described proportional counters may be used.

Most mines have high humidity and very often contain running water, this presents problems such as noise due to shorting of the high voltage across terminal connectors. The effect of this may be reduced by the use of SHV connectors and the sealing of the counter assembly and terminations in polyethylene together with silica gel desiccant. The instrumentation associated with the counters should be further protected by the use of plastic sheeting. Care should also be taken to avoid condensation when installing measuring equipment in mines. Condensation problems were reduced by allowing the counting system to warm up prior to being taken underground.

A4.2.2 Neutron detection in boreholes.

Proportional counters such as those described above have long been used as "Downhole detectors" for neutron logging techniques utilising artificial neutron sources. The sensitivity required by these techniques is much lower than that required to measure the low level natural flux and thus existing commercial logging systems cannot easily be used. Because of the lack of commercially available detectors a high sensitivity down hole neutron detection system was developed jointly with the physics department at the University of Bath. The system was primarily developed to enable the natural neutron flux to be measured in moderately deep (50-100 m) boreholes. The detection system was developed around a Centronics 150EB BF_3 proportional counter which was enclosed in a stainless steel probe unit together with integrated HV power supply, amplifier, single channel analyser and low voltage power supply. The probe was connected to the surface via a steel logging cable through which the primary power and signal were transmitted. Development of this unit is still being carried out at the University of Bath.

A4.3 Instrumentation.

Two types of analyser/counter configurations were used for counting pulses from the proportional counters described above. Initially a simple system similar to that described in NORDSTROM et al (1985) was used. This consisted of a Canberra 2006 Pre Amp, 2012 Spec Amp, 2031 Pulse Analyser, 3105 HV supply and 2089 Serial Scanner/Printer and was used for measurements made in April of 1985 at Rosemanowes Quarry. The use of this system for measuring neutron flux in the environment was severely limited as it was mains powered and only semi-portable.

A battery operated Canberra Series 10 portable multi channel analyser (MCA) which had a dwell time of up to 40 seconds in multi channel scaling (MCS) mode was used in situations where mains power was not available. The Series 10 MCA was also capable of pulse height analysis (PHA). In the field its internal NiCd batteries were supplemented by external lead acid 12V batteries. The current drain on the supplementary supply (whilst running the BF_3 proportional counter) was 1.25 Amps, thus with two 12V, 30 Amp hour

batteries connected in parallel collection of counts over periods in excess of 48 hours was possible. Schematic diagrams of both these systems are shown in Figs A4.7 and A4.8.

A4.3.2 Operating parameters.

Parameters varied to optimise counting conditions for the BF_3 and ^3He proportional detectors were high voltage (HV), amplification (gain), discrimination levels and pulse shaping. Initial settings were obtained from manufacturers literature prior to optimising the system. Optimised operating parameters used for the measurement of neutron flux with the BF_3 and ^3He counters are given in Table A4.1. Using these parameters the pulse height spectra shown in Figs A4.10 and A4.11 were obtained.

A4.4 Measurement of detector background.

The presence of background counts in either of the described amplification systems was checked by removing the detector and shielding the unconnected termination. The system was then operated under the conditions described above. In either case no counts were recorded in the region of interest over a 24 hour period. This indicates that background in the electronics of the amplification systems is nil.

Background counts due to the detectors were harder to quantify since in mines we are measuring "background" levels in rocks which are shielded from cosmic rays and further shielding of the detector would be impractical. The background of the BF_3 detector must be at least as low as the minimum recorded count rate. Two measurements one in the Bath stone mine at Corsham and the other in Wookey Hole gave count rates of less than 0.0020 counts per second. This must therefore be taken as the highest possible background. In practice the actual background should be much lower due to the particularly good discrimination of this detector against gamma and beta background. The background of the ^3He detector has not yet been quantified but from results obtained so far should be less than 0.005 counts per second.

The measurement of detector backgrounds will be significantly improved once a probe has been developed which may be totally immersed in water. Suspending such a detector

covered with a thin Cd shield in an underground lake will enable very low backgrounds to be measured (as the water will thermalise fast neutrons which will be subsequently absorbed by the Cd cover).

A4.5 Methods of measurement.

Because of the large variety of conditions met at each measuring site procedures were generally governed by local constraints, such as rock type, availability of suitable boreholes etc. However the following general procedure was applied:-

(1) Where possible measurements were carried out by inserting the detector into dry cylindrical boreholes (typically > 7.5 cm in diameter and > 3m in length), otherwise measurements were made against the wall or at the centre of small chambers. Measurements boreholes were taken to reflect the equilibrium flux present in the rock matrix, whilst those in other situations were taken to be less than the equilibrium flux due to absorption of neutrons by air, and geometric effects.

(2) The total neutron flux was the first measurement carried out at each site. This was made by placing the counter (wrapped in thin polyethylene sheeting) in or at site of measurement. Neutron counts were integrated over as long a period as possible to obtain good statistics. Neutron flux was then calculated by dividing the count rate (s^{-1}) by the sensitivity of the respective counter. The flux so measured was the flux of all neutrons with energies up to 30 KeV (Thermal and Epi-cadmium neutrons).

(3) A further measurement was generally made in an identical manner to that described above except that the counter was covered by a 0.5 mm thick Cd tube. The neutron flux so measured was the flux of all neutrons with energies between 0.3 eV and 30 KeV (Epi-cadmium neutrons).

This epi-cadmium flux was then subtracted from the total neutron flux measured in (2) to obtain the flux of neutrons with energies between 0 and 0.3 eV (thermal neutrons).

(4) At a later stage the ^3He counter described above was purchased and calibrated against the Centronics BF_3 counter. An attempt was then made to use the ^3He counter was to measure the neutron flux in a borehole at the Rosemanowes geothermal energy site.

A4.6 Results of BF^3 and ^3He counter measurements.

Measurements were made with the detector in a number of different positions (ie/ at different depths in the borehole, in the centre of a small chamber, at the side of a small chamber and in long passage ways) to obtain a comparison between epi-cadmium ratios (R_{Cd}) and total flux values. A detailed description of measurement sites is given in Appendix 2. Raw experimental data such as counting rates are given for each of the sites in Tables A4.2(a) to (i). Neutron flux measurements based on this data are presented and discussed in Section 3.

Table A4.1 Standard operating conditions for the Centronics 150 EB70/50L BF_3 and Harshaw ^3He neutron detectors.

(a) Centronics BF_3 using laboratory BIN based single channel analyser :-

High Voltage :- 3,600 V
High Voltage polarity :- positive
Pre-amplifier gain jumper :- position A to C
Spectroscopy amplifier gain :- coarse=16, fine=1.0
Time constant :- slow
Pulse analyser :- ΔE = 10V, low level window 1.5 V, window 8V
Sensitivity 242 counts min^{-1} per unit neutron flux (cm^{-2} S^{-1})

(b) Centronics BF_3 using portable series 10 MCA based multi channel analyser :-

High Voltage :- 3,600 V
High Voltage polarity :- positive
Pre-amplifier gain jumper :- position A to C
Amplifier gain :- 16
Time constant :- slow
Low level window :- ch = 60 (0.010 V)
Peak ch = 450 (0.078 V)
Sensitivity 242 counts min^{-1} per unit neutron flux (cm^{-2} S^{-1})

(c) Harshaw ^3He using portable Series 10 multi channel analyser (50m cable):-

High Voltage :- 1,250 V
High Voltage polarity :- positive
Pre-amplifier gain jumper :- position A to C
Amplifier gain :- 64
Time constant :- slow
Low level window :- ch = 70 (0.0024 V)
Peak ch = 150 (0.0052 V)

Table A4.2.(a) Results of measurements of neutron flux carried out at Rosemanowes Quarry.

SITE	TOTAL COUNTS	$2\sqrt{}$	TIME S	COUNT RATE S^{-1}	+/-
Surface (FM11)	28865	170	72000	0.4009	0.00236
Borehole C (April 85) (FM12, 13, 14)					
2.38m into face	7557	86	122400	0.0601	0.00070
4.18m into face	3454	59	93600	0.0369	0.00063
5.98m into face	12261	111	259200	0.0473	0.00043
Borehole C (May 87) (FM 15)					
3.80m into face	1420	38	40000	0.0355	0.00095
3.80m " " + Cd	232	15	32000	0.0073	0.00048
Borehole B (FM 16)					
3.80m into face	469	22	17940	0.0261	0.00123
Borehole C (June 87) (FM17)					
4.50m into face	2034	45	48000	0.0424	0.00094
Borehole C ^{3}He Counter (June 87)					
4.50 m into face	953	31	54780	0.0174	0.00056
Deep Verticle Borehole --- ^{3}He counter					
50m below surface	263	16	52200	0.0050	0.00031

Table A4.2.(b) Results of measurements of neutron flux carried out at South Crofty Mine

SITE	TOTAL COUNTS	$2\sqrt{}$	TIME S	COUNT RATE S^{-1}	+/-
Borehole A (FM20)					
No Cd shielding	2358	49	160000	0.0147	0.00030
Cd shielded	471	22	80000	0.0059	0.00027
Borehole B (FM21)					
No Cd shielding	1342	37	88000	0.0153	0.00042
Cd shielded	342	19	64000	0.0053	0.00029
Centre of small chamber (FM22)					
No Cd shielding	789	28	64000	0.0123	0.00044
Cd shielding	133	12	32000	0.0042	0.00036
Wall of small chamber (FM23)					
No Cd shielding	570	24	48000	0.0119	0.00050
Cd shielded	109	10	32000	0.0034	0.00033

Table A4.2.(c) Results of measurements of neutron flux carried out at Pendarves Mine.

SITE	TOTAL COUNTS	$2\sqrt{}$	TIME S	COUNT RATE S^{-1}	+/-
Borehole A (FM24)					
No Cd shielding	709	27	56000	0.0127	0.00048
Cd shielded	154	12	32000	0.0048	0.00039
Centre of passage (FM 25)					
No Cd shielding	404	20	56000	0.0072	0.00036
Cd shielded	47	7	24000	0.0020	0.00029

Table A4.2.(d) Results of measurements of neutron flux in Rosevale Mine.

SITE	TOTAL COUNTS	$2\sqrt{}$	TIME S	COUNT RATE S^{-1}	+/-
Centre of passage (FM27)					
No Cd shielding	396	19.9	80000	0.0050	0.00025

Table 5.4.1(e) Results of measurements of neutron flux carried out at Nottingham Castle.

SITE	TOTAL COUNTS	$2\sqrt{}$	TIME S	COUNT RATE S^{-1}	+/-
Surface (FM1)	3492	59	8000	0.4365	0.00739
Sandstone cavern 20m below surface					
Away from the wall (FM3)					
No Cd shielding	1219	35	84000	0.0145	0.00042
Cd shielded	542	23	79980	0.0068	0.00029
Close to the wall (FM2)					
No Cd shielding	385	20	28000	0.0138	0.00070
Cd shielded	730	27	88000	0.0083	0.00031
Centre of chamber (FM4)					
No Cd shielding	1775	42	128000	0.0139	0.00033

Table A4.2.(f) Results of measurements of neutron flux carried out at Bath University.

SITE	TOTAL COUNTS	$2\sqrt{}$	TIME S	COUNT RATE S^{-1}	+/-
Surface (in hut) (FM5)					
No Cd shielding	84402	290	160000	0.528	0.0018
Cd shielded	7952	89	160000	0.0497	0.0006

Table A4.2.(g) Results of measurements of neutron flux carried out at Bath University in a Sand Pit (bulk density = 1.6 gcm^{-3}).

Depth below surface (m)		TOTAL COUNTS	$2\sqrt{S}$	TIME S^{-1}	COUNT RATE +/-	
Surface	(FM6)	3811	62	9561	0.399	0.006
0.50	(FM7)	37669	194	80937	0.465	0.002
1.20	(FM8)	16429	128	50699	0.324	0.003

Table A4.2.(h) Results of measurements of neutron flux carried out at Bath Stone Mine (cavern 30m below surface).

SITE	TOTAL COUNTS	$2\sqrt{S}$	TIME S	COUNT RATE S^{-1}	+/-
Mined slot (FM9)					
No Cd shielding	567	24	100000	0.00567	0.00024
Cd shielded	382	20	152000	0.00251	0.00013
Centre of chamber (FM10)					
No Cd shielding	736	27	144000	0.00511	0.00019
Cd shielded	216	15	112000	0.00193	0.00013

Table A4.2.(i) Results of measurements of neutron flux carried out at Wookey Hole Cave (cavern 50 m below surface).

SITE	TOTAL COUNTS	$2\sqrt{S}$	TIME S	COUNT RATE S^{-1}	+/-
Centre of chamber (FM26)					
No Cd shielding	293	17	74575	0.00393	0.00023
Cd shielded	12	3.5	6526	0.00184	0.00054

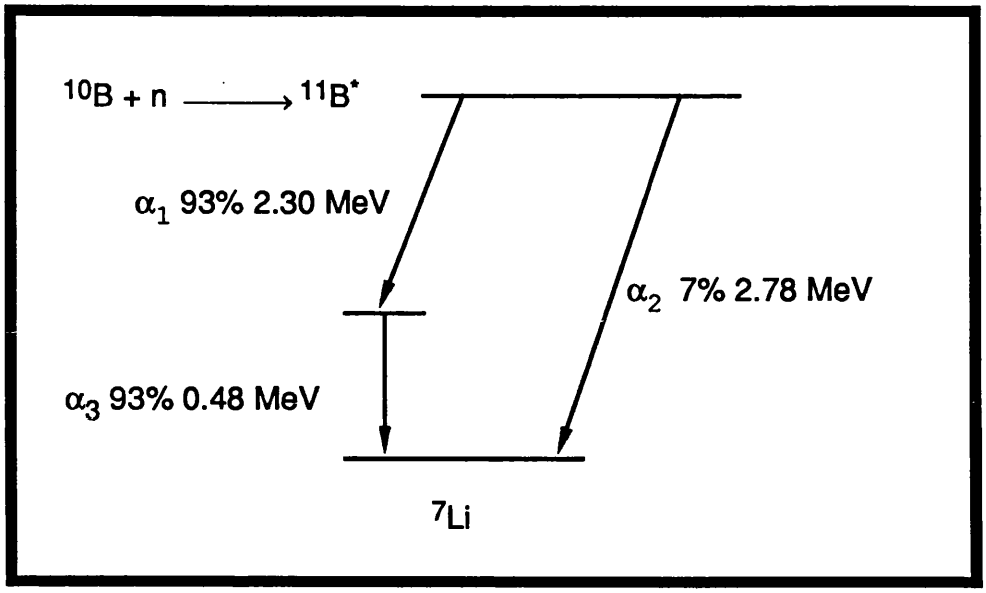

Particles	Kinetic energy MeV
α_1 + Li_1 recoil nucleus	2.30
α_1	1.47
Li_1 recoil nucleus	0.83
α_2 + Li_2 recoil nucleus	2.78
α_2	1.77
Li_2 recoil nucleus	1.01
α_3	0.48

Fig A4.1 Decay scheme and energy partition for the reaction $^{10}B(n,\alpha)^7Li$.

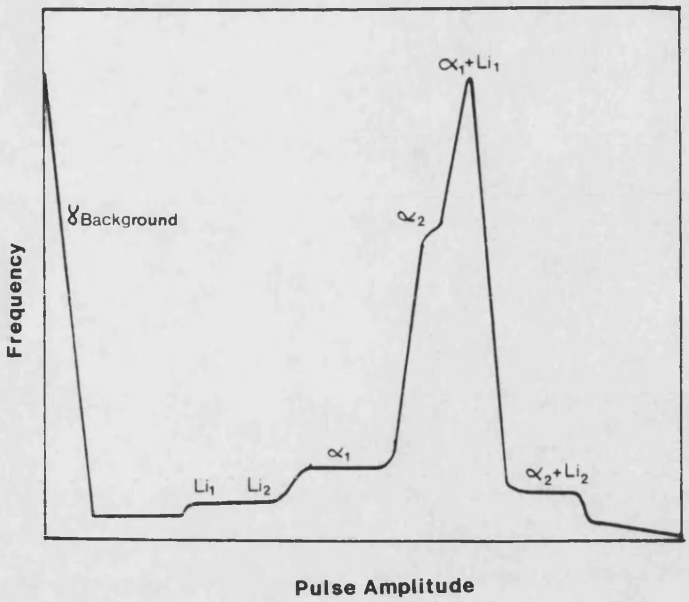

Fig A4.2 Theoretical pulse height spectrum for a typical BF_3 filled proportional counter.

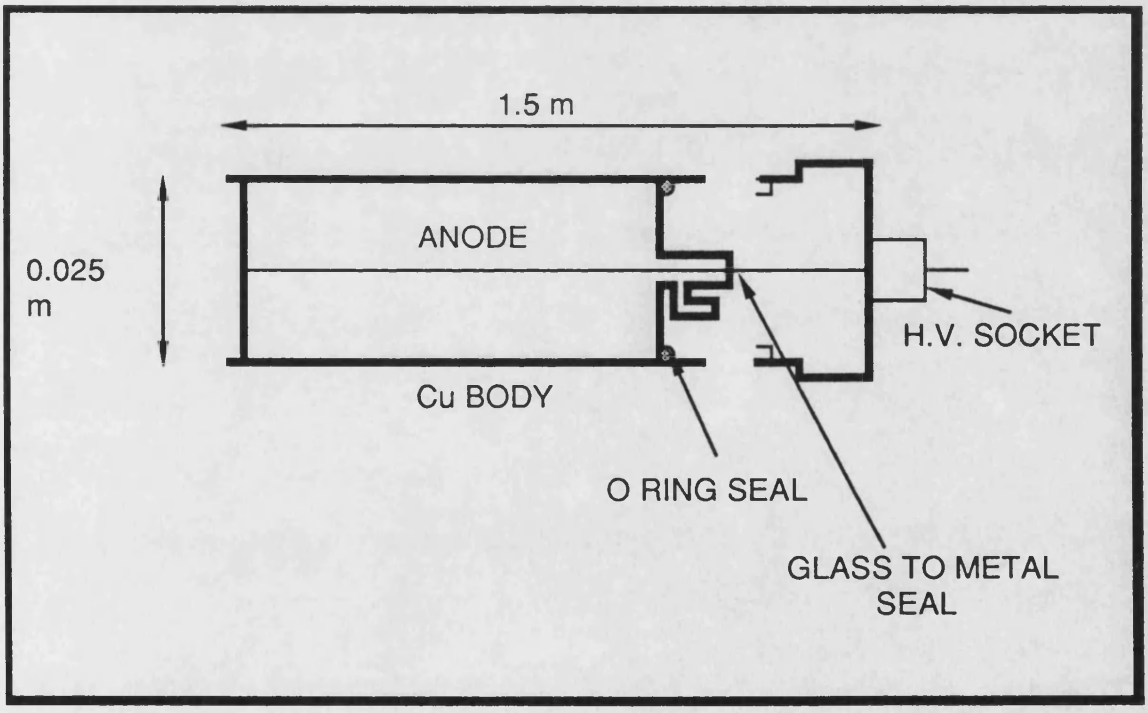

Fig A4.3 Schematic diagram showing the components of the Centronics BF_3 proportional counter.

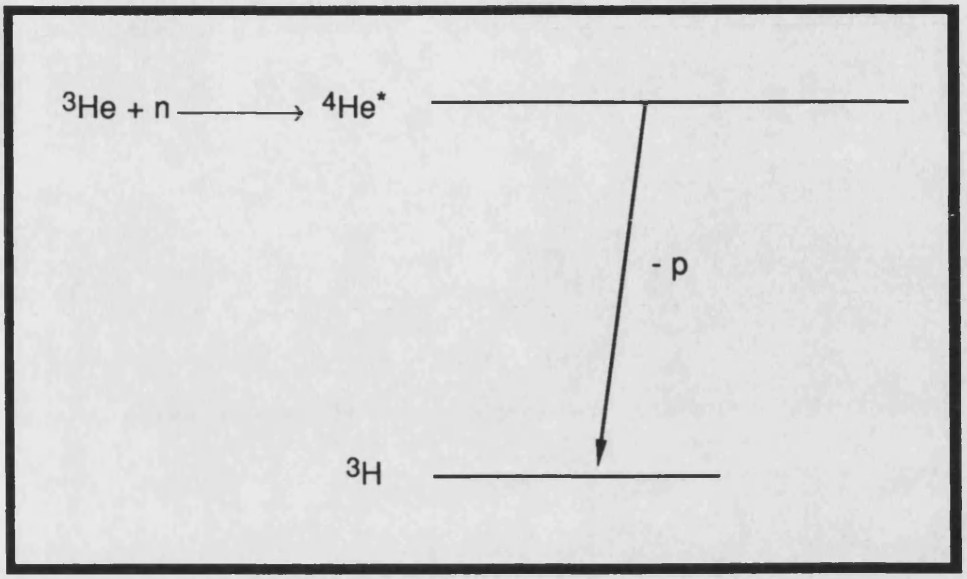

Fig A4.4 Energy decay scheme for the reaction $^3He(n,p)^3H$.

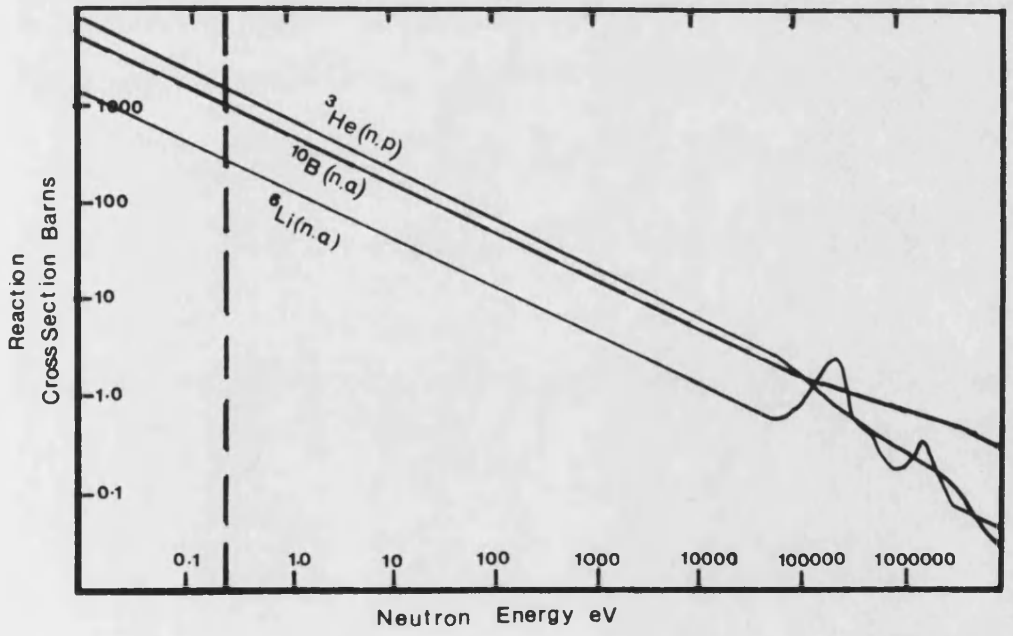

Fig A4.5 The variation of reaction cross-section with neutron energy for the reactions $^3He(n,p)$, $^{10}B(n,\alpha)$ and $^6Li(n,\alpha)$.

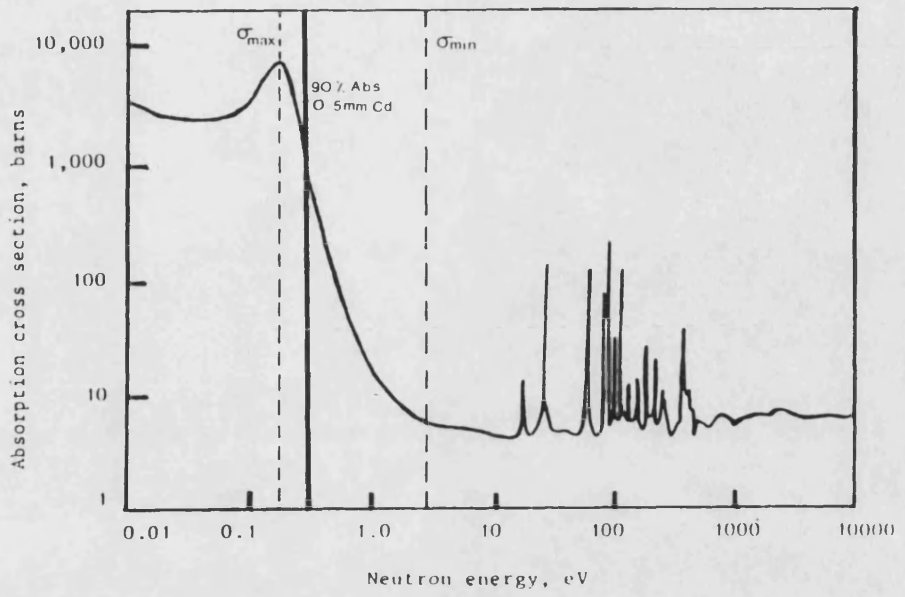

Fig A4.6 The variation of reaction cross-section with neutron energy for the reaction Cd(n,γ).

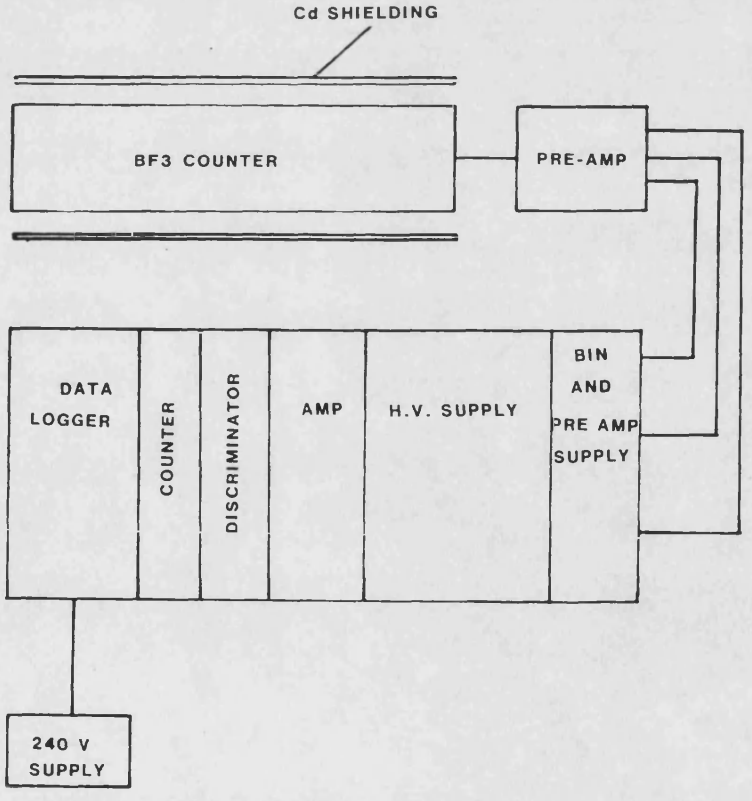

Fig A4.7 Schematic diagram of the laboratory based neutron counting system.

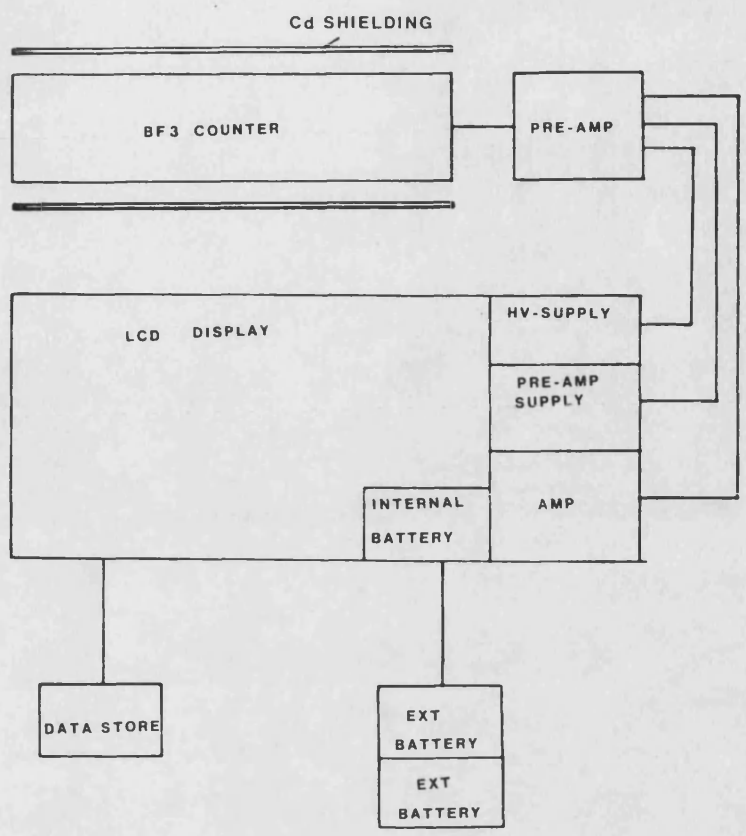

Fig A4.8 Schematic diagram of the portable neutron counting system based on a Canberra Pakard series 10 MCA.

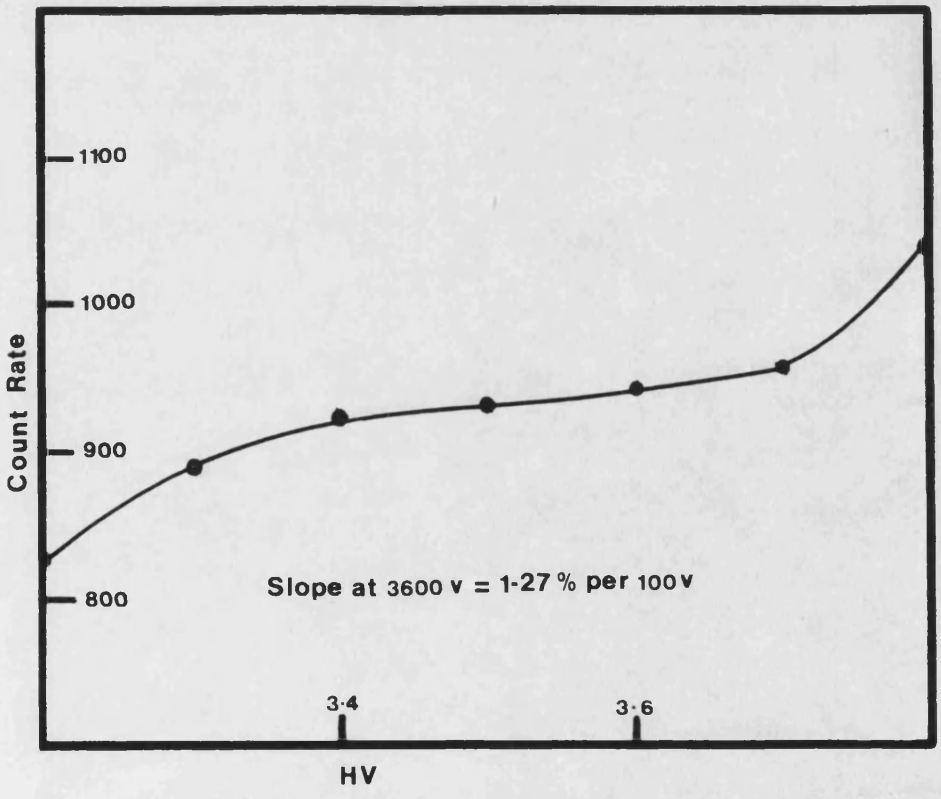

Fig A4.9 Plot of applied high voltage (HV) vs countrate for the Centronics EB150 BF_3 proportional counter.

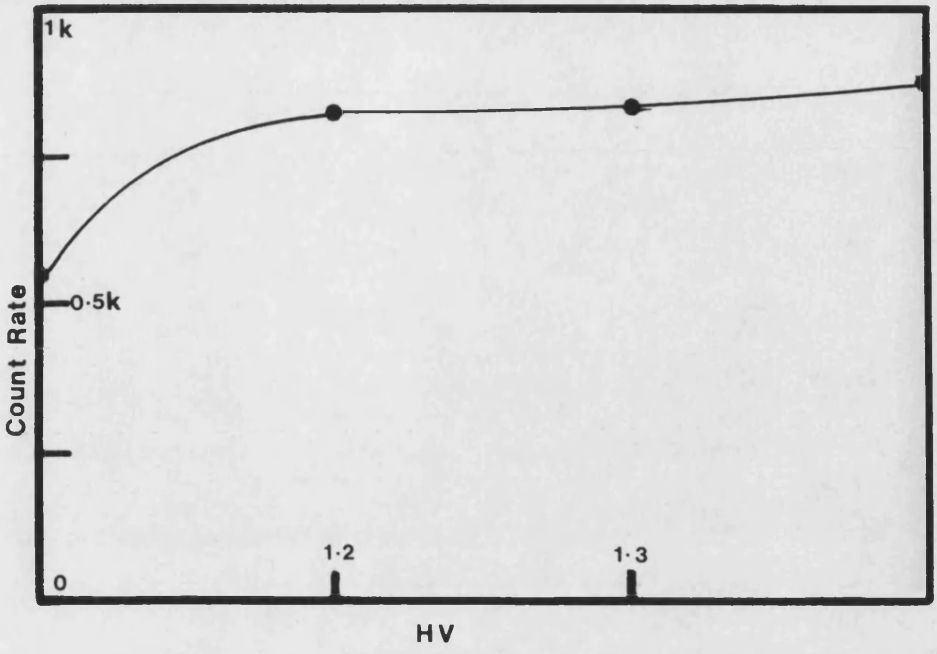

Fig A4.10 Plot of applied high voltage (HV) vs countrate for the Harshaw ^{3}He proportional counter.

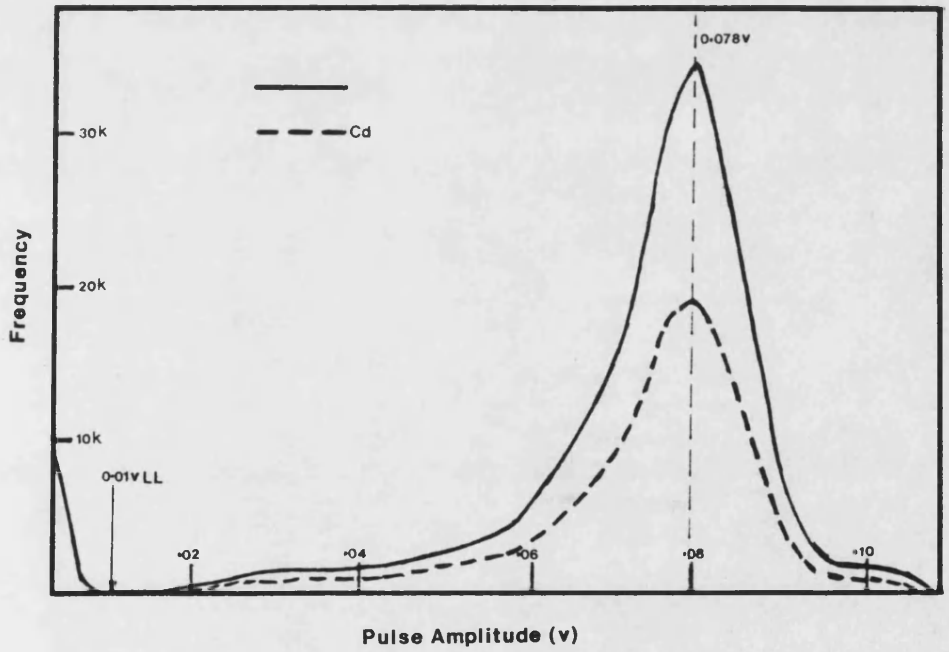

Fig A4.11 Pulse height spectra obtained using the Centronics EB150 BF_3 proportional counter under standard operating conditions (see table A4.), voltages correspond to those after the pre-amplifier.

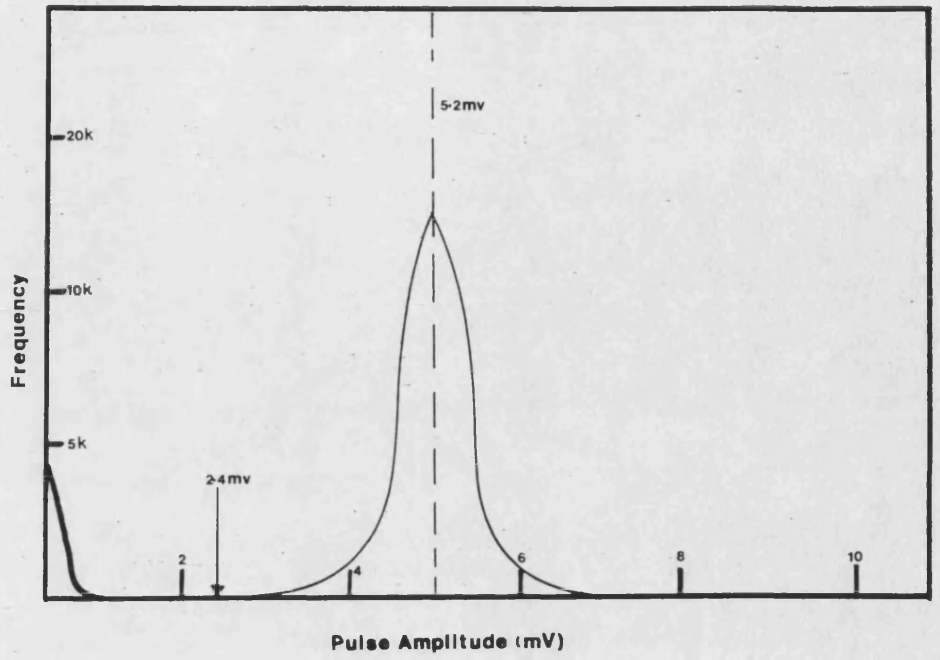

Fig A4.12 Pulse height spectra obtained using the Harshaw ^{3}He proportional counter under standard operating conditions (see Table A4.), voltages correspond to those after the pre-amplifier.

APPENDIX 5 COMPUTER PROGRAMS

This section contains a listing of the computer program "Isotope Production" that calculate the production rate of neutrons and isotopes in rock matrices below the Earth's surface. To save space the a listing of the data output routine has been omitted.

```
REM PROGRAM "ISOTOPE PRODUCTION" LAST EDITED 1 MAY 89  BS
REM CALCULATES NEUTRON FLUX AND IN-SITU ISOTOPE PRODUCTION DUE TO SURFACE PHENOMENA

SUB-ROUTINE 1 INITIALISE ARRAYS AND VARIABLES AND INPUT DATA.
DIM ELEMENT$(25), ATOMWT(25), PZ(25), RZ(25), CROSSECT(25), ABUND(25, 5), ERRCROSSECT(25), ERRABUND(25, 5), SIGMA(25)
DIM ERRSIGMA(25), TEMPABUND(25, 5), AST$(25), ID$(5)
DIM DEPTH(10), NPMU(10), NPPIPRO(10), NPSPF(10), NPALPH(10), NPTOT(10), NFLUX(10)
DIM HPP(10), HPLI(10), HPB(10), HMU6LI(10), HMU16O(10), HMU28SI(10)
DIM CPP(10), CPN(10), CPO(10), CMU16O(10), CMU17O(10), CMU15N(10)
DIM CLPK(10), CLPCA(10), CLPNG(10), CLPKNA(10), CLRAT(10), CLMU39K(10), CLMU40CA(10)
DIM AR37PK(10), AR37PCA(10), AR37PFE(10), AR37PNA(10), AR37MU39K(10), AR37MU40CA(10)
DIM AR39PK(10), AR39PCA(10), AR39PFE(10), AR39PKNA(10), AR39PCANA(10), AR39MU39K(10), AR39MU40K(10), AR39MU40CA(10),
AR39MU42CA(10)
REM READ DATA
FOR I = 1 TO 24
READ ELEMENT$(I), ATOMWT(I), CROSSECT(I), ERRCROSSECT(I), PZ(I), RZ(I)
FOR X = 1 TO 5
READ TEMPABUND(I, X)
ERRABUND(I, X) = TEMPABUND(I, X) * .1
NEXT X
NEXT I
REM DATA FRACTIONAL ABUNDANCES (PARKER., 1968) CROSS SECTIONS FROM BNL 325., 1958)
REM ELEMENT    AT/WT    ABS C/S    +/-      PZ      RZ       STRIPA       GRANITE      SANDSTONE  CARBONATE  CLAY/SHALE
DATA   LI,       6.94 ,    71.000,   1.000,     ,     ,    0.000011,    0.000040,    0.000015 ,  0.000005 ,  0.000060
DATA   B ,      10.81 ,   755.000,   2.000,     ,     ,    0.000004,    0.000015,    0.000035 ,  0.000020 ,  0.000100
DATA   NA,      22.99 ,     0.505,   0.010,   1.0,    0.42 ,  0.030200,    0.027700,    0.003300 ,  0.000400 ,  0.006600
DATA   MG,      24.31 ,     0.063,   0.003,   0.93,   0.46 ,  0.001570,    0.005600,    0.007000 ,  0.047000 ,  0.013400
DATA   AL,      26.98 ,     0.230,   0.005,   0.76 ,  0.51 ,  0.074100,    0.077000,    0.025000 ,  0.004200 ,  0.104500
DATA   SI,      28.08 ,     0.160,   0.020,   0.84 ,  0.56 ,  0.359000,    0.323000,    0.368000 ,  0.240000 ,  0.238000
```

```
DATA    CL,      35.45 ,    33.600,   1.100,    ,     ,      0.000160,   0.000240,   0.000010 ,   0.000150 ,   0.000160
DATA    K ,      39.10 ,     2.070,   0.070,  1.54 ,  0.79 ,  0.038400,   0.033400,   0.010700 ,   0.002700 ,   0.022800
DATA    CA,      40.08 ,     0.440,   0.020,  1.90 ,  0.84 ,  0.005150,   0.015800,   0.039100 ,   0.302300 ,   0.025300
DATA    TI,      47.90 ,     5.800,   0.400,    ,     ,      0.000480,   0.002300,   0.001500 ,   0.000400 ,   0.004500
DATA    CR,      51.99 ,     3.100,   0.200,    ,     ,      0.0000017,  0.000025,   0.000035 ,   0.000011 ,   0.000100
DATA    MN,      54.93 ,    13.200,   0.200,    ,     ,      0.000460,   0.000600,   0.000050 ,   0.001100 ,   0.000670
DATA    FE,      55.85 ,     2.530,   0.060,  3.28,   0.90 ,  0.009300,   0.027000,   0.009800 ,   0.003800 ,   0.033000
DATA    CO,      58.93 ,    37.000,   1.500,    ,     ,      0.0000007,  0.000005,   0.0000003,  0.0000001,  0.000020
DATA    NI,      58.71 ,     4.800,   0.200,    ,     ,      0.000008,   0.000008,   0.000002 ,   0.000020 ,   0.000095
DATA    SM,     150.35 ,  5600.00,   200.,      ,     ,      0.0000114,  0.000009,   0.000010 ,   0.0000013,  0.0000065
DATA    GD,     157.25 , 46000.00,  1000.,      ,     ,      0.0000129,  0.000009,   0.000010 ,   0.0000013,  0.0000065
DATA    BE,       9.01 ,     0.009,   0.001,    ,     ,      0.0000055,  0.0000055,  0.0000005,  0.0000005,  0.000003
DATA    O,       15.99 ,     0.00,    0.00 ,  1.0,    0.28 ,  0.480000,   0.487000,   0.480000 ,   0.479600 ,   0.528000
DATA    F,       18.99 ,     0.009,   0.001,    ,     ,      0.000440,   0.000800,   0.000270 ,   0.000330 ,   0.000500
DATA    C,       12.00 ,     4.700,   0.47 ,    ,     ,      0.000300,   0.000300,   0.010000 ,   0.090690 ,   0.010000
DATA    U,      238.03 ,    50.00 ,   0.5  ,    ,     ,      0.000044,   0.0000035,  0.00000045, 0.0000022,  0.0000037
DATA    TH,     232.04 ,    14.00 ,   0.14 ,    ,     ,      0.000033,   0.000018,   0.0000017,  0.0000017,  0.000012
DATA    N,       14.00 ,    10.5  ,   0.11 ,    ,     ,      0.000020,   0.000020,   0.000005 ,   0.000005 ,   0.000600
REM TITLE FOR CALCULATION
CLS : PRINT "  INPUT TITLE FOR CALCULATION"
INPUT TITLE$
REM ROUTINE TO ALLOW DATA MODIFICATION DUE TO CHEMICAL ANALYSIS OF SPECIFIC ROCK SAMPLE.
FOR X = 1 TO 5: READ ID$(X): NEXT X
DATA STRIPA GRANITE, AVERAGE GRANITE,SANDSTONE,LIMESTONE,CLAY/SHALE
5 CLS : PRINT "ENTER NUMBER FOR ROCK MATRIX TYPE"
PRINT : PRINT : PRINT "      1    STRIPA GRANITE"
PRINT "      2    AVERAGE GRANITE"
PRINT "      3    SANDSTONE"
PRINT "      4    LIMESTONE"
```

```
PRINT "       5     CLAY/SHALE"
PRINT : INPUT "       ", ID
PRINT : PRINT : PRINT USING "     YOU HAVE SELECTED \            \ "; ID$(ID)
PRINT : PRINT "       CONFIRM WITH Y OR N"
7 Q$ = INKEY$
IF Q$ = "Y" GOTO 9
IF Q$ = "N" GOTO 5
IF Q$ <> "Y" OR Q$ <> "N" THEN GOTO 7
9 FOR I = 1 TO 24
CLS : PRINT USING "AMEND DATA FOR \  \       Y  OR  N"; ELEMENT$(I)
12 OPT$ = INKEY$
IF OPT$ = "Y" GOTO 14
IF OPT$ = "N" THEN ABUND(I, ID) = TEMPABUND(I, ID)
IF OPT$ = "N" THEN ERRABUND(I, ID) = TEMPABUND(I, ID) / 10
IF OPT$ = "N" THEN GOTO 16
IF OPT$ <> "Y" OR OPT$ <> "N" THEN GOTO 12
14 CLS : PRINT "INPUT ABUNDANCE (PPM) AND ERROR (PPM) FOR "; ELEMENT$(I)
PRINT : PRINT : INPUT ABUND(I, ID), ERRABUND(I, ID)
ABUND(I, ID) = ABUND(I, ID) * .000001
ERRABUND(I, ID) = ERRABUND(I, ID) * .000001
IF ERRABUND(I, ID) < .00000001# THEN ERRABUND(I, ID) = ABUND(I, ID) / 10
AST$(I) = "*": GOTO 18
16 AST$(I) = ""
18 NEXT I

SUB-ROUTINE 2 CALULATION OF MACROSCOPIC NEUTRON ABSORPTION CROSS-SECTION
FOR I = 1 TO 17
SIGMA(I) = (ABUND(I, ID) / ATOMWT(I)) * CROSSECT(I)
ERRSIGMA(I) = (((ERRABUND(I, ID) / ABUND(I, ID)) ^ 2 + (ERRCROSSECT(I) / CROSSECT(I)) ^ 2) ^ .5) * SIGMA(I)
```

```
NEXT I
REM SUMMATION NACS = NEUTRON ABSORPTION CROSS SECTION
FOR I = 1 TO 17
SUMSIGMA = SUMSIGMA + SIGMA(I)
ERRSUMSIGMA = ERRSUMSIGMA + (ERRSIGMA(I) ^ 2)
SUMABUND = SUMABUND + ABUND(I, ID)
NEXT I
ERRSUMSIGMA = ERRSUMSIGMA ^ .5
NACS = SUMSIGMA * .6023: ERRNACS = ERRSUMSIGMA * .6023: REM CM2/G
REM RESULTS ON SCREEN
GOSUB 1000
PRINT "     ******  DO YOU REQUIRE HARD COPY ?   Y OR N  ******"
40 Q$ = INKEY$
IF Q$ = "Y" THEN GOSUB 1500
IF Q$ = "N" GOTO 100
IF Q$ = "Y" GOTO 100
IF Q$ <> "Y" OR Q$ <> "N" THEN GOTO 40

SUB-ROUTINE 3   CALULATION OF NEUTRON YIELD FORM (A,N) AND SPONTANEOUS FISSION REACTIONS.
DIM NYU(15), NYTH(15), MSP(15), ERRORNU(15), ERRORNT(15)
DIM A(15, 4), B(15, 4), N(14)
REM  DATA READ
FOR I = 1 TO 12
READ MSP(I), NYU(I), NYTH(I)
ERRORNU(I) = NYU(I) * .08
ERRORNT(I) = NYTH(I) * .08
NEXT I
DATA 652,21.4,9.24    :          REM LI
DATA 623,254 ,86.6    :          REM BE
```

```
DATA 619,64.2,18.7    :          REM B
DATA 609,0.236,0.0785            REM O
DATA 531,31.6,12.5    :          REM F
DATA 503,12.5,5.75    :          REM NA
DATA 520,5.52,2.33    :          REM MG
DATA 493,4.88,2.39    :          REM AL
DATA 501,0.681,0.320             REM SI
DATA 455,0.366,0.087             REM K
DATA 453,0.016,0.004             REM CA
DATA 395,0.166,0.189             REM FE
REM IDENTIFY ABUNDANCE DATA
FOR I = 1 TO 12
READ N(I): NEXT I
DATA  1,18,2,19,20,3,4,5,6,8,9,13
UCONC = ABUND(22, ID) * 1000000!: ERRUCONC = ERRABUND(22, ID) * 1000000!
IF ERRUCONC < .001 THEN ERRUCONC = UCONC * .05
THCONC = ABUND(23, ID) * 1000000!: ERRTHCONC = ERRABUND(23, ID) * 1000000!
IF ERRTHCONC < .001 THEN ERRTHCONC = THCONC * .05
REM CALCULATION ERRORS AND NEUTRON YIELDS
X = 0
Y = 0
Z = 0
ERRORX = 0
ERROTY = 0
ERRORZ = 0
FOR I = 1 TO 12
A(I, 1) = MSP(I) * ABUND(N(I), ID): REM STOPPING POWER
B(I, 1) = ERRABUND(N(I), ID) * MSP(I): REM ERROR STOPPING POWER
A(I, 2) = MSP(I) * ABUND(N(I), ID) * NYU(I): REM N-YIELD U
```

```
B(I, 2) = ((((ERRABUND(N(I), ID) / ABUND(N(I), ID)) ^ 2) + ((ERRORNU(I) / NYU(I)) ^ 2)) ^ .5) * A(I, 2)
A(I, 3) = MSP(I) * ABUND(N(I), ID) * NYTH(I): REM N-YIELD TH
B(I, 3) = ((((ERRABUND(N(I), ID) / ABUND(N(I), ID)) ^ 2) + ((ERRORNT(I) / NYTH(I)) ^ 2)) ^ .5) * A(I, 3)
NEXT I
REM  SUMMATION
FOR I = 1 TO 12
X = X + A(I, 1)          : REM SUM STOPING POWER
Y = Y + A(I, 2)          : REM SUM N-YIELD U
Z = Z + A(I, 3)          : REM SUM N-YIELD TH
ERRORX = ERRORX + (B(I, 1) ^ 2)
ERRORY = ERRORY + (B(I, 2) ^ 2)
ERRORZ = ERRORZ + (B(I, 3) ^ 2)
NEXT I
REM FINAL CALC
ERRORX = ERRORX ^ .5
ERRORY = ERRORY ^ .5
ERRORZ = ERRORZ ^ .5
XSUMERROR = ERRORX
YSUMERROR = ERRORY
ZSUMERROR = ERRORZ
NYIELDURAN = Y / X     : REM SUM N-YIELD U/SUM STOPPING POWER
NYIELDTHOR = Z / X     : REM SUM N-YIELD TH/SUM STOPPING POWER
ERRORY = ((ERRORY / Y) ^ 2 + (ERRORX / X) ^ 2) ^ .5 * Y / X: REM ERROR IN URANIUM N YIELD
ERRORZ = ((ERRORZ / Z) ^ 2 + (ERRORX / X) ^ 2) ^ .5 * Z / X : REM ERROR IN THORIUM N YIELD

REM  NEUTRON PRODUCTION CALC
NURAN = UCONC * NYIELDURAN      : REM NETRONS PER YEAR PER G
NTHOR = THCONC * NYIELDTHOR     : REM NEUTRONS PER YEAR PER G
U238ATOMS = UCONC * 6.02E+17 * .9927 / 238.03: REM UCONC IN PPM
LAMBDASFU238 = 8.5E-17: REM YEARS^-1
```

```
NPSPF = U238ATOMS * LAMBDASFU238 * 2.03 : REM NEUTRONS PER YEAR PER G ROCK
NEUTSF = NPSPF / UCONC                                    : REM NEUTRON PER YEAR PER UG U
ERRORNURAN = ((ERRORY / NYIELDURAN) ^ 2 + (ERRUCONC / UCONC) ^ 2) ^ .5 * NYIELDURAN * UCONC
ERRORNTHOR = ((ERRORZ / NYIELDTHOR) ^ 2 + (ERRTHCONC / THCONC) ^ 2) ^ .5 * NYIELDTHOR * THCONC
ERRORSFURAN = (((ERRUCONC / UCONC) ^ 2 + .025 ^ 2) ^ .5) * NPSPF
REM NPALPH = NEUT.PROD.ALPHA-N   NPSPF = NEUT.PROD.SPONT.FISSION    TO PASS TO NEUTFLUX CALC (200)
NPALPH = NYIELDURAN * UCONC + NYIELDTHOR * THCONC: TOTAL = NPALPH + NPSPF
TOTALERROR = (ERRORNURAN ^ 2 + ERRORNTHOR ^ 2 + ERRORSFURAN ^ 2) ^ .5
REM RESULTS TO SCREEN
GOSUB 2000
PRINT : PRINT "DO YOU REQUIRE HARD COPY ?  Y OR N"
180 Q$ = INKEY$
IF Q$ = "Y" THEN GOSUB 2500
IF Q$ = "N" GOTO 200
IF Q$ = "Y" GOTO 200
IF Q$ <> "Y" OR Q$ <> "N" THEN GOTO 180

SUB-ROUTINE 4 CALCULATION OF NEUTRON PRODUCTION FROM COSMIC RAYS.
INPUT " LATITUDE  (N=+, S=-)              ", LAT
INPUT " LONGITUDE  (E=+, W=-)             ", LNG
INPUT " ALTITUDE OF SITE (METRES ASL)       ", ALT
INPUT " DENSITY OF ROCK MATRIX (G/CM3)       ", DENSITY
300 REM ***  GEOMAGNETIC LATITUDE CALC ***
PI = 3.141593
B = (90 - LAT) * PI / 180
A = ABS(LNG + 69) * PI / 180: REM 69 = LONG GEOMNP
C = (90 - 78.3) * PI / 180: REM 78.3 = LAT GEOMNP
COSA = COS(B) * COS(C) + SIN(B) * SIN(C) * COS(A)
TANA = ((1 - COSA ^ 2) / COSA ^ 2) ^ .5
```

```
GEOMLAT = 90 - ATN(TANA) * 180 / PI
IF GEOMLAT < 0 THEN GEOMLAT = -GEOMLAT
REM CALC ALT AND LAT FACTORS FOR PION/PROTON AND MUON PROD. OF NEUTRONS
REM NORMALISED TO 1 FOR SEA LEVEL AND >60N RESPECTIVELY.  MEASUREMENTS MADE AT 40 N GEOMAGNETIC
REM MUST BE CORRECTED BY MULTIPLICATION BY 1.57.
IF GEOMLAT < 32.5 GOTO 315
LATFACPIPRO = -.000025196# * GEOMLAT ^ 3 + .0032249 * GEOMLAT ^ 2 - .112447 * GEOMLAT + 1.582842
GOTO 320
315 LATFACPIPRO = 2.0818E-05 * GEOMLAT ^ 3 - .000922913# * GEOMLAT ^ 2 + .018778 * GEOMLAT + .119907
320 IF LATFACPIPRO > 1 THEN LATFACPIPRO = 1
LATFACMU = .014 * (GEOMLAT - 5) + .33       : REM LAT DEPENDENCE MUONS AT SEA LEVEL
IF LATFACMU < .33 THEN
LATFACMU = .33
ELSEIF LATFACMU > 1! THEN
LATFACMU = 1!
END IF
REM ALTFACPIPRO = MEAN COSMOGENIC NUCLIDE PROD. RATE REL. TO SEA LEVEL (YOKOYAMA ET AL 1977)
ALTFACPIPRO = 9.4558E-11 * ALT ^ 3 + 9.88E-08 * ALT ^ 2 + .0008529 * ALT + .98363
IF ALTFACPIPRO < 1 THEN ALTFACPIPRO = 1
ALTFACMU = 6.02E-12 * ALT ^ 3 + 1.4E-07 * ALT ^ 2 + .000278 * ALT + .977
IF ALTFACMU < 1 THEN ALTFACMU = 1
REM *******  CALC NEUTRON PRODUCTION IN N/G/A AT DEPTHS 0.1 TO 100 M *******
FOR D = 1 TO 7:  REM  ********************  START  LOOP  ****************************
READ DEPTH(D)
DATA 1,2,3,5,40,80,100
THICK = 100 * DEPTH(D) * DENSITY: REM ROCK THICKNESS G/CM2
REM CALC NPMU = NEUT PROD BY MUONS AT DEPTH(D) FOR >60 N
IF DEPTH(D) < .1 THEN NPMU(D) = 115: GOTO 330: REM SKIP FOR LOW DEPTHS SINCE MUON PROD <<< THAN PION/PROTON
LNTHICK = LOG(THICK)
```

```
NPMU(D) = -14.40356 + (25.9471 * LNTHICK) - (14.0439 * LNTHICK ^ 2) + (3.8153 * LNTHICK ^ 3) - (.545453 * LNTHICK ^ 4) + (.038989 * LNTHICK
^ 5) - (.0011027 * LNTHICK ^ 6)
NPMU(D) = EXP(NPMU(D))
NPMU(D) = NPMU(D) * 1.2195: REM CORRECT MUON PROD TO LATITUDES > 60 N.
330 NPMU(D) = NPMU(D) * ALTFACMU * LATFACMU: REM CORR MUON PRODUCTION
IF NPMU(D) < 0 THEN NPMU(D) = 0
340 REM CALC NPPIPRO =NEUT PROD BY PION/PROTONS SEE YAMASHITA ET AL 1966
NPPIPRO = 1190 * EXP(-THICK / 170)
REM 1190 = SEA LEVEL INTENSITY >60 DEG. N   170 = ATTENUATION LENGTH SEE YAMASHITA ET AL 1966.
NPPIPRO(D) = NPPIPRO * ALTFACPIPRO * LATFACPIPRO: REM CORR NPPIPRO
REM CALC NPSPF AND NPALPH = NEUT PROD BY SF AND N,A REACTIONS
NPSPF(D) = NPSPF: REM N/G/A
NPALPH(D) = NPALPH: REM N/G/A
REM CALC TOTAL NEUTRON PRODUCTION (N/G/A) AND FLUX
NPTOT(D) = NPMU(D) + NPPIPRO(D) + NPALPH(D) + NPSPF(D)
IF DEPTH(D) < .1 THEN GOTO 345: REM CALC FOR NON EQUILIBRIUM REGION
NFLUX(D) = NPTOT(D) / (NACS * 3600 * 24 * 365): REM PER CM2 PER SECOND
GOTO 346
345 REM CORRECT FOR NON-EQUIL REGION AS O'BRIEN ET AL 1978
CORR = .2992857 + .0496428 * THICK - .00130357# * THICK ^ 2 + .0000125# * THICK ^ 3
NFLUX(D) = NPTOT(D) * CORR / (NACS * 3600 * 24 * 365): REM PER CM2 PER SECOND
SUB-ROUTINE 5  SUM M_Z P_Z  TO AID CALCULATION OF ISOTOPE PRODUCTION RATES FROM ⁻μ INTERACTIONS
347 REM SUM MZPZ FOR O,NA,MG,AL,SI,K,CA,FE.
SUMMZPZ = (ABUND(19, ID) * PZ(19)) / 16 + (ABUND(3, ID) * PZ(3)) / 23
SUMMZPZ = SUMMZPZ + (ABUND(4, ID) * PZ(4)) / 24.31 + (ABUND(5, ID) * PZ(5)) / 26.98 + (ABUND(6, ID) * PZ(6)) / 28.08
SUMMZPZ = SUMMZPZ + (ABUND(8, ID) * PZ(8)) / 39.1 + (ABUND(9, ID) * PZ(9)) / 40.01 + (ABUND(13, ID) * PZ(13)) / 55.85
```

```
REM ******* SUB-ROUTINE 6          3H
346 REM HPP = H-3 PROD BY SPALLATION - SEE YOYOYAMA ET AL 1977
LICONC = ABUND(1, ID): BCONC = ABUND(2, ID): REM FRACTIONAL ABUND TAKE AS EQUIV TO G IN THIS CASE.
LAMBDAH3 = .693 / 12.43: REM H-3 DECAY CONST. A-1
DEPTHATTEN = EXP(-THICK / 170): REM DEPTH ATTENUATION OF REACTIONS SIMILAR TO THAT FOR N PRODUCTION
HPPCORR = ALTFACPIPRO * LATFACPIPRO * DEPTHATTEN
HPP(D) = 117 * HPPCORR: REM ATOMS / G / A (FROM SPALL OF LIGHT ELEMENTS) AT SEA LEVEL AND > 60 GEO LAT
HPLI(D) = (LICONC * .0742 * 6.02E+23 / 6.94) * 9.4E-22 * NFLUX(D) * 60 * 60 * 24 * 365   : REM LI6(N,A)H3 /G/A
HPB(D) = (BCONC * .1961 * 6.02E+23 / 10.81) * 1E-24 * NFLUX(D) * 60 * 60 * 24 * 365    : REM B10(N,2A)H3 /G/A
REM              ND    ,   MZ                    , PZ,  RZ ,  RP
HMU6LI(D) = (NPMU(D) * 2.14 * ((ABUND(1, ID) * .075) / 6.94) * 1 * .05 * .09) / SUMMZPZ
HMU16O(D) = (NPMU(D) * 2.14 * ((ABUND(19, ID) * .99) / 16) * 1 * .28 * .05) / SUMMZPZ
HMU28SI(D) = (NPMU(D) * 2.14 * ((ABUND(6, ID) * .92) / 28.08) * .84 * .56 * .026) / SUMMZPZ

REM ******* SUB-ROUTINE 7          14C
347 REM CPP = C-14 PROD BY SPALLATION- SEE YOYOYAMA ET AL 1977
NCONC = ABUND(24, ID): OCONC = ABUND(19, ID): REM FRACTIONAL ABUND TAKE AS EQUIV TO G IN THIS CASE.
LAMBDAC14 = .693 / 5730: REM C-14 DECAY CONST. A-1
DEPTHATTEN = EXP(-THICK / 170): REM DEPTH ATTENUATION OF REACTIONS SIMILAR TO THAT FOR N PRODUCTION
CPPCORR = ALTFACPIPRO * LATFACPIPRO * DEPTHATTEN
CPP(D) = 20.79 * CPPCORR: REM ATOMS / G / A (FROM SPALL OF LIGHT ELEMENTS) AT SEA LEVEL AND > 60 GEO LAT
CPN(D) = (NCONC * .9963 * 6.02E+23 / 14) * 1.83E-24 * NFLUX(D) * 365 * 24 * 60 * 60: REM N14(N,P)C14 /G/A
CPO(D) = (OCONC * .00038 * 6.02E+23 / 16) * 2.35E-25 * NFLUX(D) * 365 * 24 * 60 * 60: REM O17(N,A)C14 /G/A
REM              ND    ,   MZ              , PZ,  RZ ,  RP
CMU16O(D) = (NPMU(D) * 2.14 * ((ABUND(19, ID) * .99) / 16) * 1 * .28 * .08) / SUMMZPZ
CMU17O(D) = (NPMU(D) * 2.14 * ((ABUND(19, ID) * .00038) / 16) * 1 * .28 * .05) / SUMMZPZ
CMU15N(D) = (NPMU(D) * 2.14 * ((ABUND(24, ID) * .00366) / 14) * .1 * .28 * .2) / SUMMZPZ
```

```
REM ******* SUB-ROUTINE 8          36Cl
350 REM CLPK OR CLPCA = CL-36 PROD. BY K OR CA SPALLATION- SEE YOYOYAMA ET AL 1977
CLCONC = ABUND(7, ID): KCONC = ABUND(8, ID): CACONC = ABUND(9, ID): REM FRACTIONAL ABUND TAKE AS EQUIV TO G IN THIS CASE.
LAMBDACL36 = .693 / 305000: REM CL36 DECAY CONST. A-1
DEPTHATTEN = EXP(-THICK / 170): REM DEPTH ATTENUATION OF K/CA REACTIONS SIMILAR TO THAT FOR N PRODUCTION
KCACORR = ALTFACPIPRO * LATFACPIPRO * DEPTHATTEN
CLPK(D) = 404 * KCONC * KCACORR: REM ATOMS / G / A (FROM K SPALL) AT SEA LEVEL AND > 60 GEO LAT
CLPCA(D) = 120 * CACONC * KCACORR: REM ATOMS / G / A (FROM CA SPALL) AT SEA LEVEL AND > 60 GEO LAT
CLPKNA(D) = (KCONC * .93 * 6.02E+23 / 39.1) * 4.3E-27 * NFLUX(D) * 365 * 24 * 60 * 60: REM K39(N,A)CL36 /G/A
CLPNG(D) = (CLCONC * .76 * 6.02E+23 / 35.453) * 4.36E-23 * NFLUX(D) * 365 * 24 * 60 * 60: REM CL35(N,G)CL36 /G/A
CL3537AT = CLCONC * 6.02E+23 / 35.453
CLRAT(D) = ((CLPK(D) + CLPCA(D) + CLPKNA(D) + CLPNG(D)) / LAMBDACL36) / CL3537AT
REM            ND    ,   MZ      , PZ   , RZ , RP
CLMU39K(D) = (NPMU(D) * 2.14 * ((KCONC * .93) / 39) * 1.54 * .79 * .02) / SUMMZPZ
CLMU40CA(D) = (NPMU(D) * 2.14 * ((CACONC * .97) / 40) * 1.9 * .84 * .0026) / SUMMZPZ

REM *******SUB-ROUTINE 9 37AR
370 REM AR37PK, AR37PCA OR AR37PFE = AR-37 PROD BY K, CA OR FE SPALLATION- SEE YOYOYAMA ET AL 1977
FECONC = ABUND(13, ID): KCONC = ABUND(8, ID): CACONC = ABUND(9, ID):
LAMBDAAR37 = .693 / .0959: REM AR-37 DECAY CONST. A-1
DEPTHATTEN = EXP(-THICK / 170): REM DEPTH ATTENUATION OF K/CA/FE REACTIONS SIMILAR TO THAT FOR N PROD
KCAFECORR = ALTFACPIPRO * LATFACPIPRO * DEPTHATTEN
AR37PK(D) = 20.8 * KCONC * KCAFECORR: REM ATOMS / G / A (FROM K SPALL) AT SEA LEVEL AND > 60 GEO LAT
AR37PCA(D) = 595 * CACONC * KCAFECORR: REM ATOMS / G / A (FROM CA SPALL) AT SEA LEVEL AND > 60 GEO LAT
AR37PFE(D) = 72 * FECONC * KCAFECORR: REM ATOMS / G / A (FROM FE SPALL) AT SEA LEVEL AND > 60 GEO LA
AR37PNA(D) = (CACONC * .9694 * 6.02E+23 / 40.08) * 2.4E-27 * NFLUX(D) * 365 * 24 * 60 * 60: REM CA40(N,A)AR37 /G/A
REM              ND    ,   MZ      , PZ   , RZ , RP
AR37MU39K(D) = (NPMU(D) * 2.14 * ((KCONC * .93) / 39) * 1.54 * .79 * .09) / SUMMZPZ
AR37MU40CA(D) = (NPMU(D) * 2.14 * ((CACONC * .97) / 40) * 1.9 * .84 * .018) / SUMMZPZ
```

```
REM ******* SUB-ROUTINE 10          39AR
380 REM AR39PK, AR39PCA OR AR39PFE = AR-39 PROD BY K, CA OR FE SPALLATION- SEE YOYOYAMA ET AL 1977
FECONC = ABUND(13, ID): KCONC = ABUND(8, ID): CACONC = ABUND(9, ID): REM FRACTIONAL ABUND TAKE AS EQUIV TO G IN THIS CASE.
LAMBDAAR39 = .693 / 269: REM AR-39 DECAY CONST. A-1
DEPTHATTEN = EXP(-THICK / 170): REM DEPTH ATTENUATION OF K/CA/FE REACTIONS SIMILAR TO THAT FOR N PRODUCTION
KCAFECORR = ALTFACPIPRO * LATFACPIPRO * DEPTHATTEN
AR39PK(D) = 910 * KCONC * KCAFECORR: REM ATOMS / G / A (FROM K SPALL) AT SEA LEVEL AND > 60 GEO LAT
AR39PCA(D) = 116 * CACONC * KCAFECORR: REM ATOMS / G / A (FROM CA SPALL) AT SEA LEVEL AND > 60 GEO LAT
AR39PFE(D) = 8 * FECONC * KCAFECORR: REM ATOMS / G / A (FROM FE SPALL) AT SEA LEVEL AND > 60 GEO LA
AR39PKNA(D) = (KCONC * .9326 * 6.02E+23 / 39.01) * 1.6E-26 * NFLUX(D) * 365 * 24 * 60 * 60: REM K39(N,P)AR39 /G/A
AR39PCANA(D) = (CACONC * .00647 * 6.02E+23 / 40.08) * 1.6E-26 * NFLUX(D) * 365 * 24 * 60 * 60: REM CA42(N,A)AR39 /G/A
REM                ND    ,   MZ       , PZ   , RZ , RP
AR39MU39K(D) = (NPMU(D) * 2.14 * ((KCONC * .93) / 39) * 1.54 * .79 * .62) / SUMMZPZ
AR39MU40K(D) = (NPMU(D) * 2.14 * ((KCONC * .000117) / 39) * 1.54 * .79 * .5) / SUMMZPZ
AR39MU40CA(D) = (NPMU(D) * 2.14 * ((CACONC * .97) / 40) * 1.9 * .84 * .004) / SUMMZPZ
AR39MU42CA(D) = (NPMU(D) * 2.14 * ((CACONC * .00647) / 40) * 1.9 * .84 * .018) / SUMMZPZ
```

Sub-routine 1 initialise arrays and variables and input data.

ELEMENT$(25)	Name of element i
ID$(5)	Identity of standard rock types
ATOMWT(25)	Atomic weight of element i
PZ(25)	Probability of $^{-}\mu$ reaching 1S level of element i relative to that for oxygen
RZ(25)	Probability of nuclear $^{-}\mu$ capture from 1S level of element i
CROSSECT(25)	Absorption cross-section of element i
ERRCROSSECT(25)	Error in absorption cross-section of element i
ABUND(25,5)	Fractional abundance of element i for each of 5 average rock types
ERRABUND(25.5)	Error in fractional abundance of element i for each of 5 average rock types

Sub-routine 2 calculation of macroscopic neutron absorption cross-section.

For methodology see Section 3.1.2.2. Equation 3.1

Variables :-

SIGMA(25)	Macroscopic absorption cross-section for particular element
ERRSIGMA(25)	Error in macroscopic absorption cross-section for particular element
SUMSIGMA	Sum of of elemental components
ERRSUMSIGMA	Sum of errors in elemental components
SUMABUND	Sum of fractional abundances
NACS	Macroscopic neutron absorption cross-section (Σ_a (cm^2g^{-1}))

Sub-routine 3 calculation of neutron yield form (α,n) and spontaneous fission reactions.

Sub-routine 3a calculation of neutron yield form (α,n) reactions.

For methodology see Section 2.1.3

Variables :-

NYU(15)	Neutron yield due to α particles from U decay chain for element i
ERRORNU(15)	Error in neutron yield due to α particles from U decay chain for element i (8%)
NYTH(15)	Neutron yield due to α particles from Th decay chain for element i
ERRORNT(15)	Error in neutron yield due to α particles from Th decay chain for element i (8%)
MSP(15)	Mass stopping power for element i at 6.8 MeV.
A(15,4)	A(i,1) = mass stopping power of element i x abundance of element i
	A(i,2) = mass stopping power of element i x abundance of element i x neutron yield from U
	A(i,3) = mass stopping power of element i x abundance of element i x neutron yield from Th
B(15,4)	B(i,1) = Error in mass stopping power of element i x abundance of element i
	B(i,2) Error in mass stopping power of element i x abundance of element i x neutron yield fromU
	B(i,3) = Error in stopping power of element i x abundance of element i x neutron yield from Th
N(14)	Array holding identification number of elements :- Li, Be, B, O, F, Na, Mg, Al, Si, K, Ca, Fe
UCONC	Uranium concentration in ppm
ERRUCONC	Error in uranium concentration
THCONC	Thorium concentration
ERRTHCONC	Error in Thorium concentration
X	Sum of stopping power/abundance products
ERRORX	Error in sum of stopping power/abundance products
Y	Sum of stopping power/abundance/uranium yield products
ERRORY	Error in sum of stopping power/abundance/uranium yield products
Z	Sum of stopping power/abundance/thorium yield products
ERRORZ	Error in sum of stopping power/abundance/thorium yield products
XSUMERROR	Equivalent to ERRORX
YSUMERROR	Equivalent to ERRORY
ZSUMERROR	Equivalent to ERRORZ
NYIELDURAN	Total neutron yield per year per ppm uranium due to (α,n) reactions
NYIELDTHOR	Total neutron yield per year per ppm Thorium due to (α,n) reactions

Sub-routine 3b calculation of neutron yield from spontaneous fission of ^{238}U.

For methodology see Section 2.2.1

Variables :-

U238ATOMS	Number of ^{238}U atoms per gram of rock
LAMBDAFU238	Spontaneous fission halflife of ^{238}U
NPSPF	Neutron production from spontaneous fission per ppm U per year

Sub-routine 3c calculation of neutron yield from spontaneous fission of ^{238}U and (α,n) reactions.

Variables :-

NURAN	Neutron production from U induced (α,n) reactions per g rock per year
NTHOR	Neutron production from Th induced (α,n) reactions per g rock per year
NPSPF	Neutron production from spontaneous fission per g rock per year
ERRORNURAN	Error in neutron production from (α,n) reactions on rock
ERRORNTHOR	Error in neutron production from (α,n) reactions on rock
ERRORSFURAN	Error in neutron production from spontaneous fission on rock
NPALH	Total neutron production from (α,n) reactions per g rock per year
TOTAL	Total neutron yield from spontaneous fission and (α,n) reactions per g rock per year
ERRORTOTAL	Error in total neutron yield from spontaneous fission and (α,n) reactions per g rock per year

Sub-routine 4 Calculation of neutron production from cosmic rays.

Sub-routine 4a calculation of geomagnetic latitude.

Variables:-

LAT	Geographic latitude (degrees)
LNG	Geographic longitude (degrees)
ALT	Altitude in metres above mean sea level
DENSITY	Density of rock matrix in g per cm^2
GEOMLAT	Geomagnetic latitude

Sub-routine 4b calculation of correction factors for geomagnetic and altitude effects

For methodology see Section 2.3 and 2.4, equations 2.23, 2.23 and 2.27

Variables:-

LATFACPIPRO	Geomagnetic latitude correction factor for proton and pion production (R_{pl})
LATFACMU	Geomagnetic latitude correction factor for negative muon production ($R_{\mu l}$)
ALTFACPIPRO	Altitude correction factor for proton and pion production (R_{pa})
ALTFACMU	Altitude correction factor for negative muon production ($R_{\mu a}$)

Sub-routine 4c calculate neutron production rate and flux from cosmic ray and other interactions

For methodology see Section 2.3, 2.4 and 3.2, equations 2.24, 2.31, 2.32 and 3.9.

Variables:-

DEPTH(10) Depth below the Earth's surface at which production is to be calculated in metres

THICK	Depth below the Earth's surface at which production is to be calculated in g cm^{-2}
CORR	Correction factor to be applied at depths less than 0.1 m due to the escape of neutrons
NPMU(10)	Neutrons produced by negative muons at given depths below the surface (P_{μ})
NPPIPRO(10)	Neutrons produced by protons and pions at given depths below the surface (P_p)
NPSPF(10)	Neutrons produced by spontaneous fission at given depths below the surface (P_f)
NPALPH(10)	Neutrons produced by (α,n) reactions at given depths below the surface (P_{α})
NPTOT(10)	Total neutron production rate at given depths below the surface (P_{tot})
NFLUX(10)	Total neutron flux at given depths below the surface (Φ)

Sub-routine 5 sum $M_z P_z$ to aid calculation of isotope production rates from $^{-}\mu$ interactions

Sub-routines 6 to 10 :-calculate production of ^{3}H, ^{14}C, ^{36}Cl, ^{37}Ar and ^{39}Ar

Sub-routine 6 ^{3}H

For methodology see Section 4.2

Variables :-

HPP(10)	^{3}H production due to pions and protons at given depths below the surface
HPLI(10)	^{3}H production due $^{6}Li(n,\alpha)$ reactions at given depths below the surface
HPB(10)	^{3}H production due $^{11}B(n,2\alpha)$ reactions at given depths below the surface
HMU6LI(10)	^{3}H production due to ^{6}Li ($^{-}\mu$) reactions at given depths below the surface
HMU16O(10)	^{3}H production due to ^{16}O ($^{-}\mu$) reactions at given depths below the surface
HMU28SI(10)	^{3}H production due to ^{28}Si ($^{-}\mu$) reactions at given depths below the surface

Sub-routine 7 ^{14}C

For methodology see Section 4.3

Variables :-

CPP(10)	^{14}C production due to pions and protons at given depths below the surface
CPN(10)	^{14}C production due $^{14}N(n,p)$ reactions at given depths below the surface
CPO(10)	^{14}C production due $^{17}O(n,\alpha)$ reactions at given depths below the surface
CMU16O(10)	^{14}C production due to ^{16}O ($^{-}\mu$) reactions at given depths below the surface
CMU17O(10)	^{14}C production due to ^{17}O ($^{-}\mu$) reactions at given depths below the surface
CMU15N(10)	^{14}C production due to ^{15}N ($^{-}\mu$) reactions at given depths below the surface

Sub-routine 8 ^{36}Cl

For methodology see Section 4.4

Variables :-

CLPK(10)	^{36}Cl production due to pions and protons with K at given depths below the surface
CLPCA(10)	^{36}Cl production due to pions and protons with Ca at given depths below the surface
CLPNG(10)	^{36}Cl production due $^{35}Cl(n,\gamma)$ reactions at given depths below the surface
CLPKNA(10)	^{36}Cl production due $^{39}K(n,\alpha)$ reactions at given depths below the surface
CLMU39K(10)	^{36}Cl production due ^{39}K ($^{-}\mu$) reactions at given depths below the surface
CLMU40CA(10)	^{36}Cl production due $^{40}Ca(^{-}\mu)$ reactions at given depths below the surface
CLRAT(10)	$^{36}Cl/Cl$ ratios at given depths below the Earth's surface.

Sub-routine 9 ^{37}Ar

For methodology see Section 4.5

Variables :-

AR37PK(10)	^{37}Ar production due to pions and protons with K at given depths below the surface
AR37PCA(10)	^{37}Ar production due to pions and protons with Ca at given depths below the surface
AR37PFE(10)	^{37}Ar production due to pions and protons with Fe at given depths below the surface
AR37PNA(10)	^{37}Ar production due $^{40}Ca(n,\alpha)$ reactions at given depths below the surface
AR37MU39K(10)	^{37}Ar production due $^{39}K(^{-}\mu)$ reactions at given depths below the surface
AR37MU40CA(10)	^{37}Ar production due $^{40}Ca(^{-}\mu)$ reactions at given depths below the surface

Sub-routine 10 ^{39}Ar

For methodology see Section 4.5

Variables :-

AR39PK(10)	^{39}Ar production due to pions and protons with K at given depths below the surface
AR39PCA(10)	^{39}Ar production due to pions and protons with Ca at given depths below the surface
AR39PFE(10)	^{39}Ar production due to pions and protons with Fe at given depths below the surface
AR39PKNA(10)	^{39}Ar production due $^{39}K(n,p)$ reactions at given depths below the surface
AR39PCANA(10)	^{39}Ar production due $^{42}Ca(n,\alpha)$ reactions at given depths below the surface
AR39MU39K(10)	^{39}Ar production due $^{39}K(^{-}\mu)$ reactions at given depths below the surface
AR39MU40K(10)	^{39}Ar production due $^{40}K(^{-}\mu)$ reactions at given depths below the surface
AR39MU40CA(10)	^{39}Ar production due $^{40}Ca(^{-}\mu)$ reactions at given depths below the surface
AR39MU42CA(10)	^{39}Ar production due $^{42}Ca(^{-}\mu)$ reactions at given depths below the surface

APPENDIX 6. TREATMENT OF ERRORS.

The standard deviation (σ) of data in this thesis has been calculated using the formulae :-

$$\sigma_x^2 = \frac{1}{N_0 - 1} \sum_{i=1}^{N_0} (x_i - x)^2 \qquad \text{Eqn. A6.1}$$

where N_0 is the number of samples or measurements, x_i is the value measured, x is the mean of the measured values. If the number of samples is large, and a normal distribution of values about a mean is assumed a :-

1σ error gives 65 % confidence that the result is a member of the sampled population.

2σ error gives 95 % confidence that the result is a member of the sampled population.

Unless stated otherwise all reported errors are quoted to 65% confidence ie/ 1σ.

The coefficient of variation (S) is defined as :-

$$S = \frac{\sigma_x}{x} 100 \qquad \text{Eqn. A6.2}$$

where σ_x is the calculated standard deviation for the population for which x is the mean.

For the purpose of assessing the influence of ranges in composition over geological formations on production rates of isotopes and neutron flux, it is assumed that the sampled mean represents the true mean and that the distribution is normally distributed. Whilst this assumption may not always be true for rock matrices whose minor elements are log-normally distributed (MIDDLETON., 1963) it allows the use of standard error propagation procedures (BEVINGTON., 1969) for addition, subtraction, multiplication and division :-

$$\sigma_{x+y} = \sqrt[2]{\sigma_x^2 + \sigma_y^2} \qquad \text{Eqn. A6.3}$$

$$\sigma_{x-y} = \sqrt[2]{\sigma_x^2 + \sigma_y^2} \qquad \text{Eqn. A6.4}$$

$$\sigma_{xy} = xy \sqrt{\left(\frac{\sigma}{x}\right)^2 + \left(\frac{\sigma}{y}\right)^2} \qquad \text{Eqn. A6.5}$$

$$\sigma_{x/y} = x/y \sqrt{\left(\frac{\sigma}{x}\right)^2 + \left(\frac{\sigma}{y}\right)^2} \qquad \text{Eqn. A6.6}$$

Also if σ_x is small compared with x then the error in ln(x), σ_x is :-

$$\sigma_{\ln x} = \frac{\sigma_x}{x} \qquad \text{Eqn. A6.7}$$

Methods used for both linear and non linear fitting have been adapted for Hewlett Packard Basic from Fortran programmes described in BEVINGTON., (1969).